



Republic of Iraq  
Ministry of Higher Education and Scientific Research  
University of Misan/College of Engineering  
Civil Engineering Department



# **NONLINEAR FINITE ELEMENT ANALYSIS OF REINFORCED CONCRETE HAUNCHED BEAMS**

**A THESIS  
SUBMITTED TO THE COLLEGE OF ENGINEERING OF  
MISAN UNIVERSITY IN PARTIAL FULFILLMENT OF  
THE REQUIREMENTS FOR THE DEGREE OF MASTER  
IN CIVIL ENGINEERING  
(STRUCTURES)**

**BY  
ALI WATHIQ ABDULGHANI  
B.Sc. in Civil Engineering, 2016**

**Supervised by  
Assist. Prof. Dr. Abdulkhaliq Abdulyimah Jaafer**

**April 2019**

**Sha'aban 1440**



# Dedication

- ❖ To whom stood beside me and took care of me over the years, to my family and close friend.
- ❖ To all those who supported and helped me, made the difficult easy, especially to my supervisor Assist. Prof. Dr. Abdulkhaliq A. Jaafer.

I present my effort to them with all of my respect and appreciation.

## **ACKNOWLEDGEMENTS**

First of all, all my thanks for **Allah** who led me during my way to complete this work.

I would like to express my cordial thanks and deepest gratitude to my supervisor **Asst. Prof. Dr. Abdulkhaliq A. Jaafer**, whom I had the honor of being under his supervision, for his advice, help, and encouragement during the course of this study.

I would like to extend my thanks to **Prof. Dr. Ahmed K. Al-Shara** Dean of the college of engineering, and **Asst. Prof. Dr. Abbas O. Dawood**, the Head of Civil Engineering Department.

Special thanks go to **my mother** for her great efforts. Also, thanks go to **my brothers** and **my close friend**.

Special thanks also go to **Asst. Prof. Dr. Saad F. Resan**, **Asst. Prof. Dr. Bahaa Hussain**, **Mr. Mustafa Raheem**, and **Mr. Mohammed Mahood** for their effort in helping me in ANSYS program.

**Ali Wathiq Abdulghani**

**2018**

## ***CERTIFICATION***

I certify that the thesis titled "**Nonlinear Finite Element Analysis of Reinforced Concrete Haunched Beams**" which is being submitted by **Ali Wathiq Abdulghani** and prepared under my supervision at the University of Misan, Department of Civil Engineering, in partial fulfillment of the requirements for the Degree of Master of Science in Civil Engineering (Structures).

Signature:

Asst. Prof. Dr. Abdulkhaliq A. Jaafer

Date:

In view of the available recommendations, I forward this thesis for discussion by the examining committee.

Signature:

Assist. Prof. Dr. Abbas O. Dawood

(Head of Civil Eng. Department)

Date:

## Committee Report

We certify that we have read this thesis titled " **Nonlinear Finite Element Analysis of Reinforced Concrete Haunched Beams** " which is being submitted by **Ali Wathiq Abdulghani**, and as Examining Committee, examined the student in its contents. In our opinion, the thesis is adequate for award of degree of Master of Science in Civil Engineering.

Signature: 

Name: Prof. Dr. Anis A. Mohamad Ali

(Chairman)


Date: / /

Signature: 

Name: Assist. Prof. Dr. Sa'ad F. Resan

(Member)

Date: / /

Signature: 

Name: Assist. Prof. Dr. Abbas O. Dawood

(Member)

Date: / /

Signature: 

Name: Assist. Prof. Dr. Abdulkhaliq A. Jaafer

(Supervisor)

Date: / /

### Approval of the College of Engineering

Signature:

Name: Prof. Dr. Ahmed K. Al-Shara

Dean, College of Engineering

Date: / /

## **ABSTRACT**

This study presents a numerical investigation of the flexural and shear behavior of a reinforced concrete haunched beams (RCHBs). Normal and high strength concrete with or without opening tested as simply supported beam. Also, strengthening by carbon fiber reinforced polymer (CFRP) is performed.

This work is divided into three phases. The verification process was carried out on solid RCHBs analyzed by nonlinear finite element method by ANSYS to ascertain the accuracy and validity of FE procedure. These validated beams presented by several researchers. The results of the validation showed a well matching between the finite element model and the experimental tests involving the load-deflection curves and crack pattern. Also, parametric study was done for three series with different types of haunch beams. The first series involved inverted haunched beams. While, the second and third series included haunched beams with positive and negative haunch sign respectively. Several parameters including increasing  $f'_c$ , amount of shear reinforcement, existence of transverse opening, presence of longitudinal opening and using CFRP sheet for retrofitting the beams were performed. The results showed that these beams had higher energy dissipation. Increasing the haunch angle reduced the shear carrying capacity. Increasing in the  $f'_c$  enhanced the ultimate shear strength for beams that fail in shear. Also, the existence of the transverse and longitudinal opening led to decrease in the stiffness and strength of these beams. Maximum decreasing occurred by lateral opening (28% h) by (29%) when the presence of the opening was near the smaller depth for RCHBs (vertex). Maximum reduction occurred in the longitudinal opening (28% h) mm by (39%). In addition, reinforcing the opening and increasing  $f'_c$  restored the lost strength and enhanced the ductility.

Using CFRP sheet to strengthening the RCHBs with and without opening showed a good improvement in the ultimate strength. Using CFRP sheet to

strengthening the beams with transverse opening restored most of the lost strength due to the existence of the opening. CFRP sheet in several beams restored the lost strength completely with gaining additional strength with increasing in the ductility and making the cracks more propagated.

Beams with an opening showed less spread of cracks. Beams with CFRP sheet increased the amount of propagated cracks along the beam. Changing  $f'_c$  did not affected the crack pattern for RCHBs with positive haunch angle but increasing the  $f'_c$  for inverted RCHBs developed more shear and flexural cracks.



# CONTENTS

<b>Title</b>		<b>Page No.</b>
Acknowledgments		I
Certification		II
Committee Report		III
Abstract		IV
Contents		VI
Nomenclatures		X
Abbreviations		XIII
List of Figure		XIV
List of Tables		XIX
<b>Section No.</b>	<b>Title</b>	<b>Page No.</b>
<b>Chapter One: Introduction</b>		
1.1	Introduction	1
1.2	Advantages and Disadvantages of Haunched Beams	2
1.3	Application of Non-Prismatic Beams.	3
1.4	Code Recommendation	5
1.5	General Behavior of Haunched Member	6
1.6	Stress Distribution over Cross Section	7
1.7	Stress Flow in Non-Prismatic Members	8
1.8	Fiber Reinforced Polymers (FRP)	9
1.9	Objectives of the Study	10
1.10	Thesis Scope	11
<b>Chapter Two: Literature Review</b>		
2.1	Introduction	12
2.2	Experimental and Theoretical Studies of RCHBs	12

<b>Section No.</b>	<b>Title</b>	<b>Page No.</b>
2.3	Experimental and Theoretical Studies of Reinforced Concrete Members with and without Opening Strengthened by FRP	28
2.4	Summary	32
<b>Chapter Three: Finite Element Formulation and Mathematical Model</b>		
3.1	Introduction	33
3.2	Nonlinear Finite Element Analysis of Structures	33
3.3	Basic Steps in Finite Element Method	34
3.4	Finite Element Formulation	35
3.4.1	Basic Finite Element Relationships	35
3.4.2	Strain-Displacement Matrix	38
3.4.3	Element Stiffness Matrix	40
3.5	Material Modeling	41
3.5.1	Concrete Modeling	41
A	Plasticity Approach	41
B	Material Nonlinearity	42
C	Multilinear Stress-Strain Relationship	43
C.1	Tensile Behavior of High Strength Concrete	48
D	Post - Cracking Model (Tension Stiffening Model)	49
E	Failure Criteria for Concrete	51
F	Cracking Modeling	54
G	Shear Transfer and Tensile Crack Coefficient	55
H	Crushing Modeling	56
3.5.2	Reinforcement Behavior	56
3.5.3	CFRP Behavior	57
3.6	ANSYS Computer Program	57
3.7	Nonlinear Solution Techniques	58

<b>Section No.</b>	<b>Title</b>	<b>Page No.</b>
3.8	Analysis Termination Criteria	60
3.9	Convergence Criteria	61
3.10	ANSYS Finite Element Model	62
3.10.1	SOLID65 Element Description	62
3.10.1.1	Shape Functions of SOLID65 Element	62
3.10.1.2	Input Data for SOLID65	63
3.10.2	LINK180 Element Description	64
3.10.3	SOLID185 Element Description	67
3.10.4	SHELL41 Element (Membrane Shell)	67
3.10.4.1	Shell41 Input Data	68
<b>Chapter Four: Presentation and Discussion of Results</b>		
4.1	Introduction	70
4.2	Procedure of Study	70
4.3	Verification Process	71
4.4	Theoretical Investigation	76
4.4.1	Series One	77
4.4.2	Series Two	81
4.4.3	Series Three	88
4.5	Presentation and Discussion of Results	91
4.5.1	Series One	91
4.5.1.1	Load-Deflection Relationship	91
4.5.1.2	Crack Pattern	99
4.5.2	Series Two	109
4.5.2.1	Load-Deflection Relationship	109
4.5.2.2	Cracking Pattern	119

<b>Section No.</b>	<b>Title</b>	<b>Page No.</b>
4.5.3	Series Three	126
4.5.3.1	Load-Deflection Relationship	126
4.5.3.2	Crack Pattern	130
4.6	Energy Dissipation of RCHBs	133
4.7	Shear Stress Distribution of Models	134
4.8	CFRP Stress and Strain	137
Chapter Five: Conclusions and Recommendations		
5.1	Conclusions	141
5.2	Recommendations for Future Works	143
References		
	References	144
Appendices		
A	Finite Element Modeling	155
B	Shear Stress Distribution of Series Two	165

## NOMENCLATURES

Symbol	Description	Unit
$A$	Cross-sectional area	$\text{mm}^2$
$b$	Beam width	mm
$d$	Effective depth	mm
$E$	Modulus of elasticity	MPa
$E_c$	Modulus of elasticity of concrete	MPa
$E_s$	Modulus of elasticity of reinforcing bars	MPa
$E_T$	Strain hardening modulus	
$F$	Function of principal state ( $\sigma_{xp}, \sigma_{yp}, \sigma_{zp}$ )	
$f_t$	Ultimate uniaxial tensile strength of concrete	MPa
$f_r$	Modulus of rupture of concrete	MPa
$f_{cb}$	Ultimate biaxial compressive strength	MPa
$f_1$	Ultimate compressive strength for a state of biaxial compression superimposed on hydrostatic stress state	MPa
$f_c'$	Compressive strength of concrete cylinder	MPa
$f_y$	Yielding stress of steel reinforcement	MPa
$f_2$	Ultimate compressive strength for a state of uniaxial compression superimposed on hydrostatic stress state	MPa
$f_c$	Concrete ultimate uniaxial compressive strength	MPa
$f_y$	Steel yield strength	MPa
$f_u$	Steel ultimate tensile strength	MPa
$f_{cr}, \epsilon_{cr}$	Cracking stress and strain	MPa
$h$	Height of the cross section	mm
$I_1$	First stress invariant	
$J_2$	Second deviatoric stress invariant	

Symbol	Description	Unit
$L$	Span length of the beam	mm
$L_e$	Effective length	mm
$P$ and $V$	Any applied force on the structure	kN
$P_{cr}$	Cracking load	kN
$P_u$	Ultimate load	kN
$u, v, w$	Displacement components in x,y and z coordinates	mm
$W_{ext}, W_{int}$	External and internal work	
$x, y, z$	Global coordinate	
$\alpha$	Haunch angle with horizontal line	Degree
$\beta$	Shear transfer coefficient	
$B_t, \beta_c$	Opened and closed shear transfer coefficient	
$\gamma$	Shear strain	
$\varepsilon$	Normal strain	mm/mm
$\varepsilon_o$	Strain at ultimate compressive stress $f_c$	
$\varepsilon_u$	Ultimate strain	
$\zeta, \eta$	Local coordinates	
$\sigma$	Normal stress	MPa
$\sigma_h^a$	Ambient hydrostatic stress state	MPa
$\sigma_{xp}$	Principal stress in the x – direction.	MPa
$\sigma_{yp}$	Principal stress in the y – direction.	MPa
$\sigma_{zp}$	Principal stress in the z – direction.	MPa
$\sigma_h$	Hydrostatic stress	MPa
$\tau$	Shear stress	MPa
$\nu$	Poisson's ratio	
$[A]^T$	Transpose of matrix [A]	

<b>Symbol</b>	<b>Description</b>	<b>Unit</b>
$[A]^{-1}$	Inverse of matrix $[A]$	
$[B]$	Strain-displacement matrix	
$[D]$	Constitutive matrix	
$[J]$	Jacobian matrix	
$[K]$	Overall stiffness matrix	
$[K]_e$	Element stiffness matrix	
$[L]$	Differential operator matrix	
$[N]$	Matrix of shape functions	
$[T]$	Transformation matrix	
$\{a\}$	Nodal displacement vector	
$\{F^a\}$	Vector of applied loads	
$\{f\}$	Load vector	
$\{u\}$	Displacement vector	
$\{\varepsilon\}$	Strain vector	
$\{\sigma\}$	Stress vector	

## ABBREVIATIONS

<b>Symbol</b>	<b>Description</b>
ACI	American Concrete Institute
ANSYS	(ANalysis SYStem) Computer Program
APDL	Ansys Parametric Design Language
BS	British Standards (BSI: British Standards Institute)
CFRP	Carbon Fiber Reinforced Polymer
EC	Euro Code
FE	Finite Element
FEA	Finite Element Analysis
FEM	Finite Element Method
FRP	Fiber Reinforced Polymer
GFRP	Glass Fiber Reinforced Polymer
HSC	High Strength Concrete
NSC	Normal Strength Concrete
RC	Reinforced Concrete
RCHBs	Reinforced Concrete Haunched Beams
PSC	Prestress Concrete



## LIST OF FIGURES

<b>Fig. No.</b>	<b>Title</b>	<b>Page</b>
1-1	Types of Non-prismatic Members	2
1-2	Typical Haunched Members in Building and Bridge	3
1-3	Example of Recess Beams. (a) Floor beams, (b) Ground beam, (c) Stepped beam, (d) Strengthened beam	4
1-4	Shear Resistance Components of the Varied-Depth Concrete Members	5
1-5	Stress Distribution: (a) Prismatic beam; (b) Haunched beam	7
1-6	Stress Distribution in Non-prismatic Members: (a) Normal Stresses of Pure Moment; (b) Shear Stresses of Constant Shear Force	8
1-7	Principal Stress Contour for: (a) Stepped beam (b) Haunched Beam	9
1-8	Application Method of CFRP Sheet	10
2-1	Geometry and Loading Condition for the Test Specimens	16
2-2	Specimen Testing Layout	17
2-3	Testing of Experimental and Theoretical Specimen	18
2-4	Geometry and Loading Condition for the test Specimens	21
2-5	Testing Condition for the Orr et al. Specimens	22
2-6	Specimen Testing of Hou et al.	23
2-7	Crack Pattern of Shear Beams	25
2-8	Tested Models of Hou et al. Study	27
2-9	Strengthening for Beams with Large Openings	31
3-1	Finite Element Discretization	34
3-2	Non-Linear Material Response	42
3-3	Uniaxial Compressive Strain Curve for Concrete with Different Strength	43
<b>Fig. No.</b>	<b>Title</b>	<b>Page</b>

3-4	Simplified Stress-Strain for NSC	45
3-5	Stress-Strain Curve of HSC in Compression	46
3-6	Typical Stress-Strain Curves for Concrete in Uniaxial Compression Test (a)Axial and Lateral Strains. (b) Volumetric Strain ( $\epsilon_v = \epsilon_1 + \epsilon_2 + \epsilon_3$ )	47
3-7	Stress-Volumetric Strain Curves	47
3-8	Typical Tensile Stress-Strain Curve for Concrete	49
3-9	Pre and Post-Cracking Behavior of Normal Strength Concrete	50
3-10	Profile of the Failure Surface as Function of Five Parameters	54
3-11	Cracking Modeling	55
3-12	Modeling of Reinforcing Bars	56
3-13	Modeling of CFRP Sheet	57
3-14	Basic Technique for Solving the Nonlinear Equation (a) Incremental. (b) Iterative. (c) Incremental-Iterative.	59
3-15	SOLID65 Element for Representing the Concrete	63
3-16	LINK180 for Representing Steel Reinforcement	65
3-17	Models for Reinforcement in Reinforced Concrete	66
3-18	SOLID 185 Used to Model Steel Plates and Supports	67
3-19	SHELL41 Geometry	68
4-1	Load-Deflection Curves for Theoretical and Experimental Beams	73
4-2	Crack Pattern for Theoretical and Experimental Beam	75
4-3	Series One Beams Details (1L1,2L1 and 3L1 Consequently)	78
4-4	Reinforcement Details for Beams with Stirrups	80
4-5	Details of Three Beams with Different Opening Location	80
4-6	Beams with CFRP Sheet	81
4-7	Geometry and Reinforcement Details of RCHBs	82
4-8	Reinforcement Distribution of RCHBs	83
<b>Fig. No.</b>	<b>Title</b>	<b>Page</b>

4-9	Details of Three RCHBs have Transverse Opening with Different Positions	86
4-10	Details of Three RCHBs have Longitudinal Opening with Different Sizes	86
4-11	Reinforcement Details of Beam with an Opening	87
4-12	Details of Strengthened RCHBs by CFRP	87
4-13	Details of RCHBs in Series Three	88
4-14	Flexural Beam with Mid-Span Opening (NHB-TO1)	89
4-15	RCHBs Retrofitted by CFRP Sheet	90
4-16	Relationship Between the Ultimate Load and the Haunch Angle	93
4-17	Effect of the Compressive Strength on the Ultimate Load and the Deflection on the Inverted RCHBs without Shear Reinforcement	93
4-18	Effect of the Compressive Strength on the Ultimate Load and the Deflection on the Inverted RCHBs with Shear Reinforcement	94
4-19	Load-deflection Curve for Effect of Increasing the Haunch Angle	94
4-20	Load-deflection Curve for Effect of Increasing $f'_c$ for Beams without Shear Reinforcement	95
4-21	Load-Deflection Curve for Effect of Presence of Stirrups with Different Spacing	95
4-22	Load-Deflection Curve for Effect of Increasing $f'_c$ for Beams with Shear Reinforcement	96
4-23	Load-Deflection Curve of Beams with Transverse Opening	97
4-24	Load-Deflection Curve for Beams with Lateral Opening Strengthened by Increasing $f'_c$	97
4-25	Load-deflection Curve for Beam with Lateral Opening Retrofitted by CFRP Sheet	98
4-26	Load-Deflection Curve for Beam Retrofitted by CFRP Sheet	98
4-27	Integration Points in Concrete Solid Element	100
<b>Fig. No.</b>	<b>Title</b>	<b>Page</b>

4-28	Cracking Sign	100
4-29	Cracking Signs Occurring in FE Models	101
4-30	Crack Pattern for Series Two Beams	103
4-31	Relationship Between the Ultimate Load and Haunch Angle	111
4-32	Effect of the Compressive Strength on the Ultimate Load and the Deflection of RCHBs with Shear Reinforcement	111
4-33	Effect of the Compressive Strength on the Ultimate Load and the Deflection of RCHBs without Shear Reinforcement	112
4-34	Load-Deflection Curve for Effect of Increasing the Haunch Angle on the Ultimate Load for RCHBs with Stirrups	112
4-35	load-Deflection Curve for Effect of Increasing $f'_c$ for RCHBs	113
4-36	Load-deflection curve for Effect of Increasing $f'_c$ for RCHBs without Shear Reinforcement	113
4-37	Load-Deflection Curve for Beams with Transverse Opening	114
4-38	Load-Deflection Curve for Beams with Longitudinal Opening	115
4-39	Load-Deflection Curve for Beam with Opening Strengthened by Steel Reinforcement	115
4-40	Load-Deflection Curve for Beams with Lateral Opening Strengthened by Increasing $f'_c$	116
4-41	Load-Deflection Curve of Beam with Longitudinal Opening Strengthened by Increasing $f'_c$	117
4-42	Load-Deflection Curve of Beam with Transverse Opening Strengthened by CFRP Sheet	118
4-43	Load-Deflection Curve of Beam with Longitudinal Opening Strengthened by CFRP Sheet	118
4-44	RCHBs with Different $f'_c$ Equal to 40 and 50 MPa (HB40-6 and HB50-6)	120
4-45	RCHBs with Different $f'_c$ Equal to 40 and 50 MPa (HB40-6 and HB50-6)	121
4-46	Load-Deflection Curve for Effect of Increasing the Haunch Angle for RCHBs with Negative Haunch	127
4-47	Load-Deflection Curve for RCHBs with Opening	127
<b>Fig. No.</b>	<b>Title</b>	<b>Page</b>

4-48	Load-Deflection Curve for RCHBs with Opening Strengthened by CFRP Sheet	128
4-49	Load-Deflection Curve for RCHB Strengthened by CFRP Sheet Around the Beam	129
4-50	Load-Deflection curve for RCHB Strengthened by CFRP Sheet at the Bottom Surface of the Beam	129
4-51	Crack Pattern for RCHBs of Series Three	131
4-52	Energy dissipation capacity for inverted RCHBs for (a) Haunch angle (b) CFRP sheet for beam with opening (c) CFRP strips for solid RCHB	133
4-53	Shear Distribution of the Series Two Models	134
4-54	Stress and Strain of CFRP Sheet for Beams in Series One	137
4-55	Stress and Strain of CFRP Sheet for Beams in Series Two	139
4-56	Stress and Strain of CFRP Sheet for Beams in Series Three	139
A-1	Haunched Beam Modeling	160
A-2	Details of the Flexural and Shear Reinforcement	161
A-3	Loading and Boundary Condition of RCHBs	162
B-1	Shear Stress Distribution for Series Two Beams	168

## LIST OF TABLES

<b>Table</b>	<b>Title</b>	<b>Page</b>
3-1	Material properties for CFRP sheet	57
3-2	SOLID65 input data	64
3-3	Input data of CFRP sheet	69
3-4	Material properties for CFRP element	69
4-1	Verification results include the failure load	72
4-2	Verification results include maximum deflection	73
4-3	Details of specimens (Series 1)	79
4-3	(continued) Details of specimens (Series 1)	80
4-4	Properties details of RCHBs	82
4-5	Steel reinforcement properties	83
4-6	Details of specimens (Series 2)	85
4-6	(continued) Details of specimens (Series 2)	86
4-7	Details of specimens (Series 3)	89
4-8	Results of inverted RCHBs in series one	83
4-9	Results of RCHBs in series two	110
4-10	Results of RCHBs in series three	126
4-11	Maximum stresses and strain in CFRP of the strengthened beams	138
A-1	Used element of a model in ANSYS	155
A-2	Real constant of the used element in ANSYS	156
A-3	Material properties for concrete.	157
A-4	Material properties for Ø25 rebar (longitudinal bar)	158
A-5	Material properties for Ø10 rebar (stirrups)	158
A-6	Material properties for CFRP sheet	158
A-7	Material properties for steel plate	159
A-8	The analysis commands in ANSYS	163
A-9	The analysis commands	163

<b>Table</b>	<b>Title</b>	<b>Page</b>
A-10	The solution commands	164
A-11	Commands for finishing analysis	164

# CHAPTER ONE

## INTRODUCTION

---

---

### **1.1 Introduction**

Members with non-prismatic section have been exists in different structures involving bridges and buildings. Since the previous century exactly at the first ten-years, an increasing in usage of haunched beams as a structural member instead of prismatic member became more common. In addition, that structural engineers looking for ideal low weight with high strength structures by redistribute the materials through the member.

Along with the new enhancements in structural engineering, many attention has been drawn to find better combinations for modeling non-prismatic components. This was not only the result of the using of non-prismatic members in different geometries, also for a research now realized that these packages could be effectively applied to model and simulate certain phenomena or structural situations as inelastic behavior, crack propagation, and dependence of various materials [1].

Non-prismatic beams included two types, first type is haunched beam and the second is stepped beam. Haunched beam is the structural member that has cross section thicker at the support region than in the mid-span and vice versa. It used in building and bridge construction for structural and architectural reasons [1]. There are several shapes of haunched beams according to the haunch type (bigger haunch and smaller haunch) and inclination angle sign (positive and negative). While, the stepped beam is an example of non-prismatic beams that can be used to support a split-level floor, in theaters, and in private housing for aesthetic reasons as appeared in Fig. (1-1).



Both haunched and stepped beam provides additional need for reinforcement detailing to fulfill the stress concentration at point of changing depth. [2].

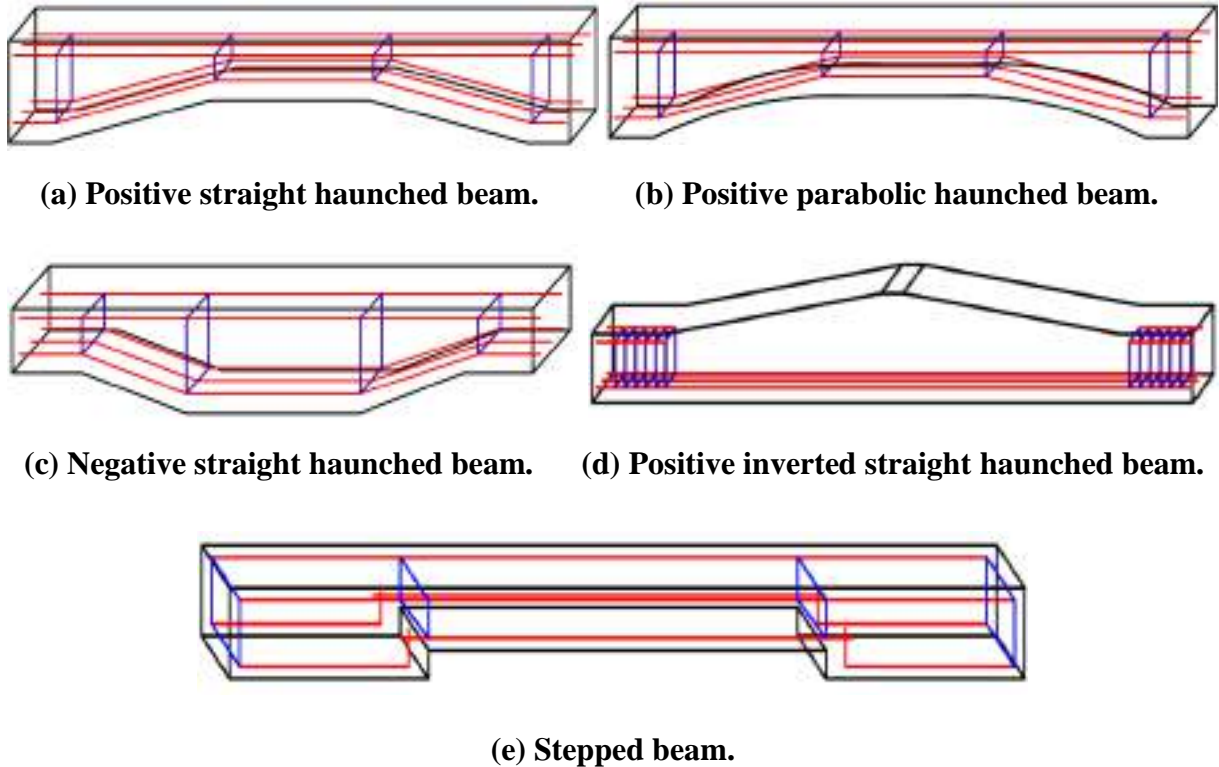


Figure (1-1): Types of non-prismatic members [3].

## **1.2 Advantages and Disadvantages of Haunched Beams**

Structural engineer and architect predominately use RCHBs in reinforced concrete (RC) buildings because haunched beam provide many advantages in comparison with prismatic beams [4] as follows:

- 1) Haunched beams enhance the lateral stiffness of structure basically, which permit to the structural designer to control code recommendation.
- 2) This type of beams increases efficiency in using concrete with steel reinforcement.
- 3) Using this type of beams reduce the self-weight of the structures with an agreed lateral stiffness.

- 4) Haunched beams provide more spaces for the placement of the building's electrical, air conditioning, sewage services...etc.

The main disadvantage of these types of beams are unfavorable in a common structural solution in buildings because of higher construction costs, as special formwork and worker with high quality in construction [4]. During an earthquake, failure of structure starts at points of weakness. The weakness occurred in this kind of beams at point of discontinuity of the member mass (varying in cross section). When structures have a discontinuity are called under the term "irregular structures". Irregularities in structure members have a contribution in a big portion of the urban infrastructure. Presence of irregularities in buildings may be one of the main reasons for structures failure during the earthquakes. For example, soft-floor structures are more structures that have been marked. The irregularities in members affect the performance structural of structures. The wise height changes in the hardness and mass make the dynamic characteristics of these buildings different from the normal construction [5].

### **1.3 Application of Non-Prismatic Beams**

RCHBs are frequently used in form of simply supported case or continuous bridge as crosswise double cantilever, hammer head beam Plate, precast roof girders [6] as demonstrated in Fig. (1-2).



**Figure (1-2): Typical haunched members in building and bridge [7].**

Non-prismatic beams are used also in ships and submarines because they are necessary for these types of structures to conserve both space and weight. For example, in modern structures where utility pipes and ducts are being accommodated below the floor beams in the space overhead the false ceiling. The usage of a non-prismatic beam with an opening will let to this equipment to pass inside the beam, eliminating amount of dead space as shown in Fig. (1-3 a).

This would reduce the height of each storey leading to significant savings in the material and construction costs. Similarly, non-prismatic beam can be properly placed as ground beam as shown in Fig. (1-3 b) in residential structures, where present service pipes frequently obstruct the building of tie beams that attach the newly built columns to present ones. Using non-prismatic tie beams permits the building to progress without the necessity of repositioning these pipes. A non-prismatic beam in the form of a stepped beam be able to be applied to support a split level floor as demonstrated in Fig. (1-3 c). This application usually exist in theatres and in houses designed for aesthetic reasons. Finally, in structures that been strengthened, there might be a need to add a new utility ducts, and this is often a difficult due to limited headroom. In this case, an opening can be creating in the present beam to harmonize this equipment [2].

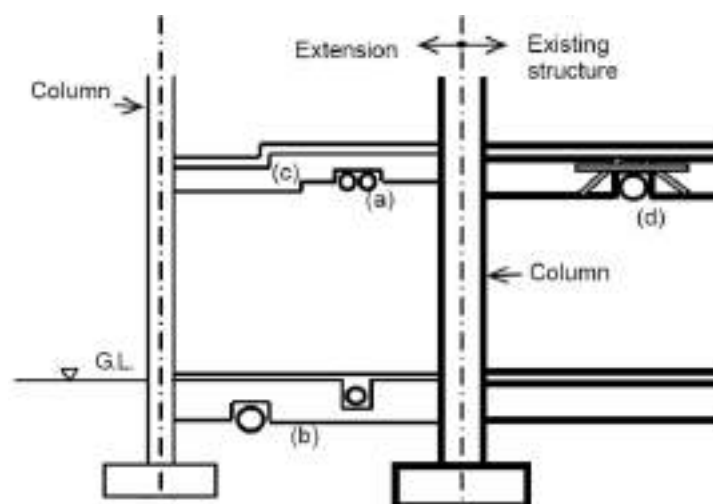


**Figure (1-3):** Examples of recess beams. (a) floor beams, (b) ground beam, (c) stepped beam, (d) strengthened beam [2].

## 1.4 Code Recommendation

Reinforced concrete guidelines ACI 318-11[8] and BS-5400[9] do not show specified recommendations about haunched members. While German code (DIN 1045-1, 2001) [10] and a few textbooks such as (Park and Paulay 1975[11], MacGregor 1997[12], Muttoni et al. 1997[13], and Nielsen 1999[14]) have some abridged recommendations for the shear design of these types of members [15].

The German code DIN 1045-01 [10] explains the shear resistance mechanism of haunched beams and provides detailed design guides in the clause 10.3.2. As explained below and from Fig. (1-4), the shear design ( $V_{ED}$ ) for haunched beams is introduced as follows:

$$V_{ED} = V_{ED0} - V_{ccd} - V_{td} - V_{pd} \leq V\alpha_{Rd}$$

Where:

$V_{ED0}$  : Shear force due to dead loads and live loads,

$V_{ccd}$  : Design shear resistance due to inclination of compression chord of beam,

$V_{td}$  : Design shear resistance component of inclined longitudinal tension

Reinforcements,

$V_{pd}$  : Design shear resistance component of prestressed force,

$V\alpha_{Rd}$  : Design value of shear bearing capacity of haunched beams at design section.

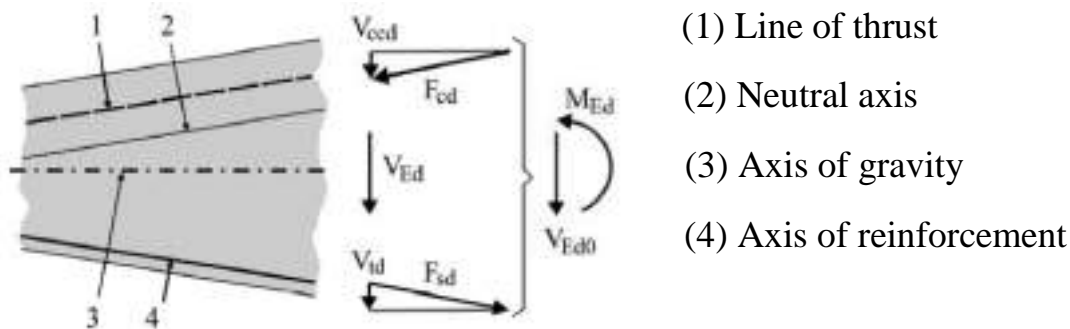


**Figure (1-4): Shear resistance components of the varied-depth concrete members [10]**

In members without prestressing and horizontal longitudinal tension reinforcement, the values of  $V_{pd}$  and  $V_{td}$  are equal zero.

## **1.5 General Behavior of Haunched Beams**

The behavior of haunched member taking in considering the shear stress is different from the behavior of prismatic members, because of the following reasons: (a) the slope of the main internal tension or compression in these types of beam produces a vertical component possibly, capable to resist shear forces. (b) The varying in cross section towards the supports is unlikely. (c) The dissimilarity of cross section along the member and the discontinuity of the axis of the centroid. The discontinuity of the centroidal axis in RCHBs causes a strong coupling between bending moment, shear and axial forces [3].

The coupling effect becomes more significant with an increase in depth of the end segments. In case of the stepped members, the existence of the null areas causes softening of the member stiffness [3]. RCHBs behavior tends to be less shear strength than in prismatic one with an increase in deflection. In RCHBs, such a crack would cause failure unless it was crossed by reinforcement. Cracking of these beams start with fine flexural cracks. With a further increase of load, these flexural cracks turned into flexure-shear cracks with the appearance of more shear cracks. The flexure-shear cracks expand in length and increased in size toward the loading zone. By increasing of more load, shear compression failure occurs for beams of big haunch, while instability failure occurs in beams with small haunch.

First diagonal cracks occur near the support for beams of smaller haunch and near the load point for beams of bigger haunch. Beams with bigger haunch are stiffer than beams with smaller haunch. The change in angle of haunch inclination affects the behavior at failure, thus bringing about two distinct types. For beams with small depth at the support, the failure is caused by an instability

type of failure. This is due to the formation of a major crack above the line joining the load point to the support. The major crack after propagation creates a weak arch in the upper part, thus bringing about the failure of the beam. This arch transfers a bigger shear of load to the support and is capable of resisting more rotation about the load point, until the crushing of concrete [15].

## **1.6 Stress Distribution over Cross Section**

Subjecting to the same internal forces, the distribution of stress through the cross section of a haunched member is dissimilar than the apportionment of stresses than in prismatic one for the same geometry. In 1963, Timoshenko [3] explained that shear stress distribution over a cross section of a bar, in the form of a cantilever wedge, it is in opposite direction to that of prismatic bars as revealed in Fig. (1-5). Timoshenko stated that: “In many cases the practical shear stresses are of no great importance and only the normal bending stresses are considered. Then the formula for maximum bending stress, derived for prismatic beams, can be used with sufficient accuracy for bars of variable cross section, provided the variation of the cross section is not too rapid”. Because of this statement, the prismatic beam formulas are usually used for non-prismatic beams and the influence of shear stresses is neglected [3].

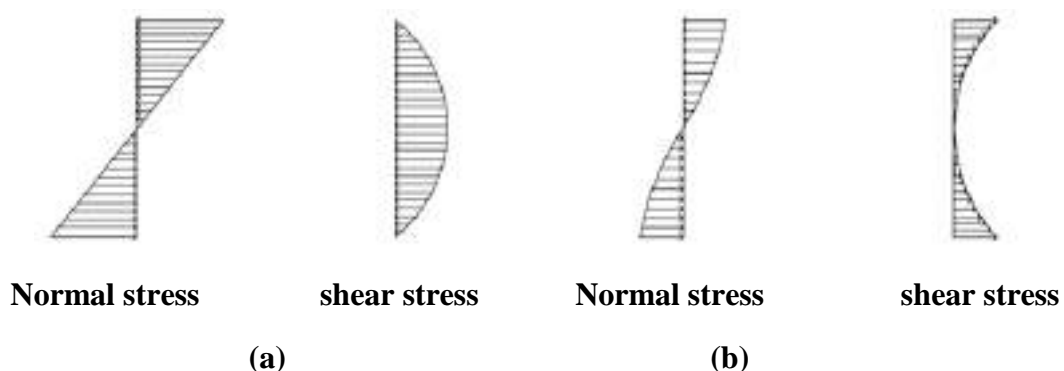


**Figure (1-5): Stress distribution: (a) prismatic beam; (b) haunched beam [3].**

The apportionment of stresses at different locations of stepped and haunched cantilevers with rectangular cross sections obtained from finite

element analysis (FEA) were presented in Fig. (1-6). In this Figure, normal stresses are due to pure bending, whereas shear stress is due to constant shear force. It can be seen that the apportionment of stresses differs in each structural member depending on the manner of changing of the cross section. Also, the neutral axis is above the centroidal axis in the haunch zone and near the step of the haunched and stepped members, respectively [3].

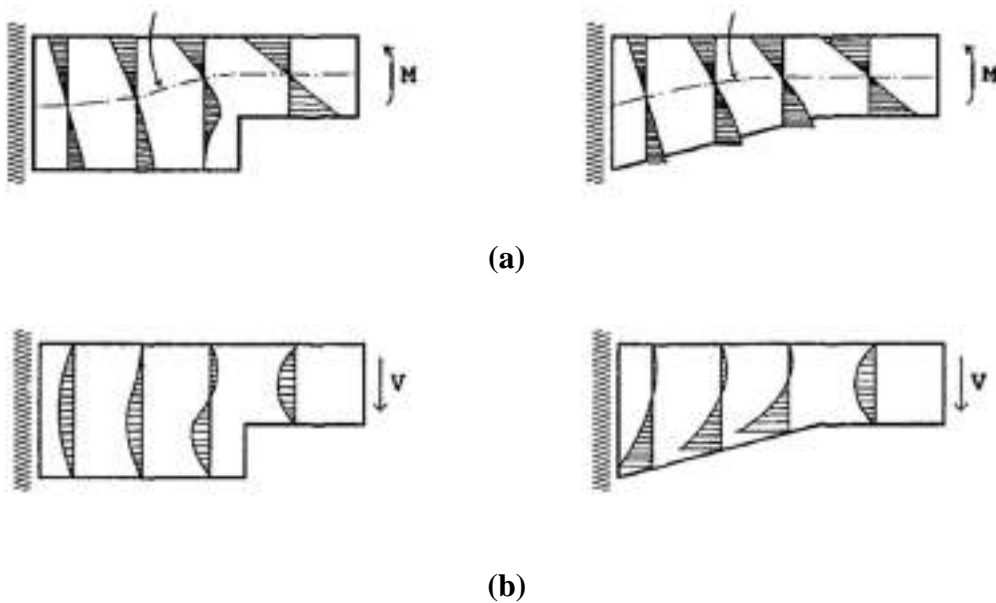


**Figure (1-6): Stress distribution in cantilever nonprismatic members: (a) normal stresses of pure moment; (b) shear stresses of constant shear force [3].**

### **1.7 Stress Flow in Non-Prismatic Members**

The points of discontinuities cause disturbances in the stress flow. In stepped members, due to the abrupt change of the cross section, parts of the member are subjected to significantly small stresses, denoted as "Null area" as demonstrated in Fig. (1-7 a). Due to their small contribution, the existence of the null areas results in a reduction of the member stiffness. In haunched members, there are "kinks area" on the centroidal axis that exhibit slope discontinuities as revealed in Fig. (1-7 b).



The overall behavior of haunched members is like to that of stepped members, except that the reduction in stiffness due to stress flow in end segments is less significant [3].

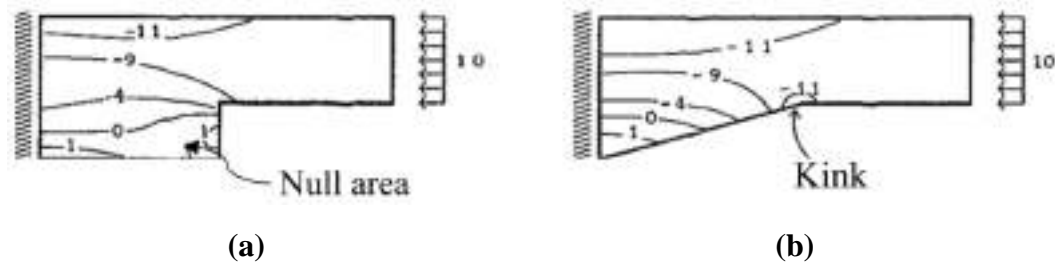


**Figure (1-7): Principal stress contour for cantilever: (a) stepped beam (b) haunched beam [3].**

## **1.8 Fiber Reinforced Polymers (FRP)**

Carbon fiber reinforced polymers (CFRP) is an abbreviation of carbon fiber polymers and is a composite of fiber and polymer material. CFRP sheets are widely accepted in the industry as the most externally enhanced materials used for retrofitting the structural members. In addition, FRP sheets consists of thin profiles which make them desirable when aesthetics is a concern or when the access is limited [16].

The material FRP produces many advantages in comparison with the another material in structural engineering. CFRP provide large stiffness-to-weight ratio, high strength ( $E > 165000$  MPa, tensile strength  $> 2400$  MPa), light weight, and reduced mechanical fixing. The main disadvantages are erratic plastic behavior, less ductility, high cost, and need for epoxy for the bonding with concrete (cohesion material) to work [16].

The most usually used CFRP retrofitting technique is the manual application of wet lay-up (hand lay-up) or prefabricated systems using cold cured adhesive bonding. The major and the most important trait of this method is that the fibers of externally bonded FRP composites are in parallel direction as



workable with the direction of principal tensile stresses [17]. Typical application methods are clarified in Fig. (1-8).



(a) Hand lay-up CFRP sheets.

(b) Application of prefabricated strips.

Figure (1-8): Application method of CFRP sheet [17].

## **1.9 Objectives of the Study**

The objective of the present work is to investigate numerically the shear and flexural behavior of simply supported RCHBs under static load. Compressive strength of concrete, presence of a transverse opening, existence of a longitudinal opening, and use of CFRP sheet to strengthening these beams are considered as parameters in this study.

The study consists of three series with different haunch types. The first and second series are to investigate the behavior of RCHBs resisting shear forces while the third series is to investigate the behavior of these beams resisting bending moment. The analysis of RCHBs were done by using nonlinear three-dimensional finite element method (FEM) using ANSYS; validity of the used procedure is examined by comparing their outputs with the literatures.

## **1.10 Thesis Layout**

The study is offered in five chapters, as follows:

- ✚ **Chapter One:** presented a general introduction for the non-prismatic beam, advantages and application of non-prismatic beams, and general definition of the FRP with its applications.
  
- ✚ **Chapter Two:** presented literature review concerning the experimental and theoretical studies of the RCHBs.
  
- ✚ **Chapter Three:** presented material modeling, and the basic finite element relationships with representation of concrete and reinforcing steel and the solution of nonlinear equations.
  
- ✚ **Chapter Four:** presented the analysis results acquired from FE computer program.
  
- ✚ **Chapter Five:** summarized the conclusions and recommendations.

# CHAPTER TWO

## LITERATURE REVIEW

---

---

### **2.1 Introduction**

This chapter aims to provide a brief review of previous experimental and analytical investigations of structural behavior of RCHBs. The first part presented previous investigators who suggested various design and analysis methods to obtain a proper behavior of RCHBs and to appraise the ultimate capacity of this type of members. While the second Part presented the studies of RC beams with and without opening strengthen by CFRP are presented.

### **2.2 Experimental and Theoretical Studies of RCHBs**

In 1983, Stefanou [18] explained the application of the codes of practice for British, American and Russian to calculate the maximum shear capacity of RCHBs. The process included testing of 24 non-prismatic beams. The major parameters were the main longitudinal reinforcement, existence of stirrups, beams depth at supports, and inclination of the haunch angle of beams. According to the outcomes of the study, the existence of inclination on the upper surface (positive inverted haunch) was less effective than that on the bottom (negative haunch). The influence of either slope was greater in beam with stirrups than without stirrups. The predicted strength of RCHBs were almost the same as in American and British codes. The estimated strength for members without stirrups was somewhat more safe than those for members with stirrups.

In 1988, El-Niema [15] described how to calculate the maximum capacity of shear strength for RCHBs. The experimental study involved testing ten beams with T- cross section. Ultimate shear force of RCHBs from these experiments was

estimated and that significantly influenced by changing the haunched angle. Specific expression was proposed for evaluating shear strength of RCHBs and verified using results of ten distinct experiments. The suggested formula was acceptable for predicting the shear capacity of these types of members with T-cross section. The results proved that the large haunch at supports over beam with haunch enhanced load capacity and reduced amount of the deflection for these beams. Also, larger haunch at the support was better than smaller haunch. An equation was suggested to estimate the ultimate shear strength for these types of beams, which is presents the ultimate shear force of RCHBs in terms of the concrete strength, the stirrups influence, and the dowel action. A suggested equation is modified from the ACI code terms for shear design. The modification in equation of design included the angle of haunch and the dowel contribution. The following terms (Eq. 2.1) was proposed for the nominal shear stress of RCHBs:

$$V_u/bd_s = v_u = v (1 + 1.7 \tan \alpha) + P_v f_{yv} + 0.25 P_w f_{yw} \sin \alpha \quad \dots(2.1)$$

When,

$V_c$  : Shear stress of the concrete section

$\nu$ : Poisson ratio,

$\alpha$ : Haunch angle,

$P_w$  and  $P_v$ : ratio of longitudinal and web reinforcement, respectively;

$f_{yw}$  and  $f_{yv}$ : yield stress in longitudinal and transverse reinforcement, respectively.

In 1991, El-Mezaini et al. [3] investigated the linear elastic behavior of frames with non-prismatic members by using iso-parametric plane stress finite elements. Four frame models with haunched beam analyzed with different shapes of haunch such as stepped members, members with straight haunches, and members with parabolic haunch. Stiffness, carryover factors, and fixed end

moments for such members were computed for full frames with non-prismatic members. The result revealed that there was a large dissimilarity between the behavior of prismatic and non-prismatic beams. In the case of stepped members, the existence of the null areas causes softening of the member stiffness, and if the member is axially restrained, arching action takes place, producing a significant axial thrust that affects the force distribution in the structure.

In 1994, Colunga [19] showed a checking study about the concerns with regard to the design of seismic for RCHBs. The study-included analysis of 12-story RC building to confirm that the existing design practices did not prefer enough capacity to the lateral loads for the building and that disadvantageous failure mechanism could occur. According to the finding of this investigation and results of other investigations, the existing design procedure for these members were untrusted in evolving their ductile behavior in both bending and shear. Also, the failure mechanisms related to the existing design practices were not only unwanted but also related to slighter base shear capacities.

In 2000, Ozay and Topcu [20], presented a more realistic and comprehensive static analysis technique for structures having non-prismatic members. A general stiffness matrix for non-prismatic members that is applicable to Timoshenko beam theory was derived in the proposed method. The stiffness coefficients were determined for constant, linear, and parabolic height variations of members, employing analytical and (or) numerical integration techniques. A computer program has been coded in Fortran which analyses two-dimensional frames using the proposed stiffness matrix and fixed-end forces for a wide range of external loads. Uniform, triangular, and trapezoidal distributed loads over the entire member or along any part of it, are taken into consideration to determine the fixed-end forces. The accuracy of the proposed analysis technique was verified by comparing the results of the numerical examples with those obtained from the general analysis program SAP90 using a large number of sub elements.

In 2004, Tan [2] devoted a wide experimental with numerical study to evaluate the capability of application of Strut-and-Tie method in the design and analysis of non-prismatic concrete beams. Seven simply supported beams were designed and tested with considering many parameters such as the recess width, location of recess, and usage of FRP plates. Test results revealed that the crucial loads exceeded loads of the design for all studied models. Strut-and-Tie method was appropriate for design non- prismatic beams. Also, the Strut-and-Tie method provides lower bound for the failure load, and this method suggested a simple and straightforward solution that was based on established principles to an otherwise complicated problem. Non-prismatic beams with a transverse recess exhibited different performance to the beams with a transverse opening with respect to displacement, cracking characteristics, and failure load behavior. For non-prismatic beams with a recess in the tension region, any increasing in the size of the recess results reduction in the load failure, higher cracking propagation and smaller service load deflection. Beams with recess introduced and subsequently retrofitted by FRP plates showed satisfactory performance with respect to strength, deflection at the mid-span and crack width. However, the failure tends to be non-ductile and sudden.

Colunga et al. [4] in 2008, carried out two groups of tests to provide a wide result on the behavior of RCHBs for shear under static loading. Ten prototype RCHBs with and without shear reinforcement designed to develop a shear failure divided into two series as revealed in Fig. (2-1). The first series was consisting of five beams without stirrups (four of them were haunched beams and one was prismatic). The second group of tests consisted of five beams with stirrups (four of them were haunched beams and one prismatic). The studied parameters were haunch angle (varied from  $3^\circ$  to  $12^\circ$ ), compressive strength, and amount of shear reinforcement. It was observed from experimental results that RCHBs develop an arch mechanism which allows the damage to be distributed along the haunched

length before the main diagonal crack develops. RCHBs have different shear behavior than existed in prismatic beams. RCHBs had higher deformation and energy dissipation capacities in comparison with prismatic members. Crack propagation in RCHBs was higher than found in prismatic beams. Also, the angle of inclination of the principal shear crack decreases as the haunch angle increases. The suggested equation to calculate the ultimate shear strength of RCHBs was a function of the haunch angle and influenced particularly by three parameters: (a) the contribution of the concrete, (b) the contribution of the vertical force introduced by the inclined longitudinal steel reinforcement and, (c) the contribution of the transverse shear reinforcement.

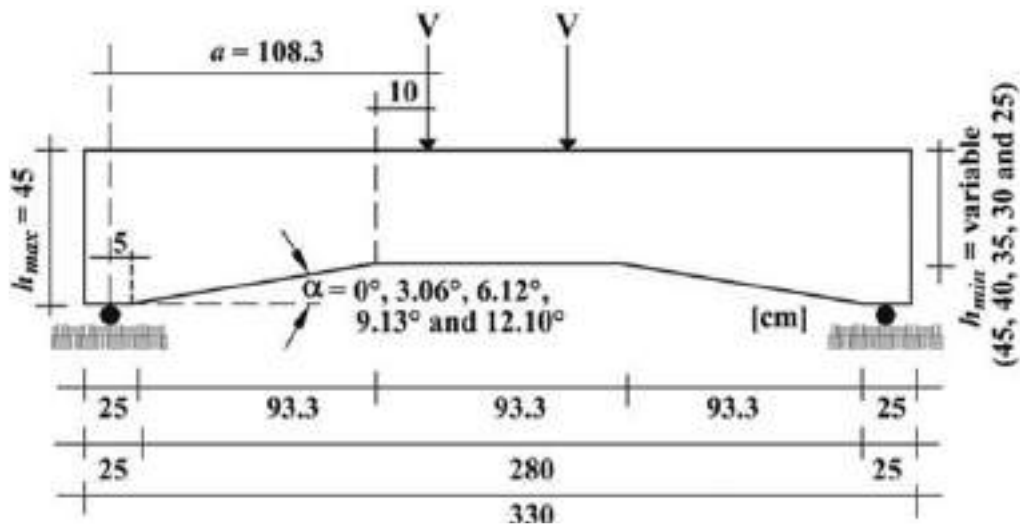
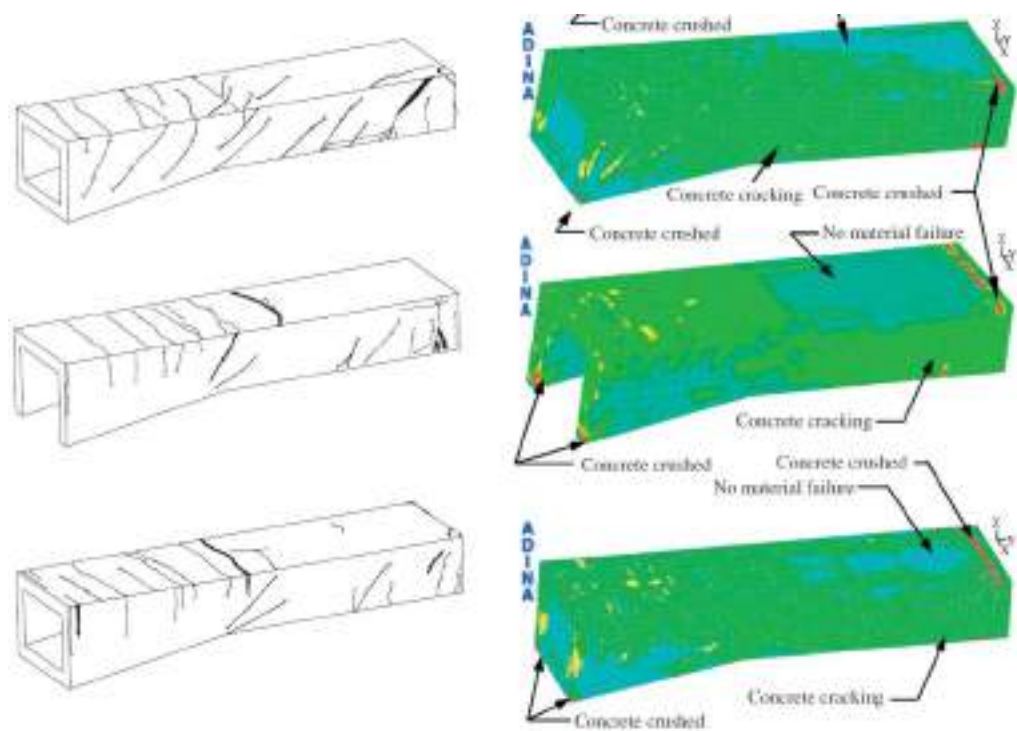


Figure (2-1): Geometry and loading condition for the test specimens [4].

In 2009, Galal et al. [21] performed an analytical and experimental approach to inspect the behavior of RC haunched girder with thin-walled shape and hollow girders when it was exposed to centric and eccentric loads. Five examinations were performed on intermediate-scale sand-box girders to examine the action of load eccentricity and the influence of bottom slabs on their maximum load capacities, failure mode, and load–displacement relationship. Also, the test specimens was analyzed by using ADINA software, and the nonlinear FEA had been conducted. The investigation outcomes exhibited that a significant reduction in ultimate load and the ductility of girders with open sections when tested under



eccentric loading. The girder behavior improved significantly when this open section turned into full span section. Different failure mechanisms were obtained for girders exposed to centric versus eccentric loads. Centric loads resulted in flexure-dominated plastic failure, whilst eccentric loads resulted in additional contributions from the brittle torsion and shear mechanisms as revealed in Fig. (2-2). The use of bottom RC slabs in a haunched section or along the full girder length had a comparatively small influence on the girder behavior exposed to central loads.



**Figure (2-2): Specimen testing layout [21].**

In 2010, Megahid et al. [22] investigated the RCHBs reinforced by outer steel plates with epoxy under static load. Eighteen RCHBs (fourteen of them were concrete beams with high strength property and four remaining were normal strength RC beams). These beams having 1500 mm total length with rectangular cross-section 120×280 mm for width and depth respectively. The influence of the geometric dimension of plates, position, width and arrangements of plate, plate thickness, the haunch effect, and the concrete grade were examined. Experimental



results exhibited that the position, width, arrangements, and thickness of plate heavily affects the strength, deformation capability and failure mode of analyzed specimens. Increasing the width value and thickness of bonded plate to both sides of shear zone of beams increases cracking number and load capacity for retrofitted beam. Rising the value of the concrete grade reduces the crack spread and maximum failure load of a retrofitted beams in comparison with unstrengthen beams. The change from positive to negative haunch enhances the max. failure load and cracking propagation of the retrofitted beams.

In 2011, Rombach et al. [23] presented an experimental and numerical investigation about shear design of concrete haunched members without stirrups subjected to concentrated load at the mid-span of the beam. All the models were designed using three design ways based on statistical approaches according to the Euro code 2. Tested specimens were totally eighteen with various parameters like ratio and location of stirrups, varied inclination angle for haunch, and length of the haunch. Also, FEA by modeling these beams in ABAQUS program was utilized to understand the crack spread and the failure mechanism. Results of experimental and theoretical tests revealed that the shear strength and the crack modality of RCHBs was different from members with constant height. Also, FEM confirm the results which showed a good agreement with the experimental results as revealed in Fig. (2-3).

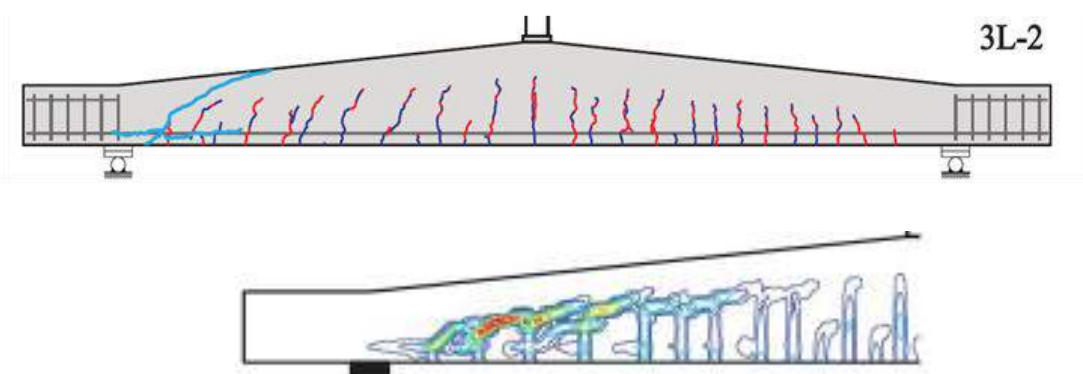


**Figure (2-3): Testing of experimental and theoretical specimen [23].**

In 2011, Qi et al. [24] devoted an inclusive experimental study to investigate the effect of the seismic loads on the performance of RCHBs transmit structures of frames-supported. The experiential proceedings included carrying out three specimens 1:3 scaled with different ratio of section height to thickness of short-leg shear-wall (RHT). Tests of frames exposed to cyclic lateral load by low-frequency with constant vertical actions, failure pattern, skeleton curves hysteresis curves, capacity of energy dispersion, and stiffness degradation laws of haunched transfer beam structures were investigated. The result exhibited that the structural rigidity and the energy dispersion has been enhanced by the RCHBs presence, the endogen force became more equally doled out and the bearing is more rationalistic with a boosting in RHT. Conclusion of this investigation was that the frame-supported short-leg shear wall structure with properly designed was good enough to resist an earthquake according to Chinese standard GB 50011-2001.

In 2012, Caldentey et al. [25] performed a numerical approach to explore the load distribution effect and changing depth on the shear strength of slender RCHBs without stirrups. Eight RC specimens (four of them were haunched beams) were exposed to different load types (point loading, uniform loading, and triangular loading). The result exhibited that the constant-depth cantilevers carried 63% more load for uniformly distributed loading than for point loading, and more than 100% for triangular loading than for point loading. Also, they concluded that the inclination of compression chord carrying shear plays a significant role in resisting shear stresses for members without stirrups and only for applied loads at a certain distance to the support. These distances are estimated by 2.5 to 3 times the effective depth of the member. For tapered beams under point load, the ACI 318-08 and EC2 codes overestimated the shear strength.

In 2013, Al-Maliki [26] performed an experimental research to investigate the behavior of hollow non-prismatic RC beams retrofit with CFRP sheets. Five

specimens of dimension (1170 length  $\times$  260 height  $\times$  150 width mm) were tested under two-point load. The parameters included the effect of section (solid or hollow), hollow opening filling (shapes and materials), and effect of retrofitting with CFRP. Four of the models were retrofitted with CFRP strip. The results illustrated that the existence of irregularity in beam depth caused a reduction in stiffness and increasing in the beam deflection when compared with solid one. Using (circle PVC pipe) was made a hollow recess in non-prismatic beams that contributed to decreasing in the load capacity and increasing in the deflections and strain compared with solid non-prismatic beams. The square longitudinal opening was filled with steel hollow pipe increased the maximum load capacity and decreased the deflection when compared with PVC pipe by about 56% and 33%. Also, the retrofit of beams by CFRP contributed to enhancing in the load capacity and ductility specially when the bonding CFRP sheet to the bottom surface of non-prismatic beams. Cracks were concentrated near support of non-prismatic beams retrofit with CFRP to formulated shear failure due to CFRP confined concrete at flexural zone and give more strength at that location.

Experimental study for RCHBs exposed to cyclic shear loads was presented by Aranda et al. [27] in 2013. Ten prototype beams with simply-support condition were tested into two groups, the first series was consisting of four haunched beams without stirrups and one prismatic. The second group of study investigated the influence of stirrups existence. Various parameters such as haunch angle, compression strength, and the presence of stirrups were included in the experimental work. Based on the results of this study, they proved that the shear behavior for cyclic loading of RCHBs is different to than existed in prismatic beams. Also, RCHB provide higher capability for the deformation and more dissipation in the energy or at least energy dissipation equal to those dissipated by prismatic ones. and finer cracks than prismatic beam as revealed in Fig. (2-4) for cyclic load test for prismatic and haunched beams.



(a) Prismatic beam without stirrups.

(b) Haunched beam with stirrups.

Figure (2-4): Geometry and loading condition for the test specimens [28].

In 2014, Orr et al. [28] presented an experimental investigation on the shear behavior of non-prismatic RCHBs through experimental tests. The study conducted on testing of nineteen RCHBs designed using three variable approaches. The first design method was used the variable angle truss model (EC2), the second design method was performed by using the compressive force path method (CFP). Finally, the third approach was designed with reference to Strut and Tie model (STM). The consequence revealed that any assumptions of some available design codes led to unconservative design for beams with non-prismatic sections under effect of shear. The EC2 beams cracked initially at the end region before limited crack progression towards the point of load application. In the STM models, cracking began in the center of the tapered zone before pervasion towards the support and the point of load application. In the CFP model, cracking began beneath the load point and raised towards the support before failure as shown in Fig. (2-5).

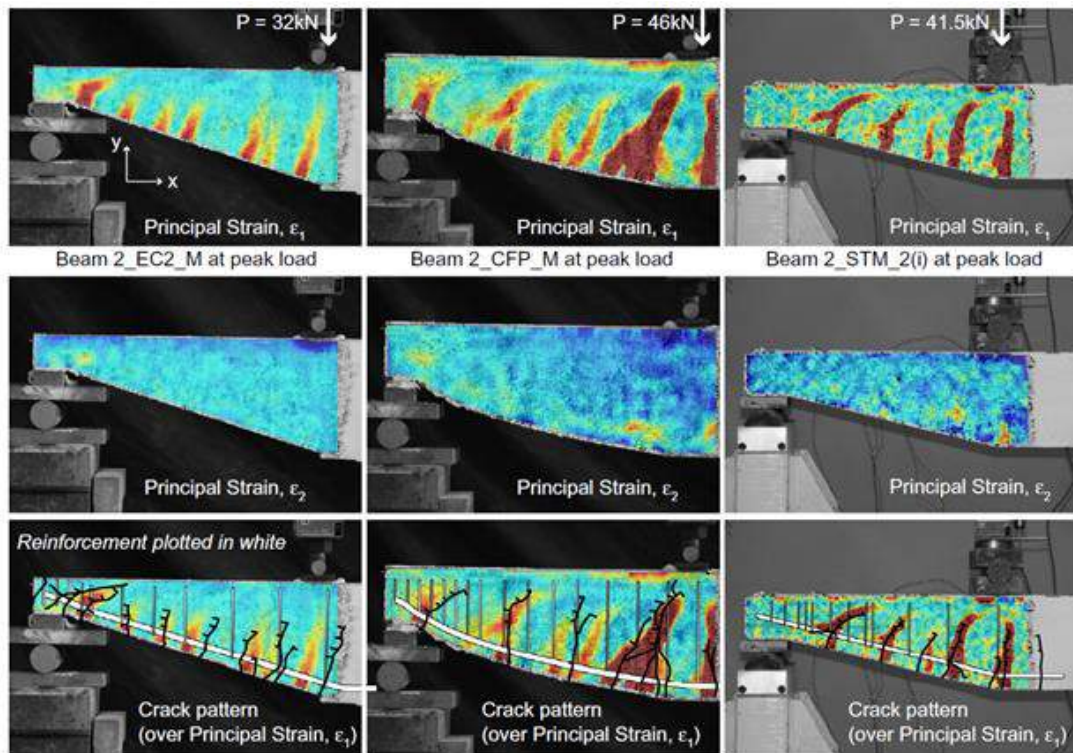


**Figure (2-5): Testing condition for the Orr et al. specimens [29].**

In 2015, Hou et al. [29] devoted an experimental and theoretical study to predict the shear failure mechanism of RCHBs. The process included testing four series of ten specimens with varied parameters such as concrete cover thickness, existence of haunched portion, organization of tensile bar, and the position of haunched portions. Non-linear FEA was utilized to assess the compression region and to confirm the results. The outcome showed that the bending position of the longitudinal bar for tension greatly affected the spreading of cracks which caused the difference in the shear capacities. More shear cracks and flexural cracks happened when stirrups were provided in RCHBs. The bigger concrete cover at the mid-span affected the crack spread but had no influence on shear capacity of these types of beams. The bent tensile rebar had a negative contribution to the shear capacity due to stress concentration, while the debonding cracks resulted in the arch action even in slender beams. The result of FEM exhibited a good matching with the experimental results as revealed in Fig. (2-6).



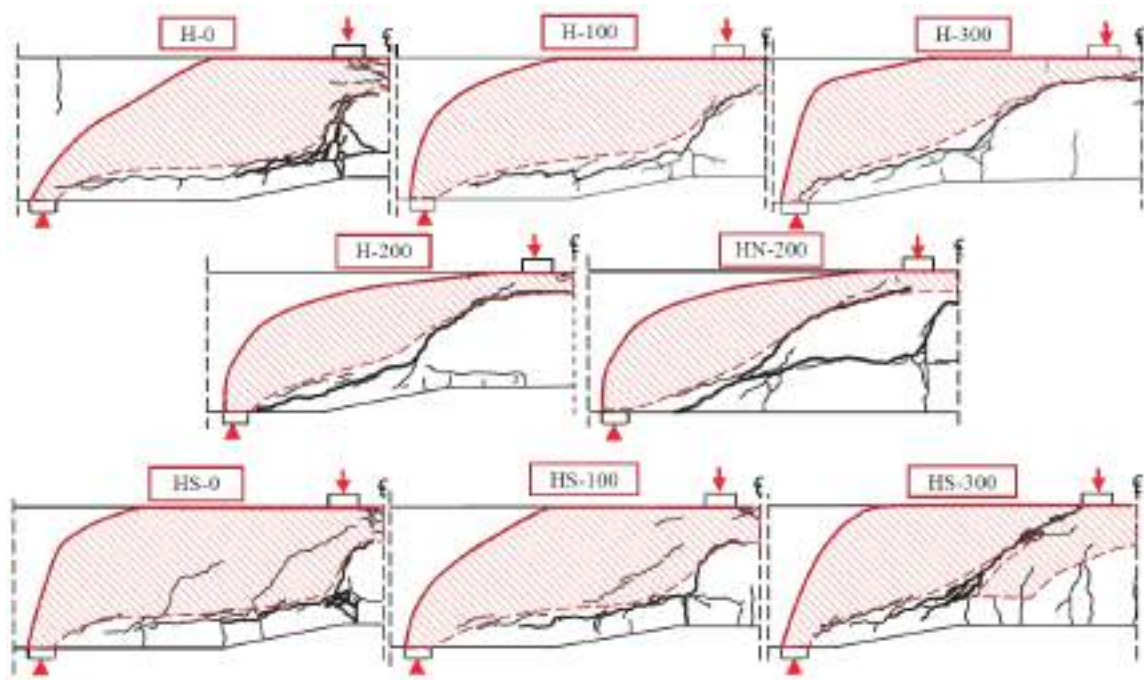


**Figure (2-6): Specimen testing of Hou et al. [30].**

Finite element method utilized to analyze RCHBs failing in shear was conducted by Dominguez et al. [30] in 2015. The research purpose was to appraise the capability and limitations of simple and complex analytical models to anticipate the structural behavior of RCHBs failing in shear. Analysis performed on eight simply supported specimens in the shape of haunched member when it exposed to static loading. The main parameters were haunch angle, ratio of stirrups, and variable compressive strength for eight specimens into two groups (the first group had four beams without any shear reinforcement while the second had four beams with shear reinforcement). Simplified nonlinear specimens in which the involvement of the main steel reinforcement and stirrups was indirectly involved were assessed using SAP2000. More complex nonlinear finite element models were assessed with ANSYS. The results observed that haunched beams have shear behavior is different to that in prismatic beams. Also, having higher capacity for deformation, more shear cracks, and more energy dissipation capacities.

In 2015, Albegmprli et al. [31] presented study about reliability analysis of shear capacity for RCHBs. This study performs stochastic and reliability analyses of the ultimate capacity of shear for RCHBs based on nonlinear FEA. The main target of this research was to inspect the influence of these parameters (such as shape of the haunch, haunch length, haunch angle, and ratio of stirrups) on the mechanistic performance and ultimate shear capacity of RCHBs. Sixty-five experimental test of RCHBs and prismatic beams were performed by means of nonlinear FEM by analysis program ATENA to confirm the qualifications of the used numerical models, the maximum shear capacity and the crack modality. The deterministic analysis results also showed excellent matching with the crucial load capacity of experimental tested specimens. RC haunched beams had greater sensitivity and severity than the RC prismatic beams. The uncertainty of geometry parameters and material properties substantially influenced the ultimate capacity of load for RCHBs.

In 2015, Dawood and Nabbat [32] studied the behavior of high strength RCHBs for shear and flexure. Twelve simply supported non-prismatic beams divided equally into two series; the first series fails in shear while the second group fails in flexure. The specimens were with or without opening, retrofitted by CFRP sheet and near surface mounted (NSM) bars for the shear and flexural beams as shown in Fig. (2-7). The experimental results revealed that retrofitting by carbon fiber bar enhanced the load failure for flexural and shear beams by 16% and 15% respectively. Existence of an openings in the RCHBs near support zone and at the mid-span reduced the ultimate load for shear and flexure respectively. When beams with openings were strengthened by CFRP sheets and bars, the ultimate load for flexural behavior beams was increased 23% to 35% respectively. While for shear behavior beam was increased by 16% to 25% respectively, in comparison with beams have an opening. CFRP sheet technique gave a better performance compared with NSM in flexure beams. Also, FEA was performed to

prove the soundness of the results which exhibited a good matching in load-displacement curve and crack patterns.



**Figure (2-7): Crack Pattern of Shear Beams [33].**

In 2016, Aziz et al. [6] performed an experimental research to investigate the shear behavior of tapered beam with self-compacted concrete. They tested six simply supported beams under two point loads. Five of them were tapered and one was prismatic rectangular beam. The dimensions of these beams were remained constant for all specimens. The adopted variables were amount of shear reinforcement, shape of the analyzed models, and retrofitting by strips of carbon fiber. The results exhibited that the tapered beams without web reinforcement have greater shear capacity and more deformation response in comparison with the prismatic beam. The CFRP strips improved the failure load of the tapered beam by 30% of prismatic beam.

In 2016, Jolly and Vijayan [33] presented a theoretical study on behavior of RCHBs under static and seismic loads. Finite element analysis by using ANSYS and ETABS programs were utilized to conduct a parametric analysis. A



comparison between experimental and numerical tests for the validation purpose which showed a good matching in load failure and crack pattern. Seismic analysis of RC framed with linear and haunched beams were carried out on eight specimens with different haunch angle. The results appeared that the haunched beam deflection was larger than of prismatic beam. The lateral stiffness of framed structures was increased with presence of non-prismatic members. Crack pattern distribution of this type of beams was dissimilar that of prismatic beam. Cracks started at the vertex because of the stress focus at this position because the sudden change in direction of longitudinal bars. Also, the outcomes appeared that the occurred deflection and tensile stress increased as haunch angle increased, while storey drift was decreased with increase in the inclination angle of haunch.

To explain the shear resistance mechanism of reinforced concrete and prestress concrete tapered beam without stirrups, a research was conducted by Hou et al. [34] in 2017. Three series of seven beams with different parameters were selected. These parameters were  $a/d$  ratio, prestress level, and variable compressive strength of concrete. The result revealed that there was no influence of the taper shape on the behavior of short beam without stirrups because of shorten of the arch action. The shear capacity of PSC tapered beam became higher than that of PSC constant depth beam because of the larger critical section. The existence of prestressing force enhanced the shear capacity of these beams. Finite element analysis was used to complement the experimental tests and to confirm the results, which revealed a good matching in load-deflection curves, crack patterns, and load capacities as appeared in Fig. (2-8).

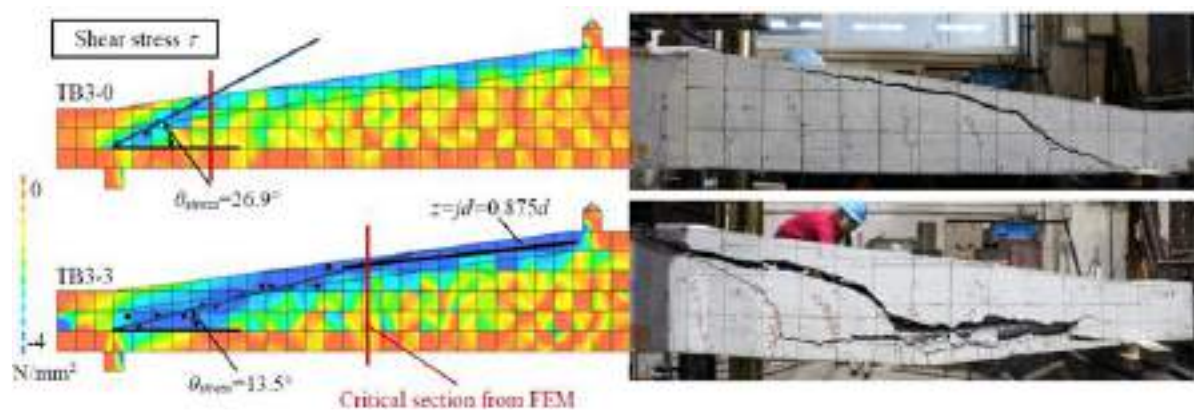


**Figure (2-8): Tested models of Hou et al. study [35].**

In 2017, a research was published about estimation of the maximum strength of continuous RCHBs for shear when exposed to cyclic load by Colunga et al. [35]. Five prototype continuous RC beams (four of them were haunched and the retained one was prismatic) designed to develop to fail in shear. Different parameters were considered in this research such as (a) haunch angle with horizontal line, (b) the effect of the bent reinforcement on the behavior for shear, (c) existence of strips effect, and (d) the inclination angle of the shear crack. The results appeared that RCHBs endure shear force similar or higher than that presented by prismatic beams, especially for increasing in the inclination haunch angle and negative bending. The extra shear strength in haunched beams at a lesser volume was because of inclined longitudinal rebar contributions and the stirrups. The inclination angle of shear cracks decreased by increasing in the inclination angle.

### **2.3 Experimental and Theoretical Studies on Reinforced Concrete Members with and without Opening Strengthened by FRP**

In 1984, Mansur and Alwist [36] tested twelve reinforced fiber RC deep beams with rectangular opening in the web. The major parameters of the study were the fiber concrete, opening location, shear span to effective depth ratio and

amount of web reinforcement. The results indicated that the locations of openings are the principal parameters that affect the behavior and strength of deep beams.

In 1996, Tan et al. [37] studied the flexural behavior of RC T-continuous beams with and without large web opening in positive and negative moment regions. Fifteen beams were tested under one-point load. The tests had indicated that the presence of web openings leads to a decrease in the cracking and ultimate strength as well as the post-cracking stiffness of continuous beams.

Abdulla et al. [38] in 2003, tested ten RC beams with openings. CFRP was used for strengthening region of the opening. The experimental program included strengthening five beams with openings, while four beams kept without strengthening. The last one was solid beam used as control beam. It was found that the opening with height of 0.6 from the beam depth reduces the capacity by 75%. The application of the CFRP sheet around the opening greatly decreased the beam deflection, controlled the cracks around the openings and increased the ultimate load capacity of the beam. The failure occurred due to a combination of shear cracking of concrete and bond failure of CFRP sheets glued to concrete surface.

In 2007, Mosallam and Banerjee [39] performed an experimental study on enhancement of the shear strength for RC beams externally strengthened by FRP composites. Nine full-scale beam specimens of three different classes, as-built (unstrengthened) were tested. The first class involved strengthening with E-glass /epoxy wet lay-up, the second class strengthened with Carbon/epoxy wet layup. The third retrofitted with procured carbon strips. Experimental results indicated that the composite systems provided substantial increase in ultimate strength of repaired and strengthened beams as compared to the pre-cracked and as-built beam specimens.

In 2007, Dawlat [40] studied experimental and theoretical behavior of RC beams, strengthened or repaired by CFRP for both flexural and shear cases of beams have been presented. The experimental program consisted of 28 beams divided into two groups (flexural and shear groups), each group has 14 beams. The study took into account the strengthened and repaired cases in using CFRP; therefore, similar beams were used once for strengthening and other for repairing to make comparison between them. The results showed that the use of CFRP as external strengthening has a significant effect on ultimate load, crack pattern and deflection. It is observed that the use of external CFRP sheet connected to the tension sides of beams could enhance the ultimate load capacity up to 160% in flexure over the capacity of the identical reference beam. The repaired beams reached 95% to 97% of ultimate load in comparison with those strengthened in the same way by CFRP; this proved the efficiency of the use of CFRP in repairing beams. The shear group of beams included beams with attached CFRP sheets on their sides at shear zones. It is observed that the use of CFRP to strengthen or repair the beams at the sides of shear zones could enhance the ultimate load capacity up to 20% in shear over the capacity of the identical reference beams. ANSYS was used. With the smeared cracking model, good prediction for post-cracking behavior was obtained. The comparison between the numerical and the experimental results asserted the validity of the numerical analysis and the methodology developed here where the maximum difference ratio in ultimate load was less than 10% for all the tested and analyzed beams.

In 2009, Najim [41] tested eight RC deep beams with cross-section of 100×750 mm and total length 1150 mm under four-point loads. Seven specimens had two rectangular openings with cross-section (100×200) mm, one in each center of the shear span, placed symmetrically about the centerline of the beam. The first specimen was solid deep beam (without openings) and the second specimen was deep beam with web openings, these beams were used as references

beams. The other beams were strengthened with CFRP laminate. The variables included the orientation, shape, and vertical anchorage of CFRP laminate. The experimental results indicated that the use of CFRP sheet to upgrade the RC deep beams with web openings had a significant effect on overall behavior such as the ultimate load, crack width and deflection. The percent of increase in the ultimate load capacity was about 100-190 %. The use of CFRP as externally strengthening system also decreased the crack width, but, it cannot change the formation of inclined crack. All the tested beams failed due to splitting the beam into two pieces through the inclined crack. In the other side, three dimensional finite element analysis was used to investigate the performance of the RC member strengthened by CFRP laminate. FE software ANSYS was utilized through this study. The comparison between the experimental and theoretical results showed reasonable agreement and asserted the validity of the numerical analysis and methodology developed in this study.

In 2011, Chin et al. [42] studied the behavior of externally strengthened RC beams with large opening at section with critical flexure and shear using CFRP laminates. All the beam specimens had a cross section of 120×300 mm with an effective span of 1800 mm. Variable parameters in this study were: the size, location, and shape of the opening. Nine beams which included a control beam, four un-strengthened and four strengthened beams were tested as shown in Fig. (2-9). The numerical modeling was conducted using a nonlinear FE program, which appeared good agreement had been obtained between the numerical analysis and experimental results. Strengthening of large circular and square openings in flexure zone could significantly restore 74-100 % of the beam original capacity, while strengthening of large circular and square openings in shear zone could only re-gain the beam capacity to about 33-35% of the original beam strength.

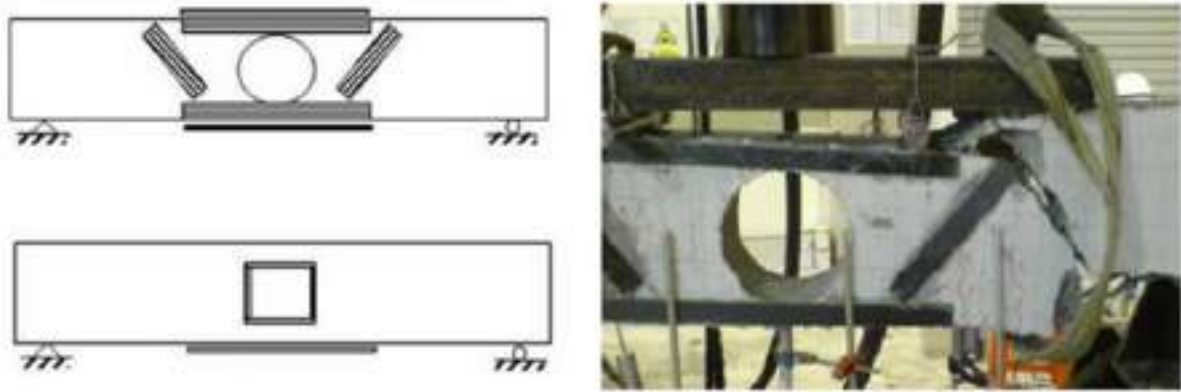


**Figure (2-9): Strengthening for beams with large openings [43].**

In 2011, Al-Dolaimy [43] tested eight continuous RC beams with cross-section of  $150 \times 250$  mm and total length 3300 mm with two spans (clear span is 1500 mm) were tested under two-point loads. Six beams, each beam contains one opening, three of which have dimensions  $200 \times 100$  mm and the three other have dimensions  $140 \times 140$  mm. The location of the openings was in the zone of max. moment and max. shear. The first beam solid continuous beam (without openings) and the second and third continuous beam with web openings were used as references beams. The other beams were strengthened with CFRP laminate. The variables included the orientation, shape, and vertical anchorage of CFRP laminate. The experimental results indicated that the use of CFRP sheet to upgrade the RC continuous beams with web openings has a significant effect on overall behavior such as the ultimate load, crack width and deflection. The percent of increase in the ultimate load capacity was about 60-106 %. On the other hand, three dimensional finite element analyses were used to investigate the performance of the R.C. member strengthened by CFRP laminate. ANSYS program was utilized through this study. Theoretical results showed reasonable agreement and asserted the validity of the numerical analysis and methodology developed in this study.

Redha [44] in 2012, investigated the flexural behavior of self-compacting concrete beams by experimentally and theoretically study. Sixteen RC beams with

or without web opening were carried out. These beams strengthened by steel fibers (with percentages 0, 0.5%, and 1%) and CFRP sheet, tested as simply supported span subjected to two-point loading. The use of CFRP sheets as external strengthening techniques for openings restored all the lost strength due to the presence of opening. Also, CFRP upgraded beam with web opening, and approximately erased the effect of opening presence.

### **2.3 Summary**

From the previous literature review, the following points may be noted:

- 1) Carbon fibers materials are one of the performances improving technique that increases the ultimate capacity and improved other characteristics of reinforced concrete beams.
- 2) This thesis will investigate the flexural and shear behavior of normal and high strength RCHBs with and without opening and strengthened with CFRP sheet.



# **CHAPTER THREE**

## **FINITE ELEMENT FORMULATION AND MATHEMATICAL MODELLING**

---

---

### **3.1 Introduction**

In structural analysis, most problems are complex and accurate solutions are obtained for their governing equations only and for limited types of structures of load characteristics and simple engineering. Thus, numerical procedures such as FEM are used to obtain approximate solutions for realistic types of problems.

FEM is an important technique provided solutions to a various problem in all engineering fields. This work applies a nonlinear FEA for RCHBs exposed to static load to study the behavior of these beams.

### **3.2 Nonlinear Finite Element Analysis of Structures**

A lot of phenomena in solid mechanics are nonlinear. However, in several applications, using linear formulation will be proper and practical solution to obtain an engineering solution. Otherwise, other problems may require analysis with nonlinear property if obtained realistic results such as high deflection and post-yielding. Depending on nonlinear sources, the nonlinear problems involve three types [45], these types are:

- a- Problems including material nonlinearity.
- b- Problems including geometric nonlinearity.
- c- Problems including both materials and geometric nonlinearity.

In finite element method, the complex structure is first divided (discretized) into a limited number of individual non-overlapping components known as 'elements' over which the variables are interpolated. These elements are



connected together in number of discrete points along their periphery known as ‘nodal points’ or ‘nodes’ as revealed in Fig. (3-1) [46].

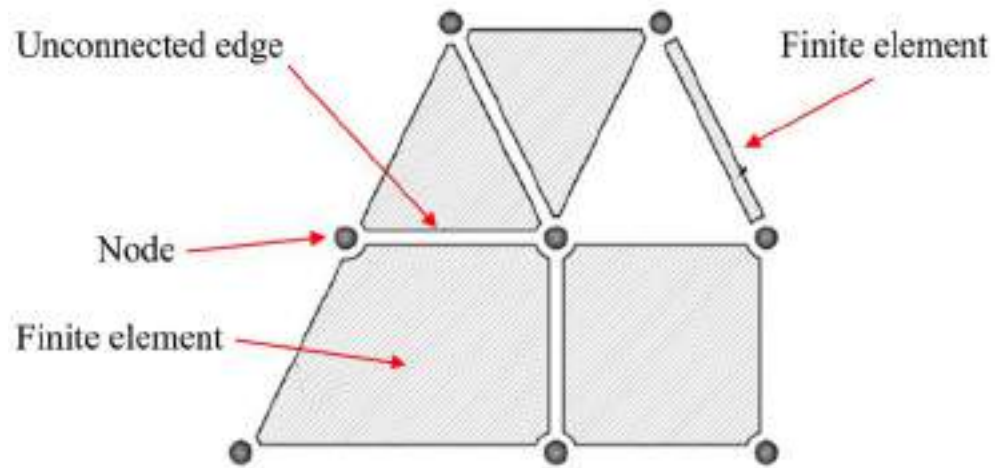


**Figure (3-1): Finite element discretization [46].**

For all elements, stiffness matrix and applied load vector are calculated and then assembled to give respectively, a global stiffness matrix with global load vector for the complete structure. The resulting rhymester of simultaneous equations is solved for unknown nodal variables which for structural problems are the displacement components [47].

### **3.3 Basic Steps in Finite Element Method**

Saeed Moaveni in 1999 [48], introduced basic steps for any problem used finite element analysis to provide a solution as shown below:

- a) Pre-processing Phase:
  - 1) Create and discretize the solution domain into finite elements; making the problem division into elements and node.
  - 2) Assuming shape function to define the physical behavior of an element; that is, to provide the element solution, the approximate continuous function is supposed.
  - 3) Develop matrices for each different element.

- 4) Assemble stiffness matrices of the current elements to present the whole problem and build a general stiffness matrix.
- 5) implement boundary conditions, initial conditions, and loading.
- 6) A group of linear or nonlinear algebraic equations are solved at the same time to get nodal outcomes, like displacement values or shear force, moments, or other significant outcome such as stresses and strains that can be evaluated for the nodes or the elements.

b) Solution Phase:

The resulting series algebraic equations is solved to obtain nodal results, such as displacement at different nodes.

c) Post Processing Phase:

Obtain additional important information, like the values of principal stresses, moment, shear force, etc.

## **3.4 Finite Element Formulation**

### **3.4.1 Basic Finite Element Relationships**

The derivation of stiffness matrix for selected element is the basic stage in any FEA, which relates  $\{a\}$  the nodal displacement vector to  $\{f\}$  the nodal force vector. Three conditions should be satisfied to derive this relation:

- 1) Compatibility of strains and displacements (kinematic condition).
- 2) Equations of equilibrium (equilibrium condition).
- 3) Stress-strain relations (constitutive relations).

By using the principle of virtual displacement, stiffness matrix of element can be determined, which states that, if the work done by the external forces on a structural system is equal to the increase in strain energy of the system for any set of tolerable virtual displacements, then the system is in equilibrium [49].

When a body is exposed to a series of exterior forces, the displacement vector at any point within the element,  $\{U\}_e$ , is given by,

$$\{U\}_e = [N]. \{a\}_e \quad \dots\dots (3.1)$$

Where,  $[N]$  is a matrix for shape functions, and  $\{a\}_e$  is the nodal displacements column vector. At any point the strain calculated by differentiating Eq. (3.1),

$$\{\varepsilon\}_e = [L]. \{U\}_e \quad \dots\dots (3.2)$$

Where,  $[L]$  is the differential operator matrix. In extended form, the strain vector can be termed as,

$$\{\varepsilon\}_e = \begin{Bmatrix} \varepsilon_x \\ \varepsilon_y \\ \varepsilon_z \\ \gamma_{xy} \\ \gamma_{yz} \\ \gamma_{xz} \end{Bmatrix} = \begin{Bmatrix} \frac{\partial u}{\partial x} \\ \frac{\partial v}{\partial y} \\ \frac{\partial w}{\partial z} \\ \frac{\partial u}{\partial y} + \frac{\partial v}{\partial x} \\ \frac{\partial v}{\partial z} + \frac{\partial w}{\partial y} \\ \frac{\partial w}{\partial x} + \frac{\partial u}{\partial z} \end{Bmatrix} \quad \dots\dots (3.3)$$

Substitution of Eq. (3.1) into Eq. (3.2) gives,

$$\{\varepsilon\}_e = [B]. \{a\}_e \quad \dots\dots (3.4)$$

where  $[B]$  is matrix of strain-nodal displacement, which is given by,

$$[B] = [L]. [N] \quad \dots\dots (3.5)$$

With the strains within the element are known, the stress vector can be illustrated by using the stress-strain relationship as:

$$\{\sigma\}_e = [D]. \{\varepsilon\}_e \quad \dots\dots (3.6)$$

where  $[D]$  is the constitutive matrix and  $\{\sigma\}_e$  is:

$$\{\sigma\}_e = [\sigma_x \sigma_y \sigma_z \tau_{xy} \tau_{yz} \tau_{xz}]^T \quad \dots\dots (3.7)$$

From Eq. (3.4) and (3.6), the stress-nodal displacement relationship can be displayed as,

$$\{\sigma\}_e = [D].[B].\{a\}_e \quad \dots\dots (3.8)$$

To depict the force-displacement relationship, a principle of virtual displacement is utilized. If a random virtual nodal displacement,  $\{a^*\}_e$ , is executed, the external work,  $W_{ext}$ , will be the same to the internal work,  $W_{int}$ ,

$$W_{ext} = W_{int} \quad \dots\dots (3.9)$$

in which

$$W_{ext} = \{a^*\}_e^T \cdot \{f\}_e \quad \dots\dots (3.10)$$

and

$$W_{int} = \int_e \{\varepsilon^*\}_e^T \cdot \{\sigma\}_e \cdot dv \quad \dots\dots (3.11)$$

where  $\{f\}_e$  is the vector of nodal force. Substitution of Eq. (3.4) into Eq. (3.11), yields,

$$W_{int} = \{a^*\}_e^T \cdot \int_v [B]^T \cdot \{\sigma\}_e \cdot dv \quad \dots\dots (3-12)$$

From Eq. (3.8) and (3.12),

$$W_{int} = \{a^*\}_e^T \cdot \int_v [B]^T \cdot [D].[B].dv \cdot \{a\}_e \quad \dots\dots (3.13)$$

Then Eq. (3.9) can be written as,

$$\{a^*\}_e^T \cdot \{f\}_e = \{a^*\}_e^T \cdot \int_v [B]^T \cdot [D].[B].dv \cdot \{a\}_e \quad \dots\dots (3.14)$$

or,

$$\{f\}_e = \int_v [B]^T \cdot [D].[B].dv \cdot \{a\}_e \quad \dots\dots (3.15)$$

letting:

$$[K]_e = \int_v [B]^T \cdot [D] \cdot [B] \cdot dv \quad \dots\dots (3.16)$$

then

$$\{f\}_e = [K]_e \cdot \{a\}_e \quad \dots\dots (3.17)$$

where,  $[K]_e$  is stiffness matrix for an element.

The comprehensive stiffness matrix,  $[K]$ , can be achieved by direct addition of the elements stiffness matrices after transforming from the local to the global coordinates, therefore,

$$[K] = \sum_n \int_v [B]^T \cdot [D] \cdot [B] \cdot dv \quad \dots\dots (3.18)$$

$\{f\}$ , the vector of total external force is then,

$$\{f\} = [K] \cdot \{a\} \quad \dots\dots (3.19)$$

where,  $\{a\}$  is the vector of unknown nodal point displacement.

### 3.4.2 Strain-Displacement Matrix

At any point in the brick element (8 nodes) the strain vector is relating to the nodal displacements vector by Eq. (3.3), which may be written in this form as:

$$\begin{Bmatrix} \varepsilon_x \\ \varepsilon_y \\ \varepsilon_z \\ \gamma_{xy} \\ \gamma_{yz} \\ \gamma_{zx} \end{Bmatrix} = \sum_{i=1}^8 \begin{Bmatrix} \frac{\partial N_i}{\partial x} & 0 & 0 \\ 0 & \frac{\partial N_i}{\partial y} & 0 \\ 0 & 0 & \frac{\partial N_i}{\partial z} \\ \frac{\partial N_i}{\partial y} & \frac{\partial N_i}{\partial x} & 0 \\ 0 & \frac{\partial N_i}{\partial z} & \frac{\partial N_i}{\partial y} \\ \frac{\partial N_i}{\partial z} & 0 & \frac{\partial N_i}{\partial x} \end{Bmatrix} \begin{Bmatrix} u_i \\ v_i \\ w_i \end{Bmatrix} \quad \dots\dots (3.20)$$

where, the 6x3 matrix is the strain-displacement matrix  $[B]$ , which includes the global shape functions derivatives,  $N_i$ .

Since the shape function are explained in term of local coordinate, then a rapport between the shape functions derivatives in the two coordinate systems must be defined. This relationship can be existing by using the chain rule as follows:

$$\begin{aligned}\frac{\partial N_i}{\partial s} &= \frac{\partial N_i}{\partial x} \cdot \frac{\partial x}{\partial s} + \frac{\partial N_i}{\partial y} \cdot \frac{\partial y}{\partial s} + \frac{\partial N_i}{\partial z} \cdot \frac{\partial z}{\partial s} \\ \frac{\partial N_i}{\partial t} &= \frac{\partial N_i}{\partial x} \cdot \frac{\partial x}{\partial t} + \frac{\partial N_i}{\partial y} \cdot \frac{\partial y}{\partial t} + \frac{\partial N_i}{\partial z} \cdot \frac{\partial z}{\partial t} \\ \frac{\partial N_i}{\partial r} &= \frac{\partial N_i}{\partial x} \cdot \frac{\partial x}{\partial r} + \frac{\partial N_i}{\partial y} \cdot \frac{\partial y}{\partial r} + \frac{\partial N_i}{\partial z} \cdot \frac{\partial z}{\partial r}\end{aligned}\quad \dots\dots (3.21)$$

In matrix form, Eq. (3.21) can be expressed as,

$$\begin{Bmatrix} \frac{\partial N_i}{\partial s} \\ \frac{\partial N_i}{\partial t} \\ \frac{\partial N_i}{\partial r} \end{Bmatrix} = \begin{bmatrix} \frac{\partial x}{\partial s} & \frac{\partial y}{\partial s} & \frac{\partial z}{\partial s} \\ \frac{\partial x}{\partial t} & \frac{\partial y}{\partial t} & \frac{\partial z}{\partial t} \\ \frac{\partial x}{\partial r} & \frac{\partial y}{\partial r} & \frac{\partial z}{\partial r} \end{bmatrix} \begin{Bmatrix} \frac{\partial N_i}{\partial x} \\ \frac{\partial N_i}{\partial y} \\ \frac{\partial N_i}{\partial z} \end{Bmatrix}\quad \dots\dots (3.22)$$

The Jacobian matrix  $[J]$  is the 3x3 matrix, therefore,

$$\begin{Bmatrix} \frac{\partial N_i}{\partial s} \\ \frac{\partial N_i}{\partial t} \\ \frac{\partial N_i}{\partial r} \end{Bmatrix} = [J] \begin{Bmatrix} \frac{\partial N_i}{\partial x} \\ \frac{\partial N_i}{\partial y} \\ \frac{\partial N_i}{\partial z} \end{Bmatrix}\quad \dots\dots (3.23)$$

The shape functions are utilized to define the element geometry for the iso-parametric element. Therefore, the Cartesian coordinates of any point within the element are given by,

$$\begin{aligned} x(s,t,r) &= \sum_{i=1}^8 N_i(s,t,r) \cdot x_i \\ y(s,t,r) &= \sum_{i=1}^8 N_i(s,t,r) \cdot y_i \\ z(s,t,r) &= \sum_{i=1}^8 N_i(s,t,r) \cdot z_i \end{aligned} \quad \dots\dots (3.24)$$

where,  $x_i$ ,  $y_i$  and  $z_i$  are the global coordinates of node  $i$ .

Making use of Eq. (3.24), the Jacobian matrix can be written as,

$$[J] = \begin{bmatrix} \sum_{i=1}^8 \frac{\partial N_i}{\partial s} \partial x_i & \sum_{i=1}^8 \frac{\partial N_i}{\partial s} \partial y_i & \sum_{i=1}^8 \frac{\partial N_i}{\partial s} \partial z_i \\ \sum_{i=1}^8 \frac{\partial N_i}{\partial t} \partial x_i & \sum_{i=1}^8 \frac{\partial N_i}{\partial t} \partial y_i & \sum_{i=1}^8 \frac{\partial N_i}{\partial t} \partial z_i \\ \sum_{i=1}^8 \frac{\partial N_i}{\partial r} \partial x_i & \sum_{i=1}^8 \frac{\partial N_i}{\partial r} \partial y_i & \sum_{i=1}^8 \frac{\partial N_i}{\partial r} \partial z_i \end{bmatrix} \quad \dots\dots (3.25)$$

By inverting the Jacobian matrix, the global derivatives of the shape functions can be attained;

$$\begin{Bmatrix} \frac{\partial N_i}{\partial x} \\ \frac{\partial N_i}{\partial y} \\ \frac{\partial N_i}{\partial z} \end{Bmatrix} = [J]^{-1} \begin{Bmatrix} \frac{\partial N_i}{\partial s} \\ \frac{\partial N_i}{\partial t} \\ \frac{\partial N_i}{\partial r} \end{Bmatrix} \quad \dots\dots (3.26)$$

### **3.4.3 Element Stiffness Matrix**

The stiffness matrix for an element as given in Eq. (3.16) can be written as:

$$[K]_e = \iiint_v [B]^T \cdot [D] \cdot [B] \cdot dv \quad \dots\dots (3.27)$$

in which  $dv$  represents the volume of the element in the global coordinates and can be expressed as:

$$dv = dx \cdot dy \cdot dz \quad \dots\dots (3.28)$$

In local coordinates it can be written as:

$$dv = |J| \cdot ds \cdot dt \cdot dr \quad \dots\dots (3.29)$$

where,  $|J|$  is the determinate of the Jacobian matrix.

Substituting Eq. (3.28) into Eq. (3.29), the element stiffness matrix is then given by,

$$[K]_e = \int_{-1}^{+1} \int_{-1}^{+1} \int_{-1}^{+1} [B]^T \cdot [D] \cdot [B] \cdot |J| \cdot ds \cdot dt \cdot dr \quad \dots\dots (3.30)$$

## **3.5 Material Modeling**

### **3.5.1 Concrete Modeling**

#### **A. Plasticity Approach**

There are many constituent models which have been established to evaluate the concrete response under different stress states. Some of the main constitutive models are the elasticity based models and the plasticity based model. The plasticity based model is relying in this work, which provides a mathematical relationship that describes the elasto-plastic response of materials.

ANSYS provides several options to characterize different kinds of material behavior, such as bilinear isotropic (with work hardening) and multi-linear isotropic hardening. For concrete, the concrete crushing in compression algorithm is similar to a plasticity law [50]. This algorithm is similar to a multilinear work hardening uniaxial stress-strain relationship based on rate independent Von-Mises yielding criterion. Rate independent plasticity constitutes an irreversible straining that occurs in a material once the yield surface is reached.



The yield term which means that value of stress that causing yield to the material, while, the rule of flow after the yield point determines the plastic straining direction. The hardening rule defines the changes in yield surface with gradually changing in yield.

Even though this approach represents the behavior in the strain hardening region, the softening in the curve can't be defined adequately by the hardening plasticity theory after the point of peak stress [51].

## **B. Material Nonlinearity**

This nonlinearity arise due to time independent behavior, like plasticity, and behavior of time dependent behavior like creep and viscoelastic / viscoplastic behavior. Stress-strain relationship is the prime feature that explains the material behavior. A nonlinear structural behavior is caused by the nonlinearity of the stress-strain curve of the material. Other factors can affect the material's stress-strain properties, such as load history, environmental circumstances, and the needed time to apply loads. A variation in nonlinear material behavior models are offered in ANSYS program, including plasticity, creep, nonlinear elastic, viscoelasticity, and hyper elasticity [45]. Fig. (3-2) shows a typical non-linearity of stress-strain curve for concrete.

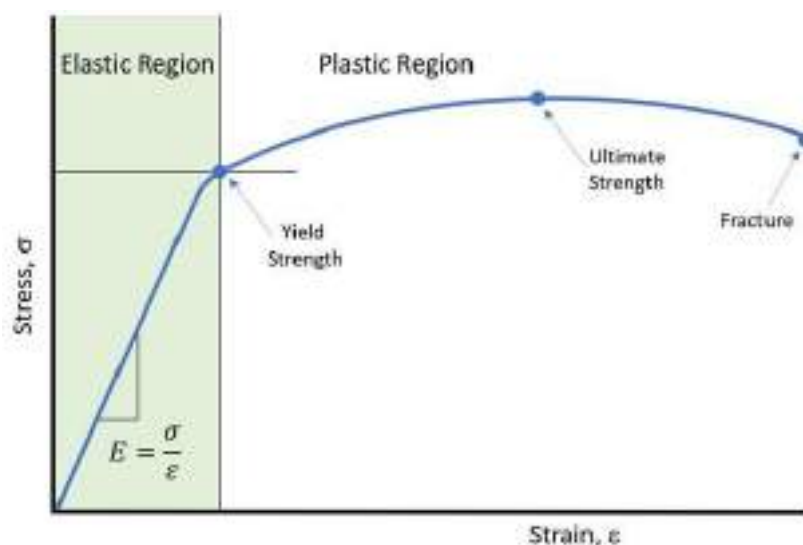


**Figure (3-2): Non-Linear Material Response [45].**

### C. Multilinear Stress-Strain Relationship

A typical stress-strain behavior for concrete exposed to uniaxial compression is illustrated in Fig. (3-1). It is approximately linear up to about (0.3-0.5) times the ultimate strength of concrete ( $f'_c$ ) [52]. Stress-strain curve explains a progressive increase in bend that occurs up to level of stress of  $(0.75 f'_c)$  to  $(0.9 f'_c)$ , after which the stress-strain curve bends pointedly and oncoming to the summit point at  $(f'_c)$  [53,54]. Then, the stress-strain curve descends until failure occurs because of the concrete crushing.

High strength concrete (HSC) behavior is linear with higher stress than the normal strength concrete (NSC). The strain at the maximum stress is approximately (0.003) (although high strength concretes have somewhat a little higher strain at peak stresses). On the descending portion of the stress-strain curve, higher strength concrete tends to behave in more brittle manner, with the fast stress dropping more than NSC as exhibited in Fig. (3-3) [52].

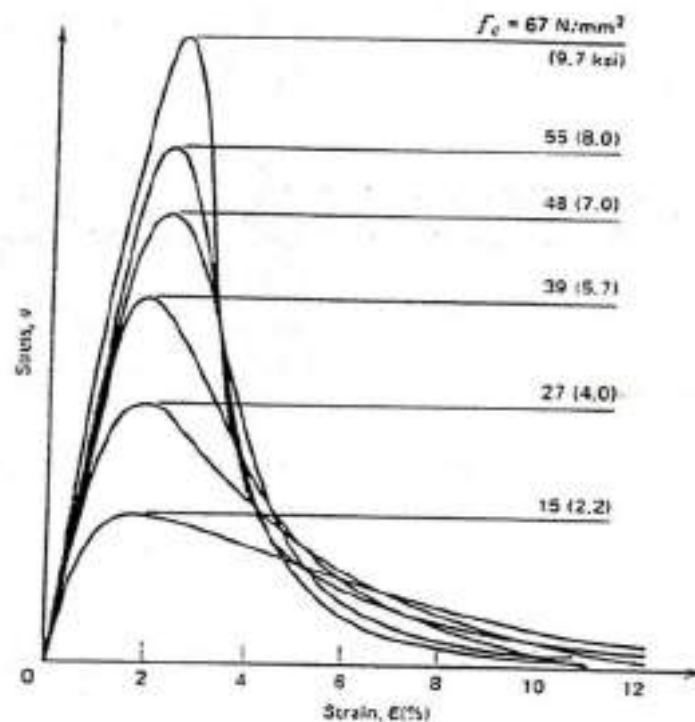


**Figure (3-3): Uniaxial compressive strain curve for concrete with different strength [52].**

Young modulus for concrete ( $E_c$ ) is a function in term of compressive strength ( $f'_c$ ). For normal strength concrete, the empirical equation found in the ACI 318M-11 is used [8],

$$E_c = 4700\sqrt{f'_c} , \quad (MPa) \quad \dots\dots (3.31)$$

For high strength concrete, Hsu and Hsu [55] reported values for the modulus of elasticity,

$$E_c = 124.31f'_c + 22653 , \quad (MPa) \quad \dots\dots (3.32)$$

Where, ( $E_c$ ) is the slope of stress-strain curve of concrete in (MPa), which equal to dividing the stress over strain.

The Poisson's ratio for concrete subjected to uniaxial compression ranges between (0.15 to 0.22). In current investigation a value of (0.2) is selected for analyzing RCHBs [56].

In ANSYS, the concrete behavior for uniaxial compression is defined by a piece-wise linear stress-strain curve, starting from the origin, and increases with positive values for stresses and strains. The slope of the first segment of the curve corresponds to the elastic modulus of the material and other segments have slopes less than first segment slope.

The idealized uniaxial stress-strain sketch for concrete specimen can be get by using the following equations for numeration the multilinear isotropic stress-strain values for the concrete as shown in Fig. (3-4) [57] as follows:

$$f_c = \varepsilon E_c \quad \text{for} \quad 0 \leq \varepsilon \leq \varepsilon_1 \quad \dots\dots (3.33)$$

$$f_c = \frac{\varepsilon E_c}{1 + \left(\frac{\varepsilon}{\varepsilon_0}\right)^2} \quad \text{for} \quad \varepsilon_1 \leq \varepsilon \leq \varepsilon_0 \quad \dots\dots (3.34)$$

$$f_c = f'_c \quad \text{for} \quad \varepsilon_0 \leq \varepsilon \leq \varepsilon_{cu} \quad \dots\dots(3.35)$$

$$\epsilon_1 = \frac{0.3 f'_c}{E_c} \quad \text{(Hooke's law)} \quad \dots\dots(3.36)$$

$$\epsilon_o = \frac{2 f'_c}{E_c} \quad \dots\dots(3.37)$$

Where;

$f'_c$  = stress at any strain  $\epsilon$ , MPa

$\epsilon$  = strain at stress  $f$

$\epsilon_o$  = strain at ultimate compressive stress  $f'_c$  and,

$E_c$  = concrete elastic modulus, MPa.

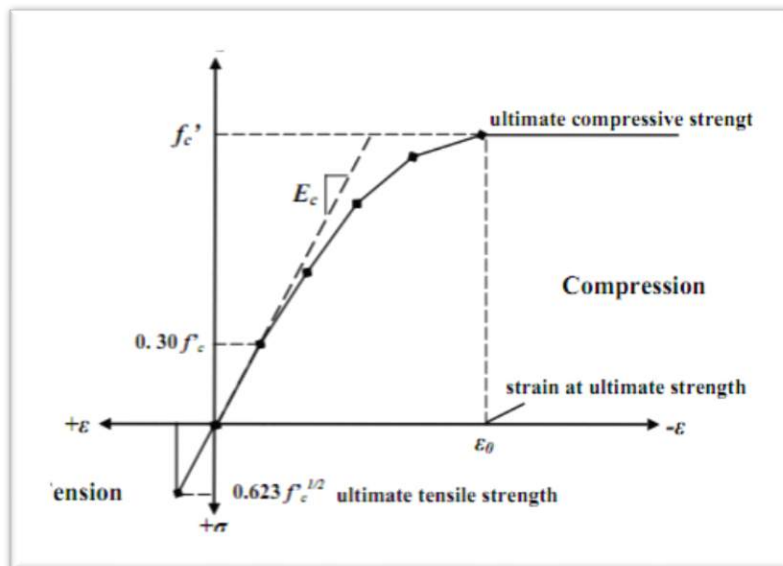


Figure (3-4): Simplified stress strain for NSC [57].

For HSC, (Hsu and Hsu 1994) [56], stress-strain equation is used

$$f_c = f'_c \frac{n \beta (\epsilon/\epsilon_o)}{n \beta - 1 + (\epsilon/\epsilon_o)^{n \beta}} \quad \dots\dots (3.38)$$

$$\beta = \left( \frac{f'_c}{65.23} \right)^3 + 2.59 \quad \dots\dots (3.39)$$

$$\epsilon_o = 1.29 \times 10^{-5} f'_c + 2.114 \times 10^{-3} \quad \dots\dots (3.40)$$

Where,  $f_c$  is the stress at any strain  $\epsilon$  in ( MPa).

$f'_c$  is the ultimate compressive strength at strain  $\epsilon_o$  in ( MPa).

$n$  is a parameter that depends on material strength,  $n=1$  for  $0 < \varepsilon < \varepsilon_0$ .

$\beta$  is a parameter that depends on the shape of the stress-strain curve.

The ascending branch of stress-strain curve for HSC is more linear and steeper and the strain at maximum strength is greater. This is because HSC is more homogenous than NSC and has less internal micro cracking for the same axial strain imposed, that becomes active only at a high load. After the maximum strength is reached, the descending branch of the curve gets steeper and drops suddenly for HSC due to the brittle failure of HSC, this behavior results because the broken surface initiates through the aggregate particles because of the greater matrix strength and this leads to form a much smoother cracked surface, thus sudden failure happens [55] as shown below.

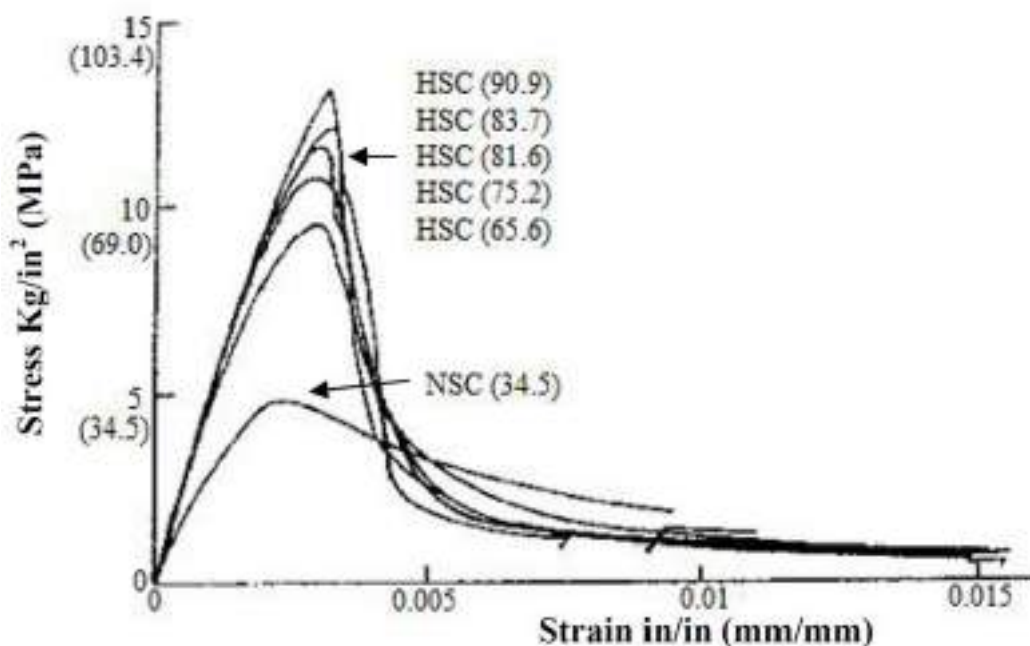
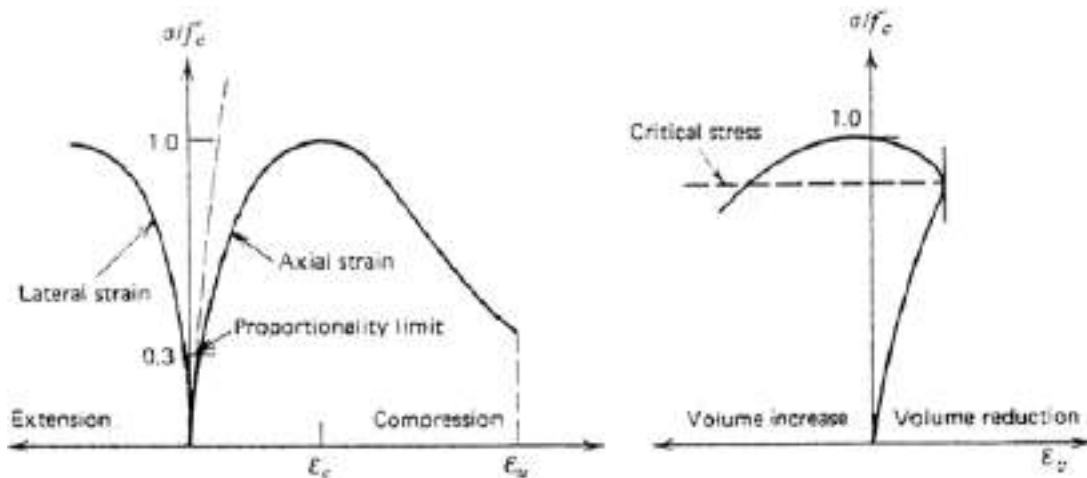


Figure (3-5): Stress-Strain Curve of HSC in Compression [55].

As revealed in Fig. (3-6) When the volumetric strain ( $\varepsilon_v = \varepsilon_1 + \varepsilon_2 + \varepsilon_3$ ) is found initially to be almost linear up to about to (here 1, 2, 3 are subscripts representing direction of principal stresses and strains). At this point, the direction (or sign) of the volumetric strain is reversed, resulting in a volumetric expansion near or at

( $f'_c$ ). The stress corresponding to the minimal value of volumetric strain beyond which no further reduction in volume occur is termed critical stress [58].



**Figure (3-6): Typical stress-strain curves for concrete in uniaxial compression test (a) Axial and lateral strains. (b) Volumetric strain ( $\epsilon_v = \epsilon_1 + \epsilon_2 + \epsilon_3$ ) [59].**

In the nearness of maximum stresses concrete subjected to compression reveals inelastic volume increase. This phenomenon, termed as volume dilatancy, is usually attributed to the gradual micro cracking in concrete during loading, as explained in Fig. (3-7) [60].

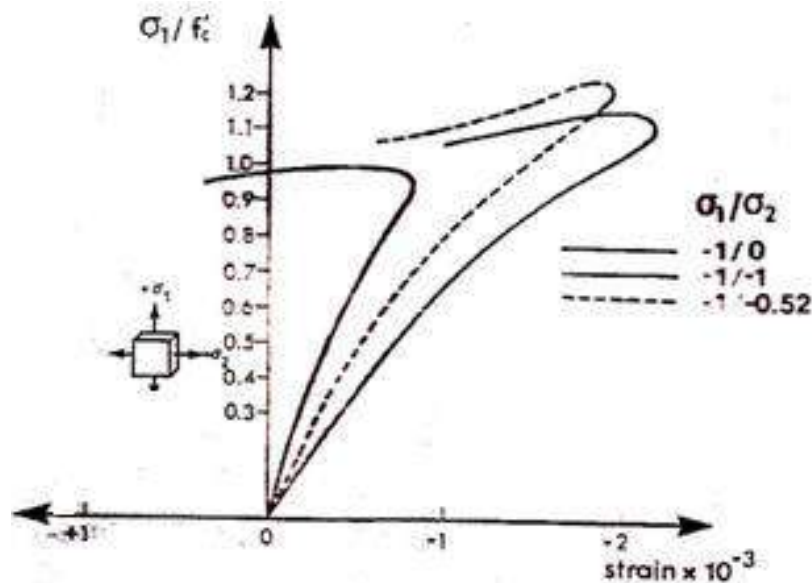


**Figure (3-7): Stress-volumetric strain curves [61].**

### C.1 Tensile Behavior of High Strength Concrete

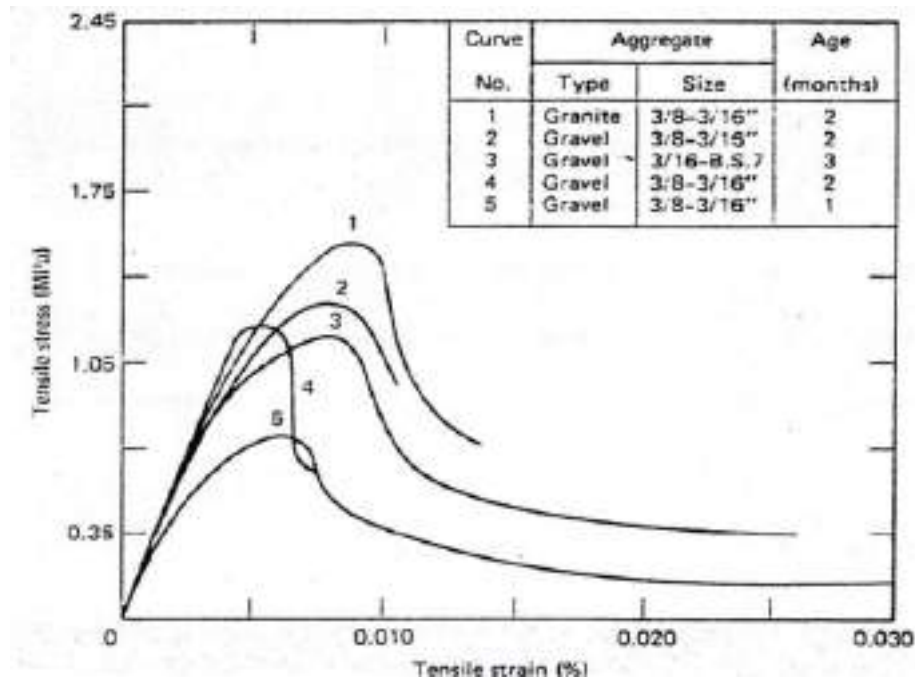
The general concrete behavior under uniaxial tensile loading is similar to an extent to the behavior of observed uniaxial compression. The crack propagation direction for uniaxial tension is normal to the stress direction. A decrement in the available load-stress capacity due to growth of every new crack and this reduction will be the reason of an increasing in the stresses at critical crack tips. The failing in tension occurs because a few connected cracks instead of numerous cracks, as it is for compressive states of stress.

The ratio between uniaxial tensile strength ( $f_t$ ) and compressive strength ( $f'_c$ ) may vary significantly but regularly ranges from (8-12) %. The modulus of elasticity under uniaxial tension is fairly higher and Poisson's ratio somewhat lower than in uniaxial compression [58].

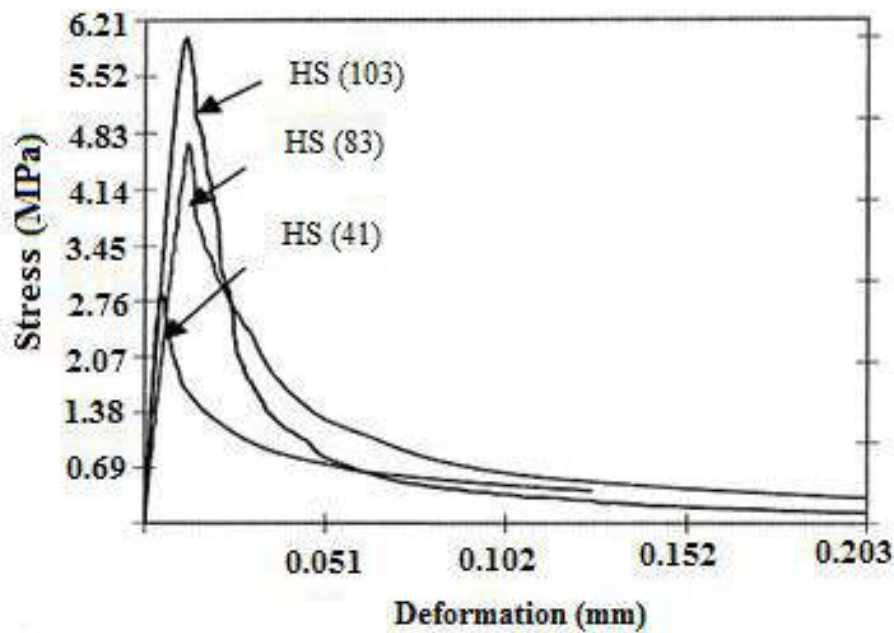
The direct tensile strength of concrete is problematic to measure and is normally taken as  $\left[ (0.3) \text{ to } \left( 0.4 \sqrt{f'_c} \right) \right]$ . Usually, either the modulus of rupture ( $f_r$ ) or the split cylinder strength ( $f_t$ ) is utilized to estimate the tensile strength of concrete. The value of the modulus of rupture of concrete differs quite extensively but is normally taken as  $\left( 0.62 \sqrt{f'_c} \right)$ . The split cylinder tensile strength is usually somewhat lower, at approximately  $\left[ (0.45) \text{ to } \left( 0.55 \sqrt{f'_c} \right) \right]$  in (MPa) [58].

The behavior of HSC exposed to uniaxial tension was studied by Li and Ansari (2000) [62] which was an experimental investigation consisted of testing (NSC and HSC) with  $f'_c$  values ranged from (41 to 103) MPa. Typical stress-deformation responses of the NSC and HSC in tension are explained in Fig. (3-8).





(a) Stress-strain relationship for NSC [55].



(b) Stress-strain relationship for HSC [62].

Figure (3-8): Typical tensile stress-strain curve for concrete [56,63].

#### D. Post - Cracking Model (Tension Stiffening Model)

Upon cracking, the stresses normal to cracked plane are released as the cracks propagate. To simulate this behavior in connection with the FE designing of RC beams, a tension stiffening concept is usually used [63]. This concept is



based on fact that some of the tensile stresses can be carried by the concrete among the cracks because of bond action between the steel bars and the surrounding concrete. This capability is gradually weakened because of the emergence of new cracks.

Additionally, to expand the numerical stability of the solution, the influence of tension stiffening was presented in several models. In the current work, the tension stiffening of RC after cracking was characterized by providing a linearly descending branch as revealed in Fig. (3-9). This model is given by:

(a) For  $\varepsilon_{cr} \leq \varepsilon_n \leq \alpha_1 \varepsilon_{cr}$

$$f_n = \left( \frac{\alpha_2 f_{cr}}{\alpha_1 - 1} \right) \left( \alpha_1 - \frac{\varepsilon}{\varepsilon_{cr}} \right) \quad \dots\dots (3.41)$$

(b) For  $\varepsilon_n \geq \alpha_1 \varepsilon_{cr}$

$$f_n = 0 \quad \dots\dots (3.42)$$

where,  $(f_n, \varepsilon_n)$  is the stress and strain normal to the crack plane,

$(f_{cr}, \varepsilon_{cr})$  is the cracking stress and strain,

$(\alpha_1)$  is the rate of stress released as the crack widens

$(\alpha_2)$  is the sudden loss of stress at the instant of cracking

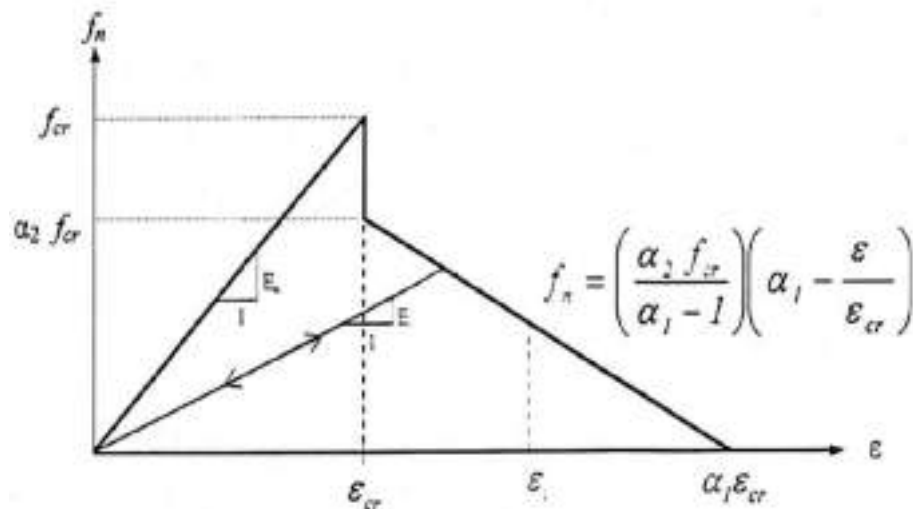


Figure (3-9): Pre and post-cracking behavior of normal strength concrete [63]

### E. Failure criteria for concrete

The actual behavior and strength of concrete materials are very complex because they depend on many factors like the mechanical and physical properties of the aggregate, cement paste and loading nature. No single mathematical model can describe the strength of real concrete materials completely under all conditions, so, simple models or criteria are utilized to represent the properties that are essential to the problem being considered [54].

Willam and Warnke, [64] developed a mathematical model able to inspect failure for concrete materials under multiaxial stress state.

Both cracking mode and crushing failure are accounted for. This model is modelled by usage of these equations:

$$\frac{F}{f_c} - S \geq 0 \quad \dots\dots (3.43)$$

where,  $(F)$  is the function of principal state  $(\sigma_{xp}, \sigma_{yp}, \sigma_{zp})$ ,  $(S)$  is the failure surface defined in term of principal stresses with five input parameters  $(f_c', f_t, f_{cb}, f_1 \text{ and } f_2)$ ,  $(f_c')$  is the peak uniaxial compressive strength,  $(f_t)$  is the peak uniaxial tensile strength,  $(f_{cb})$  is the crucial biaxial compressive strength,  $(f_1)$  is the peak compressive strength for a case of biaxial compression superimposed on hydrostatic stress state  $(\sigma_h^a)$ ,  $(f_2)$  is the crucial compressive strength for a state of uniaxial compression superimposed on hydrostatic stress state  $(\sigma_h^a)$ , and  $(\sigma_h^a)$  is the ambient hydrostatic stress state [54].

Failure surface is discrete into hydrostatic (volume changing) and deviatoric (shape changing) sections as shown in Fig. (3-10). The hydrostatic section forms a meridional plane which contains the equisectrix  $(\sigma_1 = \sigma_2 = \sigma_3)$  as an axis of revolution. The deviatoric section is located in normal plane to the equisectrix (intermittent line). Defining the deviatoric trace is done by polar coordinate  $(r, \theta)$

where  $(r)$  is the position vector locating the failure surface with angle  $(\theta)$ . The failure surface is defined as:

$$f(\sigma_m, \tau_m, \theta) = \frac{1}{2} \frac{\sigma_m}{f'_c} + \frac{1}{r(\theta)} \frac{\tau_m}{f'_c} - 1 = 0 \quad \dots\dots (3.44)$$

where,  $(\sigma_m$  and  $\tau_m)$  is the average stress components defined as:

$$\sigma_m = \frac{1}{3}(\sigma_1 + \sigma_2 + \sigma_3) = \frac{1}{3} I_1 \quad \dots\dots (3.45)$$

$$\tau_m^2 = \frac{2}{5} J_2 \quad \dots\dots (3.46)$$

where,  $(I_1)$  is the first stress invariant,  $(J_2)$  is the second deviatoric stress invariant and  $(\rho)$  is the apex of the surface.

The free parameters of failure surface  $(\rho)$  and  $(r)$  are identified from the uniaxial compressive strength  $(f'_c)$ , biaxial compressive strength  $(f_{cb})$  and uniaxial tensile strength  $(f_t)$ . If Eq. (3.44) is not satisfied, there is no attendant cracking or crushing. In another way, cracks will develop in material if any principal stress is tensile, while crushing will happen if all main stresses are compressive.

Willam and Warnke [64] succeeded in finding an expression for a failure cross section, since it can meet not only the conditions of symmetry, smoothness and convexity, but also it degenerates to circle if  $(r_1 = r_2)$ . This means that the cylindrical Von Mises model and the conical Drucker-Prager model are all special cases of Willam and Warnke failure formulation.

The failure surface can be indicated with a total of five strength parameters  $(f'_c, f_t, f_{cb}, f_1$  and  $f_2)$  in addition to an ambient hydrostatic stress state  $(\sigma_h^a)$ , as exhibited in Fig. (3-10).  $(f'_c)$  and  $(f_t)$  can be specified from two simple tests, and the other constants can be determined from Willam and Warnke [64]:

$$f_{cb} = 1.2 f'_c \quad \dots\dots (3.47)$$

$$f_1 = 1.45 f'_c \quad \dots\dots (3.48)$$

$$f_2 = 1.725 f'_c \quad \dots\dots (3.49)$$

However, these values are valid only for stress states where the condition stated below is satisfied:

$$|\sigma_h| \leq \sqrt{3} f'_c \quad \dots\dots (3.50)$$

where

$$(\sigma_h) \text{ is the hydrostatic stress state} = \frac{1}{3}(\sigma_{xp} + \sigma_{yp} + \sigma_{zp}) \quad \dots\dots (3.51)$$

The condition of Eq. (3.41) applies to stress situations with a low hydrostatic stress component.

Fig. (3-10), the lower curve represents all stress states in which  $(\theta = 0^\circ)$ , while the upper curve represents stress states for  $(\theta = 60^\circ)$ . The axis  $(\xi)$  represents hydrostatic length.

The concrete failure is categorized into four domains, each domain consisted of three principal stresses as follows:

1<sup>st</sup> domain:  $(0 \geq \sigma_1 \geq \sigma_2 \geq \sigma_3)$  (compression – compression – compression).

2<sup>nd</sup> domain:  $(\sigma_1 \geq 0 \geq \sigma_2 \geq \sigma_3)$  (tension – compression – compression).

3<sup>rd</sup> domain:  $(\sigma_1 \geq \sigma_2 \geq 0 \geq \sigma_3)$  (tension – tension – compression).

4<sup>th</sup> domain:  $(\sigma_1 \geq \sigma_2 \geq \sigma_3 \geq 0)$  (tension – tension – tension).

The concrete will crack if any principal stress is a tensile stress, while crushing will occur if all principal stresses are compressive.

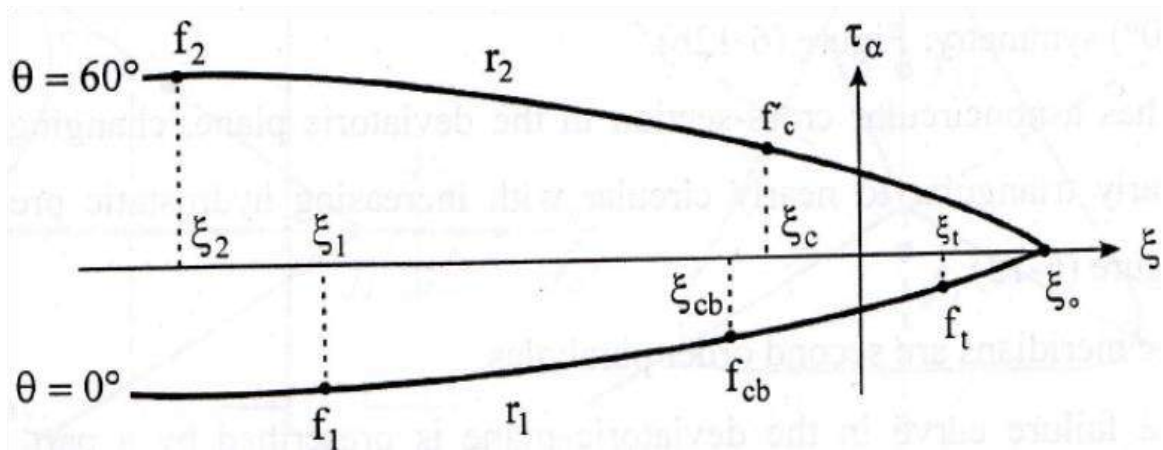


Figure (3-10): Profile of the failure surface as function of five parameters [64].

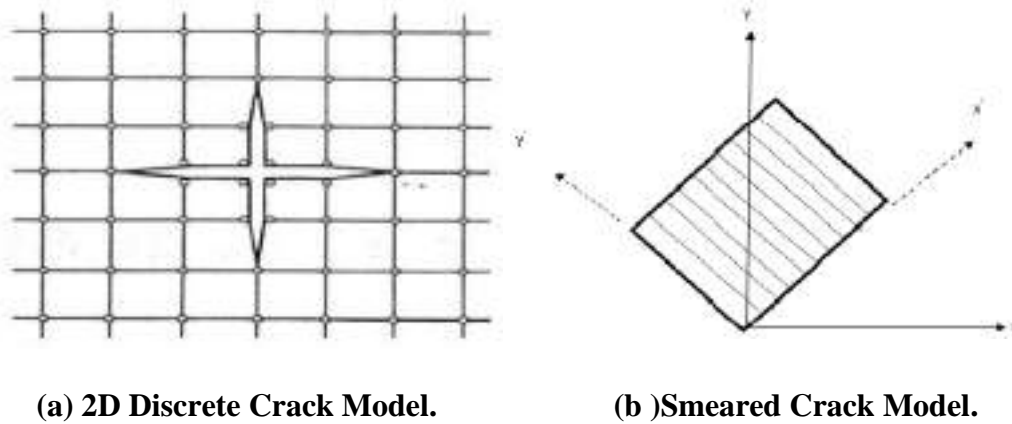
## F. Cracking modeling

The internal stresses and deflections of RC structures are affected by cracking. This phenomenon can be modeled in FE schemes either as discrete cracking approach, or as smeared cracking approach.

In the discrete cracking approach, the disconnecting or separating of the concrete element nodes through which the cracking is passing, requires additional nodes to occupying the same location, and connected by linkage elements. This physically appealing representation has computational difficulties in that it requires node renumbering after the emergence of the cracks and there is restriction on the crack propagation direction count on mesh layout [65].

The smeared crack paradigm was presented by Rashid [66]. He represents cracks as a change in the material property of the element over which the cracks are supposed to be smeared and offers cracks generation without the redefinition of the finite element topology. In this study, smeared crack model was used.

It is supposed that concrete turn into orthotropic after cracking with zero young modulus in normal direction to the crack. Both methods are exhibited in Fig (3-11).



(a) 2D Discrete Crack Model.

(b) Smearred Crack Model.

Figure (3-11): Cracking Modeling [65].

### **G. Shear Transfer and Tensile Crack Coefficient**

Concrete is supposed to behave linearly in tension up to the beginning of cracking. When concrete started to cracking, shear stiffness will reduce. However, cracked concrete can transmit shear forces partially because of aggregate interlock and property of dowel action existed in steel reinforcement. The shear transmission mechanism affected by several factors: the reinforcement ratio, bar size, bar arrangement, concrete cover depth, the concrete type and aggregate size. The coefficient of shear transfer ( $\beta$ ) represents the circumstances of the face of the crack.  $\beta_c$  and  $\beta_t$  refer to the coefficients of closed and open cracks [30].

The value of  $\beta$  ranges from 0.0 to 1.0, with 0.0 representing a smooth crack (whole shear loss) and 1.0 referring to rough crack (no shear loss). There are a number of investigations for modeling RC structures with using varied values of these coefficient. From these studies,  $\beta_t$  frequently ranges from 0.05 to 0.65, and  $\beta_c$  varies from 0.25 to 1. Using these coefficients below 0.2 will cause a problem in convergence. a number of preliminary analyses were carried out to assess the influence of  $\beta_t$  and  $\beta_c$  on the model behavior [30]. In this study,  $\beta_t$  ranged between (0.25-0.4) and  $\beta_c$  ranged between (0.3-0.9) for different specimens.

Reduction stiffness factor for cracked tensile condition for all beams equal to 0.9 was used to define this factor. There are many research studies that used for RC structures a tensile stiffness multiplier of 0.6 to simulate an abrupt dropping

in tensile stress to 60% of the rupture stress; followed by a linearly descending curve to zero stress [67,68], Padmarajaiah and Ramaswamy [69] used values ranged among 0.45 and 0.95 for PSC beams in FE for flexural test. Depending on these studies, and taking into account the good results obtained in the numerical studies by using ANSYS considering this factor equal to 0.9 [30].

## **H. Crushing Modeling**

If the material fails in uniaxial, biaxial, and triaxial compression at integration point, this material is supposed to crush at that point. Under this condition, material strength is supposed to have degraded to an extent such that the stiffness contribution of an element at this integration point [50].

### **3.5.2 Reinforcement Behavior**

Since the reinforcing bars are typically long and comparatively slender, they can commonly be supposed to be capable of transmitting axial forces only. For the FE models, the uniaxial stress - strain relation for steel was idealized as a bilinear curve, representing elastic- perfect plastic behavior, Fig. (3-12) explained this representation. This relation is supposed to be identical in tension and in compression. In present work, the ( $E_T$ ), strain hardening modulus is presumed to be the same value of yield stress approximately for the longitudinal bar and stirrups. This value was neatly chosen to obtain convergence [70]. Poisson's ratio  $\mu = 0.3$  was utilized for the steel reinforcement.

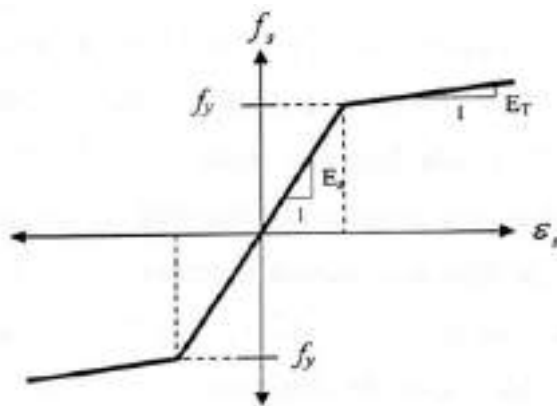


**Figure (3-12): Modeling of reinforcing bars [70].**

### 3.5.3 CFRP Behavior

Representation of CFRP sheet by linear orthotropic material. When loaded in tension, CFRP fibers do not exhibit any plastic behavior before rupture. The tensile behavior of CFRP fibers is characterized by stress-strain curve in form of linear elastic, which is sudden and can be catastrophic, as presented in Fig. (3-13). CFRP used in this study explained in Table (3-1) [71].

Table (3-1): Material properties for CFRP sheet [71].

Item	$f_y$ (MPa)	E (GPa)	Thickness (mm)	Type
CFRP	4900	240	0.167	One-direction

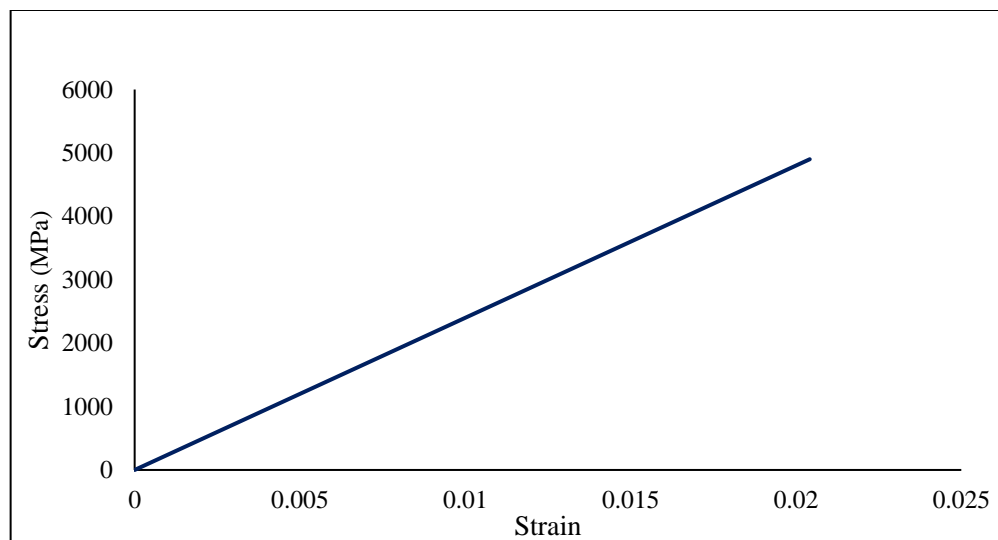


Figure (3-13): Modeling of CFRP sheet [71].

### 3.6 ANSYS Computer Program

The computer program ANSYS is a sturdy and interesting engineering finite element package that may be utilized to solve a lot of problems. FEM has become a most commonly method used to study the stress, deformation, and other engineering parameters. FEM uses complicated mathematical equations to accurately approximate how the complex structure reacts to a certain load or



condition. FE bundles like ANSYS solve thousands or millions of these equations to find a solution for a model. Handling all these equations as a whole be difficult and mostly impossible to solve manually. ANSYS is an inclusive general-purpose FE computer program that contains different elements implemented in the program. ANSYS has the capacity of solving linear and nonlinear problems including the influence of cracking, crushing, yielding of reinforcement, creep... etc. To use ANSYS or any another FEA software, one should first fully understands the underlying basic concepts and limitation of the FEM. In this work, the material parameters that must be taking into consideration to investigate the RCHBs behavior that are young modulus ( $E_c$ ), compressive strength  $f'_c$ , and the tensile strength ( $f_t$ ). Also, young modulus ( $E_s$ ) and the yielding strength ( $f_y$ ) of steel are considered. Furthermore, the geometry factors considered are the beam width, effective depth, longitudinal reinforcement area and shear reinforcement area.

### **3.7 Nonlinear Solution Techniques**

The FE derivation process returns a set of simultaneous equations:

$$[K]\{U\} = \{F^a\} \quad \dots\dots (3.52)$$

where,  $[K]$  is the stiffness matrix,  $\{U\}$  is the nodal displacements vector and  $\{F^a\}$  is the applied loads vector.

For linear elastic problems Eq. (3.52) is untied to calculate the solution of the unknown displacement  $\{U\}$ . In the case of nonlinear system, the  $[K]$  stiffness matrix is a function of the unknown displacement (or their derivatives). Then Eq. (3.51) cannot be exactly computed before determining the unknown displacement  $\{U\}$ .

There are three techniques for solving the nonlinear Eq. (3.52); the basic technique can be categorized into:

- 1) An Incremental or stepwise procedure, Fig. (3-14 a).
- 2) An iterative or Newton procedure, Fig. (3-14 b).
- 3) An Incremental- Iterative procedure, Fig. (3-14 c).

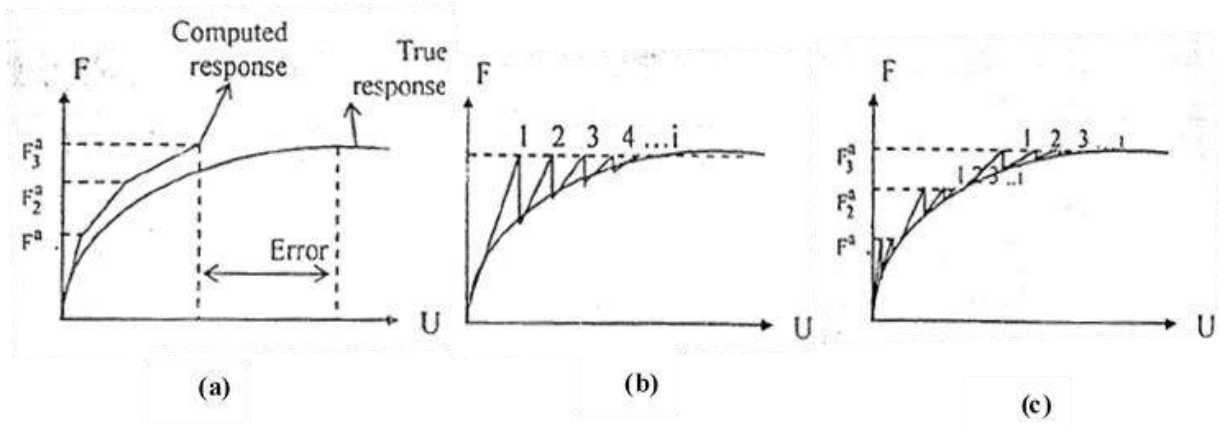


**Figure (3-14): Basic technique for solving the nonlinear equation (a) Incremental. (b) Iterative. (c) Incremental-Iterative. [72].**

In the incremental proceedings, the application load is changed in many small increments, and the structure is expected to react linearly during each increment with its stiffness recalculation based on geometry of the structural member and member end actions at the finish of the previous load increment. This is a simple procedure that does not require any iteration, except errors are probable to compile after many increments unless so fine increments are used, Fig. (3-14a).

In the iterative procedure, all applied load is in one increment at the first iteration, the out of balance forces are then computed and used in next iteration until the last converged solution will be in equilibrium, such that the internal load vector would equal the applied load vector or within some tolerance. This process can be written as:

$$[K_i^T] \{\Delta U_i\} = \{F^a\} - \{F^{nr}\} \quad \dots\dots (3.53)$$

$$\{U_{i+1}\} = \{U_i\} + \{\Delta U_i\} \quad \dots\dots (3.54)$$

where,  $[K_i^T]$  is the stiffness matrix,  $(i)$  is the subscript representing the current equilibrium iteration and  $\{F^{nr}\}$  is the internal load vector.

This procedure fails to produce information regarding the intermediate stage of loading. For structural analysis including path-dependent nonlinearities increments are in equilibrium to correctly follow the path of the applied load. This can be achieved by using the combined incremental-iterative method. In the combined-iterative procedure, a combination of an incremental and iterative scheme is utilized. The load is stratified incrementally, and iterations are performed to obtain converged solution corresponding to the stage of loading under consideration, as exhibited in Fig. (3-14c).

The incremental-iterative solution procedures have been utilized in this study. Full Newton-Raphson procedure is applied. The stiffness matrix is formed at every iteration. The benefits of this procedure may give more accurate result and used to avoid the convergence problem. The procedure disadvantage is that require large effort to form and resolve the stiffness matrix [72].

### **3.8 Analysis Termination Criteria**

In the physical examination under load control, structure collapse takes place when no further loading can be continued. This is typically indicated in the numerical tests by successively increasing iterative displacements and a continuous growth in the dissipated energy. Hence, the iterative process convergence cannot be accomplished. A maximum number of iterations for each increment are definite to stop the nonlinear solution if the convergence limit could not achieve for this study. It has been detected that the default number about (250) of iterations is generally sufficient to predict the solution divergence and failure. number of iterations Mainly depends on the type of problem and the nature of the input, range of nonlinearities, and tolerance value. In the present work a maximum range number equal (200) is adopted for load control problems.

### 3.9 Convergence Criteria

The iteration is accompanying for every incremental load until convergence is attained.

The convergence criterion for any nonlinear analysis in structural problems can be categorized into:

- 1) Force criterion.
- 2) Displacement criterion.
- 3) Stress criterion.

In displacement criterion, the incremental displacements at iteration (i) and the total displacements are determined. The solution is considered to be in convergence when the criteria of an incremental displacements is within a given tolerance for norm of the total displacements; infinite norm is used and takes the form:

$$\|\{\Delta U_i\}\| = \left(\max |\Delta U_i|\right) \leq T_n \left(\max |\Delta U_i|\right) \quad \dots\dots (3.55)$$

where, U may equal u, v, w or  $\theta_z$ .

The force criterion utilized in this study. For force criteria the norm of the residual forces at end of each iteration are tested versus the current applied forces norm as:

$$\|\{R\}\| = \left(\sum R_i^2\right)^{0.5} \leq T_n \left(\sum F_i^2\right)^{0.5} \quad \dots\dots (3.56)$$

where,  $\{R\}$  is a residual vector:

$$\{R\} = \{F^a\} - \{F^{nr}\} \quad \dots\dots (3.56)$$

To control the convergence through an analysis of model in this work, for this process as follows:

- 1) Using the full new Raphson.

- 2) Using shear transmission coefficient  $\beta_t$  and  $\beta_c$  more than 0.2 .
- 3) Tangent modulus for steel reinforcement equal approximately to the yield stress ( $f_y$ ) and input data of CFRP sheet.
- 4) The tolerance ( $T_n$ ) is taken equal to (0.005) near the ultimate load.
- 5) Increasing the iteration number to 200.

### **3.10 ANSYS Finite Element Model**

#### **3.10.1 SOLID65 Element Description**

SOLID 65 is utilized for the modeling of solid material with and without rebar (reinforcing bars). For example, this ability of solid is utilized to simulate the concrete material with its condition and properties. There is a need to define the failure surface and this is done by using the maximum compressive and tensile strength. Concrete element started to crack when the principal tensile stress is located in any direction outside the surface of the failure. After that, Young modulus will suffer dropping in its value reaching to zero in parallel direction to the principal tensile stress. Crushing begins to happen when the principal stresses are compressive and located outside the failure surface. Subsequently, Young modulus is reached to zero, and the element efficiency vanishes [73].

The most significant feature of SOLID65 is that it can represent the non-linearity of the material used. SOLID65 has an ability to cracks, crushes, plastic deformation, and creep. The element is defined by isotropic material properties. The geometry, node position, and coordinate system for SOLID65 are exhibited in Fig. (3-15) [65].

##### **3.10.1.1 Shape Functions of SOLID65 Element**

To model concrete, three dimensional brick elements are utilized. To express the displacements at any point within the element in terms of nodal displacement, shape functions for SOLID65 are utilized, which are interpolation functions.

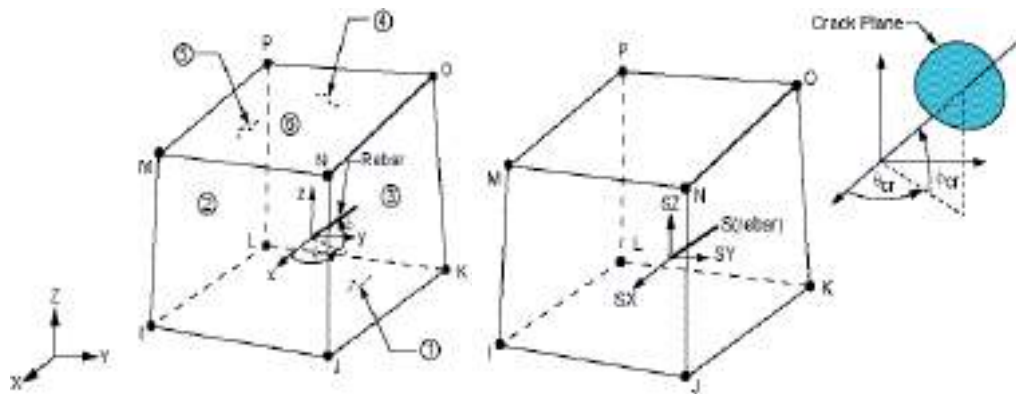
Using the shape functions, the displacement components (u, v, w) at a specific point can be found as follows [65],

$$\begin{aligned}
 u = \frac{1}{8} [ & u_I(1-s)(1-t)(1-r) + u_J(1+s)(1-t)(1-r) \\
 & + u_K(1+s)(1+t)(1-r) + u_L(1-s)(1+t)(1-r) \\
 & + u_M(1-s)(1-t)(1+r) + u_N(1+s)(1-t)(1+r) \quad \dots\dots (3.57) \\
 & + u_O(1+s)(1+t)(1+r) + u_P(1-s)(1+t)(1+r)]
 \end{aligned}$$

$$v = \frac{1}{8} [v_I(1-s)] \dots (\text{analogous to } u) \quad \dots\dots (3.58)$$

$$w = \frac{1}{8} [w_I(1-s)] \dots (\text{analogous to } u) \quad \dots\dots (3.59)$$

where, (s, t, and r) are the local coordinates and they are normalized, ranging from -1 to +1, and are not necessarily orthogonal to one another [65].



a) SOLID65 geometry      b) SOLID65 stress output

Figure (3-15): SOLID65 element for representing the concrete [65].

### 3.10.1.2 Input Data for SOLID65

Input data for SOLID65 element has one solid material and up to three rebar material in different direction. This element can contain another material through the volume of SOILID65 which defined as the rebar volume divided by the total element volume is equal to zero. Additional concrete material data such as the

shear transfer coefficient, tensile strength, and compressive strength are described in Table (3-2).

Table (3-2): SOLID65 input data.

Constant	Meaning
1	Shear transfer coefficient for open cracks
2	Shear transfer coefficient for closed cracks
3	Uniaxial tensile cracking stress
4	Uniaxial crushing stress
5	Biaxial crushing stress
6	Ambient hydrostatic stress state
7	Biaxial crushing stress under the ambient hydrostatic stress
8	Uniaxial crushing stress under the ambient hydrostatic stress.
9	Stiffness multiplier for cracked tensile condition

### **3.10.2 LINK180 Element Description**

It is a truss (or spar) element which may be utilized in many of engineering problems. LINK180 is utilized to modeling trusses, springs, links, sagging cables etc. This spar element is a uniaxial tension-compression element. As in a pin-jointed structure, no consideration of bending in this element. Plasticity and stress stiffening are contained within. The element is chosen, in this research, to modelling steel reinforcement which workings as main steel reinforcement and stirrups.

By using shape functions of the LINK180 element, the displacement components ( $u$ ,  $v$ , and  $w$ ) at a particular point can be found as follows [65]:

$$u = 1/2 [u_i(1 - s) + u_j(1 + s)] \quad \dots\dots (3.60)$$

$$v = 1/2 [v_i(1 - s) + v_j(1 + s)] \quad \dots\dots (3.61)$$

$$w = 1/2 [w_i(1 - s) + w_j(1 + s)] \quad \dots\dots (3.62)$$

A geometry, nodes positions, and coordinate system for LINK180 are presented in Fig. (3-16) [65].

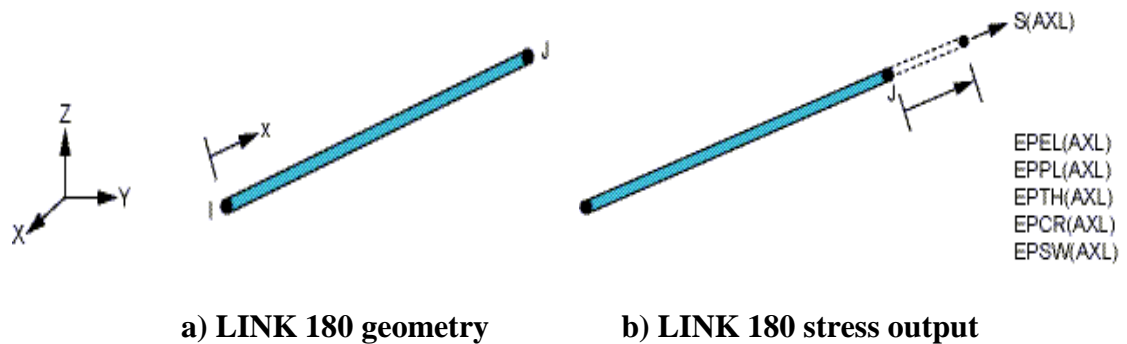


Figure (3-16): LINK180 for representing steel reinforcement [65].

Input data for LINK180 element are the cross sectional area for used bar, initial strain, and the material properties [74]. In mounting a FE model, three alternative representations of reinforcement can commonly be utilized, these are:

### 1) Discrete Representation

Discrete representation has commonly been utilized. The reinforcement in discrete modeling uses one dimensional bar that are linked to concrete mesh nodes as shown in Fig. (3-17 a). Therefore, the concrete and steel reinforcement bar will construct at the same nodes and same occupied regions. Full displacement compatibility between SOLID65 for concrete and LINK180 for steel rebar is significant benefit of the discrete representation. The weaknesses in this method that the constraint of the mesh and increase in number of the constructed elements.

### 2) Embedded Representation

The embedded representation is often used with high order iso-parametric elements. The bar element is constructed in by keeping reinforcing steel displacements compatible with an adjacent concrete element as displayed in Fig. (3-17 b). When reinforcement is complex, this model is very useful. The reinforcement steel stiffness matrix is evaluated unconnectedly and added to that



of the concrete to obtain the inclusive stiffness matrix. The disadvantage of this method is that there are extra degrees of freedom increase the computational and numerical treatment.

### 3) Smearred (Distributed) Representation

This method of modelling supposes that steel reinforcement is distributed uniformly through concrete elements in the defined region of the FE mesh as displayed in Fig. (3-17c). For example, this method is utilized for modelling wire mesh to simulate the occurred cracks, and for large structural members to decrease number of used element. Also where the presence of reinforcement does not have significantly effect on the overall structural behavior.

In discrete model method, which is utilized in this work, reinforcement is constructed by LINK180 at shared node with SOLID65. As a result, there are “perfect bond” between the concrete core and steel rebar, as presented in Fig. (3-17).

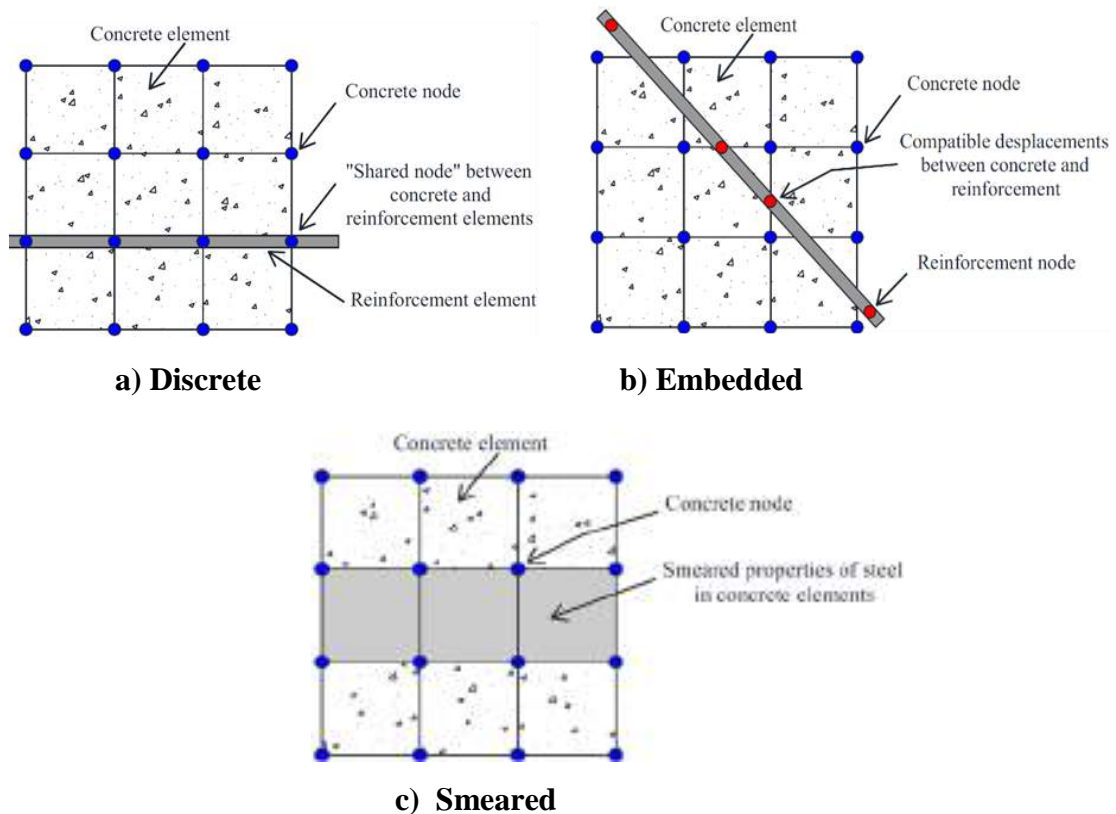
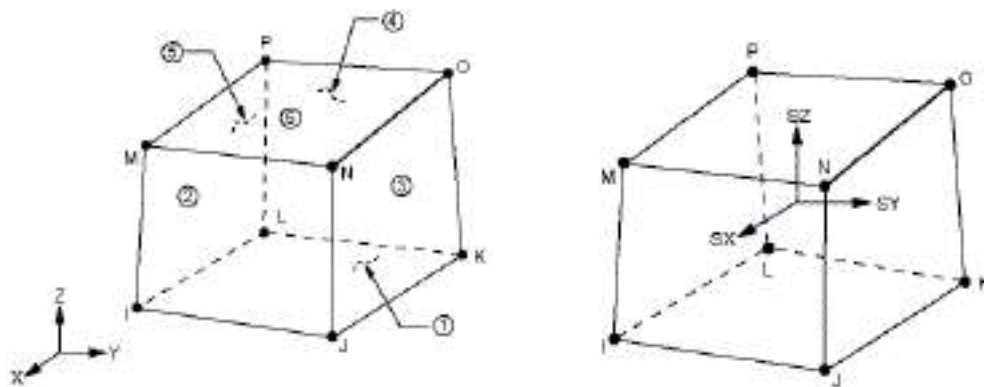


Figure (3-17): Models for reinforcement in reinforced concrete [74].

The above is termed to limitation, because from the experimental testing, cracking, crushing, and loss of concrete cover because of bond-slip failures. The desired technique for the modeling of steel reinforcement is selected based on the problem nature.

### **3.10.3 SOLID185 Element Description**

A SOLID185 element is utilized for steel plates at the supports and loading zones for the beam. This element with eight nodes, each node has three degrees of freedom. SOLID185 with translation in x, y, and z directions. A geometry and nodes positions for this element are exhibited in Fig. (3-18). SOLID185 description are took from ANSYS 15 element library.



a) SOLID 185 homogeneous  
structural solid geometry

b) SOLID 185 homogeneous  
structural solid stress output

Figure (3-18): SOLID 185 used to model steel plates and supports [65].

### **3.10.4 SHELL41 Element (Membrane Shell)**

A SHELL41 element with four nodes is utilized to simulate the CFRP strips. SHELL41 is a 3D element having membrane (in-plane) stiffness but no bending (out-of-plane) stiffness. It is destined for material with thin thickness where the element bending is in secondary importance. SHELL41 with eight nodes, each node has three degrees of freedom. Translations of SHELL41 in x, y, and z

directions [72]. Shell41 has variable thickness, large deflection, and stress stiffening as appeared in Fig. (3-19).

### 3.10.4.1 Shell41 Input Data

The element is defined by four nodes, four thicknesses, a material direction angle and the orthotropic material properties. The element may have variable thickness. The thickness is assumed to vary smoothly over the area of the element. In the present study the element has a constant thickness [71] as stated in Table (3-3).

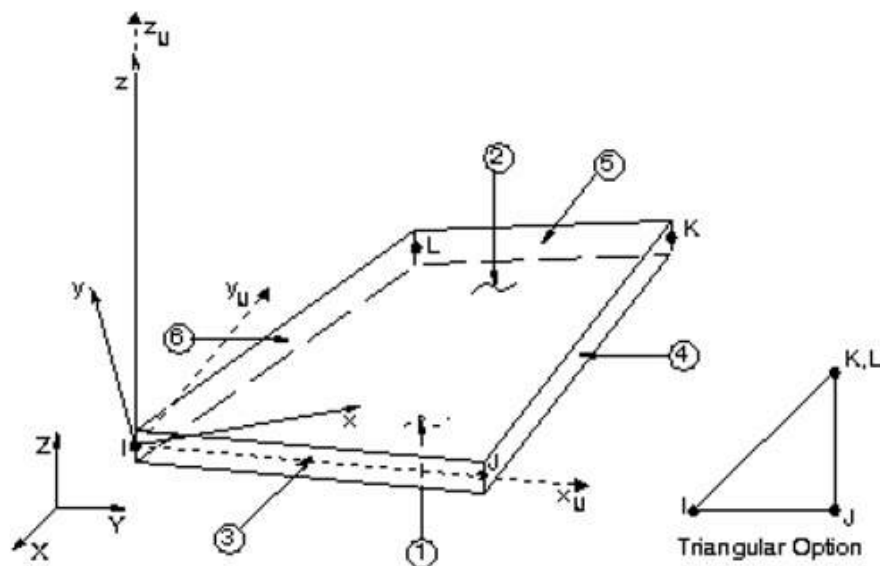


Figure (3-19): SHELL41 Geometry [71].

Carbon fiber that used in this work is in one-direction strength with modulus of elasticity in the same direction equal to (240 000 MPa). Poisson ratio of CFRP sheet equal to 0.3. Other input data like the Young modulus in lateral direction, Poisson ratio in other direction, and modulus of rigidity of the same material in all direction inserted to (1 MPa) to avoid the convergence problem during the solving process. Material properties Used in ANSYS in this work for all models used CFRP [71], are illustrated in Table (3-4).

Table (3-3): Input data of CFRP sheet.

No.	Name	Description
1	TK(I)	Shell thickness at node I
2	TK(J)	Shell thickness at node J (defaults to TK(I))
3	TK(K)	Shell thickness at node K (defaults to TK(I))
4	TK(L)	Shell thickness at node L (defaults to TK(I))
5	Thet A	Element x-axis rotation
6	EFS	Elastic foundation stiffness

Table (3-4): Material properties for CFRP element [71].

Linear orthotropic	
EX	240000
EY	1
EZ	1
PRXY	0.3
PRYZ	0
PRXZ	0
Gxy	1
Gyz	1
Gxz	1

# **CHAPTER FOUR**

## **NUMERICAL APPLICATION AND RESULTS**

---

### **4.1 Introduction**

In this chapter, RCHBs are analyzed using three dimensional FEM utilizing ANSYS 15 program. Seven numerical specimens provided from the previous experimental work are explored through this study.

The verification with experimental results are carried out to check the validity and accuracy of the FE procedure. The results obtained by FEM are compared with the experimental results in terms of load-deflection curves and crack patterns. Also, the study is conducted to determine the ultimate loads, maximum deflection. The effect of the various parameters which are expected to affect the behavior of such beams is also investigated. These parameters are:

- 1) Inclination of the haunch angle.
- 2) Compressive strength of concrete.
- 3) Presence of a transverse opening.
- 4) Presence of a longitudinal opening.
- 5) Usage of CFRP sheet to strengthening RCHBs.

### **4.2 Procedure of the Study**

In the current study, the structural behavior of simply supported rectangular cross-section RCHBs is simulated depending on available experimental tests.

Three groups of RCHBs based on experimental tests are used. The first group offered by Rombach et al. [23] which carried out on eighteen specimens having an inverted positive haunch angle fails in shear. The parameters of this research were the haunch angle and haunch length. Only two beams were utilized in this

study for the validation process. The second group presented by Colunga et al. [4] with ten beams has positive haunch angle fail in shear with different parameters such as the haunch angle and stirrups influence. Four specimens were selected from this study to the verification process. The third group was investigated by Dawood and Nabbat [33]. They tested twelve beams having negative haunch angle fails in flexure. Just one beam was validated.

### **4.3 Verification Process**

The results of numerical analysis alongside the experimental ones for specimens (2L1, 3L1, TASC $\alpha$ 1-R1, TASC $\alpha$ 2-R1, TASC $\alpha$ 3-R1, TASC $\alpha$ 4-R0, and S1) that used for the verification purpose in terms of load-deflection curve, ultimate load, maximum deflection, and crack patterns are presented in Tables (4-1) to (4-2), and Figs. (4-1) to (4-2).

Figure (4-1) shows that the predicted behavior concerning the load deflection curves is almost identical to the experimental results. The values of ultimate load are shown in Table (4-1). It can be observed that the values ratio of experimental to numerical ultimate load are between (0.96) to (1.1) with average value of (1.03).

Table (4-2), also gives the experimental and numerical values of the maximum deflection. The ratio of experimental to theoretical values of deflection are between (0.83) to (1.02) with average value of (0.97).

Crack patterns for the validated beams showed a good conforming between the experimental and theoretical are demonstrated in Fig. (4-2). Because of the simplification and assumption of the employed FEM, it seems no way to obtain crack propagation as accurately as the experimental test. This may be due to the difference between the condition of the theoretical and experimental tests. But the major reason is the nature of the concrete material. It must be noted that the obtained cracks from numerical test is larger than one exists in the experimental

test, and sometimes it was extended to areas where cracking were not physically observed. The first group (2L1 and 3L1) involved additional compression cracks near the top surface of haunch zone. The second group exactly for beams (TASC $\alpha$ 1-R1, TASC $\alpha$ 2-R1, and TASC $\alpha$ 3-R1), first cracks developed at the support more than existed in the experimental. Also, haunch zone suffers more cracks than found in the experimental test.

Third group shows flexural cracks more than regular existed in the experimental test. Extensive cracks are predicted by the FE modeling because the greater intensity of stress at the nodes.

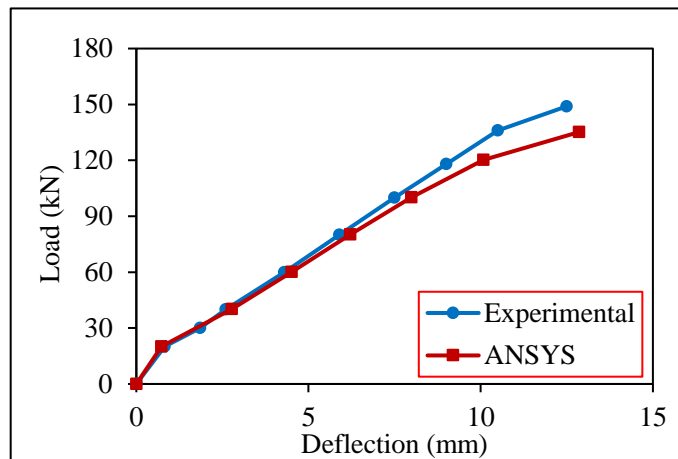
The greater intensity obtained for the numerical cracking may be due to the cracking modeling used, in which material degradation is distributed over all the volume of the element. Also, assuming perfect bond between the used elements (SOLID65, and LINK180) causes high stress concentrations in the concrete elements.

Table (4-1): Verification results include the failure load.

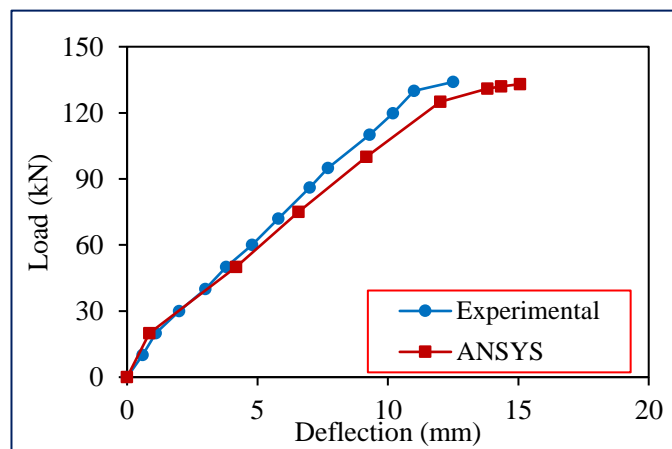
Group	Beam ID	$V_{u, Exp.}$ (kN)	$V_{u, ANS.}$ (kN)	$\frac{V_{u, Exp}}{V_{u, ANS.}}$
I	2L1	149	135	1.1
	3L1	139	133	1.04
II	TASC $\alpha$ 1-R1	210	197	1.06
	TASC $\alpha$ 2-R1	170	176	0.96
	TASC $\alpha$ 3-R1	135	124	1.09
	TASC $\alpha$ 4-R0	40	40.25	0.99
III	S1	182	182	1
Mean	-	-	-	1.03
Standard deviation	-	-	-	0.0528

Table (4-2): Verification results include maximum deflection.

Group	Beam ID	$\Delta$ , Exp. (mm)	$\Delta$ , ANS. (mm)	$\frac{\Delta, Exp}{\Delta, ANS.}$
I	2L1	12	12.85	0.93
	3L1	12.5	15	0.83
II	TASC $\alpha$ 1-R1	35	35.5	0.98
	TASC $\alpha$ 2-R1	40.5	40.86	0.99
	TASC $\alpha$ 3-R1	41.5	41.55	1
	TASC $\alpha$ 4-R0	20	19.5	1.02
III	S1	17.2	17	1.01
Mean	-	-	-	0.97
Standard deviation	-	-	-	0.0665



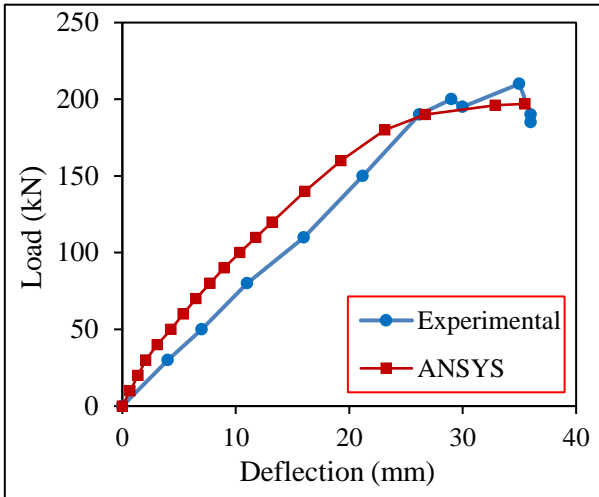
(a) Beam (2L1).



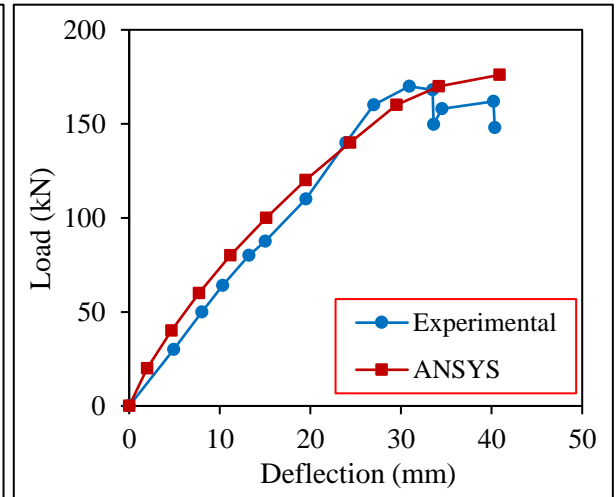
(b) Beam (3L1).

Figure (4-1): Load-deflection curves for theoretical and experimental beams.

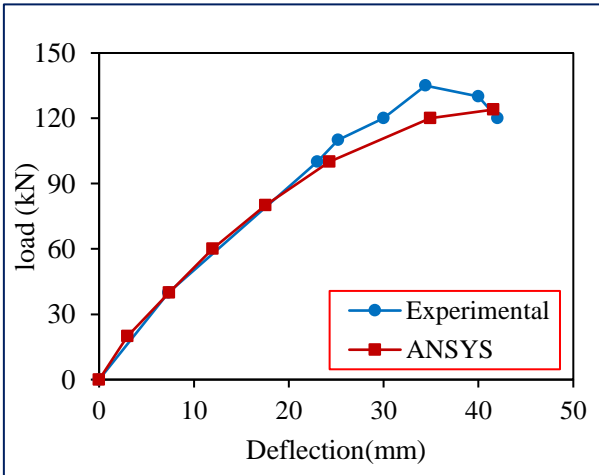




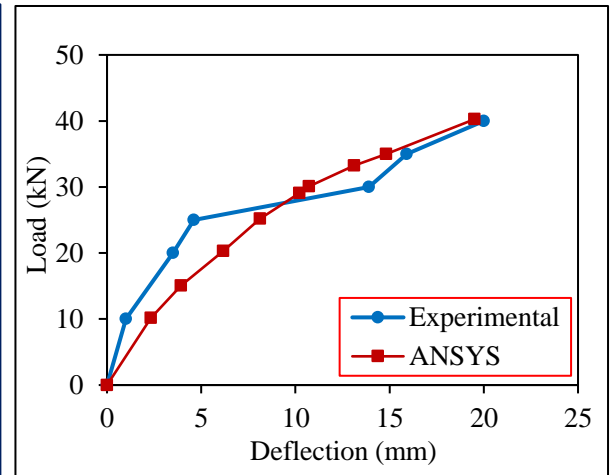
(c) Beam (TASCα1-R1).



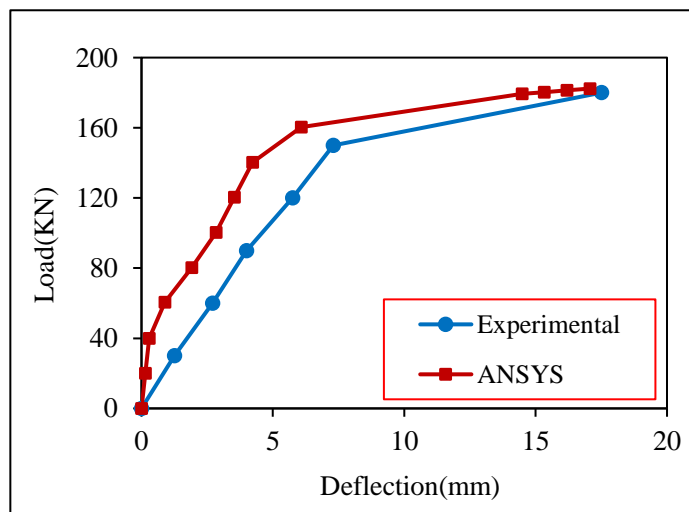
(d) Beam (TASCα2-R1).



(e) Beam (TASCα3-R1).

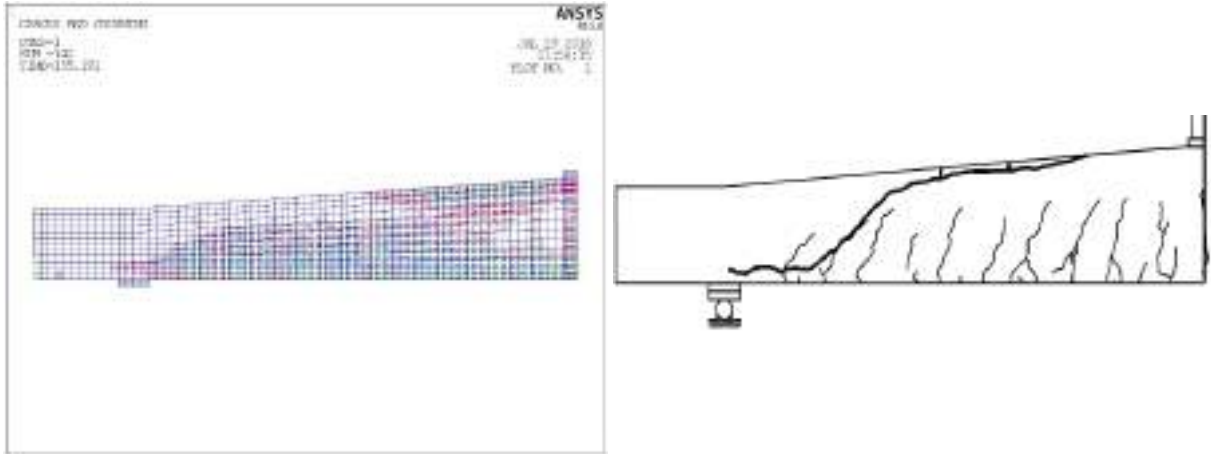


(f) Beam (TASCα4-R0).

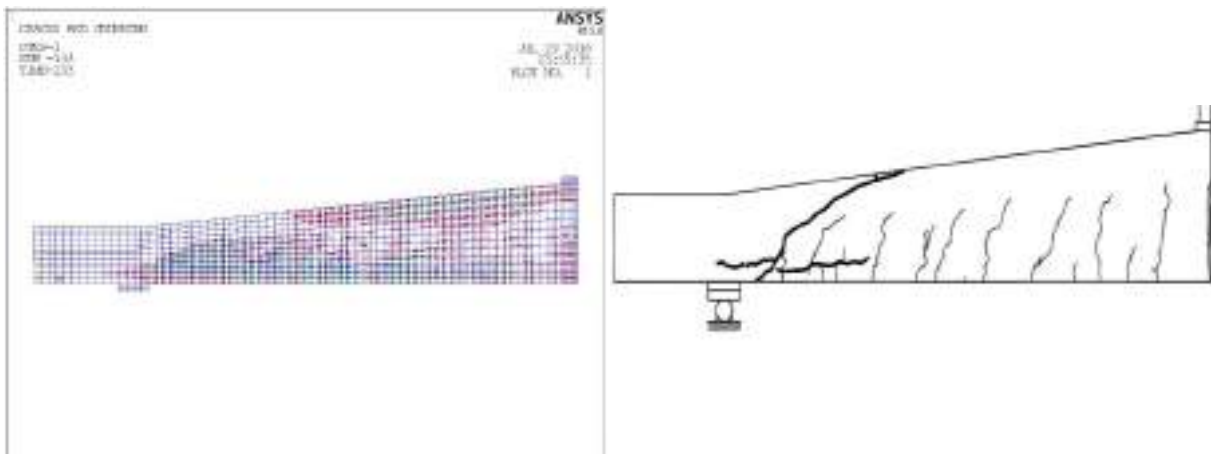


(g) Beam (S1).

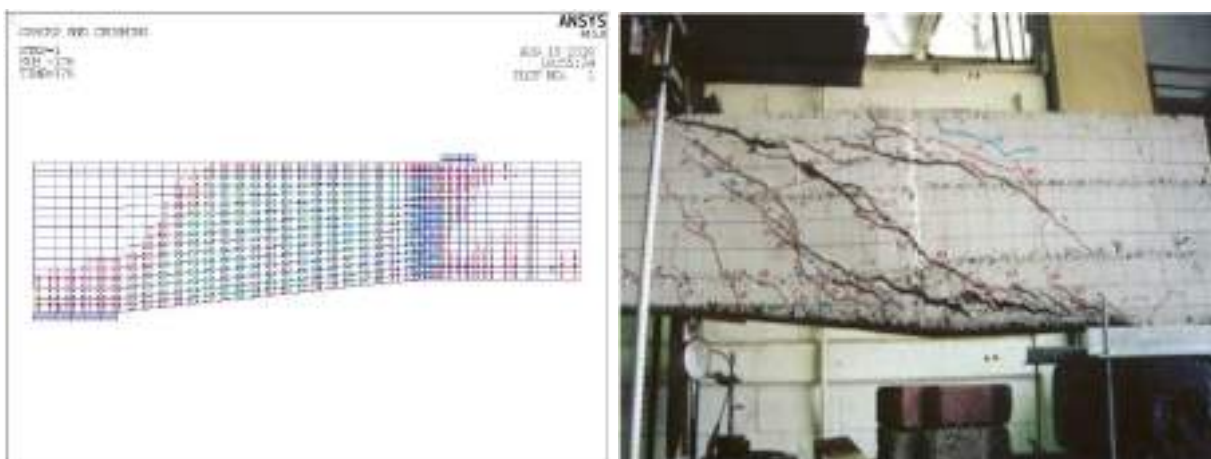
Figure (4-1): Cont.



(a) Numerical and experimental beam (2L1).

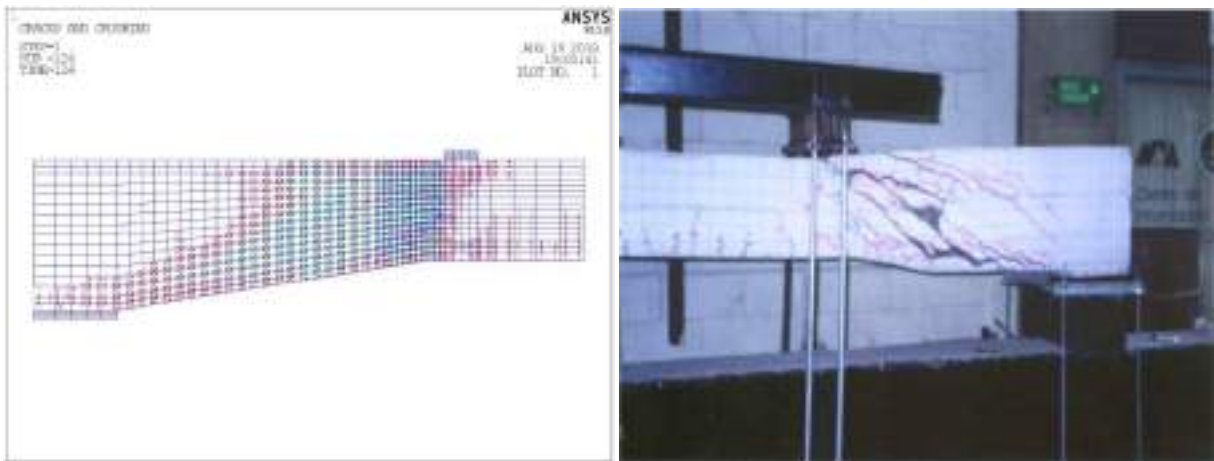


(b) Numerical and experimental beam (3L1).



(c) Numerical and experimental beam (TASC $\alpha$ 2-R1).

Figure (4-2): Crack pattern for theoretical and experimental beam.



(d) Numerical and experimental beam (TASC $\alpha$ 3-R1).



(e) Crack patterns for numerical and experimental beam (S1).

Figure (4-2): Cont.

#### **4.4 Finite Element Analysis of Haunched Beams**

In this section, the RCHBs is investigated via FEM that discussed in previous chapter. Load-deflection curves, cracking load, ultimate load, maximum deflection, cracks pattern, failure mode, and shear stress distribution are considered to explore the performance of these beams.

The investigations are divided into three series that presented the influence of different parameters on the behavior of RCHBs. The first series conducted on inverted RCHBs fail in shear.

The second series is RCHBs with positive haunch type fail in shear. The third series is RCHBs with negative haunch type fail in flexural loading. All series involve forty-three RCHBs.

#### **4.4.1 Series One**

This series consists of thirteen specimens with inverted haunch and designed to fail in shear. Haunch angle, compressive strength, amount of stirrups, presence of transverse opening, and retrofitting by CFRP sheet are the main parameters for this series.

Geometry of all beams in this series are of Rombach et al. [23]. Linear tapering dimensions are obtained by keeping constant the overall depth at the mid span of beam and decreasing depth at the supports to 340, 240, 190 mm. Haunch angles ( $\alpha$ ) with horizontal line are  $0^\circ$ ,  $3.95^\circ$  and  $5.91^\circ$  for (1L1, 2L1, and 3L1) respectively.

Beam effective length, width, and clear cover equal to 3000, 200, 40 mm respectively. The shear span to effective depth ratio ( $a/d$ ) of such members is 5. The ordered materials include reinforcement type BSt 500S (design strength  $f_y = 500$  MPa) and compressive strength  $f'_c = 30$  MPa.

Three longitudinal reinforcement bars  $\text{Ø}20$  mm were chosen to place in a beam width of 200 mm to insure the flexural side. Also, two bar  $\text{Ø}10$  mm are placed at the top of cross section. Stirrups  $\text{Ø}10$  mm are placed at the support zone with spacing @55 mm to insure this region.

Steel plate ( $25.4 \times 100 \times 200$ ) mm is used for the loading and bearing zone to distribute the applied force over an area to avoid the stress concentration at some elements as revealed in Figs. (4-3). All dimensions in presented figures are with mm.

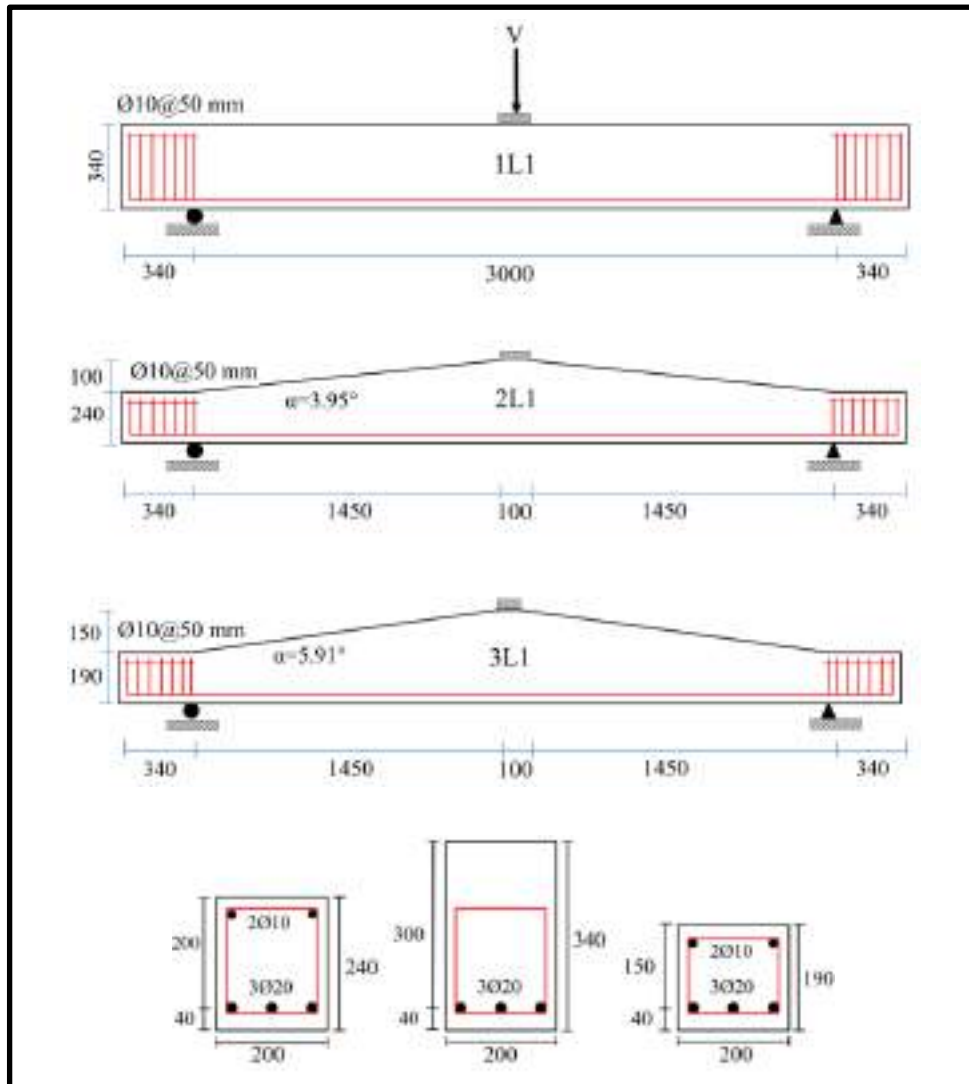


**Figure (4-3): Series one beams details.**

To investigate the effect of different parameters on the performance of inverted RCHBs in this series, thirteen specimens were carried out by different variables. These parameters include variable compressive strength, amount of shear reinforcement, creating transverse opening, and retrofitting by CFRP sheet.

Table (4-3) illustrates the variables treated of this series. The compressive strength of concrete is varying in a range comprise values of normal and high strength for beams with and without stirrups. Stirrups with different spacing (100, 150, and 200 mm) are investigated too. Compressive strength and stirrups variables are carried out on the beam with haunch angle  $5.91^\circ$  while the other parameters are carried out on the beam with haunch angle  $3.95^\circ$  with same conditions and geometry. The same Table included creating transverse opening

and beams with stirrups at variable spacing. Also included beams strengthened by CFRP sheet. As shown in Fig. (4-4) to (4-6) and Table (4-3), three beams are modeled with presence of square lateral opening (100×100) mm (39%h, 35%h, and 32%h) placed from the support at distance 275, 675, and 1150 mm respectively.

External and internal strengthening are used to enhance or restore the expected reduction of shear carrying capacity of RCHBs due to the existence of opening. These methods are:

- 1) Increasing the compressive strength of specimen with opening.
- 2) Using CFRP sheet around the opening for beams as shown in Fig. (4-6 a).
- 3) Using CFRP strips for retrofitting the solid inverted RCHBs as shown in Fig. (4-6 b).

Tensile stress and Young modulus are calculated according to recommendation and equation that presented by of ACI code. ( $f_t$ , and  $E$ ) values are calculated according to the equations  $0.62\sqrt{f'_c}$  and  $4700\sqrt{f'_c}$  respectively.  $E$  for HSC is calculated according to the presented equation by Hsu [56].

Table (4-3): Details of specimens (Series 1).

Beam ID	$\alpha$	$f'_c$ (MPa)	Opening size (mm)	Shear reinforcement	Strengthening type
1L1	0°	30	-	-	-
2L1	3.95°	30	-	-	-
3L1	5.91°	30	-	-	-
IHB50	5.91°	50	-	-	-
IHB70	5.91°	70	-	-	-
IHB30-S100	5.91°	30	-	Ø10@100mm	-
IHB30-S150	5.91°	30	-	Ø10@150mm	-
IHB30-S200	5.91°	30	-	Ø10@200mm	-

Table (4-3): (continued) Details of specimens (Series 1).

ID	$\alpha$	$f'_c$ (MPa)	Opening size (mm)	Shear reinforcement	Strengthening type
IHB50-S100	5.91°	50	-	Ø10@100mm	-
IHB70-S100	5.91°	70	-	Ø10@100mm	-
IHB30-TO1	3.95°	30	100×100	-	-
IHB30-TO2	3.95°	30	100×100	-	-
IHB30-TO3	3.95°	30	100×100	-	-
IHB40-TO1	3.95°	40	100×100	-	-
IHB30-C1	3.95°	30	100×100	-	CFRP
IHB30-C2	3.95°	30	-	-	CFRP

IHB50: Inverted haunched beam- 50 MPa compressive strength

S100: Stirrups @100 mm.

TO1,2, and 3: Beam with transverse opening with different locations.

C1 & C2 : Beam with CFRP.

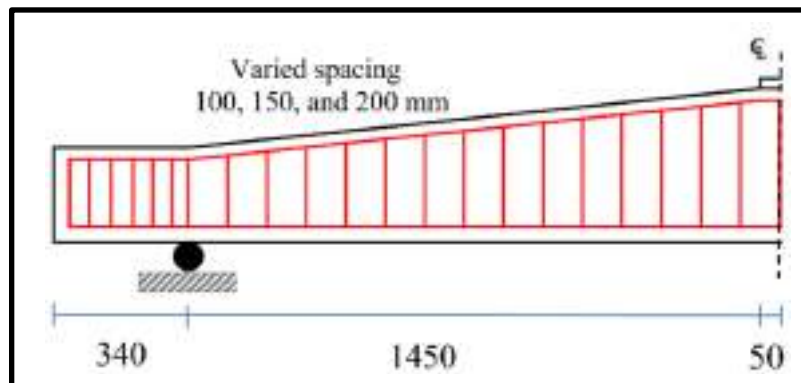


Figure (4-4): Reinforcement details for beams with stirrups.

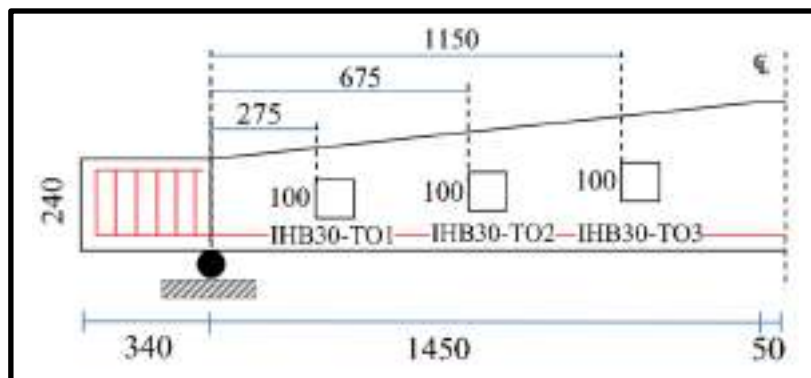
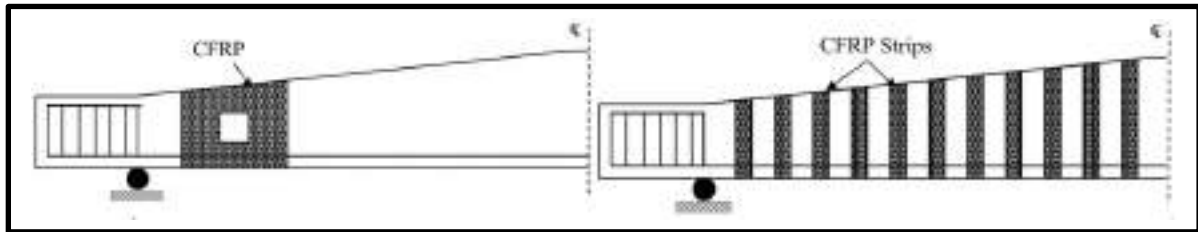


Figure (4-5): Details of three beams with different opening location.





(a) RCHB with opening used CFRP sheet. (b) Solid RCHB with CFRP strips.

Figure (4-6): Beams with CFRP sheet (IHB30-C1 and IHB30-C2) respectively.

#### 4.4.2 Series Two

A total of twenty-four simply supported RCHBs are investigated in this series, which designed to fail in shear. The haunch angle, concrete compressive strength, amount of shear reinforcement, and presence of transverse and longitudinal opening, and strengthening by CFRP sheet are the main variables regarded in this series. The dimensions of the specimens defined by Colunga et al. [4]. In all specimens, the width ( $b$ ), height ( $h$ ), effective span ( $L$ ), and shear span ( $a$ ) are 220, 450, 2800, and is 1083 mm respectively. The haunch length ( $L_h$ ) at both ends of beam is one-third of the effective span ( $L_h=L/3\approx 933$  mm). Linear tapering dimensions are obtained by keeping constant the overall depth at each beam end ( $h_{max}=450$  mm) and decreasing the overall depth at the middle to 450, 400, 350, 300, and 250 mm.

Haunch angles ( $\alpha$ ) with horizontal line are  $0^\circ$ ,  $3.07^\circ$ ,  $6.12^\circ$ ,  $9.13^\circ$ , and  $12.1^\circ$  for (RB30-0, HB30-3, HB30-6, HB30-9, and HB30-12) respectively as displayed in Fig. (4-7).

The properties of concrete and steel are shown in Tables (4-4) and (4-5). The flexural and shear reinforcement utilized in each beam are summarized in Fig. (4-8). All specimens are reinforced with  $4\text{Ø}25$  at the bottom and  $3\text{Ø}25$  at the top to insure the flexural side of the test. Also, additional stirrups added at the vertex to prevent the failure at this region. The required spacing of stirrups at the vertex



inversely proportional with the change in haunch angle value. When haunch angle increase will need to minimum spacing at this zone. All beams are simply supported subjected to two concentrated loads (V) applied at 100 mm from the vertex. Steel plate dimensions at the loading one are (25.4×100×220) mm and at the support are (25.4×250×220) mm to avoid the stress concentration as demonstrated in Fig. (4-7).

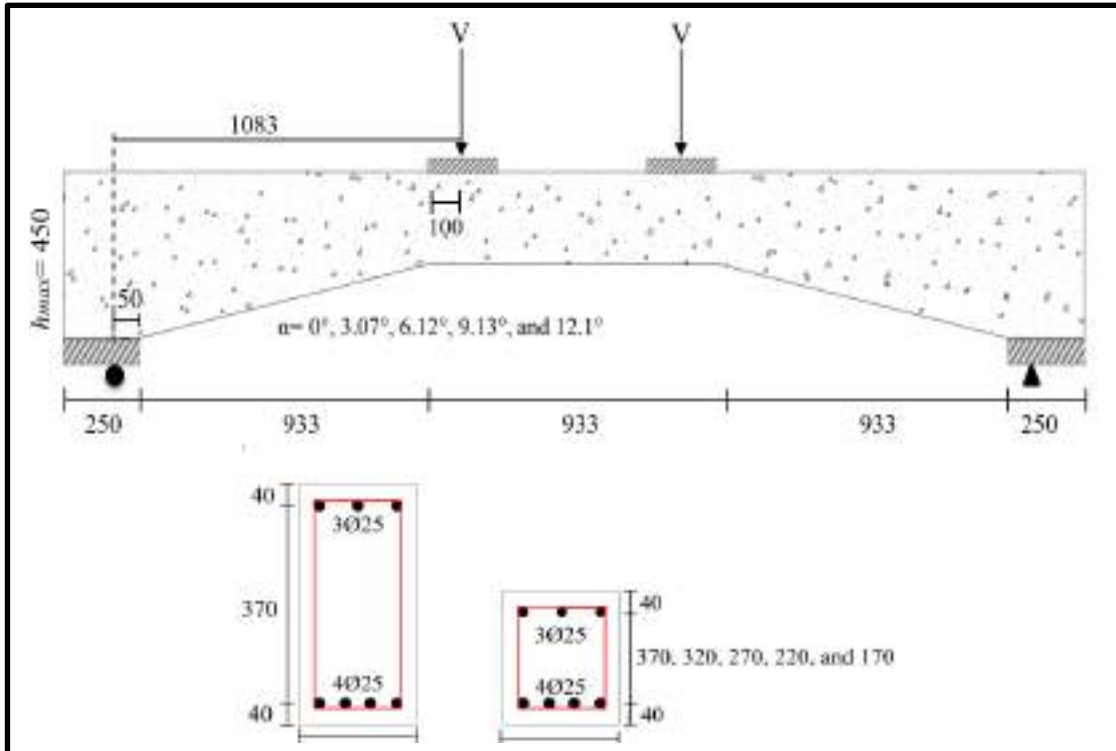


Figure (4-7): Geometry and reinforcement details of RCHBs

Table (4-4): Properties details of RCHBs.

ID	$\alpha$	$f'_c$ (MPa)	Flexural reinforcement		Shear reinforcement	
			Top	Bottom	Haunch length	Vertex
RB30-0	0°	30	3 Ø25	4 Ø25	8SØ10@185mm	
HB30-3	3.07°	30	3 Ø25	4 Ø25	8SØ10@185mm	1S Ø10
HB30-6	6.12°	30	3 Ø25	4 Ø25	8SØ10@185mm	3SØ10@140mm
HB30-9	9.13°	30	3 Ø25	4 Ø25	8SØ10@185mm	3SØ10 @75mm
HB30-12	12.1°	30	3 Ø25	4 Ø25	N/A	3SØ10@45 mm



remained beams are with transverse, longitudinal opening, and specimens used CFRP sheet.

Table (4-6) illustrate the variables treated of this series. The compressive strength of concrete is varying in a wide range comprise values of normal and high strength with different haunch angle. The same table include beams with transverse and longitudinal opening. Also involve beams strengthened and un strengthened by CFRP sheet. As shown in Fig. (4-9) and Table (4-6), three beams (HB30-TO1, HB30-TO2 and HB30-TO3) are modeled with a presence of square lateral opening (100×100) mm (28%h, 25%h, and 23%h) placed from the vertex at distance 230, 415, and 600 mm respectively. The longitudinal central square opening of (50×50), (100×100), and (125×125) mm (10% h, 22% h, and 28% h) performed at the center of cross section of beams (HB30-LO1, HB30-LO2, HB30-LO3) respectively as shown in Fig. (4-10).

External and internal strengthening are used to enhance or restore the expected reduction of shear carrying capacity of beams due to the existence of opening. These methods are:

- 1) Increasing the compressive strength of beams with transverse and longitudinal opening as shown in Table (4-6).
- 2) Using steel reinforcement around the transverse opening in perpendicular direction to the expected crack direction as shown in Fig. (4-11).
- 3) Using CFRP sheet around the beam with opening as shown in Fig. (4-12 a).
- 4) Using two layer of CFRP sheet around the beam with a longitudinal opening to restore the expected loss in strength and stiffness of RCHBs as shown in Fig. (4-12 b).

Tensile stress and Young modulus are calculated according to recommendation and equation that presented by of ACI code.  $f_t$ , and  $E$  values are calculated according to the equations  $0.62\sqrt{f'_c}$  and  $4700\sqrt{f'_c}$  respectively.  $E$  for HSC is calculated according to the equation of Hsu [56].

Table (4-6): Details of specimens (Series 2).

ID	$\alpha$	$f'_c$ (MPa)	Opening size (mm)		Shear reinforcement Ø10 mm		Strengthening type
			Lateral	Longitudinal	Haunch	Vertex	
RB30-0	0°	30	-	-	-	-	-
HB30-3	3.07°	30	-	-	@185mm	1S	-
HB30-6	6.12°	30	-	-	@185mm	3S@140mm	-
HB30-9	9.13°	30	-	-	@185mm	3S @75mm	-
HB30-12	12.1°	30	-	-	N/A	3S @45mm	-
HB40-6	6.12°	40	-	-	@185mm	3S@140mm	-
HB50-6	6.12°	50	-	-	@185mm	3S@140mm	-
HB70-6	6.12°	70	-	-	@185mm	3S@140mm	-
HB40-12	12.1°	40	-	-	N/A	3S @45mm	-
HB50-12	12.1°	50	-	-	N/A	3S@45mm	-
HB70-12	12.1°	70	-	-	N/A	3S @45mm	-
HB30-TO1	6.12°	30	100×100	-	@185mm	3S@140mm	-
HB30-TO2	6.12°	30	100×100	-	@185mm	3S@140mm	-
HB30-TO3	6.12°	30	100×100	-	@185mm	3S@140mm	-
HB30-LO1	6.12°	30	-	50×50	@185mm	3S@140mm	-
HB30-LO2	6.12°	30	-	100×100	@185mm	3S@140mm	-
HB30-LO3	6.12°	30	-	125×125	@185mm	3S@140mm	-
HB30-RO2	6.12°	30	100×100	-	@185mm	3S@140mm	Steel rebar
HB40-TO1	6.12°	40	100×100	-	@185mm	3S@140mm	$f'_c$
HB50-TO1	6.12°	50	100×100	-	@185mm	3S@140mm	$f'_c$
HB40-LO3	6.12°	40	-	125×125	@185mm	3S@140mm	$f'_c$
HB50-LO3	6.12°	50	-	125×125	@185mm	3S@140mm	$f'_c$

Table (4-6): (Continued) Details of specimens (Series 2).

ID	$\alpha$	$f'_c$ (MPa)	Opening size (mm)		Shear reinforcement $\varnothing 10$ mm		Strengthening type
			Lateral	Longitudinal	Haunch	Vertex	
HB30-CT1	6.12°	30	100×100	-	@185mm	3S@140mm	CFRP
HB30-CL3	6.12°	30	-	125×125	@185mm	3S@140mm	CFRP

HB30-3: Haunched beam- 30 compressive strength- haunch angle 3°.

TO1, 2, & 3: Beam with transverse opening with different locations.

LO1, 2, & 3: Beam with longitudinal with different sizes.

RO2: Beam with transverse opening reinforced by steel rebar.

CT1: Beam with transverse opening near the vertex reinforced by CFRP.

CL3: Beam with larger longitudinal opening reinforced by CFRP.

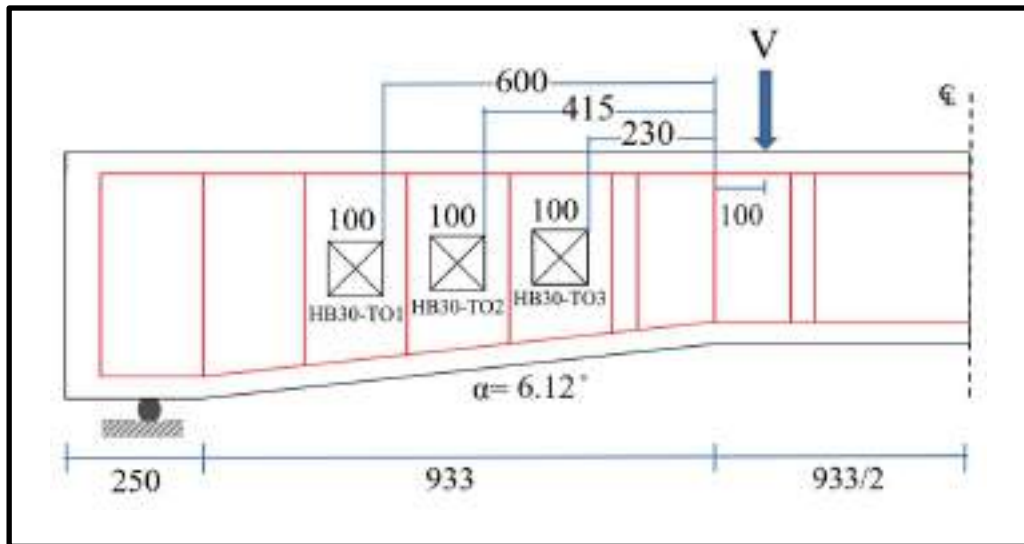


Figure (4-9): Details of three RCHBs have transverse opening with different positions.

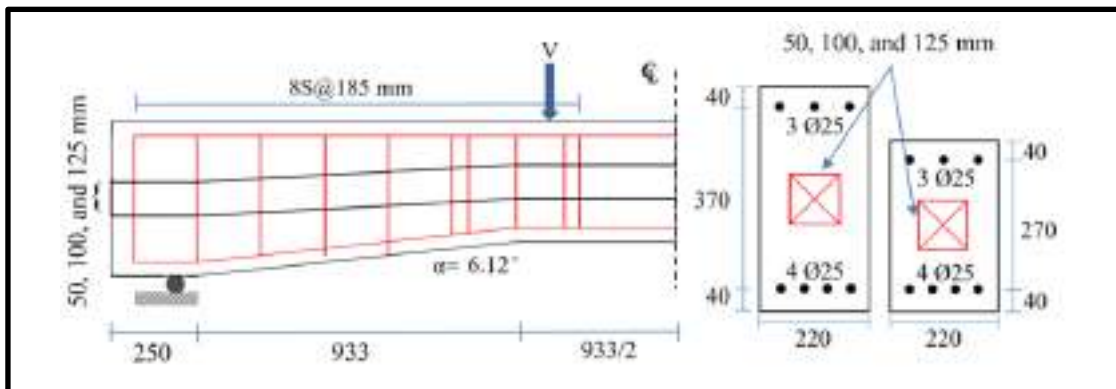


Figure (4-10): Details of three RCHBs have longitudinal opening with different sizes.

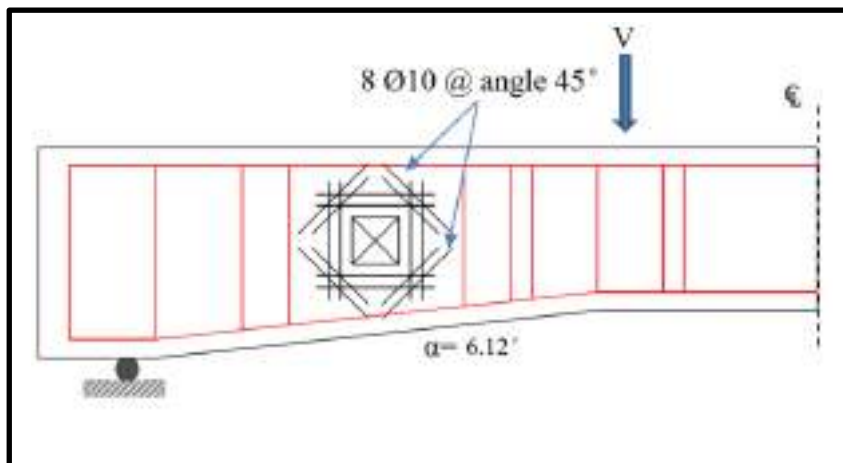
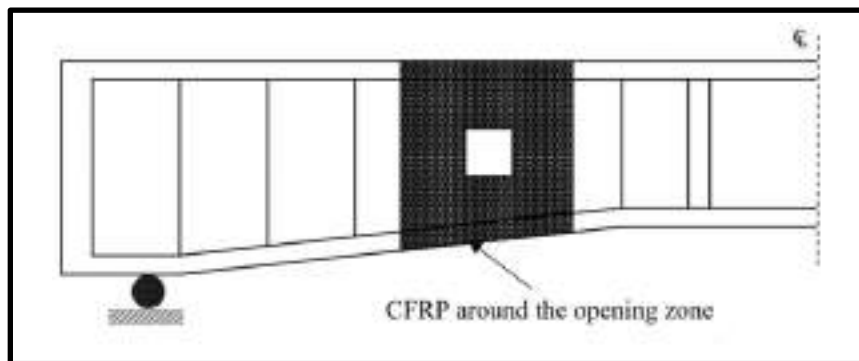
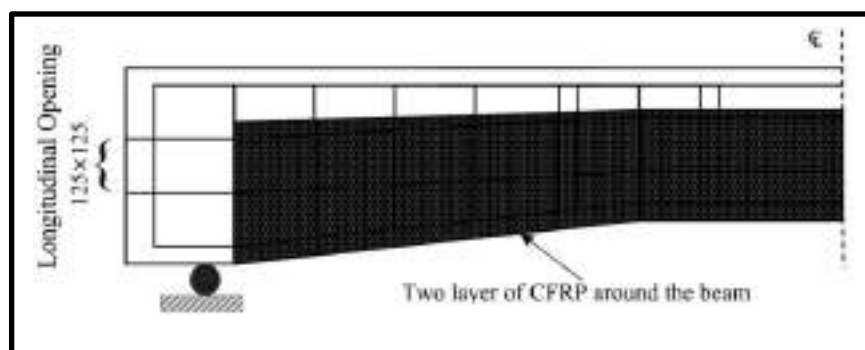


Figure (4- 11): Reinforcement details of beam with an opening (HB30-RO2).



(a) Beam (HB30-CT1) with a lateral opening retrofitted by CFRP sheet.



(b) Beam (HB30-CL3) with a longitudinal opening retrofitted by two layer of CFRP sheet.

Figure (4-12): Details of strengthened RCHBs by CFRP.

### 4.4.3 Series Three

A total of six simply supported beam (five of them are RCHBs with negative haunch angle and one prismatic) are investigated in this series, which designed to fail in flexure. The haunch angle, and presence of transverse opening and strengthened with CFRP sheet are the main variables regarded in this series. The beam width ( $b$ ), over all height ( $h$ ), and effective span ( $L$ ) are 150, 240, and 1350 mm respectively.

Stirrups  $\text{Ø}10$  mm @ 55 mm are used to insure that the failure will be in flexure with additional stirrups at the vertex  $3 \text{Ø}10@25$  mm. Also, three bottom longitudinal bars  $\text{Ø}12$  are used. Simply supported RCHBs subjects to two-point load at the vertex zone as illustrated in Fig. (4-13).  $f'_c$  for the tested beam is 63.25 MPa with tensile strength 6.47 MPa. The used steel bars with a yield stress 494 and 516 MPa for the longitudinal bars and stirrups respectively. All beams in this series are presented in Table (4-7).

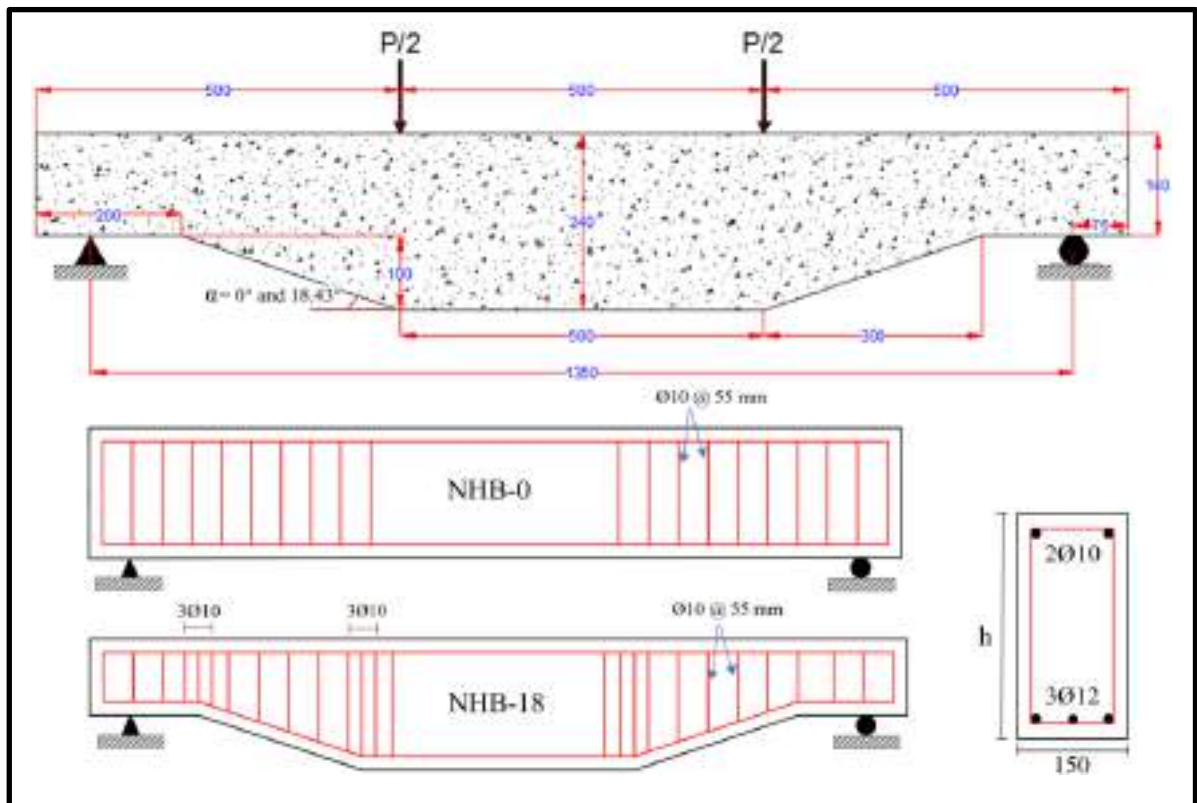


Figure (4-13): Details of RCHBs in series three.



The large rectangular transverse opening of dimension (120×140) mm (0.5 h) at the mid-span of beam (NHB-TO1) are presented with the same geometry and properties of the control beam (NHB-18) with negative haunch angle 18.34° as shown in Fig. (4-14).

External strengthening is used to enhance or compensate the expected reduction of shear carrying capacity of beams due to the existence of opening. These methods are:

- 1) Using CFRP sheet for the beam with an opening (NHB-C1) as shown in Fig. (4-15 a).
- 2) Using CFRP sheet around the beam (NHB-C2) as shown in Fig. (4-15 b).
- 3) Using CFRP sheet at the bottom of the beam (NHB-C3) as shown in Fig. (4-15 c).

Table (4-7): Details of specimens (Series 3).

ID	$\alpha^\circ$	$f'_c$ (MPa)	lateral Opening (mm)	Shear reinforcement	Retrofitting Type
NHB-0	0°	63.25	-	Ø10 @ 55 mm	-
NHB-18	-18.34°	63.25	-	Ø10 @ 55 mm	-
NHB-TO1	-18.34°	63.25	120×140 mm	Ø10 @ 55 mm	-
NHB-C1	-18.34°	63.25	120×140 mm	Ø10 @ 55 mm	CFRP
NHB-C2	-18.34°	63.25	-	Ø10 @ 55 mm	CFRP
NHB-C3	-18.34°	63.25	-	Ø10 @ 55 mm	CFRP

NHB-18°: Negative haunch beam-Haunch angle 18°.

TO1: Beam with transverse opening.

C1, C2 & C3 : Beam with CFRP.

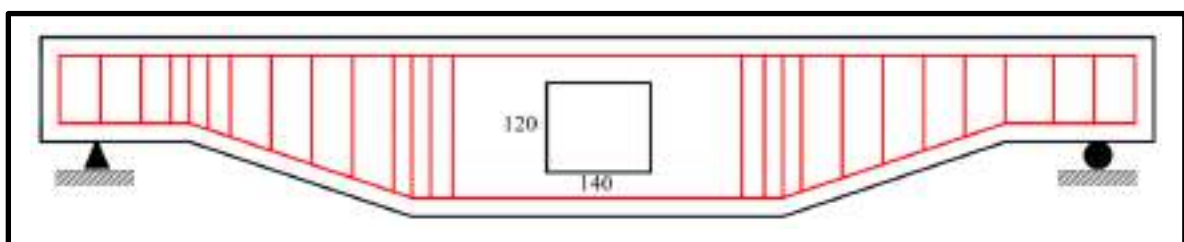
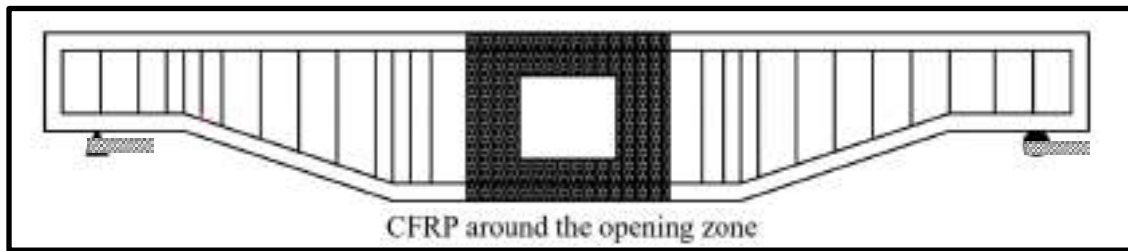
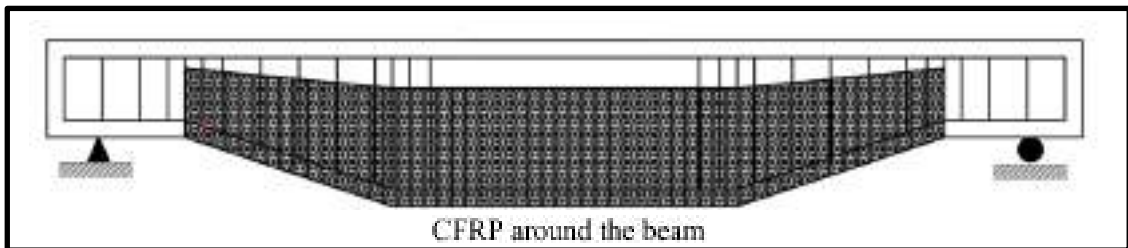


Figure (4-14): Flexural beam with mid-span opening (NHB-TO1).

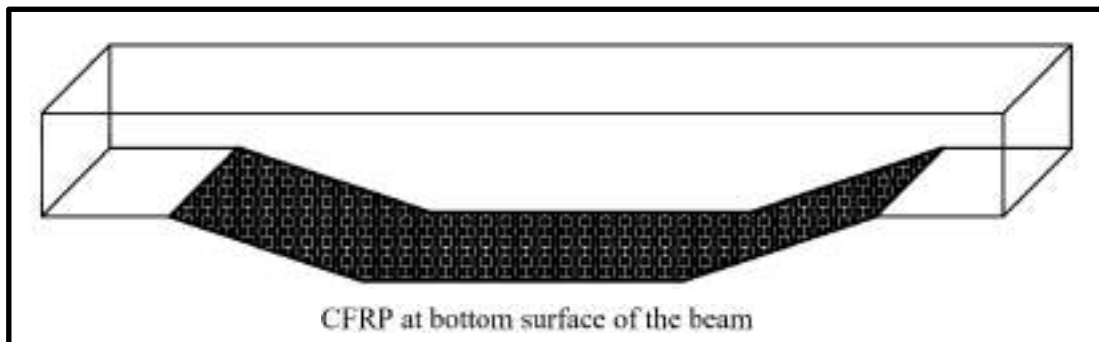




(a) Beam (NHB-C1) with CFRP sheet around the opening.



(b) Beam (NHB-C2) with CFRP around the beam.



(c) Beam (NHB-C3) with CFRP sheet at the bottom of beam.

Figure (4-15): RCHBs retrofitted by CFRP sheet.

## **4.5 Presentation and Discussion of Results**

### **4.5.1 Series One**

#### **4.5.1.1 Load-Deflection Relationship**

The numerical studies are accomplished to predict the capability of the behavior of inverted RCHBs under static shear. Used parameter are implemented to examine the influence of these parameters on the behavior of inverted RCHBs. These parameters are varied compressive strength of beams with and without stirrups, amount of stirrups, existence of the transverse opening, and using CFRP to strengthening the beams with transverse opening and strengthening the solid beams.

Results of the analysis of series one are presented in Table (4-8) and Figs. (4-16) to (4-26). The results include bar charts for the relationship between the variables and load-deflection curve. It is noticed from these figures that RCHBs appear a linear behavior till the appearance of the first diagonal cracks. At the first loading stage, trend of load-deflection curves for beams with and without shear reinforcement are almost similar until the first cracking occurs. After this stage of loading, the strength and deformation begin to dissimilar due to contribution of the stirrups.

It can be observed, that RCHBs with and without shear reinforcement have deformation capacity distinctly different with respect to the prismatic beam. After the diagonal cracks occur, the prismatic beams loses all capacity to carry the load through deformation.

In this analysis, the control beam behavior is linearly elastic up to about (22%) for prismatic beam (1L1) and (16-22%) for inverted RCHBs of the maximum failure load. Overhead this point, the load increases gradually up and reaches to the maximum load capacity.

The effect of increasing the haunch angle from  $0^\circ$  to  $3.95^\circ$  and  $5.91^\circ$  shows decreasing in the shear capacity with slight increasing in the deflection. In

addition, the prismatic beam shows a higher stiffness than RCHBs as depicted in Fig. (4-16), (4-17), and Table (4-8).

Table (4-8): Results of inverted RCHBs in series one.

Beam	Crack load (kN)	Deflection at crack load (mm)	Failure load (kN)	Maximum deflection (mm)
1L1	32	1.5	147	12.2
2L1	24	0.72	135	13
3L1	26	1.56	133	15
IHB50	34	1.16	198	22.6
IHB70	45	1.31	226	33.7
IHB30-S100	32	1.6	170	16.2
IHB30-S150	32	1.6	161	13.5
IHB30-S200	32	1.55	155	13.9
IHB50-S100	47	2.16	236	19.1
IHB70-S100	57	1.8	346	38.63
IHB30-TO1	24	1.24	109	10.7
IHB30-TO2	24	1.07	118	12
IHB30-TO3	24	1.3	124	11.3
IHB40-TO1	30	1.3	145	15.4
IHB30-C1	25	1.3	151	18.3
IHB30-C2	24	1.1	157	17.1

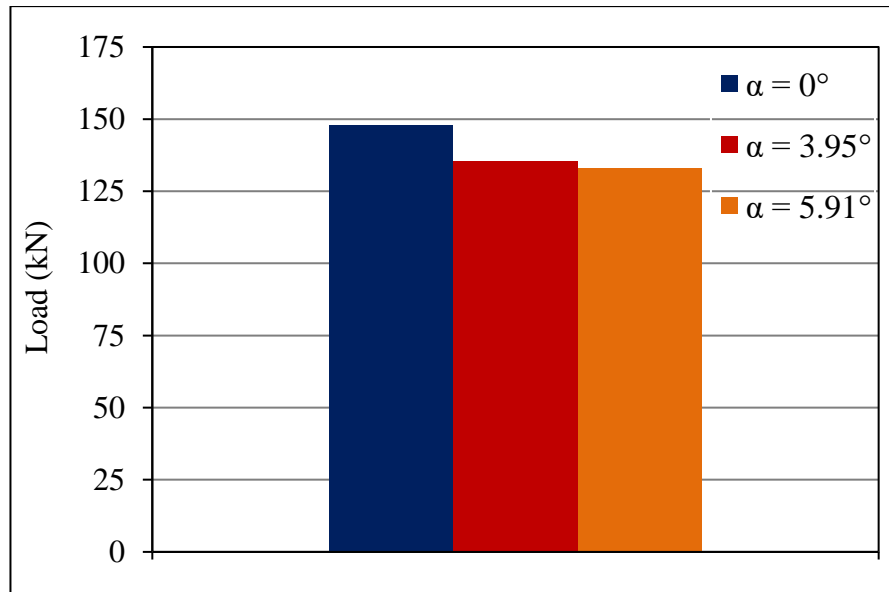


Figure (4-16): Relationship between the ultimate load and the haunch angle.

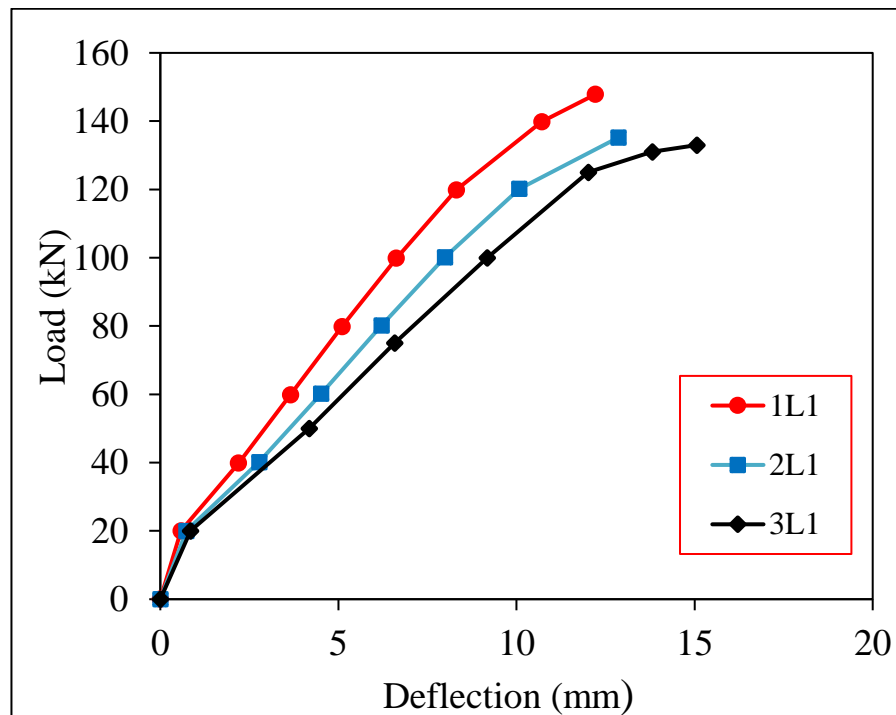
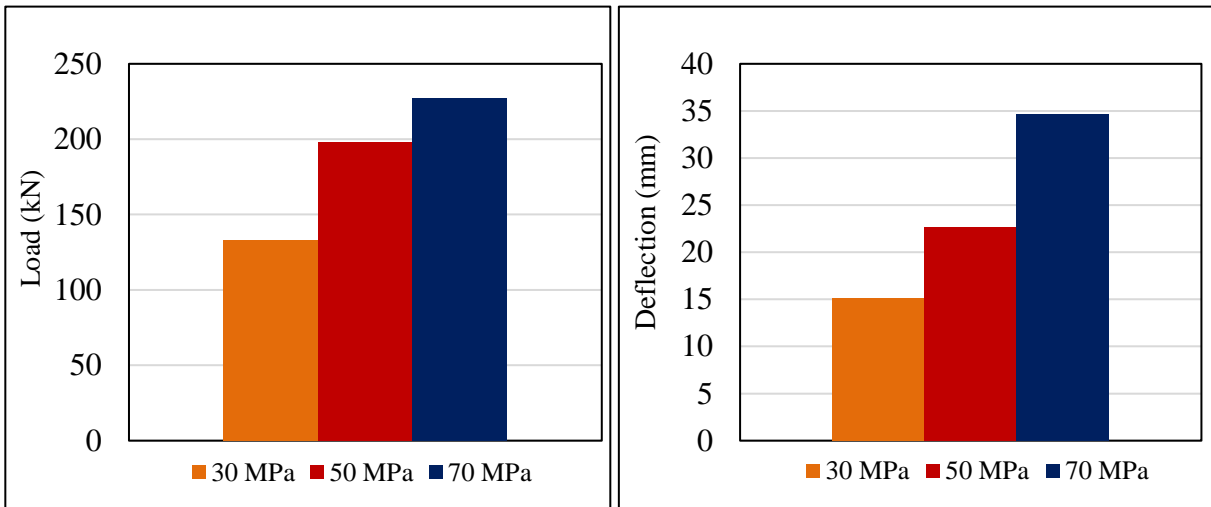


Figure (4-17): Load-deflection curve for effect of increasing the haunch angle.

For inverted RCHBs without stirrups (IHB50 and IHB70), increasing the compressive strength from 30 to 50 and 70 MPa shows increasing in the ultimate strength for shear by (49% and 70%) respectively. Also, large increase in the deflection occur by about (50% and 125%) respectively. It should be noted that

increasing to 70 MPa in beam (IHB70) without stirrups turned the failure from shear to flexural failure as demonstrated in Fig. (4-18) and (4-19).



**Figure (4-18): Effect of the compressive strength on the ultimate load and the deflection on the inverted RCHBs without shear reinforcement.**

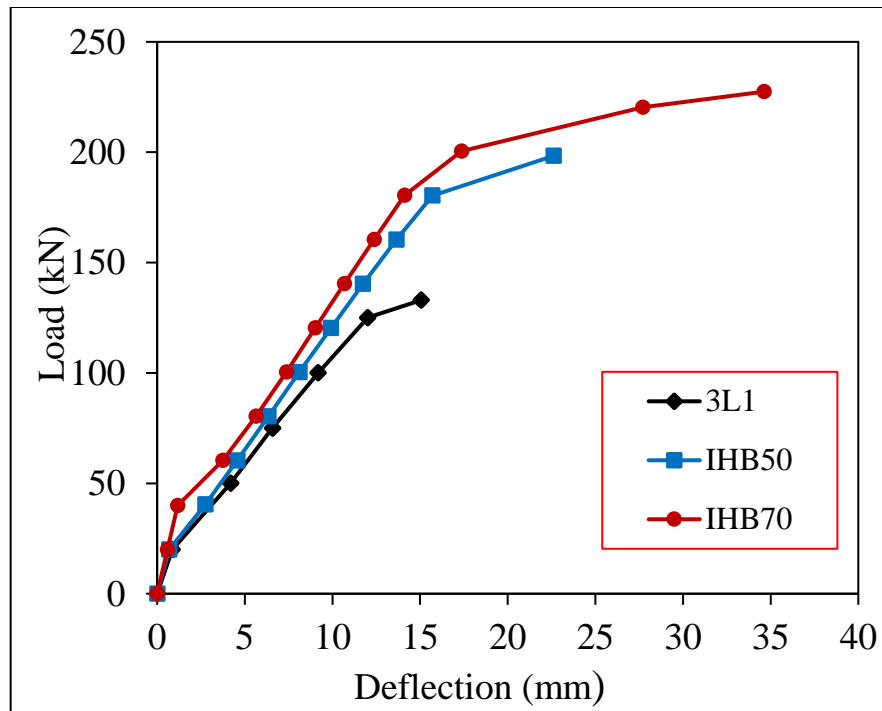


**Figure (4-19): Load-deflection curve for effect of increasing  $f'_c$  for beams without shear reinforcement.**

Presence of stirrups using  $\text{Ø}10$  mm @ (100, 150, and 200 mm) enhance the shear strength by (28%, 21%, and 17%). Using stirrups for spacing @ (150 and 200) mm caused reduction in the deflection while, for @100 mm saves the same deflection approximately as shown in Fig. (4-20).

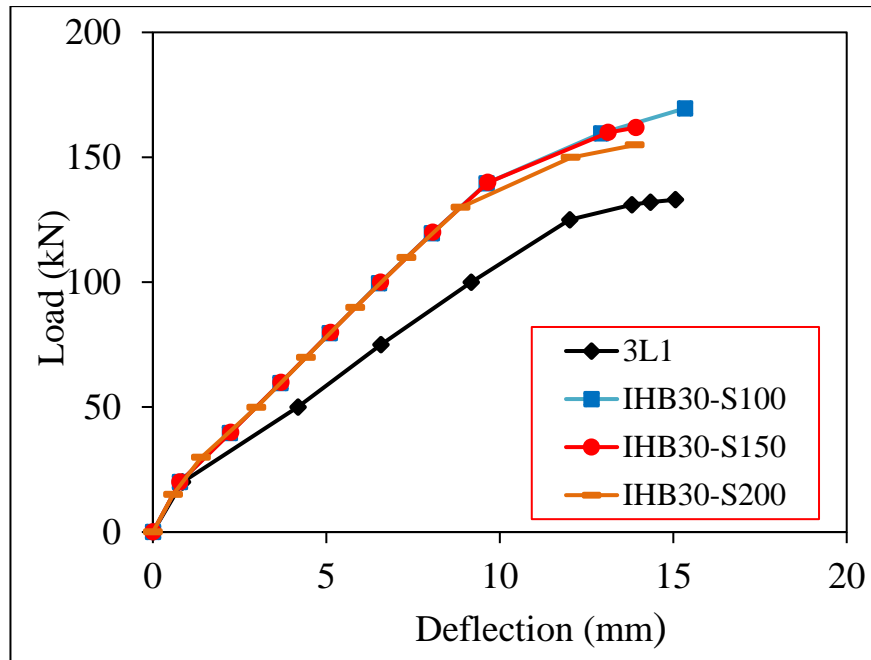


**Figure (4-20): Load-deflection curve for effect of presence of stirrups with different spacing.**

Increasing the  $f'_c$  to 50 and 70 MPa for RCHBs with stirrups (IHB50-S100 and IHB70-S100) lead to increasing in the ultimate strength of the inverted RCHBs with stirrups by (39 % and 103%) respectively in comparison with beam (IHB30-S100). The deflection increases by (18% and 138%) respectively as shown in Fig. (4-21) and (4-22). Ductility of inverted RCHBs significantly enhance with increasing the  $f'_c$  because the concrete is at the sides of the beam while in the mid-span, the steel bars control all the beam deflection in this region.

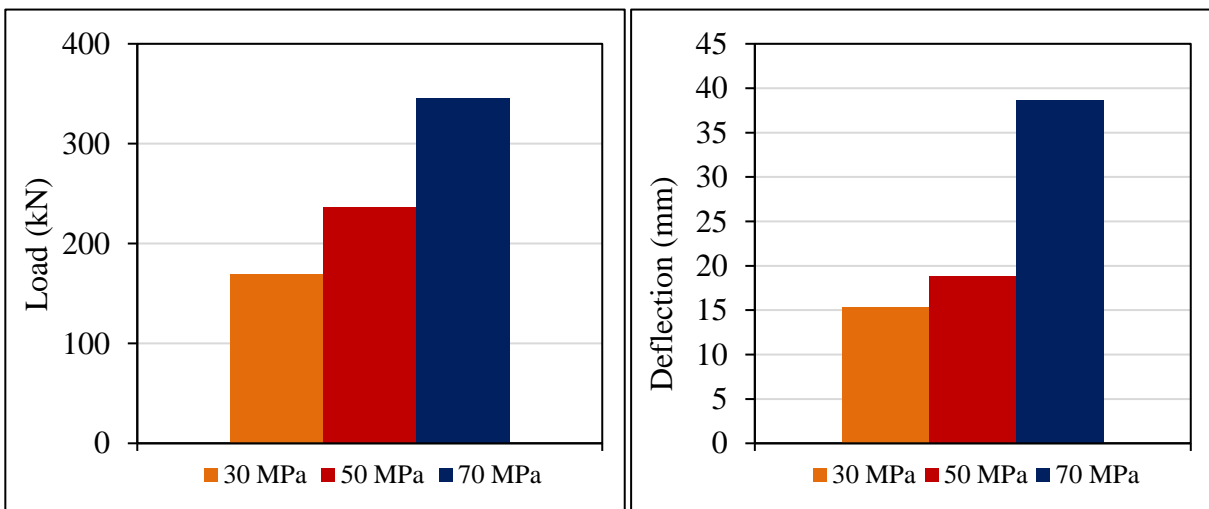


**Figure (4-21): Effect of the compressive strength on the ultimate load and the deflection on the inverted RCHBs with shear reinforcement.**

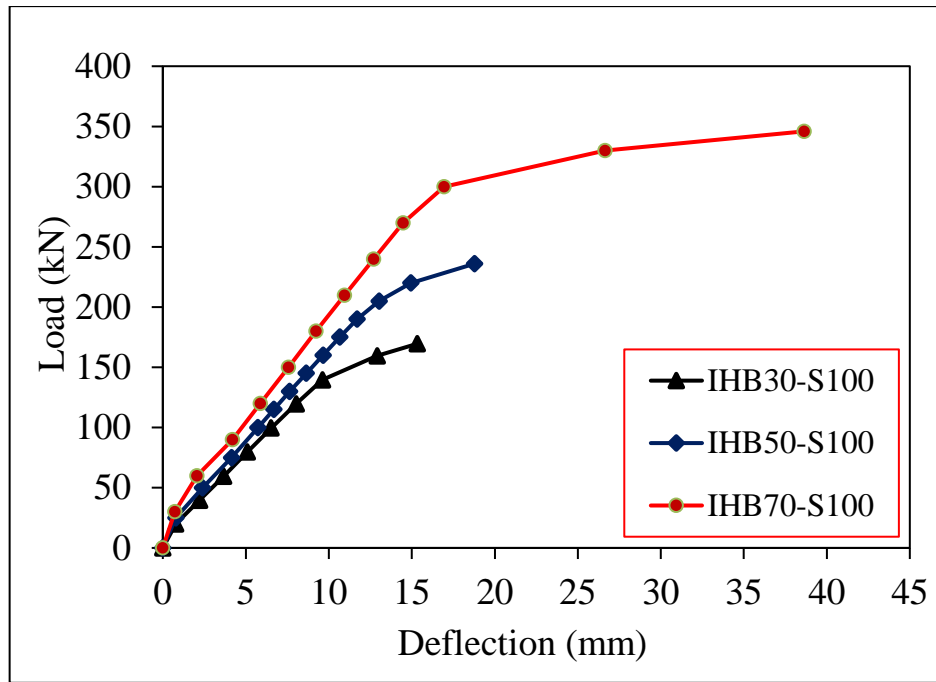


**Figure (4-22): Load-deflection curve for effect of increasing  $f'c$  for beams with shear reinforcement.**

Presence of transverse opening (100×100) mm with different location in the haunch zone affected the shear strength. Specimens (IHB30-TO1, IHB30-TO2, and IHB30-TO3) show decreasing in the shear strength and stiffness. The reduction of ultimate capacity is (20%, 13%, and 8%) for these three beams respectively when compared with the solid beam (2L1). Hence, the variance in the reduction values is due to the location of these openings. The opening position has a significant effect on the shear capacity, this effect becomes larger when the opening position is near the support due to the sensitivity of this location and to the decreasing in depth. Specimen with transverse opening near the support (IHB30-TO1) has maximum reduction in ultimate load by (20%) and in deflection by (17%). Other specimens with opening have a slight decrement in deflection as shown in Fig. (4-23).

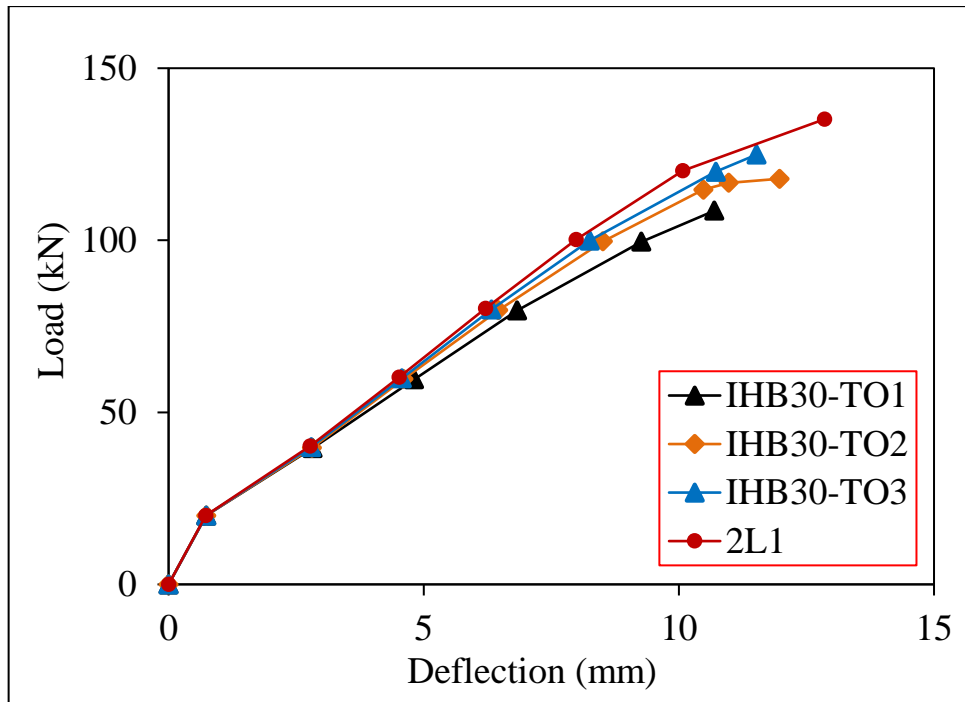


Figure (4-23): Load-deflection curve of beams with transverse opening.

One of the suggested solutions to compensate the loss in strength of specimen with an opening is raising the  $f'_c$  to 40 MPa which shows increment in the shear capacity and restoring all the loss in shear strength with gaining additional strength by (7%) as exhibited in Fig. (4-24).

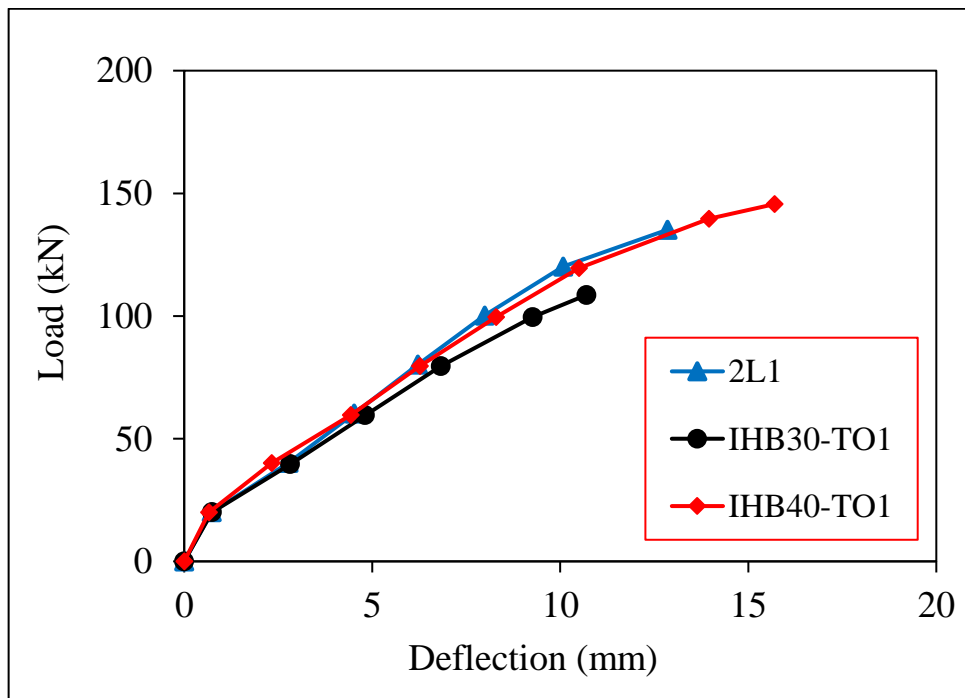


Figure (4-24): Load-deflection curve for beams with lateral opening strengthened by increasing  $f'_c$ .



Using CFRP to retrofit the RCHBs with opening near support showed compensation all the weakness and strengthening the beam by (12%) as additional strength with providing large ductility. Solid inverted RCHBs with CFRP strips has enhancing in the failure load by (16%) as shown in Fig. (4-25) and (4-26).

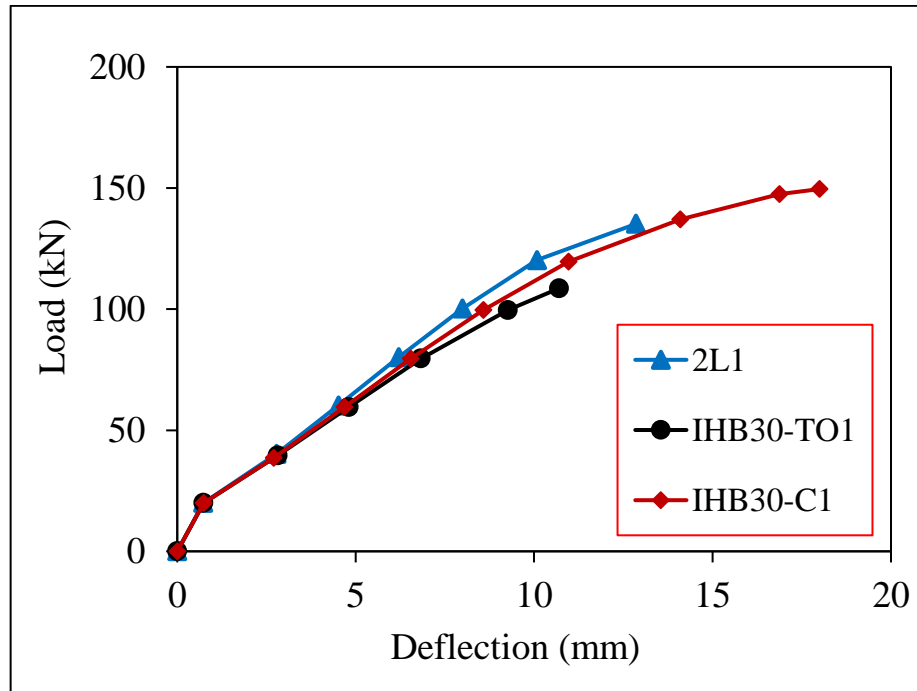


Figure (4-25): Load-deflection curve for beam with lateral opening retrofitted by CFRP sheet.

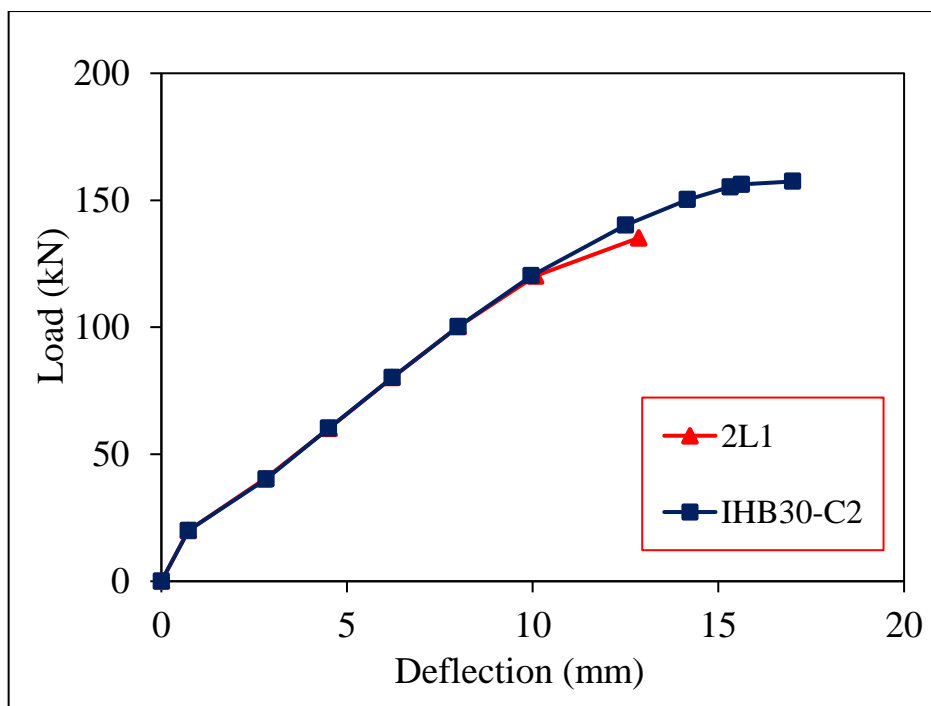


Figure (4-26): Load-deflection curve for beam retrofitted by CFRP sheet.

### **4.5.1.2 Crack Pattern**

In ANSYS computer program, the cracking or crushing types of fracture in concrete elements appear as circles at locations of these cracking or crushing, the shape of each crack and crush in concrete element is summarized as follows;

- 1) Cracking is displayed with a circle outline in the plane of the crack,
- 2) Crushing is displayed with an octahedron outline.
- 3) If the crack has opened and then closed, the circle outline will have an X designation through it.

In ANSYS, outputs, i.e. stresses and strains, are calculated at integration points of the concrete solid elements. Fig. (4-27) shows integration points in a concrete solid element [75].

Each integration point of brick element can crack in up to three different planes. The first crack at an integration point is displayed with a red circle outline. The second crack is presented with a green circle outline. While the third crack is displayed with a blue circle outline [76].

Symbols displayed at the centroid of elements are based on the state of all element's integration points. If one of these integration point through the element has crushed, the crushed symbol is shown at the centroid of the element. If any integration point has cracked or cracked and closed, the cracked symbol is shown at the element centroid. The cracked symbol is displayed at the element centroid If at least five integration points have cracked and closed. Lastly, if two or more integration point has cracked, the circle skeleton outline in the element centroid shows the average orientation of all cracked planes for that element [76].

An appearance of cracking sign occurs when a principal tensile stress exceeds the ultimate tensile strength of the concrete and appears perpendicular to the direction of the principal stress. The cracking sign appearance be perpendicular to the direction of the principal stress as explained in Fig. (4-28).

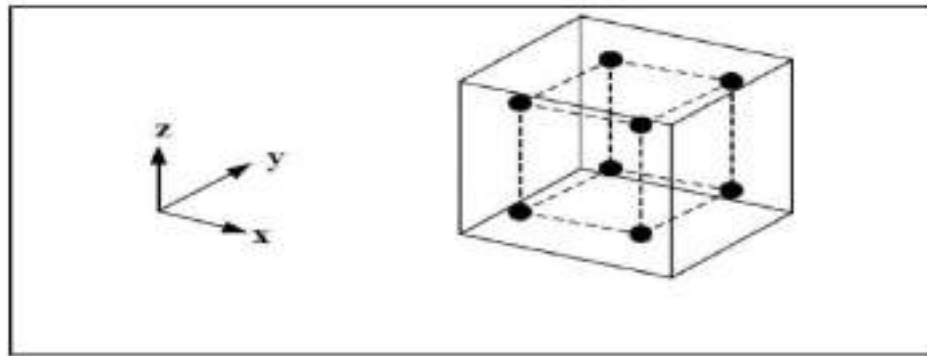


Figure (4-27): Integration points in concrete solid element [75].

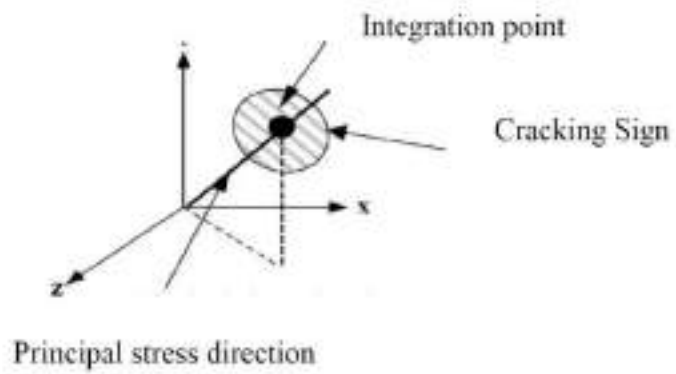
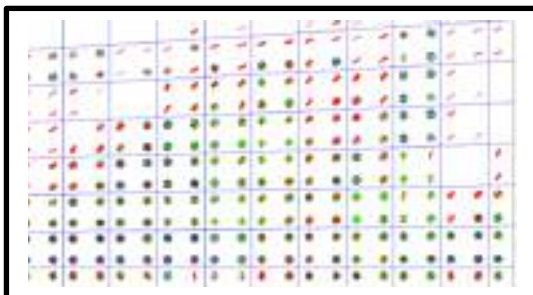
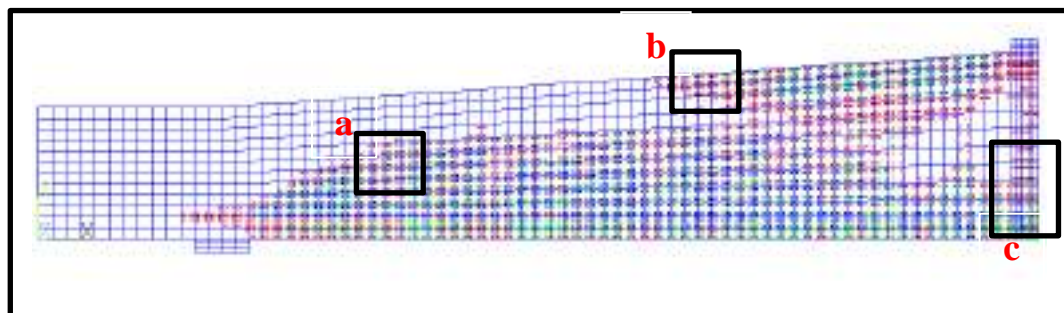
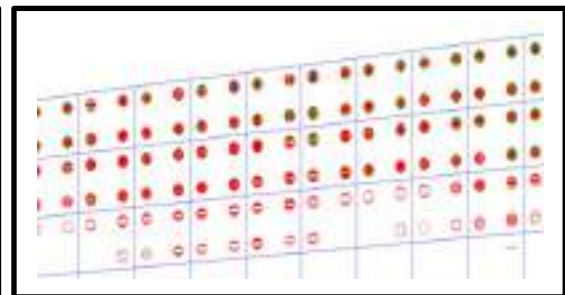


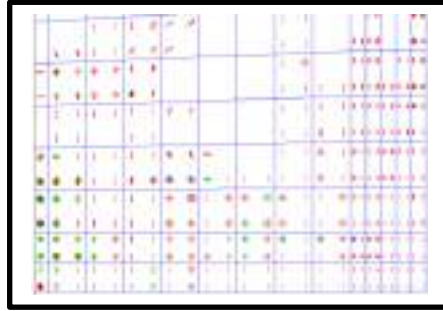
Figure (4-28): Cracking sign [75].



(a)








(b)



(c)

**Figure (4-29): Cracking signs occurring in FE models.**

The cracking signs in Figure (4-29) are explained below:

-  Sign of the flexural crack.
-  Sign of the compressive crack.
-  Sign of the diagonal tensile crack.
-  Sign of two cracks (the first crack is diagonal tensile crack and the second crack is compressive crack, it's shown with a green circle outline).
-  Sign of three cracks (the first and second cracks are diagonal tensile cracks and the third crack is compressive crack, it's shown with a blue circle outline).

The typical crack pattern at failure stage of each specimen in this series has been seen in Fig. (4-30). From these figures, it can be observed that the failure region of prismatic beam is the path from the support to the loading zone.

The first crack appeared at (16-22%) from the failure load for the all inverted RCHBs in this series. Amount of cracks increase with increasing in the applied load. For inverted RCHBs with stirrups, diagonal cracks developed in the shear span (haunch region) from the support toward the loading zone. At this stage, the failure is occurring. In the case of RCHBs without shear reinforcement, little amount of diagonal shear cracks enough to make the failure with the same path of cracks.

Crack pattern are basically affected by the attendance of parameters in comparison with the control beams as revealed in Figs. (4-30). Parameters effectiveness on the crack pattern is clarified as follows;

Increasing the inclination angle of haunch reduced the amount of propagated cracks. Shear cracks for prismatic beam is larger than inverted RCHBs. Also, flexural cracks for RCHBs is greater than prismatic one as shown in Fig. (4-30 a) to (4-30 c).

Increasing  $f'_c$  of the inverted RCHBs caused developing more shear and visible flexural cracks. Increasing  $f'_c$  to 50 and 70 MPa for inverted RCHBs without stirrups (IHB50 and IHB70) developed new flexural cracks at the mid-span of length besides more shear cracks are developed as presented in Figs. (4-30 d) and (4-30 e).

Existence of the stirrups enhanced the propagation of shear and compression cracks. More cracks developed according to the spacing of stirrups, larger amount of cracks developed for the minimum spacing (beam IHB30-S100) as displayed in Figs. (4-30 f) to (4-30 h).

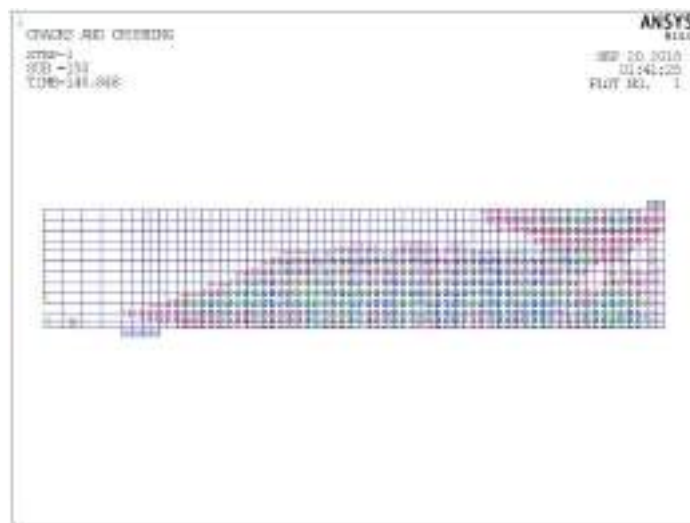
Increasing  $f'_c$  to 50 and 70 MPa for beams with stirrups (IHB50-S100 and IHB70-S100) decreased the compression cracks significantly and increased the shear and flexural cracks as shown in Fig. (4-30 i) and (4-30 j).

Existence of an opening with different location redistributed the crack propagation, decreased the compression and flexural cracks in wide range, and presented more shear cracks at the corner of the opening. For beam (IHB30-TO1) with an opening near the support, zone of the opening testified a large cracks amount while, the other zones of the beam were suffering a little cracks. Max. reduction in the cracks at the compression region occurred with beam (IHB30-TO2). As demonstrated in Fig. (4-30 k) to (4-30 m).

One of the factors affecting the pattern of cracking in this study is increasing the compressive strength of the beam containing an opening. Increasing the  $f'_c$  of the beam with an opening near the support showed that more cracks developed at the opening corners. Also, additional cracks started to develop at the top surface of the inverted RCHBs. Flexural cracks are significantly reduced due to increasing the concentration in the opening region. Also, diagonal cracks propagation is greatly enhanced as displayed in Fig. (4-30 n).

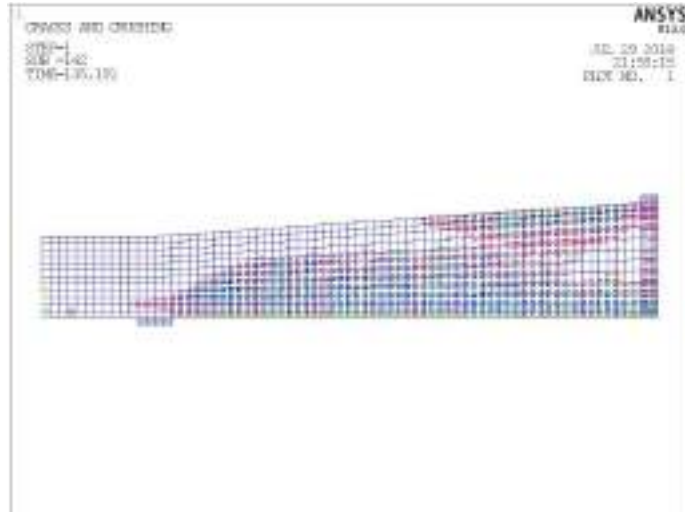
Beam (IHB30-C1) with an opening near the support strengthened with CFRP sheet greatly propagated the cracks along the haunch zone. Flexural cracks reduced due to the redistribute the stress distribution along the beam and CFRP sheet provided more stiffness to the region of opening as exhibited in Fig. (4-30 o). Using CFRP to strengthening the solid inverted RCHBs enhanced the cracks spread. Additional shear and compression cracks are presented along the haunch as displayed Fig. (4-25 p).

Energy absorption is greatly affected by increasing the compressive strength, stirrups existence, and using CFRP. Additional Cracks along the haunch which made the haunch is semi distorted with increasing in the deflection. Strengthening by CFRP is the best method to enhance the energy absorption for these beams.

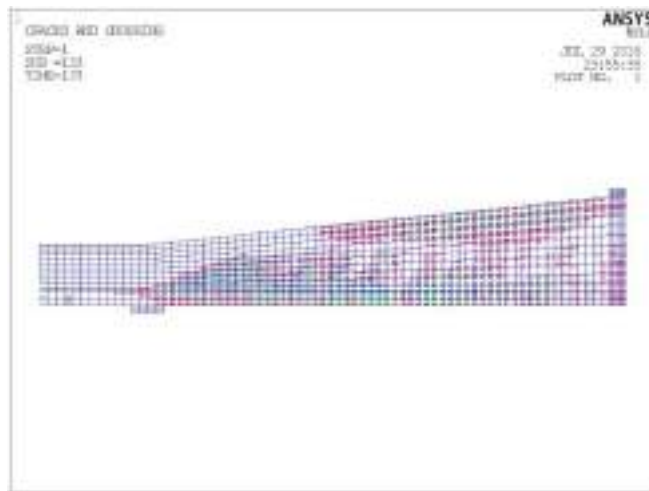


(a) Crack pattern for prismatic beam (1L1).

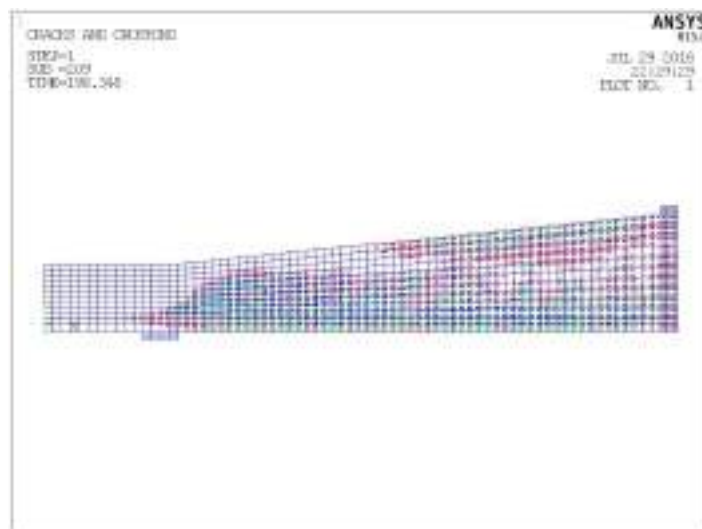
Figure (4-30): Crack pattern for series one beams.



(b) Crack pattern for beam (2L1).



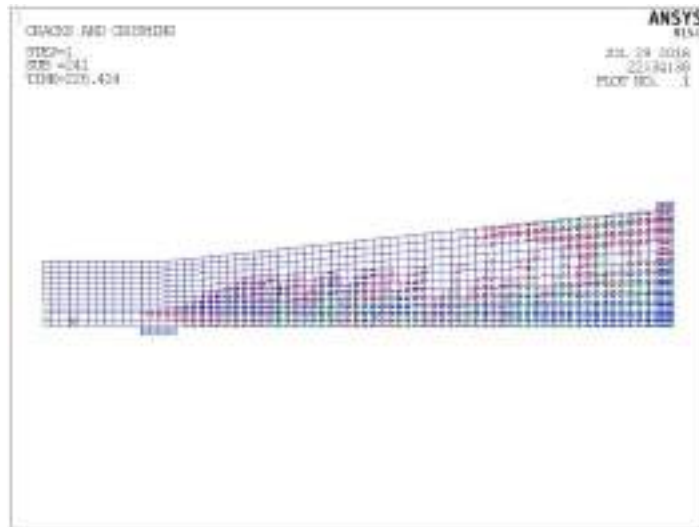
(c) Crack pattern for beam (3L1).



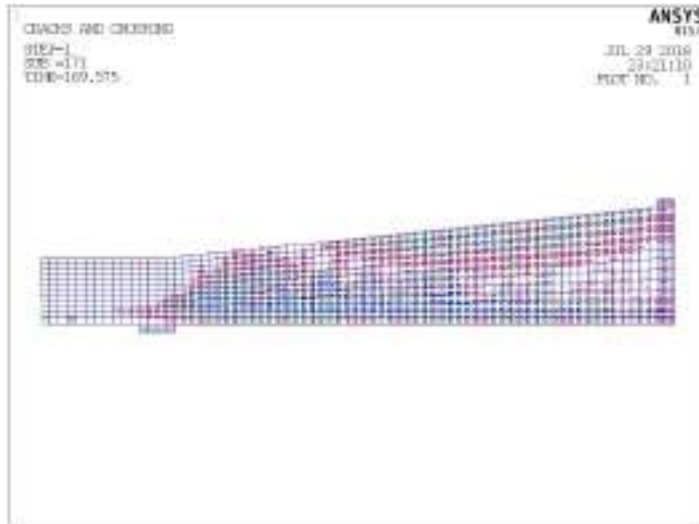
(d) Crack pattern for beam (IHB50).

Figure (4-30): Cont.

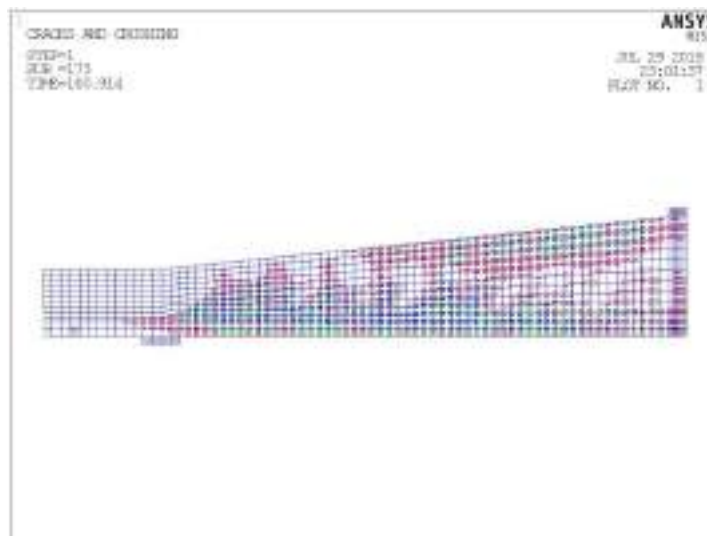




(e) Crack pattern for beam (IHB70).



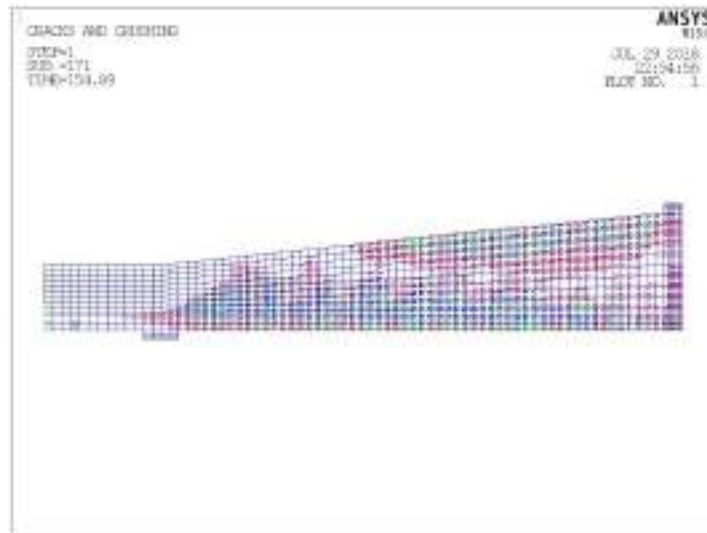
(f) Crack pattern for beam (IHB30-S100).



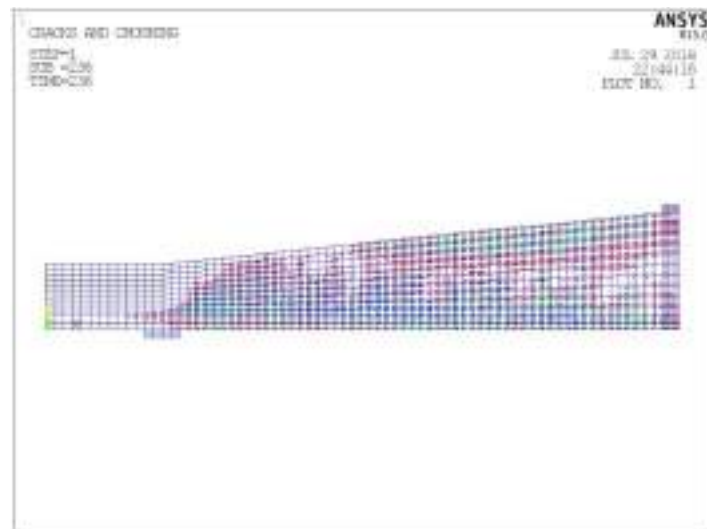
(g) Crack pattern for beam (IHB30-S150).

Figure (4-30): Cont.

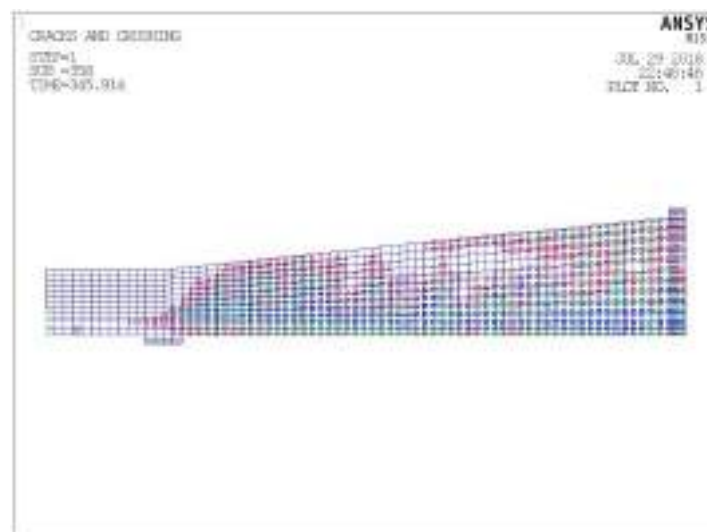




(h) Crack pattern for beam (IHB30-S200).

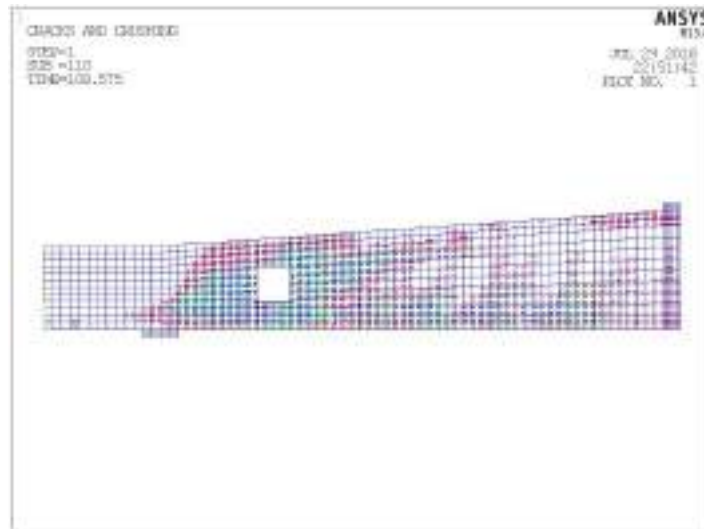


(i) Crack pattern for beam (IHB50-S100).

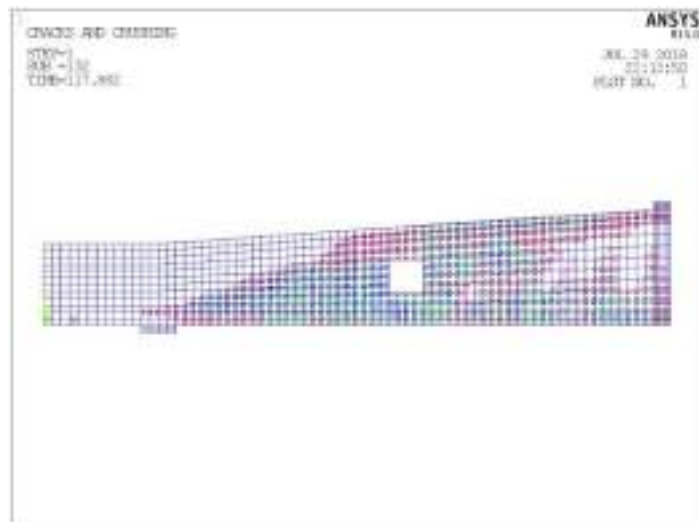


(j) Crack pattern for beam (IHB70-S100).

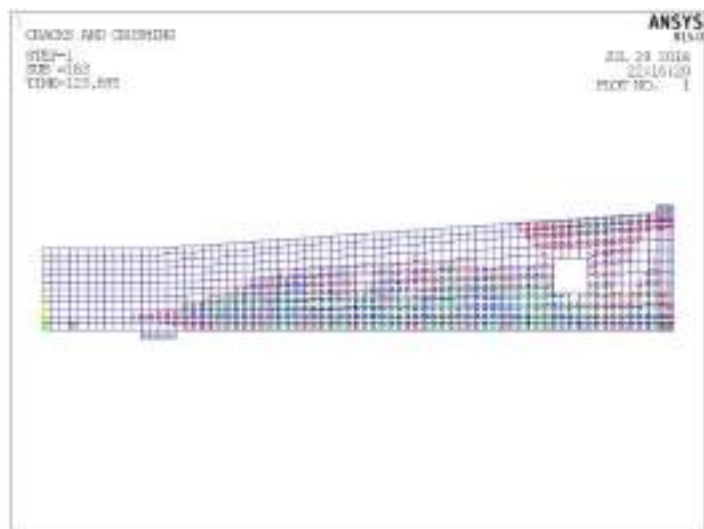
Figure (4-30): Cont.



(k) Crack pattern for beam (IHB30-TO1).

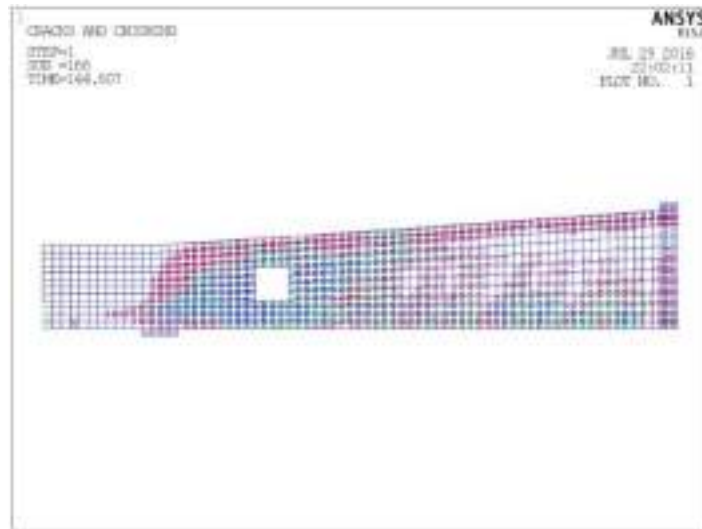


(l) Crack pattern for beam (IHB30-TO2).

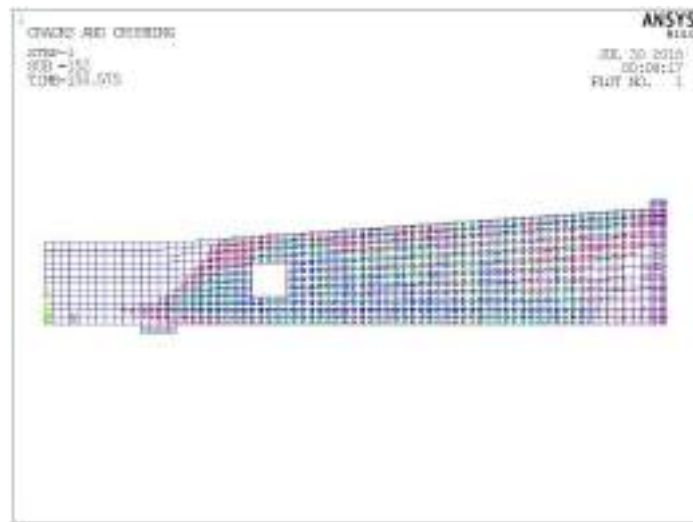


(m) Crack pattern for beam (IHB30-TO3).

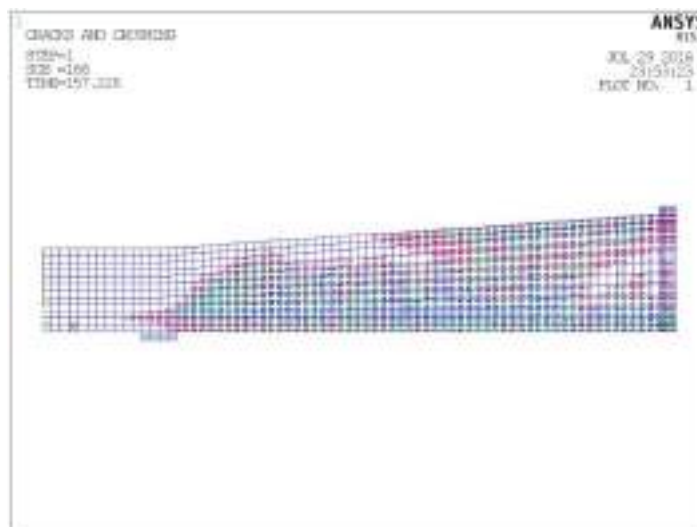
Figure (4-30): Cont.



(n) Crack pattern for beam (IHB40-T01).



(o) Crack pattern for beam (IHB30-C1).



(p) Crack pattern for beam (IHB30-C2).

Figure (4-30): Cont.

## **4.5.2 Series Two**

### **4.5.2.1 Load-Deflection Relationships**

The comparison between the experimental and theoretical analysis results for the failure load besides the deflection and crack pattern gives a confidence to implement the parameters.

The ultimate load of the modeled beams is indicating state that the beams cannot support any additional load because of the convergence failure of ANSYS.

The load-deflection curves and results of the series two beams with and without shear reinforcement are presented in Table (4-9) and Figs. (4-31) to (4-43). It is noticed from these figures that RCHBs have a linear behavior till the first cracking process.

At the first loading stage, trend of load-deflection curves for beams with and without shear reinforcement are almost similar until the first cracking occurs. After this stage of loading, the strength and deformation begin to dissimilar due to contribution of the stirrups.

From the result obtained, it can be observed that RCHBs with and without stirrups have deformation capacity distinctly different with respect to the prismatic beam. After the diagonal cracks occur, the prismatic beams lose all capacity to carry the load through deformation.

In this analysis, the load-deflection curve for specimens is linearly elastic up to about (18%) for prismatic beam and (15-30%) for RCHBs of the maximum failure load ( $V_u$ ).

Overhead this point, the load rises gradually up and reaches the nonlinearity zone to the maximum load capacity as shown below in Table (4-9).

Table (4-9): Results of RCHBs in series two.

Beam	Crack load (kN)	Deflection at crack load (mm)	Failure load (kN)	Maximum deflection (mm)
RB30-0	44	13	253	24
HB30-3	36	2.4685	184	22.1
HB30-6	25	2.175	164	25.4
HB30-9	22	2.55	117	25.95
HB30-12	11.5	2.575	38	16.3
HB40-6	33	2.675	198	28.83
HB50-6	38	3	225	31.986
HB70-6	55	4.4	257	59.7
HB40-12	13	2.375	57	18
HB50-12	17	2.8	75	21.3
HB70-12	20	2.23	137	33
HB30-TO1	25	2.6	139	22
HB30-TO2	25	2.3	127	21.2
HB30-TO3	25	2.1	117	19.3
HB30-LO1	25	2.3	135	23.2
HB30-LO2	24	2.2	115	18.6
HB30-LO3	24	2.3	101	17.2
HB30-RO2	25	2.2	152	23.3
HB40-TO1	32	2.4	156	27.75
HB50-TO1	38	2.6	189	29.74
HB40-LO3	33	2.8	136	20.3
HB50-LO3	39	3.8	170	28.24
HB30-CT1	32	3	151	25.9
HB30-CL3	32	3.75	161	35.75

The effect of increasing the haunch angle from  $0^\circ$  to  $9.13^\circ$  exhibit decreasing in the shear capacity with slight increase in the deflection as depicted in figures (4-31), and (4-32). In those figures, it can be seen that the increase in haunch angle causes decreasing in the ultimate load and increasing in deflection. It can be noticed that the prismatic beam shows a higher stiffness than RCHBs.

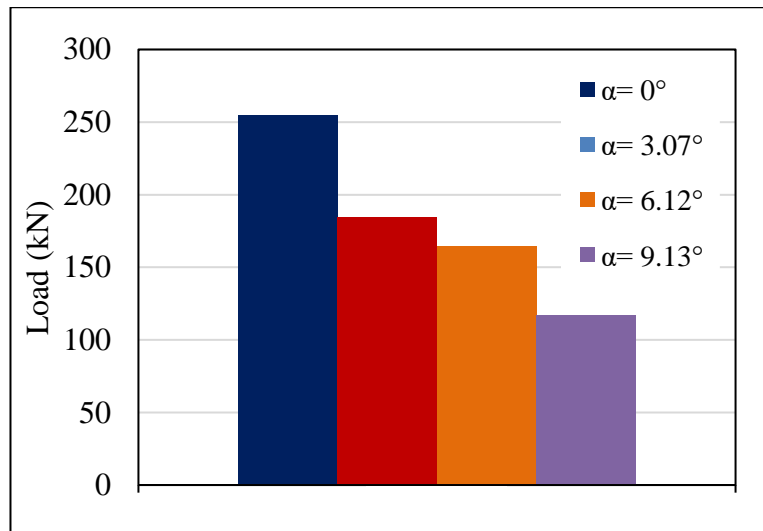


**Figure (4-31): Relationship between the ultimate load and haunch angle.**

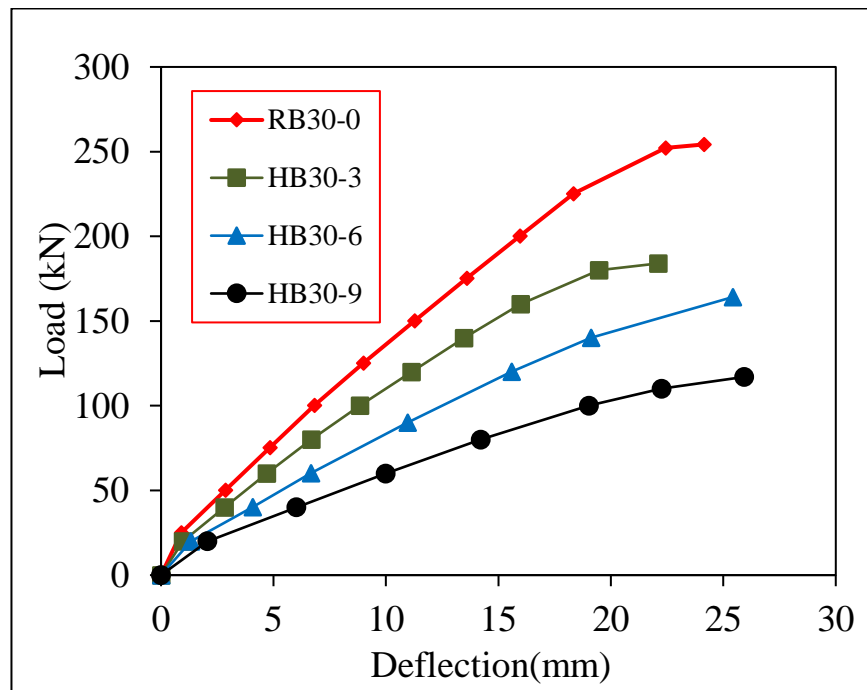


**Figure (4-32): Load-deflection curve for effect of increasing the haunch angle on the ultimate load for RCHBs with stirrups.**

Figures below show the effect of concrete compressive strength on the performance of RCHBs with and without shear reinforcement respectively. It can be noticed from these diagrams, the increasing in compressive strength enhance the ultimate shear strength, maximum deflection, and energy dissipation. Increasing  $f'_c$  of the beam with haunch angle  $6.12^\circ$  reaching to HSC degree showed that the strength enhanced by additional strength by (21%, 37%, and 57%) when the compressive stress increased to 40, 50, and 70 MPa respectively. An enhancement in the ductility of the RCHBs is presented. Also, the crack load increase at first crack as shown in Fig. (4-33) and (4-34).

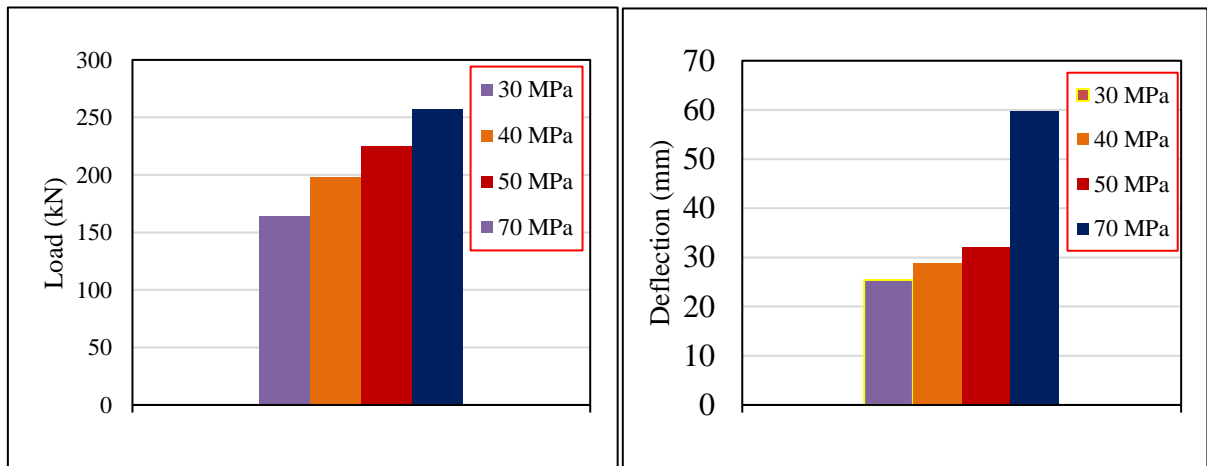


**Figure (4-33): Effect of the compressive strength on the ultimate load and the deflection of RCHBs with shear reinforcement.**

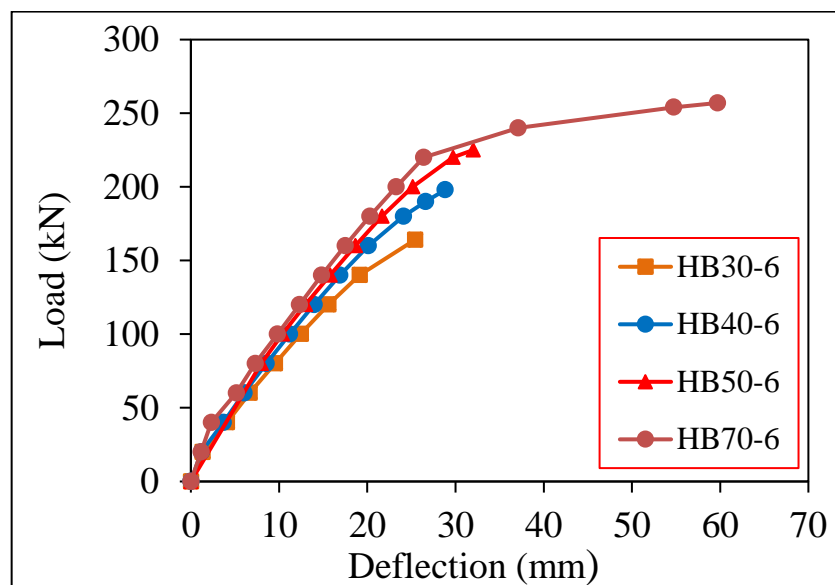


**Figure (4-34): load-deflection curve for effect of increasing  $f'_c$  for RCHBs with shear reinforcement**

Increasing the compressive strength for the RCHBs without shear reinforcement for haunch angle  $12.1^\circ$  shows less nonlinearity than beams with stirrups. Shear strength capacity of the RCHBs without shear reinforcement enhanced by (50%, 97%, and 260%) when  $f'_c$  increased to 40, 50 and 70 MPa with an increasing in the displacement by an amount less than in the beams with stirrups as expressed Fig. (4-35) and (4-36). Also, the rate of increasing in  $f'_c$  become more sensitive for the higher concrete grade.

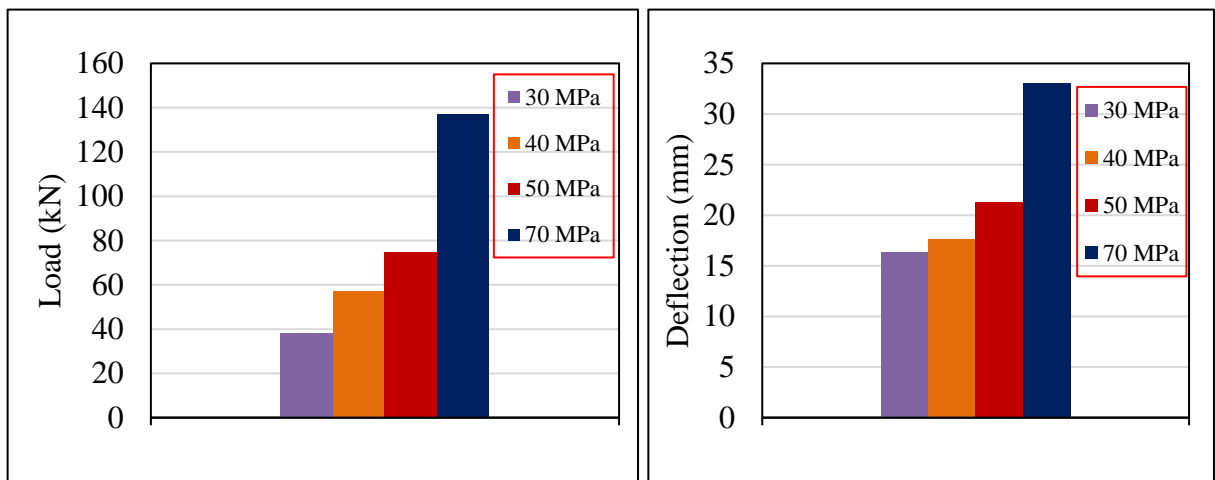


Figure (4-35): Effect of the compressive strength on the ultimate load and the deflection of RCHBs without shear reinforcement.

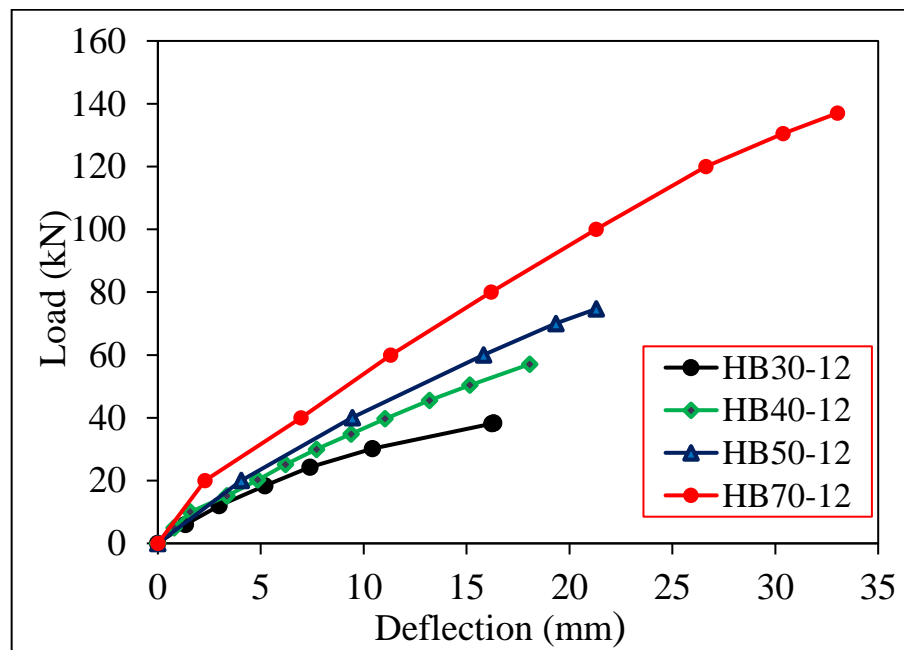
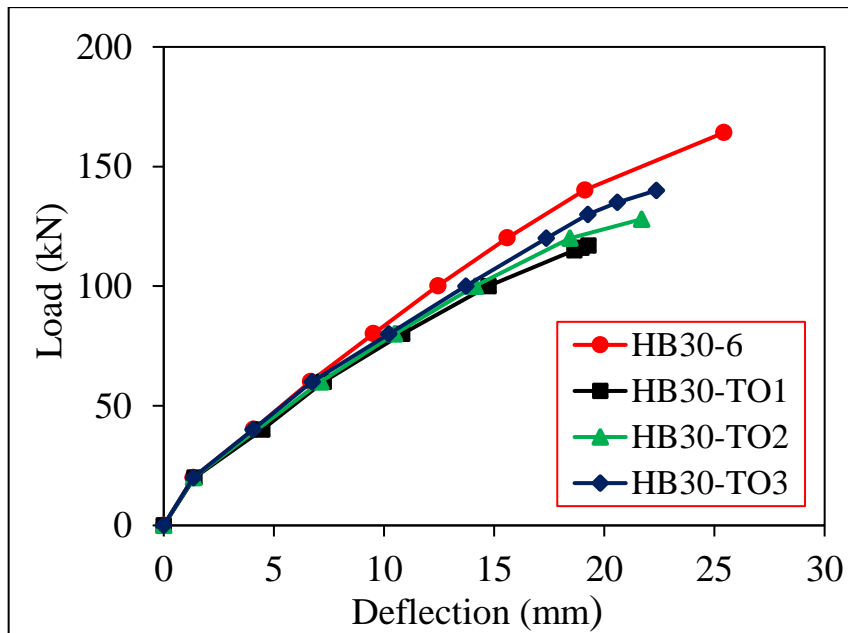


Figure (4-36): Load-deflection curve for effect of increasing  $f'_c$  for RCHBs without shear reinforcement.



The existence of a transverse square opening (100×100) mm exhibits a decreasing in the shear strength and stiffness of RCHBs. The reduction of ultimate capacity is (29%, 22%, and 15%) for specimens (HB30-TO1, HB30-TO2, and HB30-TO3) respectively. Also, the reduction in the displacement occur by (24%, 17%, and 13%) respectively in comparison with the solid beam (HB30-6). The opening position has a large influence on the shear capacity, this effect becomes large when the opening position is near the vertex due to the decreasing in depth. Specimen with an opening near the vertex (HB30-TO1) has the maximum reduction in failure load by (29%) as shown in Fig. (4-37).



**Figure (4-37): Load-deflection curve for beams with transverse opening.**

Creating a central square longitudinal opening [(50×50), (100×100), and (125×125)] mm affect the behavior of RCHBs. The effect of the opening seems more effecting whenever we move away from the support due to the decreasing in the depth. The presence of the opening causes reduction in the beam strength by (18%, 30% and 39%) for opening size (50, 100, and 125 mm) respectively. When the opening size increases, the deflection decreases as shown in Fig. (4-38).

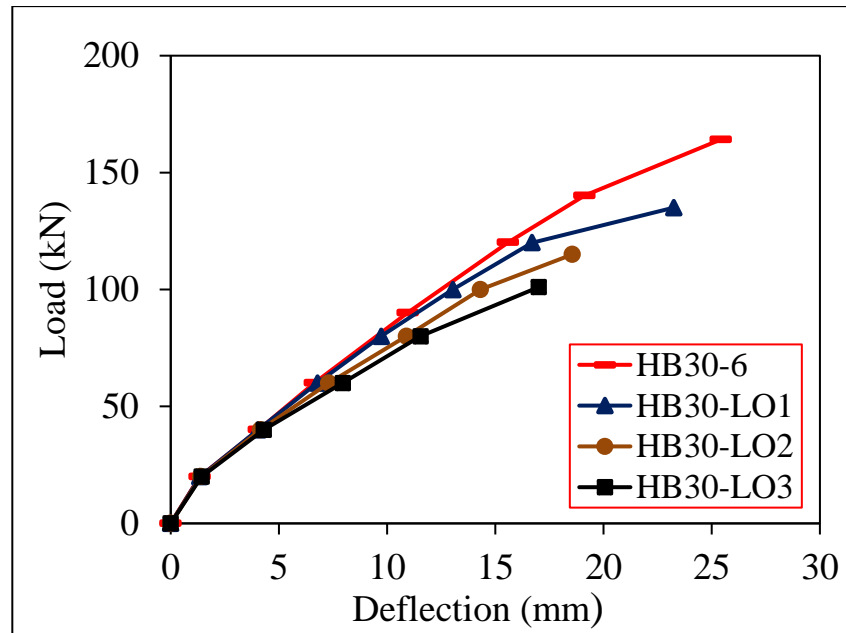


**Figure (4-38): Load-deflection curve for beams with longitudinal opening.**

Using internal strengthening by providing steel rebar  $\varnothing 10$  mm around the opening of beam with a transverse opening shows restoring most of the beam strength that reduced due to the existence of the opening. The presence of lateral opening ( $100 \times 100$ ) mm produces a reduction in ultimate strength with the ratio (22%) as mentioned above. When steel rebar are used, the weakness reduced to (8%) only when compared with the solid beam as shown in Fig. (4-39).

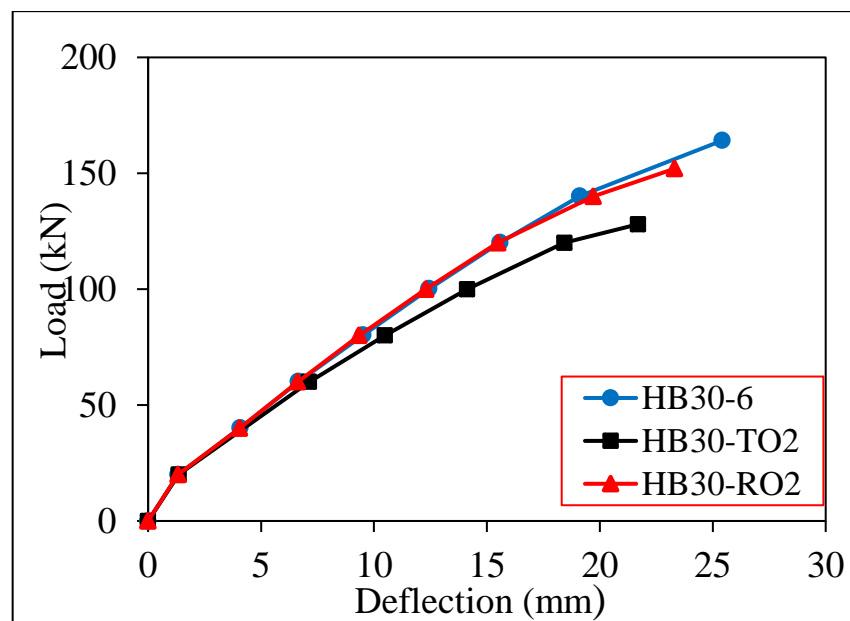


**Figure (4-39): Load-deflection curve for beam with opening strengthened by steel reinforcement.**

To restore the expected loss in strength can be treated by increasing  $f'_c$ . increasing  $f'_c$  of RCHBs with opening near the vertex (HB40-TO1 and HB50-TO1) to 40 and 50 MPa revealed that using 40 MPa compensated about (83%) from the loss in strength and increased the deflection about (9%).

Increasing in the compressive strength to 50 MPa lead to increasing in the failure load about (62%) in comparison with beam (HB30-TO1) and the behavior of beams exhibited a significant enhancement in ductility and high energy absorption as revealed in Fig. (4-40).

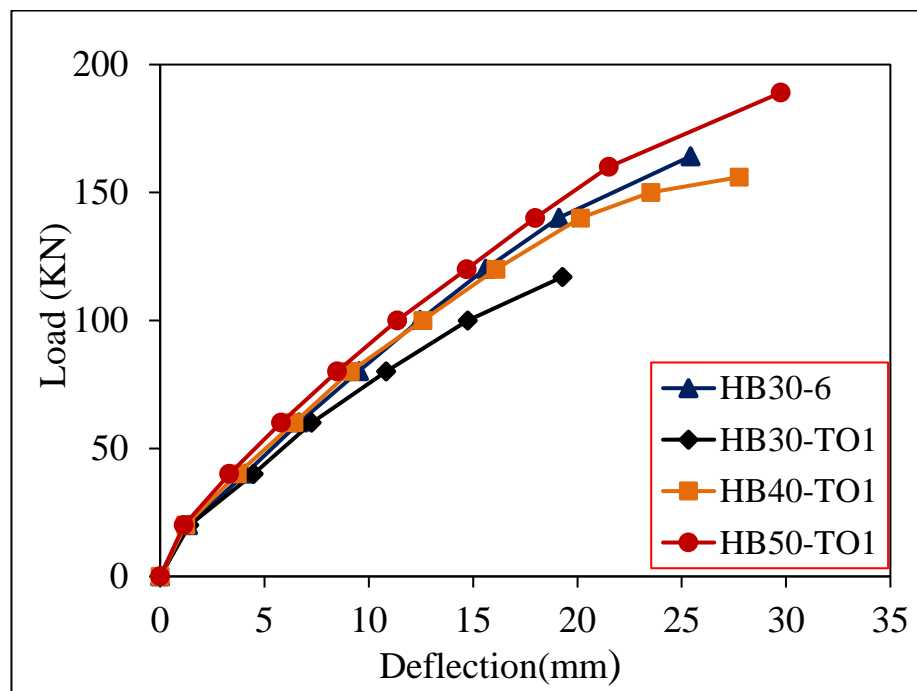


**Figure (4-40): Load-deflection curve for beams with lateral opening strengthened by increasing  $f'_c$ .**

The influence of increasing the compressive strength of the hollow RCHBs having a longitudinal opening (125×125) mm to 40 and 50 MPa shows restoring all the loss in strength and enhanced by additional strength with increase in the ductility. The enhancement in the shear capacity is by (35% and 68%) and in deflection by (18% and 64%) in comparison with hollow beam with  $f'_c$  equal to 30 MPa as demonstrated in Fig. (4-41).

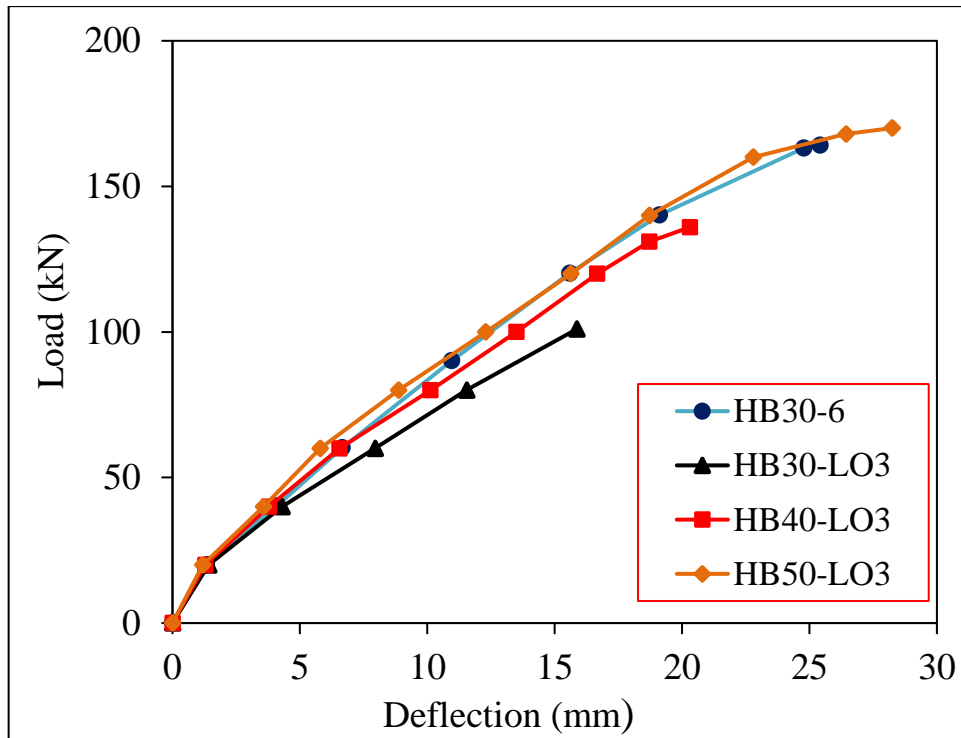


**Figure (4-41): Load-deflection curve of beam with longitudinal opening strengthened by increasing  $f'_c$ .**

Using CFRP externally to treatment the loss that occurred due to the shear failure at the opening zone and also to strengthening the performance of the solid RCHBs. the result showed that;

- 1) Retrofitting the beam (HB30-CT1) with an opening near the vertex by CFRP restored about (72%) from the occurred weakness and reduced it to (8%) after it was (29%) as shown in Fig. (4-42).
- 2) Strengthening the beam (HB30-CL3) having longitudinal opening (125×125) mm retrofitted by CFRP. Using CFRP sheet with two layer for avoidance the inability in shear strength when reduced the happened weakness in the shear capacity to less than (2%) only. Also, large increasing in the displacement by (41%) approximately in comparison with the solid beam as shown in Fig. (4-43).

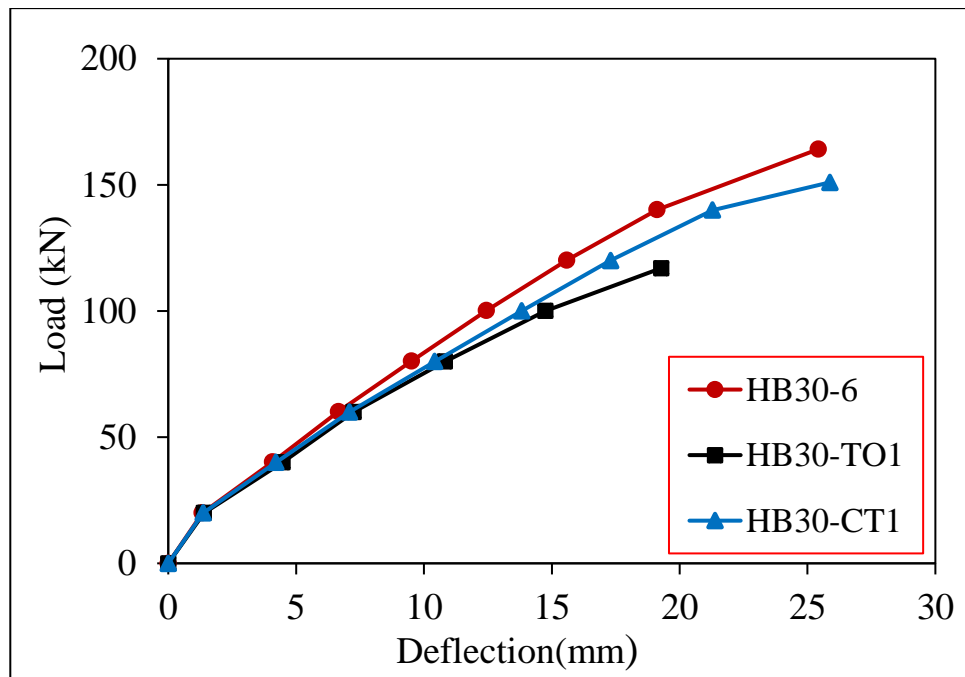


Figure (4-42): Load-deflection curve of beam with transverse opening strengthened by CFRP sheet.

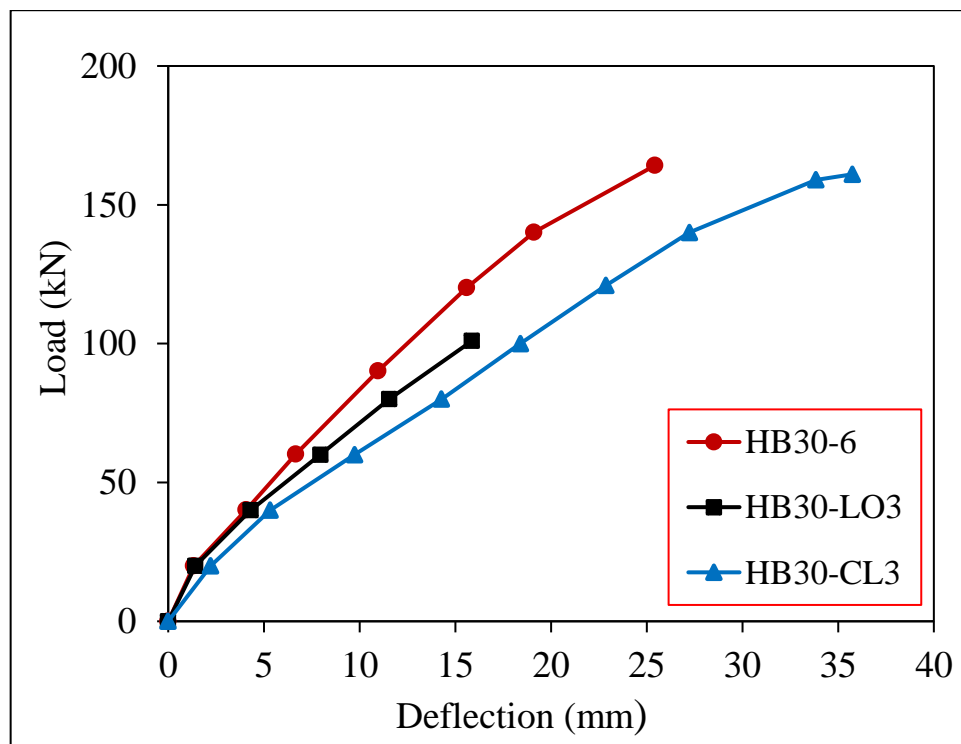


Figure (4-43): Load-deflection curve of beam with longitudinal opening strengthened by CFRP sheet.

### **4.5.2.2 Cracking Patterns**

The typical crack failure of each specimen in this series has been seen in Figs. (4-44) and (4-45).

For the prismatic beam, first crack occurs at the mid span by (17%) of the ultimate shear capacity. From these figures, it can be observed that the failure region of prismatic beam is the path from the support to the loading zone.

The first crack appeared at (15-19%) for RCHBs with stirrups and (30%) of the ultimate shear capacity for the RCHB without stirrup. Amount of cracks increase with increasing in the applied load. For RCHBs with stirrups, cracks developed firstly at the vertex then diagonal cracks developed in the shear span (haunch region) from the support toward the loading zone.

At this stage, the failure is occurring. In the case of RCHBs without shear reinforcement, the same path of cracks but a little amount of diagonal shear cracks enough to make the failure.

It can be shown from these figures, there are no failure in the vertex zone due to the presence of additional stirrups at this zone. Also, the cracks do not spread at the prismatic region for all beams.

Crack pattern are largely affected by the existence of parameters in comparison with the control beams. Parameters outcomes on the crack propagation is explained as follows;

Increasing the haunch angle causes decreasing in the amount of cracks at the flexure zone and propagate the cracks at the haunch zone as appeared in Fig. (4-45 a) to (4-45 e).

Increasing  $f'_c$  has small influence on the propagation of cracks in comparison with the beams at lower value of  $f'_c$  as illustrated in Fig. (4-44) for model with different  $f'_c$ .

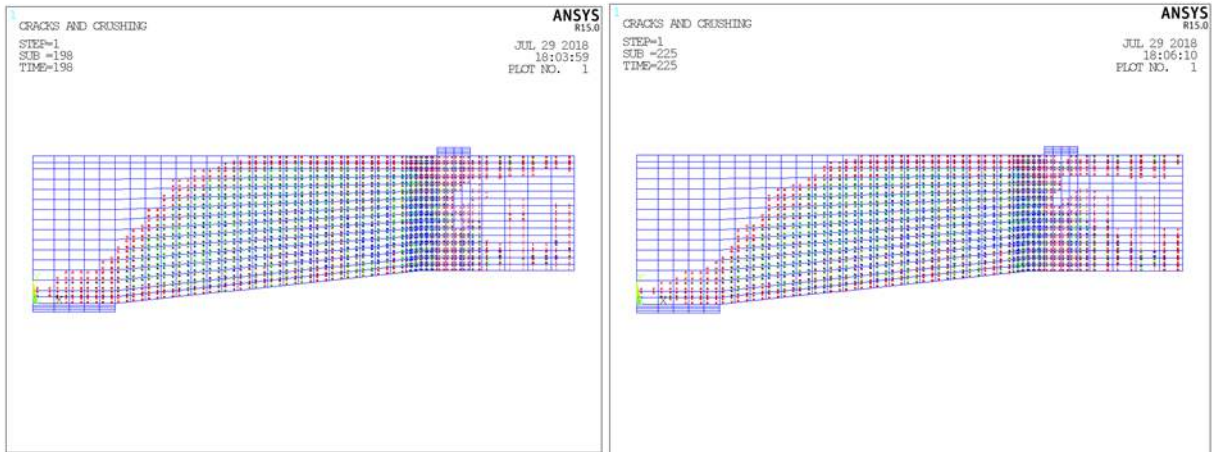


**Figure (4-44): RCHBs with different  $f'_c$  equal to 40 and 50 MPa (HB40-6 and HB50-6).**

Existence of a square opening affected the crack propagation. More shear cracks develop at the corner of the opening, all specimens with a transverse opening have a reduced crack propagation and concentrated it at the opening in comparison with the solid beam as demonstrated in Fig. (4-45 f) to (4-45 h).

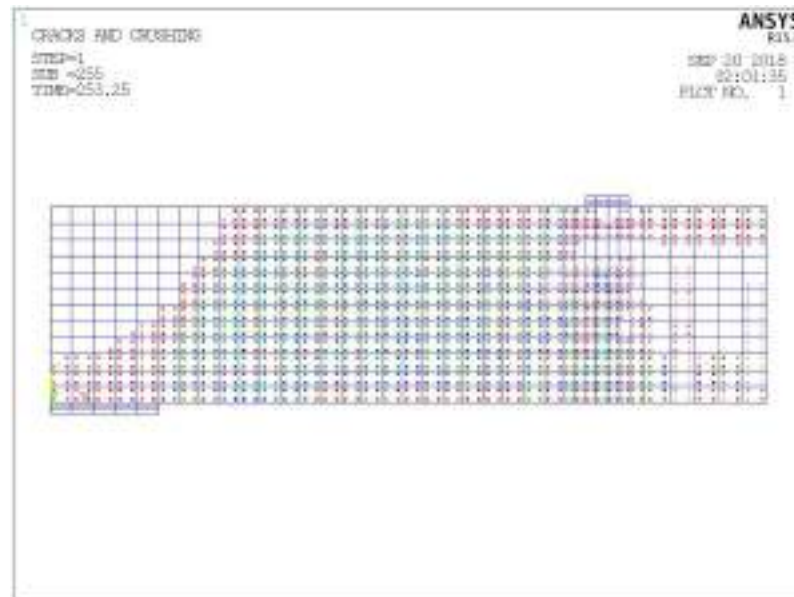
Crack pattern for hollow beams showed a cracks concentration at the corners of the opening along the haunch zone start from the support and end at the vertex with maximum spread at this zone. Increasing in the opening size caused decreasing in the cracks propagation amount as revealed in Fig. (4-45 i) to (4-45 k).

Treating the loss of the opening by the presence of reinforcement bars around the opening (HB30-RO2) made a better crack distribution. Little amount of cracks was developed at the corner of the opening and the concentration of cracks returned to the vertex which considered an index to that reinforcement works efficiently as appeared in Fig. (4-45 l).

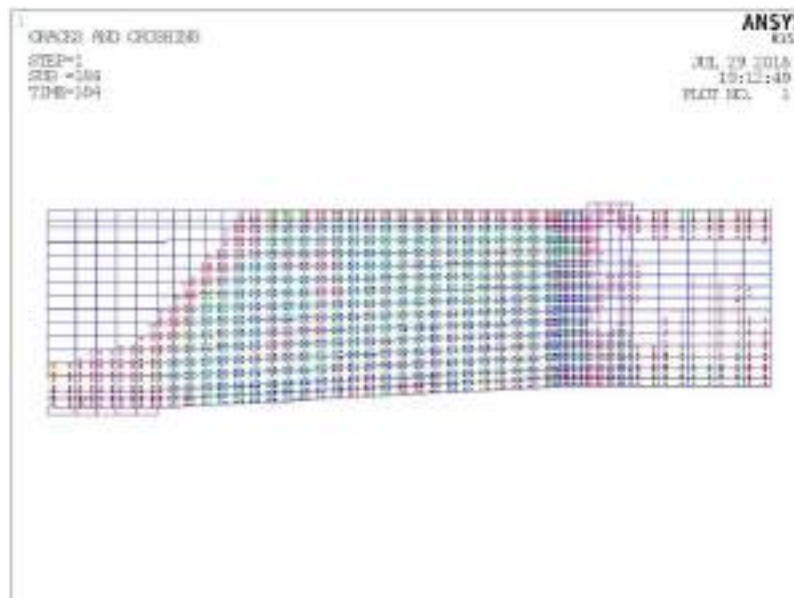
Also increasing  $f'_c$  for beams with a transverse or longitudinal opening to restore the lost strength does not affect the crack pattern.

Using CFRP sheet in the RCHBs increased the crack propagation. Beam with a transverse opening retrofitted by CFRP sheet showed more spread of cracks than in the beam without CFRP. as shown in Fig. (4-45 m).

From Fig. (4-33 n), it can be noticed that CFRP sheet with two layer for the beam with longitudinal opening showed larger amount of cracks occurred through and over the opening. Haunch zone filled with cracks which it considered a good index for ductility and energy absorption.



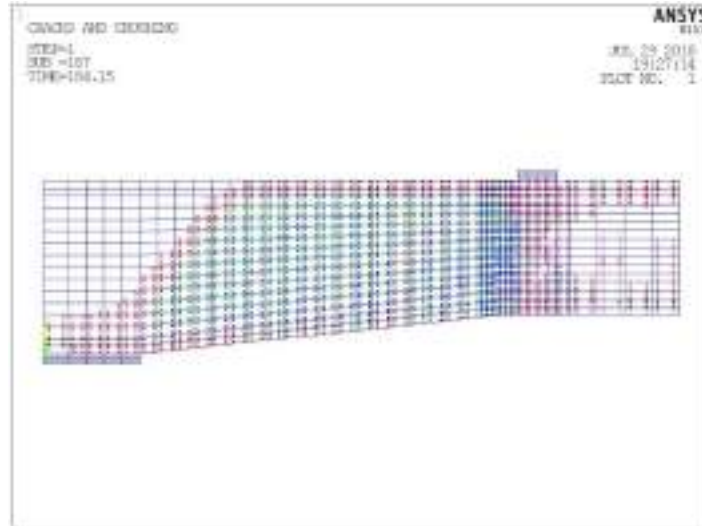
(a) Crack pattern for beam (RB30-0).



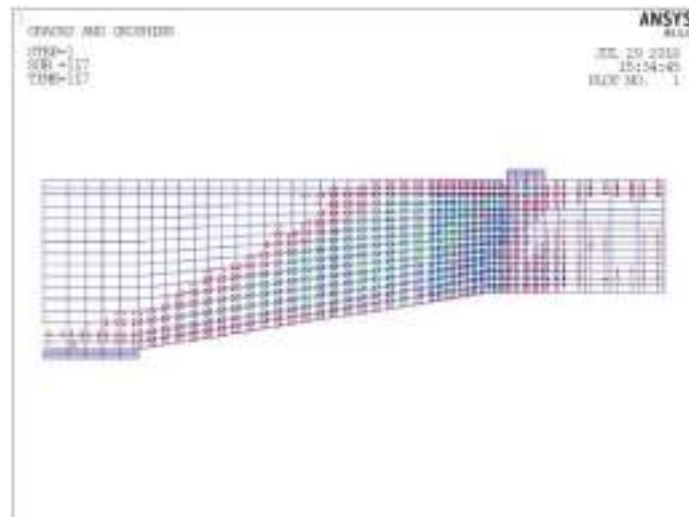
(b) Crack pattern for beam (HB30-3).

Figure (4-45): Crack pattern of the series two beams.

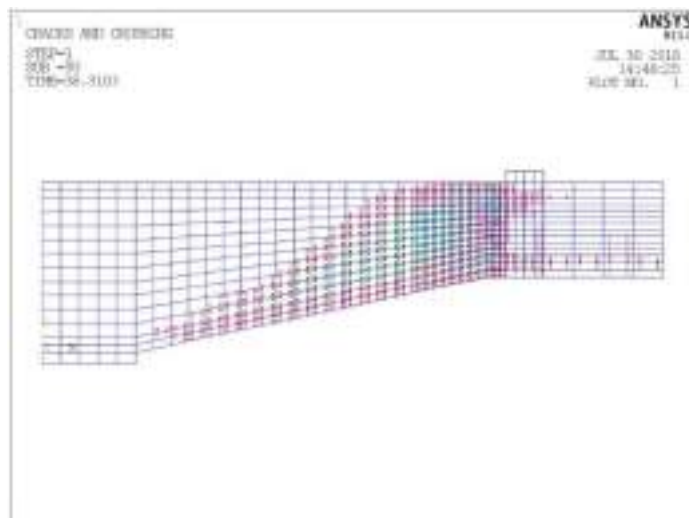




(c) Crack pattern for beam (HB30-6).

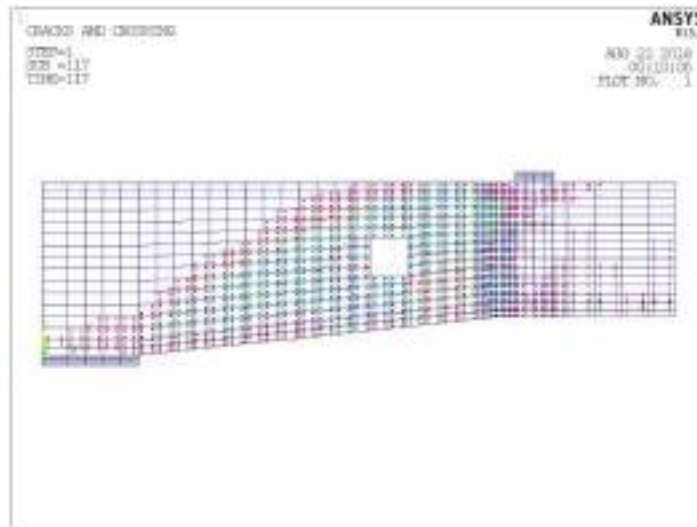


(d) Crack pattern for beam (HB30-9).

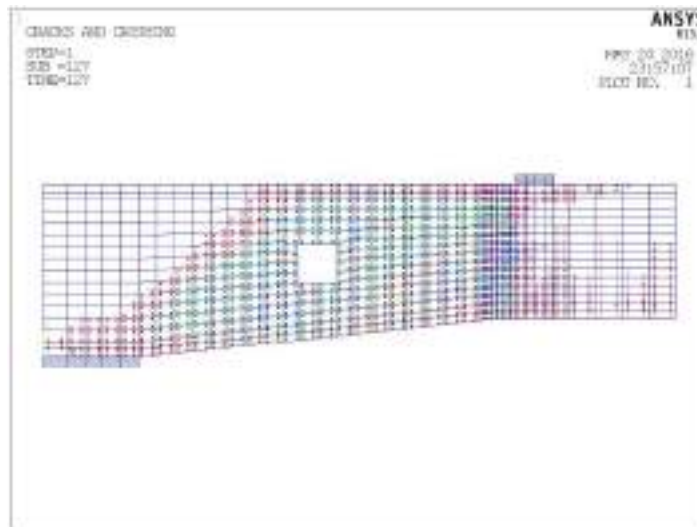


(e) Crack pattern for beam (HB30-12).

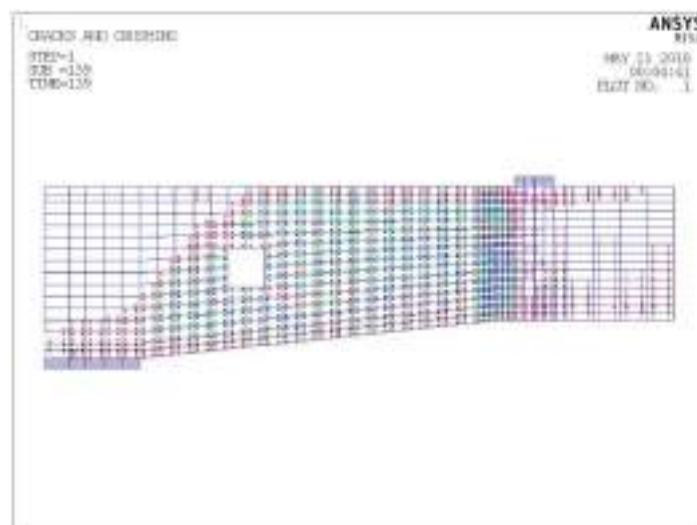
Figure (4-45): Cont.



(f) Crack pattern for beam (HB30-T01).

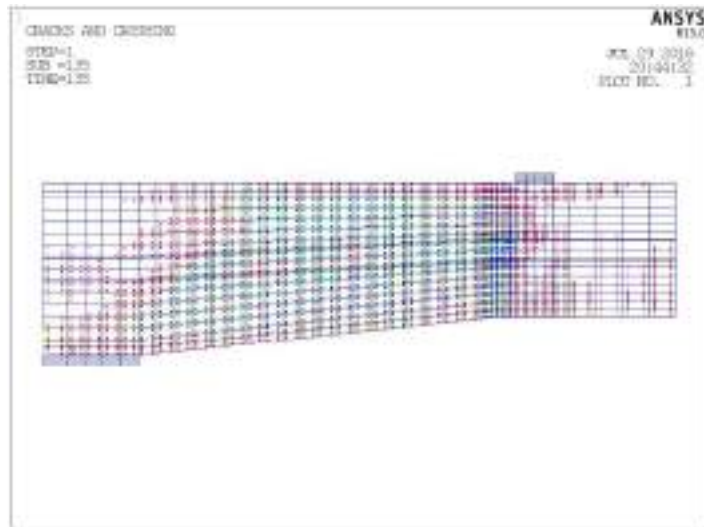


(g) Crack pattern for beam (HB30-T02).

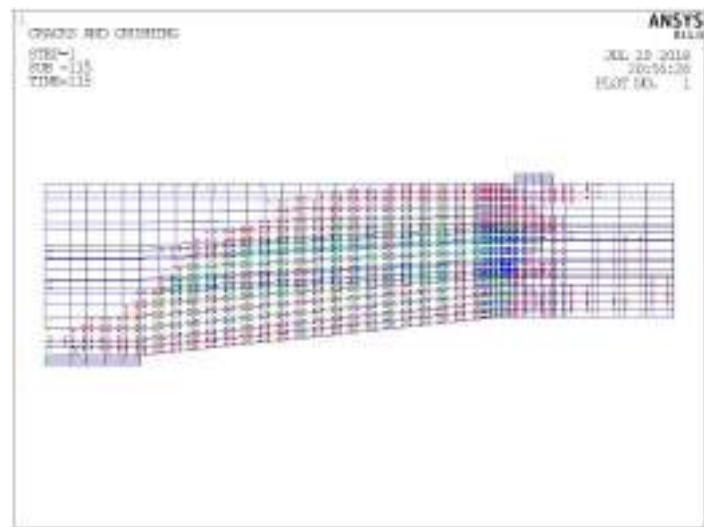


(h) Crack pattern for beam (HB30-T03).

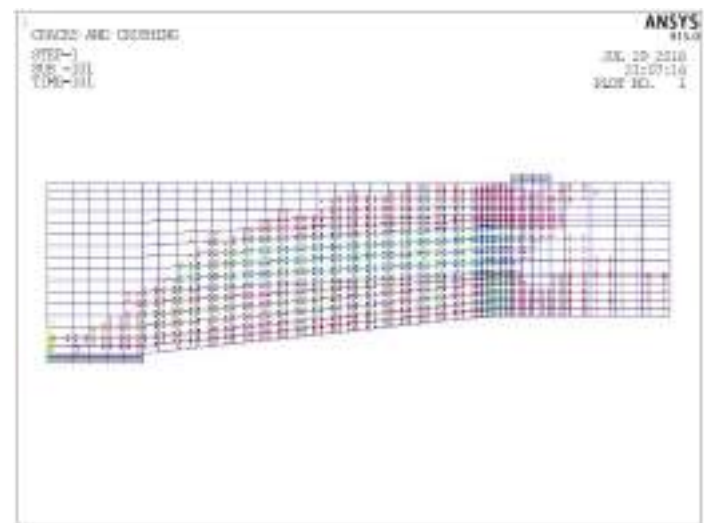
Figure (4-45): Cont.



(i) Crack pattern for beam (HB30-LO1).

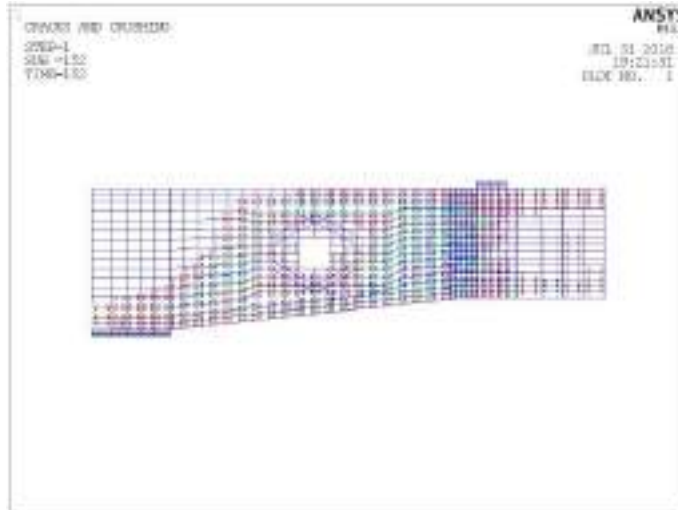


(j) Crack pattern for beam (HB30-LO2).

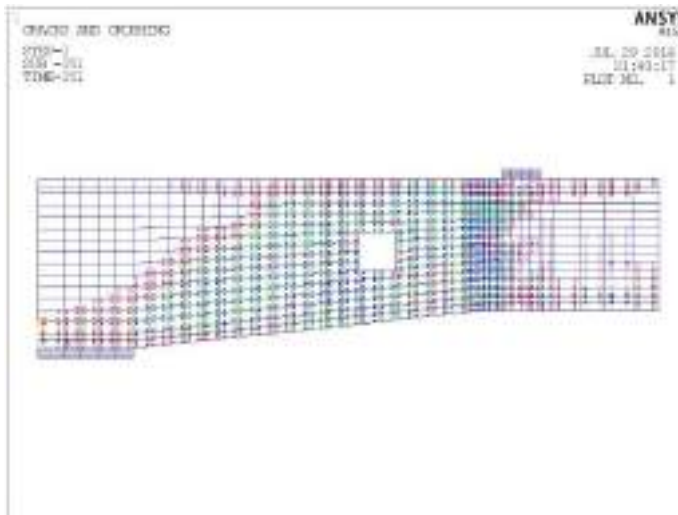


(k) Crack pattern for beam (HB30-LO3).

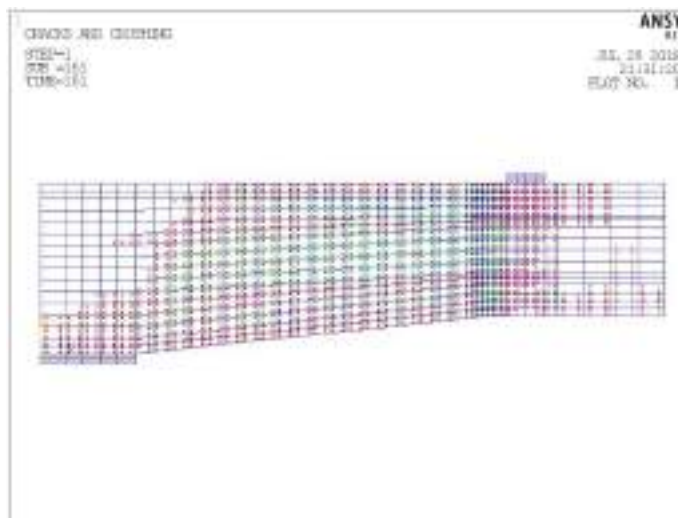
Figure (4-45): Cont.



(l) Crack pattern for beam (HB30-RO2).



(m) Crack pattern for beam (HB30-CT1).



(n) Crack pattern for beam (HB30-CL3).

Figure (4-45): Cont.

### **4.5.3 Series Three**

#### **4.5.3.1 Load-Deflection Relationship**

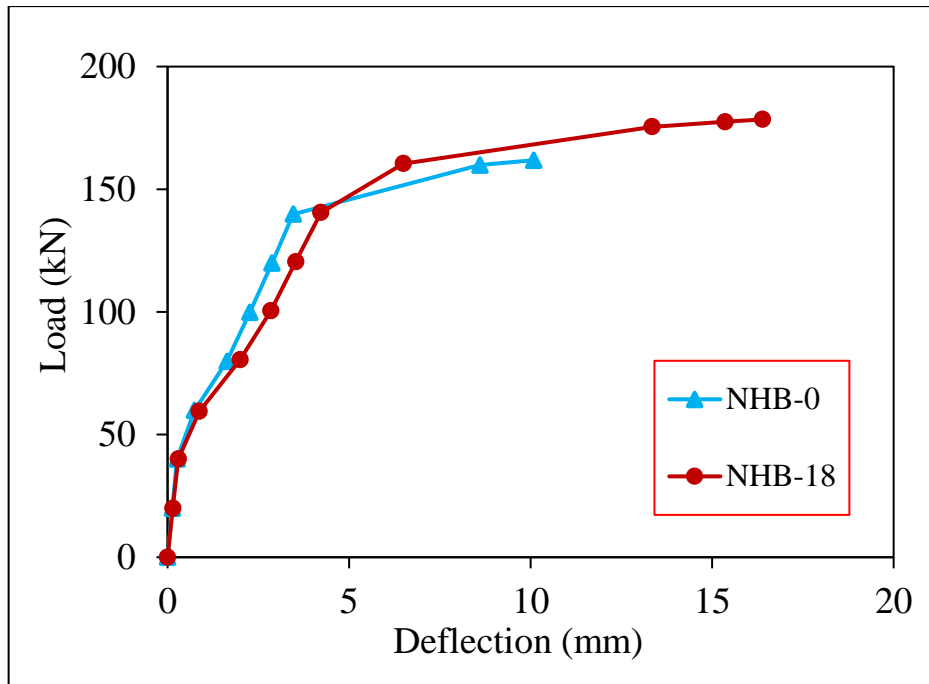
The load-deflection curve of beams in series three are presented in Fig. (4-46) to (4-50). It is noticed that the prismatic beam and RCHBs with negative haunch is linearly elastic up to about (31%) and (19-25%) respectively of the maximum failure load until appearance of first crack then, the concrete enters the zone of nonlinearity as demonstrated in Table (4-10).

Table (4-10): Results of RCHBs in series three.

Beam	Crack load (kN)	Deflection at crack load (mm)	Failure load (kN)	Max. deflection (mm)
NHB-0	51	0.57	162	10.1
NHB-18	42	0.34	178.5	16.4
NHB-TO1	42	0.34	169	13.75
NHB-C1	42	0.37	181	13.5
NHB-C2	46	0.4	240	9.25
NHB-C3	53	0.43	216.4	10.57

This group fails in flexure except some beams fails in shear due to the strengthening the flexure region.

The turning from prismatic to RCHB with negative haunch angle  $18^\circ$  increases the flexural strength by (10%) with increasing in the deflection by (62%). This haunch provides more ductility to the beam as expressed in Fig. (4-46).



**Figure (4-46): Load-deflection curve for effect of increasing the haunch angle for RCHBs with negative haunch.**

The presence of openings in this type of beams in the flexure region affect the behavior of these beams. Large transverse rectangular opening (120×140) mm causes decreasing in strength of the beam more than (5%) and in deflection more than (16%) as demonstrated in Fig. (4-47).

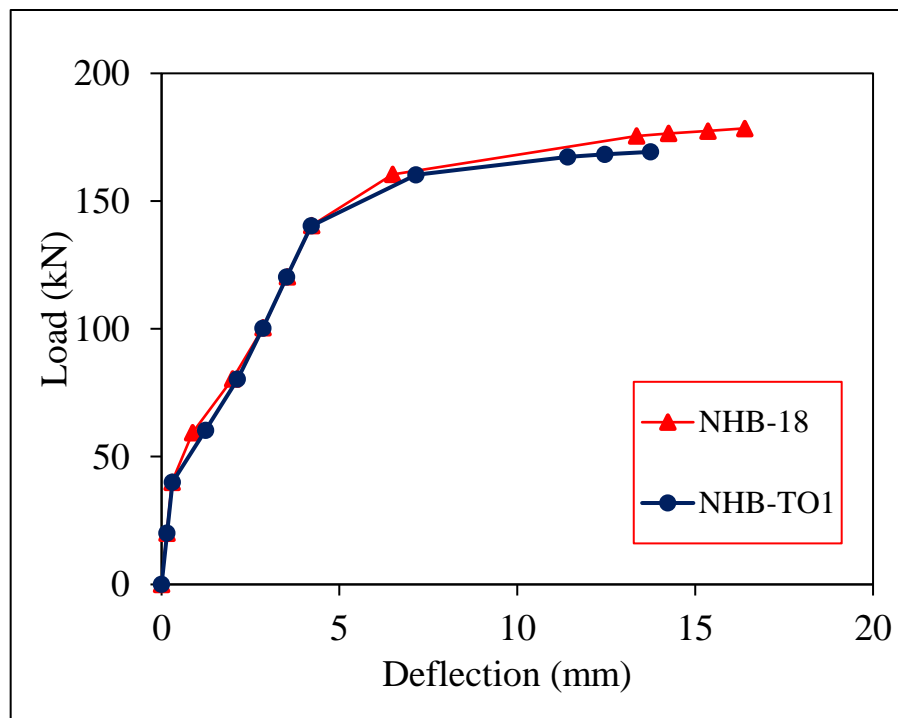


**Figure (4-47): Load-deflection curve for RCHBs with opening.**

Restoring all the weakness is accomplished by using CFRP strips around the opening (NHB-C1) with providing additional strength about (2%). CFRP strips reduce the deflection with a slight value as demonstrated in Fig. (4-48).

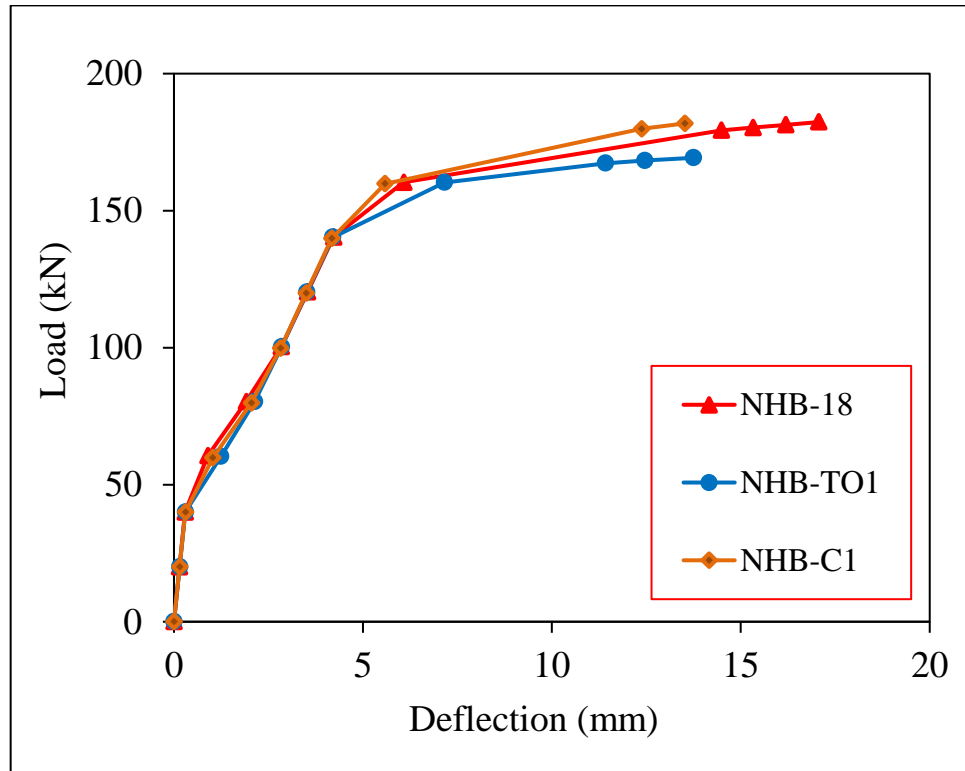


**Figure (4-48): Load-deflection curve for RCHBs with opening strengthened by CFRP sheet.**

Strengthening the solid beam in flexural side by using CFRP sheet around the beam and strip in the bottom surface of RCHB enhance the beam strength. Using CFRP sheet around the specimen (beam NHB-C2) enhance the strength of the beam by (34%) with decreasing in the deflection by (44%) as demonstrated in Fig. (4-49) with transformation in mode of failure from shear to flexure.

CFRP bottom strips for beam (NHB-C3) enhance the stiffness and strength by (21%) and reduce the deflection by (36%) as exhibited in Fig. (4-50).

Strengthening this beams transferred the failure from flexure to shear failure as occurred when used CFRP sheet in this series. This is because that CFRP sheet provided high stiffness to the flexure regions.

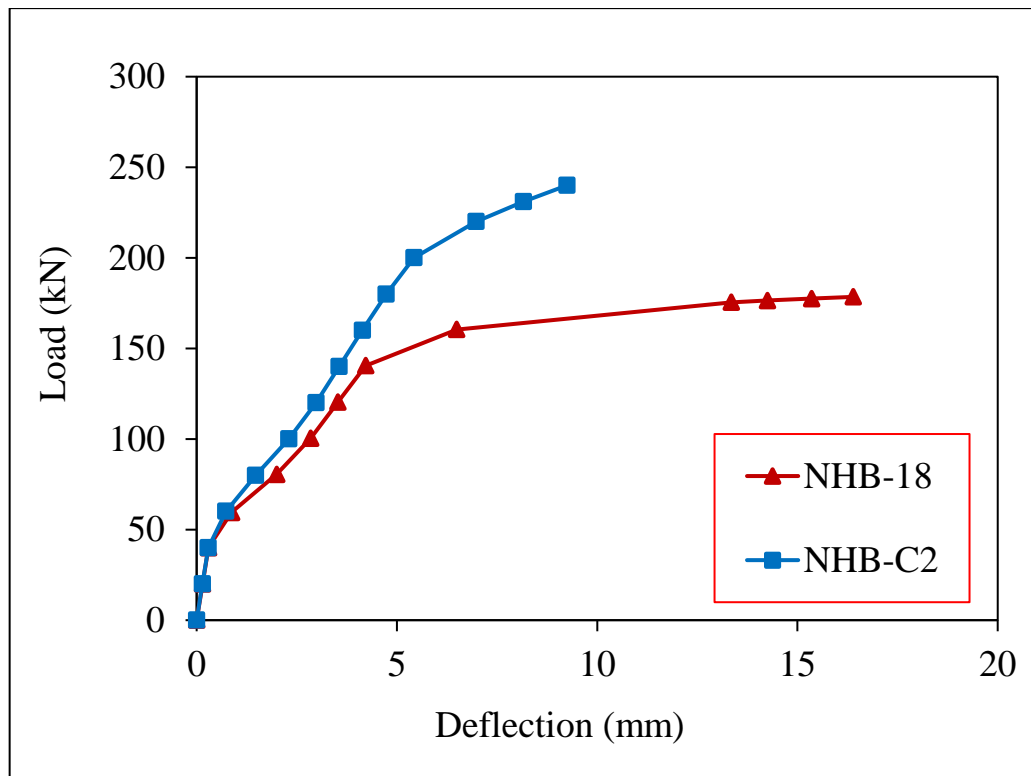


Figure (4-49): Load-deflection curve for RCHB strengthened by CFRP sheet around the beam.

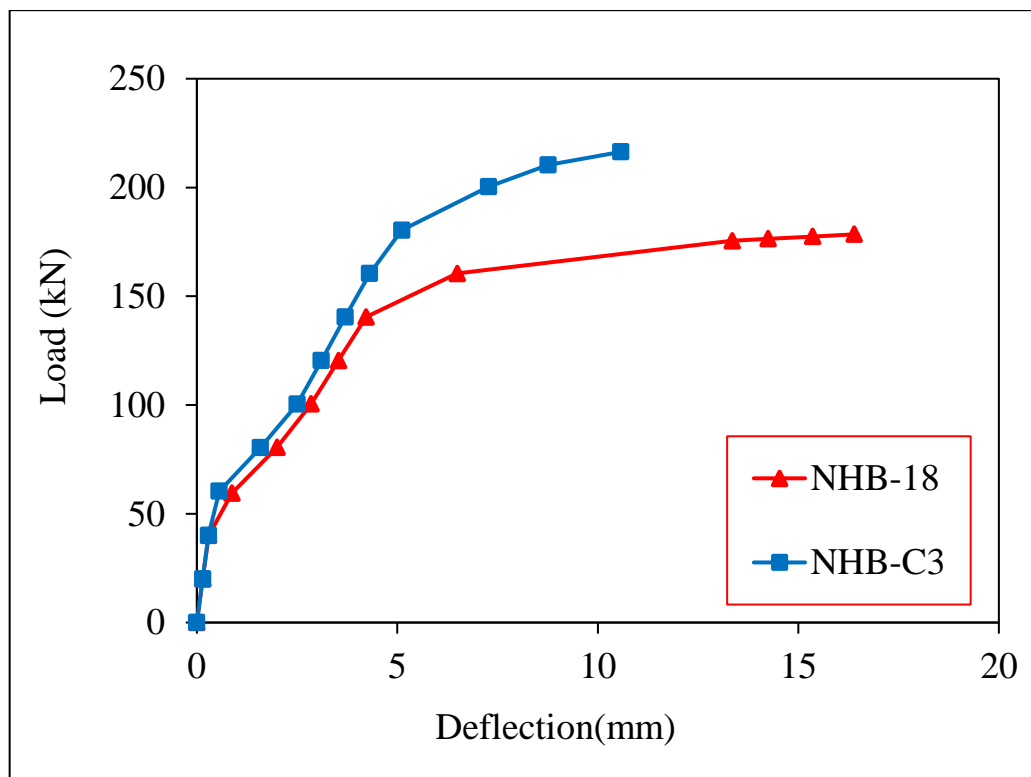


Figure (4-50): Load-deflection curve for RCHB strengthened by CFRP sheet At the bottom surface of the beam.



### **4.5.3.2 Crack Pattern**

Crack pattern of series three is the least influenced by the variables in comparison with the control beams as demonstrated in Fig. (4-51).

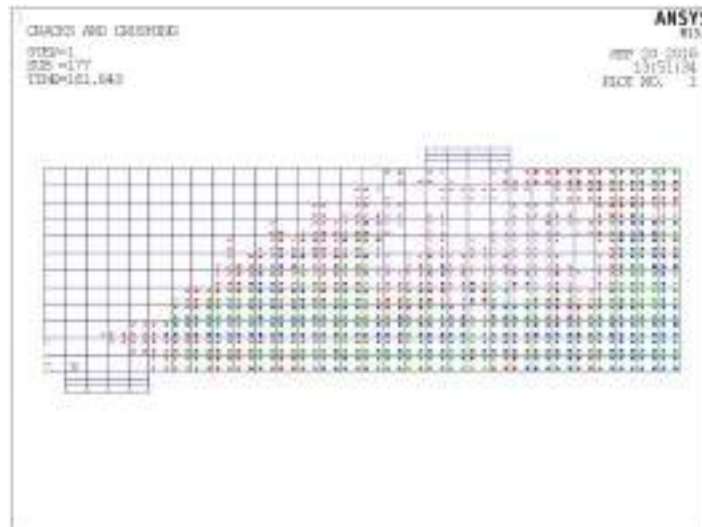
For the prismatic beam, first crack is a vertical crack started to develop at the bottom surface of the beam. Then, inclined shear cracks are developed from the support toward the loading point. Increasing in the applied load causes an increase in the flexural cracks which causes failure at the mid span of beam

First cracks started to develop at the vertex zone near the support then, flexural cracks started to develop which cause the failure in RCHBs. Additional stirrups at the vertex prevent the failure to occur at this region. Parameters effect on the crack pattern of RCHBs is explained as follows:

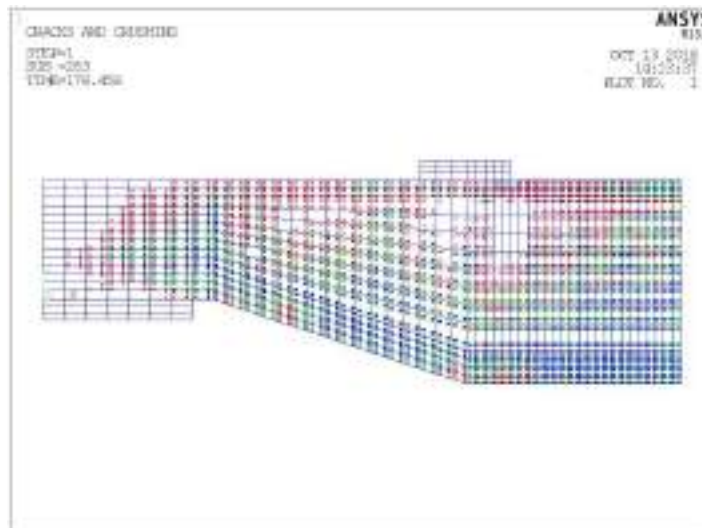
Increasing the haunch angle from 0 to 18° redistributed the propagation of cracks as demonstrated in Fig. (4-51 a) and (4-51 b).

Presence of an opening at the mid-span of RCHBs with negative haunch reduced the cracks propagation and let the cracks concentrated at the corner of the opening due to the stress concentration at this corners. Also, slight decreasing in the cracks in the haunch zone as demonstrated in Fig. (4-51 c). Using CFRP strips around the opening (NHB-C1) enhanced the cracks spread along the beam as demonstrated in Fig. (4-51 d).

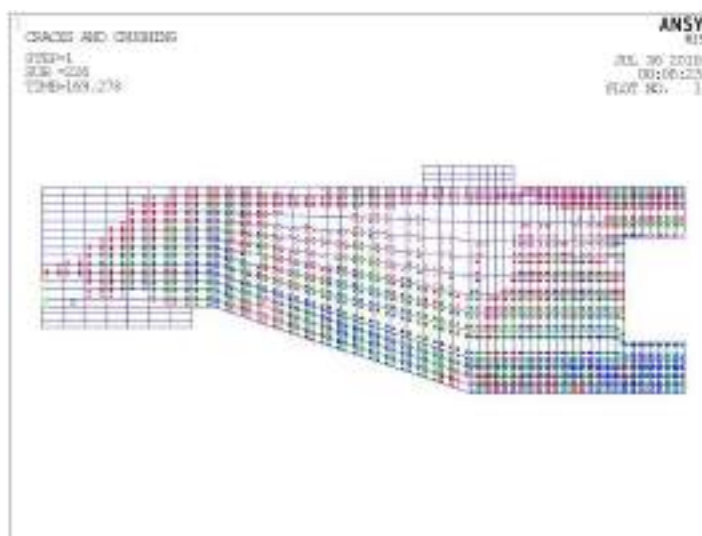
Placing CFRP sheet around the full beam (NHB-C2) provided external fortification to the beam body which make the cracks spread along the beam and made the failure at the vertex zone because this zone is considered the weak zone in the beam after retrofitting the flexure region by CFRP as appeared in Fig. (4-51 e). Also, strips of CFRP at the bottom of beam ((NHB-C2) increased the cracks spread in the zone of vertex near the support which make the failure at this region as demonstrated in Fig. (4-51 f). CFRP sheet provided additional stiffness to the mid-span region which makes it impossible for failure to occur at this region.



(a) Crack pattern for prismatic beam (NHB-0).

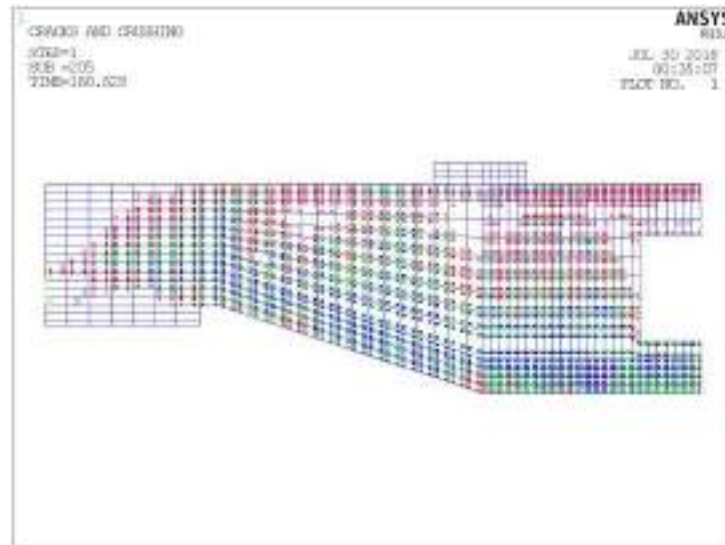


(b) Crack pattern for beam (NHB-18).

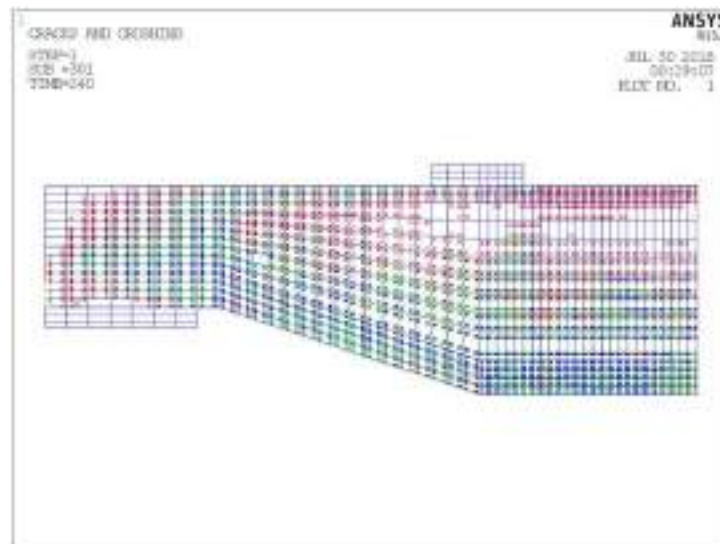


(c) Crack pattern for beam (NHB-TO1).

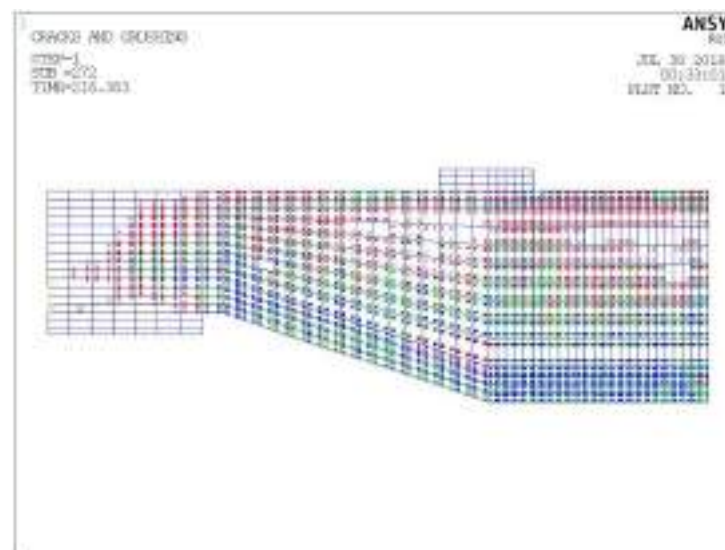
Figure (4-51): Crack pattern for RCHBs of series three.



(d) Crack pattern for beam (NHB-C1).



(e) Crack pattern for beam (NHB-C2).



(f) Crack pattern for beam (NHB-C3).

Figure (4-51): Cont.

## 4.6 Energy Dissipation of RCHBs

As shown in Fig. (4-52), the energy dissipation capacity for beams with different haunch angle with and without CFRP sheet are calculated by several indexes. These indexes are the area under the curve of the load-deflection and crack amount. For inverted RCHBs, Increasing the haunch angle enhanced the energy dissipation. Changing the haunch angle from  $3.95^\circ$  to  $5.91^\circ$  enhanced the energy absorption by 22%. Also, using CFRP sheet around the opening near the support increased the energy dissipation by 250%. Use of CFRP strips for the solid RCHB (2L1) enhanced the energy absorption by 67%. CFRP sheet make the shear zone fully distorted which allows the stresses to distribute along the beam.

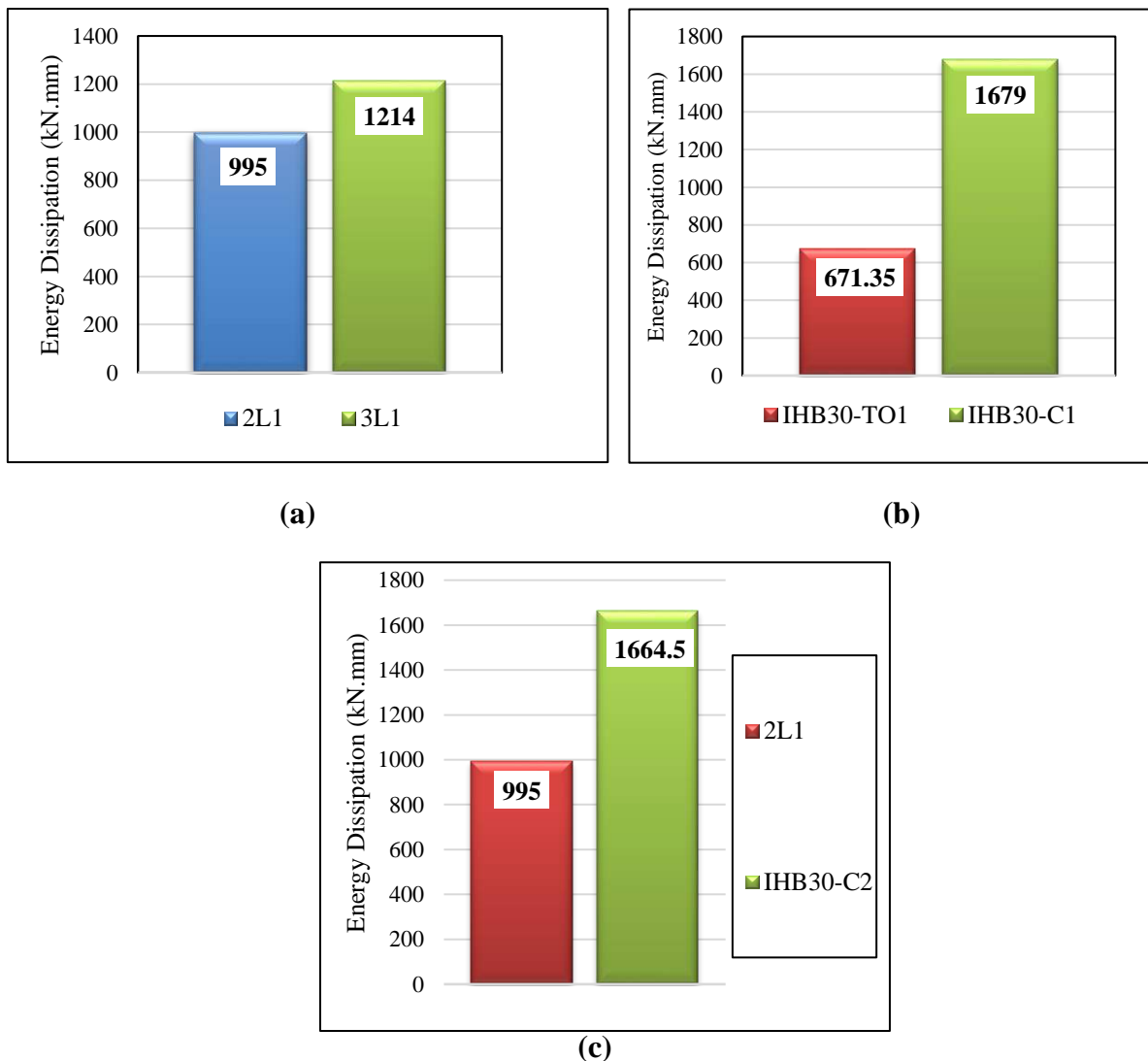
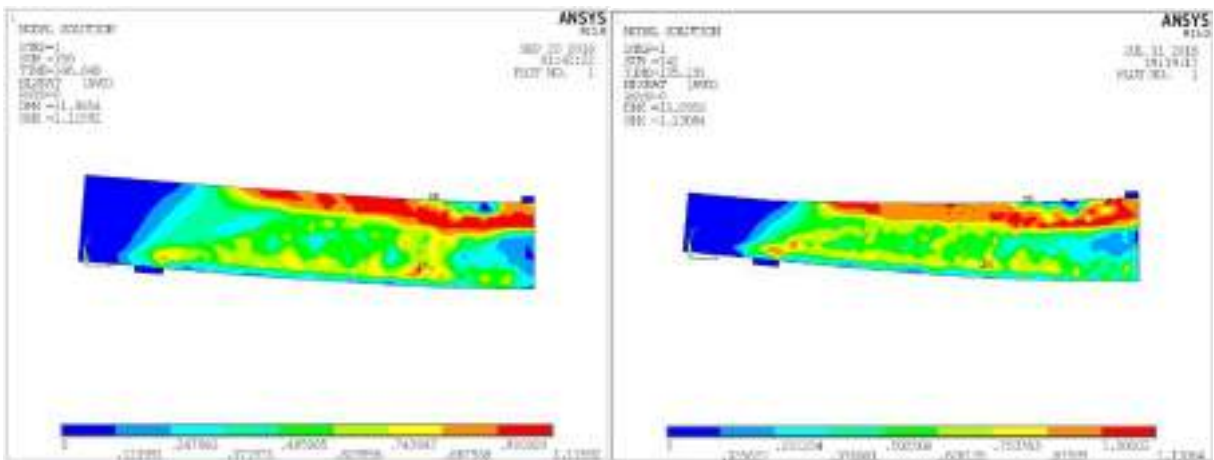


Figure (4-52): Energy dissipation capacity for inverted RCHBs for (a) Haunch angle (b) CFRP sheet for beam with opening (c) CFRP strips for solid RCHB.

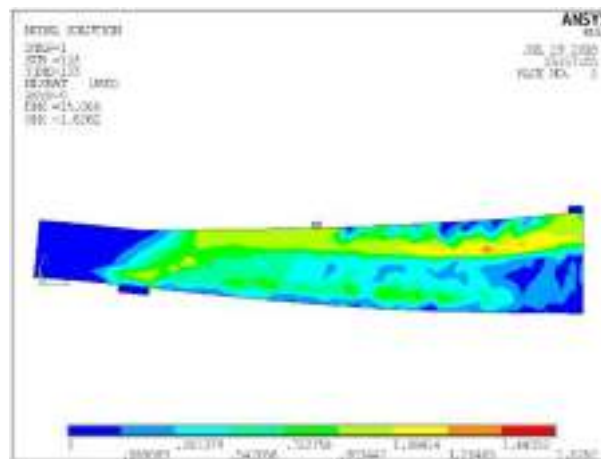
### 4.7 Shear Stress Distribution of RCHBs

Principal shear stress distribution in all beams in series one and two showed different distribution. Level of intensity ranged from colors (blue-green- yellow- brown-red) respectively in concentration, the minimum intensity is blue while maximum intensity referred in red color. In regard to the series one, the distribution of the stresses affected by all used parameters as shown below in Fig. (4-52). It must be noticed that these figures explained the path of stresses and the zones of its concentration.



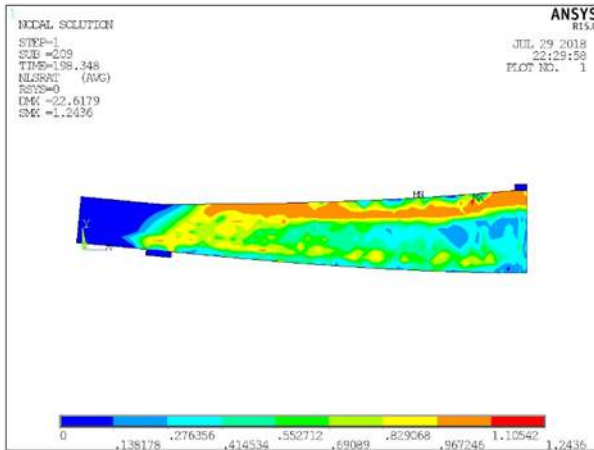
(a) Beam (1L1).

(b) Beam (2L1).

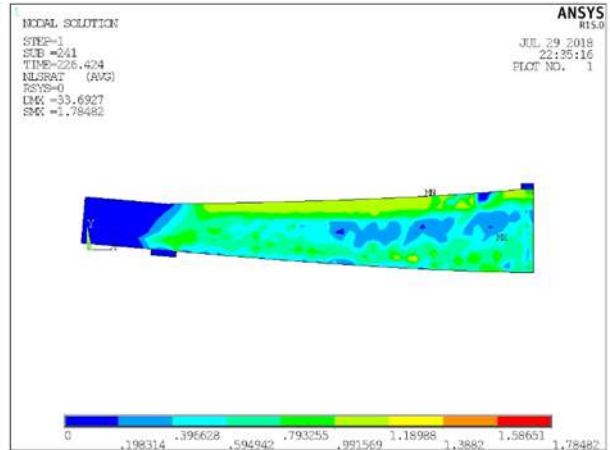


(c) Beam (3L1).

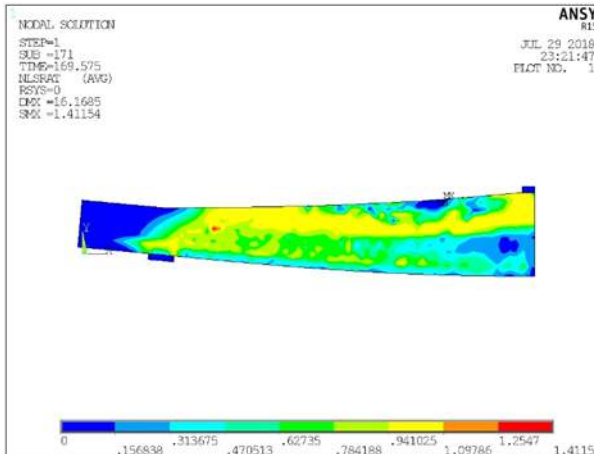
**Figure (4-53): Shear distribution of the series two models.**



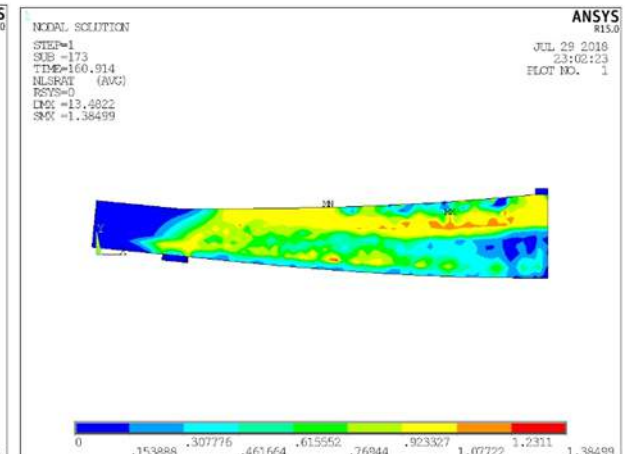
(d) Beam (IHB50).



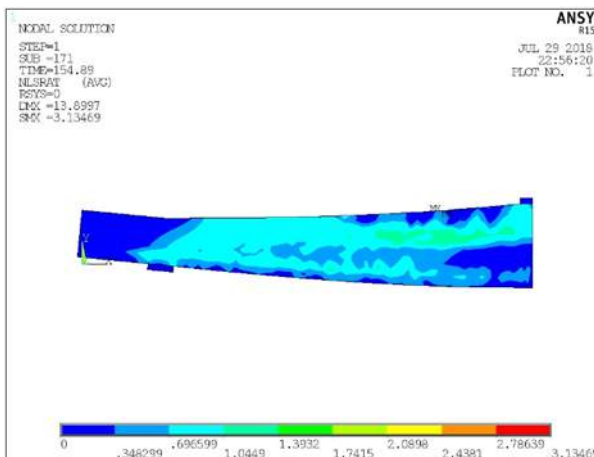
(e) Beam (IHB70).



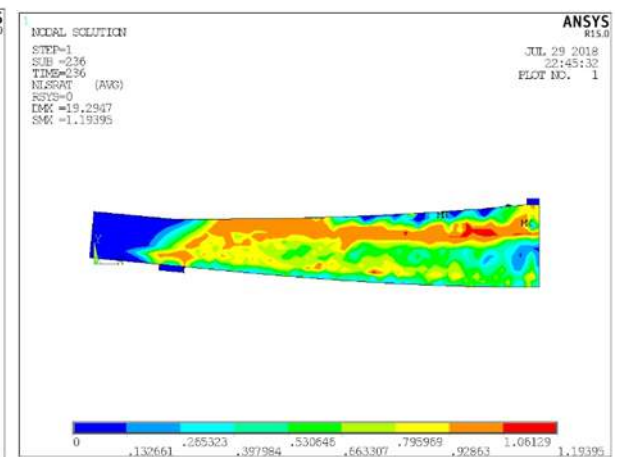
(f) Beam (IHB30-S100).



(g) Beam (IHB30-S150)



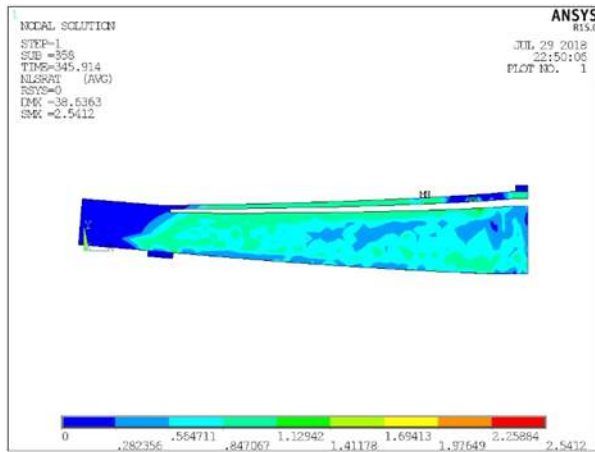
(h) Beam (IHB30-S200).



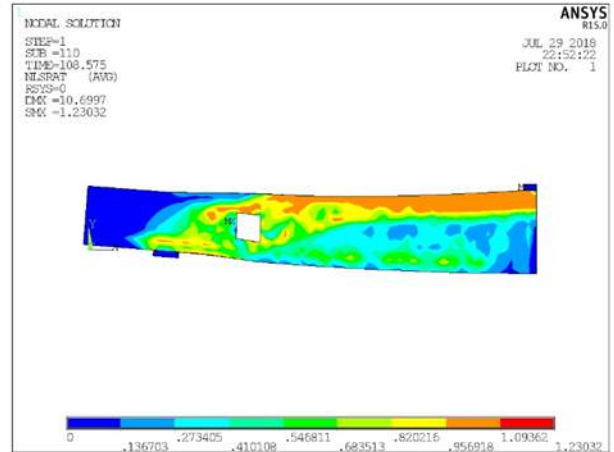
(i) Beam (IHB50-S100)

Figure (4-53): Cont.

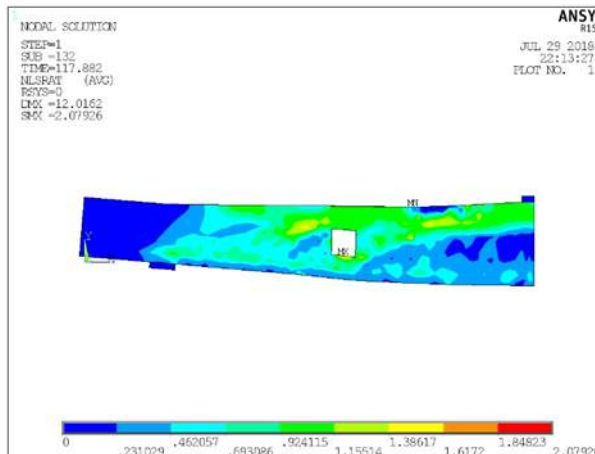




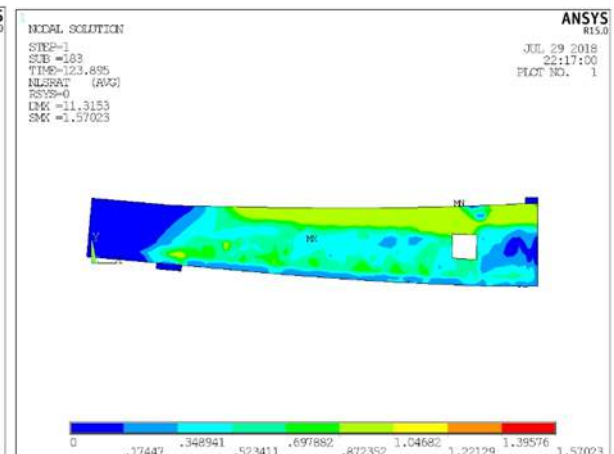
(j) Beam (IHB70-S100).



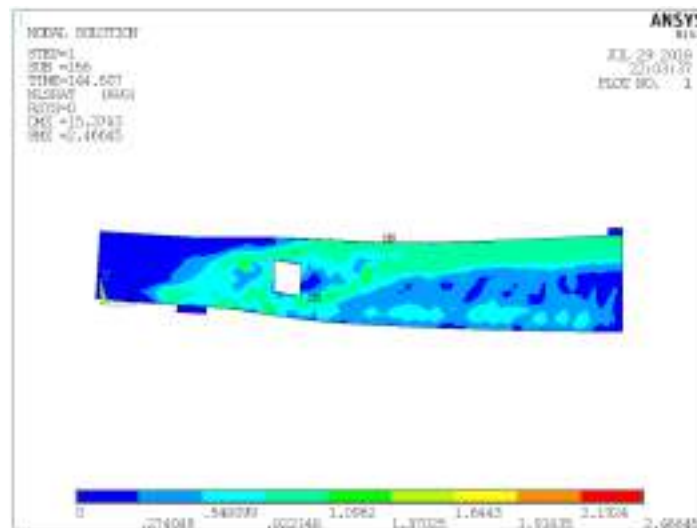
(k) Beam (IHB30-TO1).



(l) Beam (IHB30-TO2).

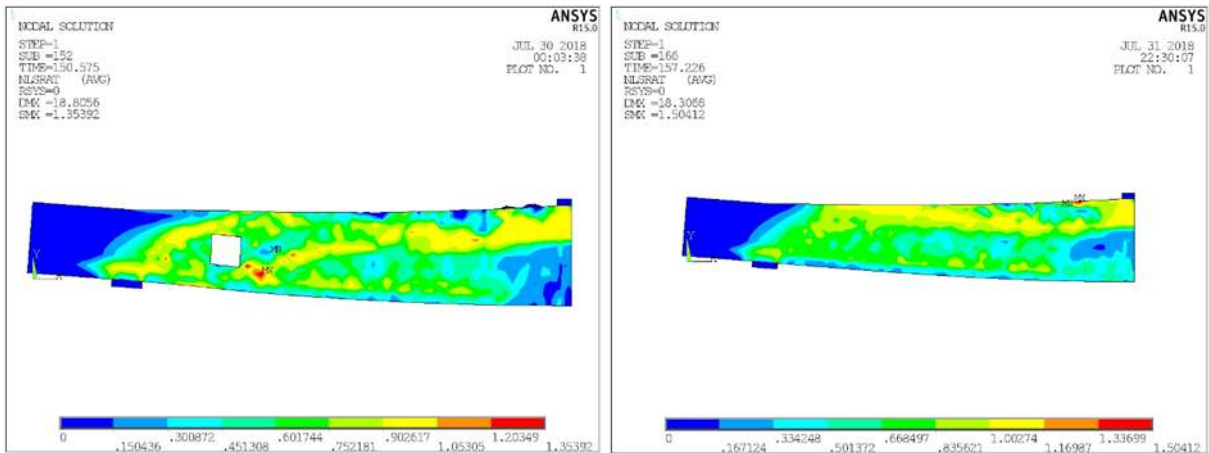


(m) Beam (IHB30-TO3).



(n) Beam (IHB40-TO1).

Figure (4-53): Cont.



(o) Beam (IHB30-C1).

(p) Beam (IHB30-C2).

Figure (4-53): Cont.

## 4.8 CFRP Stress and Strain

The finite element solutions reveal that the maximum stress developed in each CFRP strip is smaller than ultimate stress of CFRP strips which was 4900 MPa.

For the actual strengthened beams, there was no evidence that the CFRP reinforcing failed before overall failure of the beams. This was confirmed by the FEA, failure of the RCHBs occurred due to presence of the shear and flexural cracks. These cracks occur at integration points of the solid brick elements.

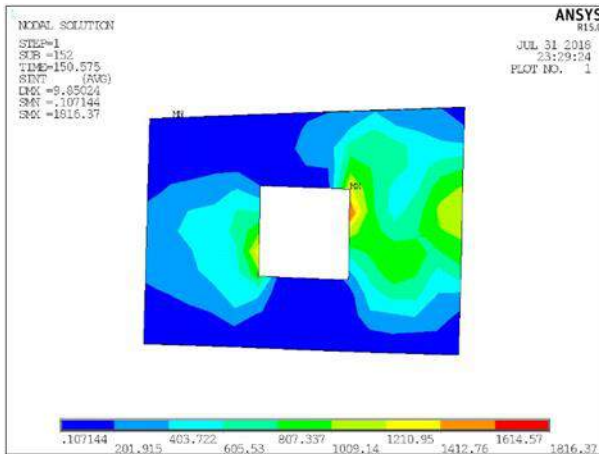
In Table (4-11), maximum stresses and strain of CFRP sheet for the last converged load step for strengthened RCHBs (IHB30-C1, IHB30-C2, HB30-CT1, HB30-CL3, NHB-C1, NHB-C2, and NHB-C3) are summarized as were recorded in ANSYS program.

Figs. (4-53) to (4-55) shows the maximum stresses and strain with their distribution for the three series respectively. The distribution of stresses in these figures give an index for using the CFRP sheet.

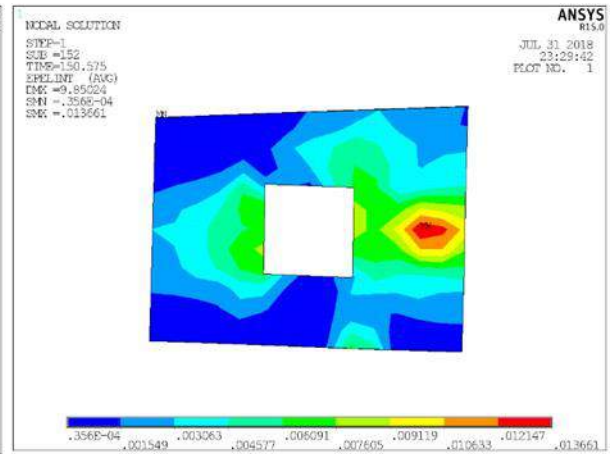


Table (4-11): Maximum stresses and strain in CFRP of the strengthened beams.

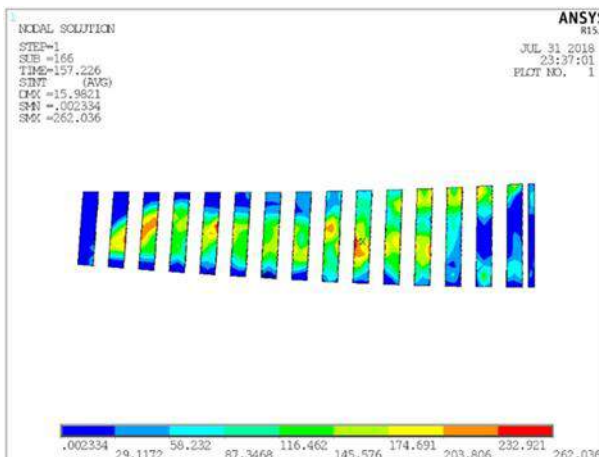
Beam	Maximum tensile stress (MPa)	Maximum tensile strain
IHB30-C1	1816	0.013661
IHB30-C2	262	0.00214
HB30-CT1	1441	0.0316
HB30-CL3	602	0.0484
NHB-C1	1746	0.0169
NHB-C2	2103	0.044
NHB-C3	2367	0.0018



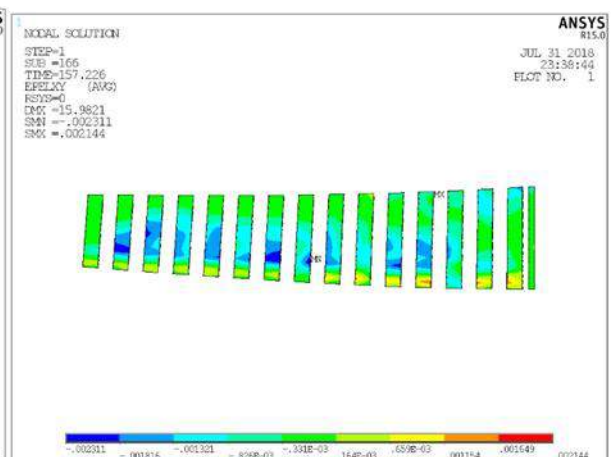
(a1) IHB30-C1 stress.



(a2) IHB30-C1 strain.

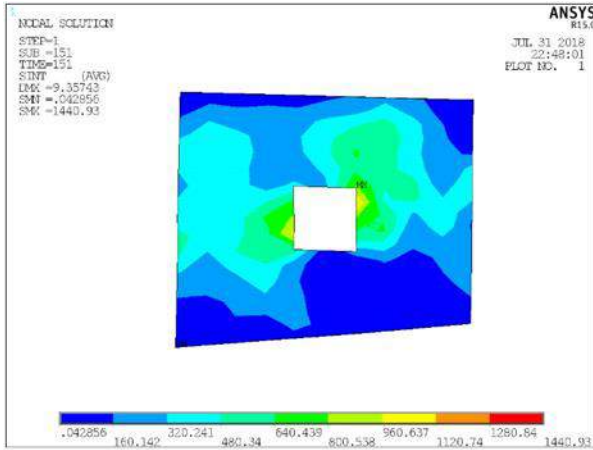


(b1) IHB30-C2 stress.

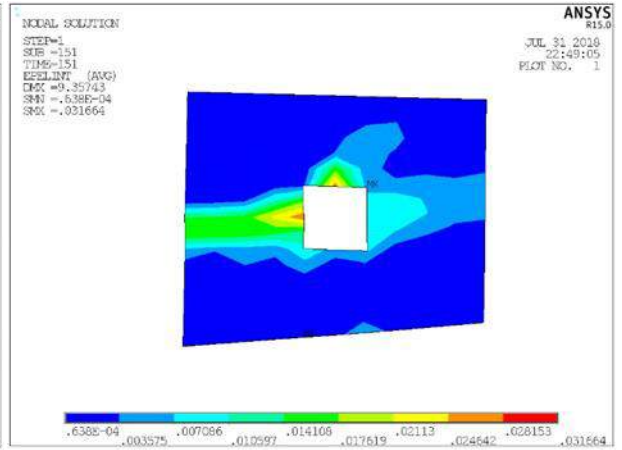


(b2) IHB30-C2 strain.

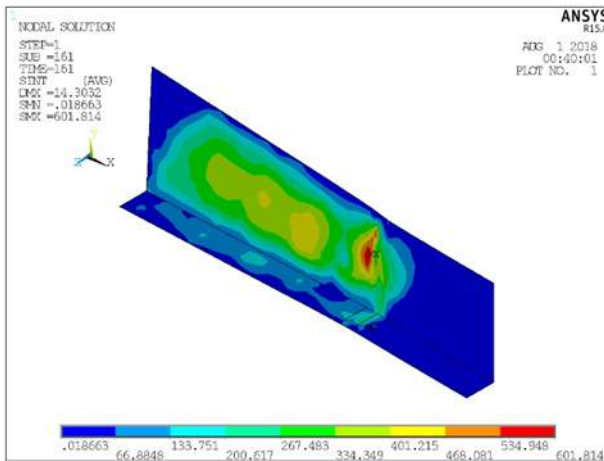
Figure (4-54): Stress and strain of CFRP sheet for beams in series one.



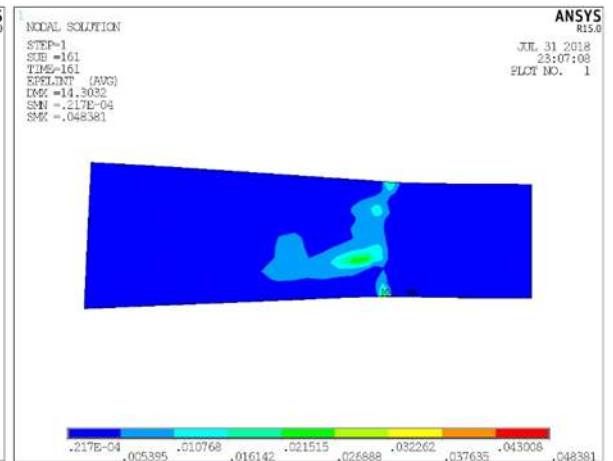
(a1) HB30-CT1 stress.



(a2) HB30-CL3 strain.

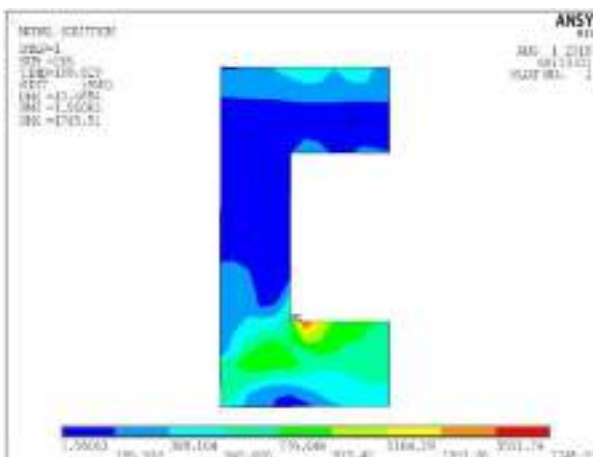


(b1) HB30-CL3 stress.

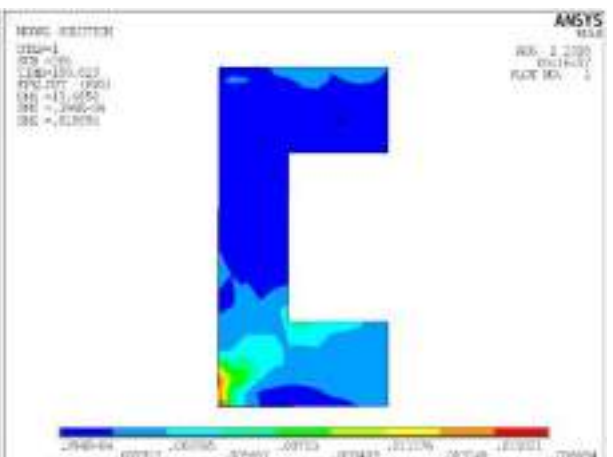


(b2) HB30-CL3 strain.

Figure (4-55): Stress and strain of CFRP sheet for beams in series two.

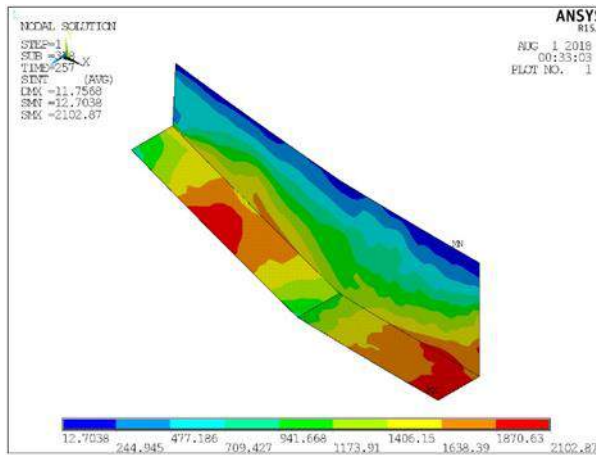


(a1) NHB-C1 stress.

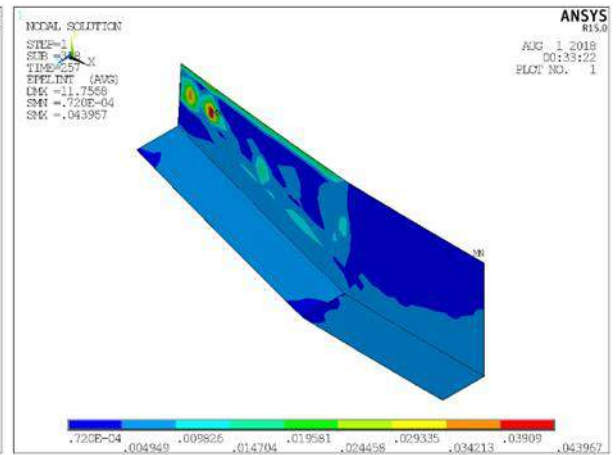


(a2) NHB-C1 strain.

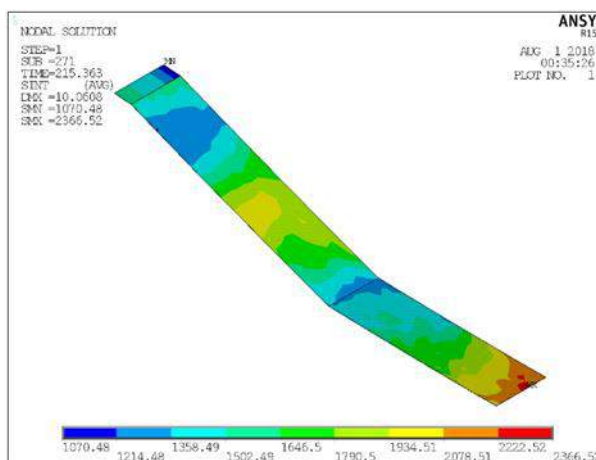
Figure (4-56): Stress and strain of CFRP sheet for beams in series three.



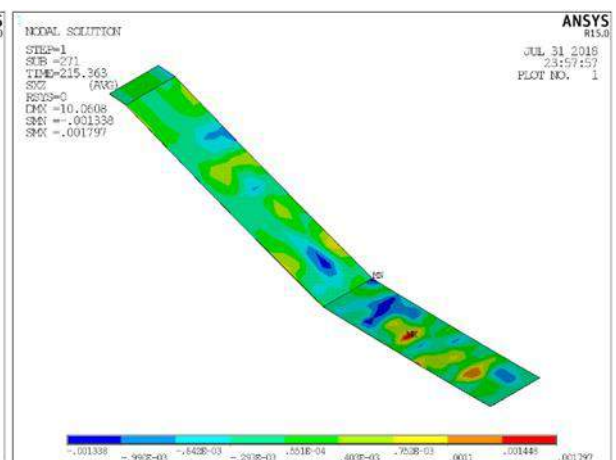
(b1) NHB-C2 stress.



(b2) NHB-C2 strain.



(c1) NHB-C3 stress.



(c2) NHB-C3 strain.

Figure (4-56): Cont.

# CHAPTER FIVE

## CONCLUSIONS AND RECOMMENDATIONS

---

### 5.1 Conclusions

The present numerical study is focused on the behavior on the shear and flexural behavior of reinforced concrete haunched beams (RCHBs). Based on the results obtained from the FEM for the RCHBs, it is concluded that the manner in which shear and flexure failure occurs varies widely. Many factors have significant effect on the shear and flexural behavior of beam at failure, and these effects can be summarized as follows:

- 1) The increasing in the haunch angle decreases the shear carrying capacity with slight increasing in the maximum deflection.
- 2) When stirrups are provided, more shear crack in RCHBs, more shear and flexural cracks occur.
- 3) Presence of a transverse opening reduces the shear strength of beam according to the opening location. The position of the opening has a large influence; this effect is large when the opening position is near the vertex due to the decrement in depth. In RCHBs with an opening at the shear zone, the maximum reduction in ultimate load was about (29%).in case of presence of opening, more shear cracks will develop at the corner of the opening.
- 4) Best location for the opening in RCHBs is position which have higher depth.
- 5) Presence of a longitudinal opening reduces the shear strength of beam according to the opening size. Maximum reduction occurred in the opening (28% h) by (39%) approximately. Cracks started from the

- support and towards the loading point with an intensity around the opening.
- 6) Reinforcement around the opening restored about (63%) of the reduction in strength, that reduced due to existence of opening. Also, Cracks concentrated at the opening corner.
  - 7) In RCHBs, the crack pattern doesn't affect by changing  $f'_c$  for RCHBs with positive haunch angle. While for inverted RCHBs, rising the  $f'_c$  increased the cracks amount in shear and flexural zone.
  - 8) Presence of a transverse opening (120×140) mm in flexural beams with negative haunch reduces the ultimate strength of beam with a slight value. Also, more shear cracks will develop at the corner of the opening with decreasing the amount of cracks in the haunch region.
  - 9) Using CFRP sheet is considered a good way to retrofitting the solid RCHBs and RCHBs with opening. CFRP sheet provided a semi complete restoring to the loss in strength due to the presence of the transverse and longitudinal opening with enhancement in the beam performance.
  - 10) CFRP sheet reduced the loss in shear strength for the beam with opening near the vertex in series one to (8%) only, when it was (29%). For longitudinal opening the lost strength reduced to less than (2%) with large ductility when two layers of CFRP sheet around the beam are used. Also. Some beams with CFRP sheet restored all the occurred loss with gaining additional strength as occurred in the inverted RCHBs and RCHBs with positive and negative haunch angle.
  - 11) Flexural RCHBs with opening can be treated by using CFRP sheet around the opening. strengthening by CFRP restored the loss in strength of the beam but with less ductility due to the material linearity nature of

CFRP sheet.

- 12) Energy dissipation increases by changing the haunch angle and using the CFRP sheet. Increasing the haunch angle increase the energy absorption. The enhancement is (22%). Also, using CFRP sheet around the opening and for the solid RCHB enhanced the energy absorption by 250% and 67% respectively.

## **5.2 Recommendation for Future Works**

Extra investigation to understand the basic behavior of RC beams is required. The following suggestions are recommended:

- 1) Studying the torsion strength of RCHBs with different inclination angles for haunch.
- 2) Investigation of the RCHBs behavior when strengthened with CFRP bar and GFRP sheet.
- 3) Study of the behavior of prestressed RCHBs under general types of loading (experimentally and numerically).
- 4) Detailed study of behavior in RC haunched deep beams.

## REFERENCES

---

- [1] ACI Committee-363. "State of the Art Report on High Strength Concrete", American Concrete Institute, Detroit, 1997.
- [2] Tan, K.H., "Design of Non-Prismatic RC Beams Using Strut and Tie Model", Journal of Advanced Concrete Technology, Vol.2, pp.249-256, March 2004.
- [3] El-Mezaini, N., Balkaya, C., and Citipitioglu, E., "Analysis of Frames with Non-Prismatic Members", Journal of Structural Engineering, Vol. 117, No.6, pp.1573-1592, 1991.
- [4] Colunga, A.T., Aranda. H.I.A., and Cuevasa, O.M.L. "Behavior of Reinforced Concrete Haunched Beams Subjected to Static Shear Loading", Journal Engineering Structures, Vol.30, pp. 478–492, 2008.
- [5] Priyanka, V.M, Kumar. M.P., Kumar, G.V.S., and Vishalakshi, D, "Effect of Haunched Beams in Moment Resisting RC Frames", Vol. 8, Issue 9, pp. 1187–1199, 2017.
- [6] Aziz, A.H., Hassan, H.F., and AbdulRazzaq, F.M., "Experimental Study on Shear Behavior of Reinforced Self-Compacted Concrete Tapered Beams", Civil and Environmental Research, Vol.8, No.8, pp.11-22, 2016.
- [7] Ahmed, A. M., Farghal, O.M., and Sayed, A.M., " Numerical Analysis of Statical Shear Behaviour of Reinforced Concrete Haunched Beams Strengthened by Using Externally Bounded Steel Plates by ANSYS

- Program" *Journal of Scientific and Engineering Research*, Vol. 5, No.2, pp.210-223, 2018.
- [8] ACI Committee 318, "Building Code Requirements for Structural Concrete and Commentary", American Concrete Institute, Farmington Hills, MI 48331, USA, pp.155-202, 2011.
- [9] BS 5400-1, "Steel, Concrete and Composite Bridges. General Statement", British Standards Institute, London, 1988.
- [10] DIN 1045-1 "Concrete, Reinforcement and Prestressed Concrete Structures, Part 1: Design", Deutsches Institut für Normung e.V, 2001.
- [11] Park R. and Paulay T. "Reinforced Concrete Structures", John Wiley and Sons, USA, 1975.
- [12] MacGregor J. G. and Wight J. K., "Reinforced Concrete-Mechanics and Design", fourth edition, Pearson-Prentice Hall, USA, 2005.
- [13] Muttoni A., Shwartz J. and Thürlimann B., "Design of Concrete Structures with Stress Fields", Birkhäuser, Germany, 1997.
- [14] Nielsen M. P., "Limit Analysis and Concrete Plasticity", second edition, CRC Press, USA, 1999.
- [15] El-Niema, E. I., "Investigation of Concrete Haunched T-Beam under Shear", *Journal of Structural Engineer*, Vol.114, No.4, pp.917-930, April, 1988.



- [16] Resheq, A.S., "Strengthening of Continuous Reinforced Concrete Beams by CFRP Laminates". PhD Thesis, University of Technology, Iraq, 2010.
- [17] Ayyad, A.J., "Finite Element Modeling of Reinforced Concrete Columns Strengthened Externally with CFRP Sheets ", M.Sc Thesis, The Islamic University–Gaza, Palestine, October, 2016.
- [18] Stefanou, G.D. "Shear Resistance of Reinforced Concrete Beams with Non-Prismatic Section", Engineering Fracture Mechanics, Vol. 18. No.3, pp.613-666, 1983.
- [19] Colunga, A.T., "the Concerns Regarding the Seismic Design of Reinforced Concrete Haunched Beam", ACI Structural Journal, Vol.91, No.3, pp.287-293, 1994.
- [20] Ozay, G., and Topcu, A., "Analysis of Frames with Non-Prismatic Members", Canadian. Journal of Civil Engineering, Vol.27, No.1, pp.17–25, 2000.
- [21] Galal, K., and Yang, Q., "Experimental and Analytical Behavior of Haunched Thin-Walled RC Girders and Box Girders", Thin-Walled Structures, Vol.47, No. pp.202–218, 2009.
- [22] Megahid, A.E., Rashwan M.M., and Sayed A.M., "Static Behavior of Reinforced High Strength Concrete Haunched Beams Strengthened by Using Epoxy Bonded External Steel Plate", Journal of Engineering Sciences, Vol.38, No.6, pp.1391-1428, 2010.

- [23] Rombach, G.A., Kohl, M., and Nghiep, V.H., "Shear Design of Concrete Members without Shear Reinforcement", *Procedia Engineering*, Vol.14, pp.134–140, 2011.
- [24] Qi, Y., Zhu, C., Zhong, S., Wang, F., and Xiang, Y., "Seismic Performance of Haunched Beam Transfer Structures of Frame-Supported Short-leg Shearwall with Varied Ratio of Short-leg Shearwall Section Height to Thickness ", *Advanced Materials Research*, Vol.255-260, pp.2308-2312, 2011.
- [25] Caldentey, A.P., Padilla, P., Muttoni, A., Ruiz, M.F., " Effect of Load Distribution and Variable Depth on Shear Resistance of Slender Beams without Stirrups", *ACI Structural Journal*, Vol.109, pp.595-603, 2012.
- [26] Al-Maliki, H.N.G.M., "Experimental Behavior of Hollow Non-Prismatic Reinforced Concrete Beams Retrofit with CFRP Sheets.", *Journal of Engineering and Development*, Vol.17, No.5, pp.224–237, November 2013.
- [27] Aranda, H.I.A., Colunga, A.T., and Vega, A.G., "Behavior of Reinforced Concrete Haunched Beams Subjected to Cyclic Shear Loading", *Engineering Structures*, Vol.49, pp.27–42, 2013.
- [28] Orr, J.J., Ibell, T.J., Darby, A.P., and Evernden, M., "Shear Behaviour of Non-Prismatic Steel Reinforced Concrete Beams", *Engineering Structures*, Vol.71, pp.48–59, 2014.
- [29] Hou, C., Matsumoto, K., and Niwa, J., "Shear Failure Mechanism of Reinforced Concrete Haunched Beams", *Journal of JSCE*, Vol.3, pp.230-245, 2015.

- [30] Domínguez, E.A.G., Colunga, A.T., and Luna, G.J., "Nonlinear finite element modeling of reinforced concrete haunched beams designed to develop a shear failure", *Engineering Structures*, Vol. 105, pp.99–122, 2015.
- [31] Albegmpri, H.M.A., Cevik, A., and Kurtoglu, A.E., "Reliability Analysis of Reinforced Concrete Haunched Beams Shear Capacity Based on Stochastic Nonlinear FE Analysis", *Computers and Concrete*, Vol.15, No.2, PP.259-277, 2015.
- [32] Dawood, M.B., and Nabbat, R.A., "Flexural and Shear Strength of Non-Prismatic Reinforced High Strength Concrete Beams with Opening and Strengthened with NSM-CFRP Bars", *International Journal of Civil Engineering and Technology (IJCIET)*, Vol. 6, Issue 9, pp. 93-103, 2015.
- [33] Jolly, A., and Vijayan, V., "Structural Behaviour of Reinforced Concrete Haunched Beam Study on ANSYS and ETABS", *International Journal of Innovative Science, Engineering & Technology*, Vol. 3, Issue 8, pp.495-500, 2016.
- [34] Hou, C., Nakamura, T., Iwanaga, T., and Niwa, J., "Shear Behavior of Reinforced Concrete and Prestressed Concrete Tapered Beams without Stirrups", *Journal of JSCE*, Vol.5, pp.170-189, 2017.
- [35] Colunga, A.T., Californias, L.A.U., and Aranda, H.I.A., "Assessment of the Shear Strength of Continuous Reinforced Concrete Haunched Beam Based upon Cyclic Testing", *Journal of Building Engineering*, JOBE257, pp.1-38, 2017.

- [36] Mansur, M.A., and Alwist, W.A.M., "Reinforced Fibre Concrete Deep Beams with Web Openings", *The International Journal of Cement Composites and Lightweight Concrete*, Vol.5, No.4, pp.263-271, 1984.
- [37] Tian, K.H., Mansur, M.A., and Huang, L.M., "Reinforced Concrete T-Beams with Large Web Openings in Positive and Negative Moment Regions", *ACI Structural Journal*, Vol. 93, No.3, pp.277-289, 1996.
- [38] Abdulla, H.A., Torkey, A.M., Haggag, H.A., and Abu-Amira, A.F., "Design Against Crack at the Opening in the Reinforced Concrete Beam Strengthened with Composite Sheet", *Composite Structure Journal*, No.60, pp.197-204, 2003.
- [39] Mosallam, A.S., and Banerjee, S., "Shear Enhancement of Reinforced Concrete Beams Strengthened with FRP Composite Laminates", *Composites Part B: Engineering*, Vol. 38 Issue 5-6 pp.781-793, 2007.
- [40] Dawlat, D.A., "Experimental and Theoretical Investigation of the Behavior of Reinforced Concrete Beams Strengthened by Fiber Reinforced Polymer", Ph. D. Thesis, University of Baghdad, College of Engineering, Iraq, 2007.
- [41] Najim, W.N., " Experimental and Theoretical Investigation of the Behavior of RC Deep Beams with Openings Strengthened by CFRP Laminates", M.Sc. Thesis, College of Engineering, University of Babylon, Iraq, 2009.
- [42] Chin, S.C, Shafiq, N., and Nuruddin, M.F., "Finite Element Modelling of RC Beams with Large Opening at Critical Flexure and Shear Strengthened with CRFP Laminates" 7th International Conference on Steel & Aluminium Structures 13th-15th July 2011 Kuching, Sarawak, Malaysia, 2011.

- [43] Al-Dolaimy, A., "Structural Behavior of Continuous Reinforced Concrete Beams with Openings and Strengthened by CFRP Laminates", M.Sc. Thesis, College of Engineering of University of Babylon, Iraq, 2011.
- [44] AbdulRedha, D.A., "Flexural Behavior of Steel Fiber Self-Compacting Concrete Beams". M.Sc. Thesis, College of Engineering, University of Babylon, Iraq, 2012.
- [45] Dobrzański, L.A., Pusz, A., Nowak, A.J., and Górnjak, M., "Application of FEM for Solving Various Issues in Material Engineering", Journal of Achievements in Materials and Manufacturing Engineering, Vol.42, Issue 12, pp.134-141, 2010,
- [46] Madenci, E., and Guven, I., "the Finite Element Method and Application in Engineering Using ANSYS", Springer New York Heidelberg Dordrecht London, 2nd Edition, ISBN:978-1-4899-7550-8, (2015).
- [47] Hinton, E., and Owen, D.R.J., "An Introduction to Finite Element Computations", Pineridge Press limited, Swansea, U. K., 1979.
- [48] Moaveni, S., "Finite Element Analysis Theory and Application with ANSYS", Prentice Hall, Upper Saddle River, New Jersey 07458, 1999.
- [49] Zienkiewicz, O.C., "The Finite Element Method", 3rd Ed., McGraw-Hill Book Company, New York, 1977.

## *References*

---

- [50] Fanning, P., "Nonlinear Model of Reinforced and Post-Tensioned Concrete Beams", *Electronic Journal of Structural Engineering*, Vol.2, pp.111-119, 2001.
- [51] Kwak, H., and Filippou, F.C., "Finite Element Analysis of Reinforced Concrete Structures Under Monotonic Load", Department of Civil Engineering / University of California / Berkeley / California, USA, Report No. UCB SEMM-90/14, November, 1990.
- [52] Wischers, G., "Application of Effects of Compressive Loads on Concrete", *Betontechnische Berichte*, No.2 and 3, Duesseldorf, Germany, 1978.
- [53] Guide to Quality Control and Testing of High-Strength Concrete Reported by ACI Committee 363.2R-92.
- [54] Chen, W.F., "Plasticity in Reinforced Concrete", McGraw-Hill, 1982.
- [55] Hsu, L.S., and Hsu, C.T.T., "Complete Stress-Strain Behaviour of High-Strength Concrete under Compression", *Magazine of Concrete Research (ASCE Journal)*, Vol.46, No.169, pp.301-312, 1994.
- [56] ASCE Committee on Concrete and Masonry Structures, "A State of the Art Report on the Finite Element Analysis of Reinforced Concrete structures", ASCE Special Publication, 1981.
- [57] Desayi, P., and Krishnan, S., "Equation for the Stress-Strain Curve of Concrete", *Journal of the American Concrete Institute*, Vol.61, No.3, pp.345-350, March, 1964.

## *References*

---

- [58] Chen, W.F. and Saleeb, A.F., "Constitutive Equations for Engineering Materials", West Lafayette, Indiana, December 1981.
- [59] Balbool, A. N.A., "Prestressed Fiber Reinforced Polymer (FRP) for Strengthening of Concrete Members", Ph.D. Thesis, University of Baghdad, Civil Engineering Department, Iraq, 2009.
- [60] Kupfer, H. P., Hilsdorf, H. K., and Rusch, H., "Behavior of Concrete under Biaxial Stresses", ACI Journal, Proceedings, Vol.66, No.8, pp.656-666, 1969
- [61] Ali, M.S., "Experimental and Theoretical Investigation of Concrete Slabs on Grade ", Ph.D.Thesis, College of Engineering, University of Basrah, Iraq, 2010.
- [62] Li, Q., and Ansari, F., "High-Strength Concrete in Uniaxial Tension", ACI Structural Journal, Vol.97, No.1, pp.49-57, 2000.
- [63] Banzant, Z.P., "Comment on Orthotropic Models for Concrete and Geomaterials", Journal of Engineering Mechanics Division, ASCE, Vol.106, No. 3, pp. 849-865, 1983.
- [64] Willam, K., and Warnke, E., "Constitutive Model for the Triaxial Behavior of Concrete", Proceedings International Association for Bridge and Structural Engineering, Vol.19, pp. pp. 1-30, Bergamo, Italy, 1975.
- [65] ANSYS, "Analysis Guide", Version 11, Swanson Analysis System Inc., 2007.

- [66] Rashid, Y.R., "Analysis of Prestress Concrete Pressure Vessels", *Journal Nuclear Engineering and Design*, Vol.7, No.4, pp.334-344, 1968.
- [67] Hawileh, R.A., Rahman, A., and Tabatabai, H., "Nonlinear Finite Element Analysis and Modeling of Precast Hybrid Beam–Column Connection Subjected to Cyclic Loads", *Applied Mathematical Modelling*, Vol. 34, pp. 2562-2583, 2010.
- [68] Hawileh, R.A., Abdalla, J.A., and Tanarlan, M.H., "Modeling of Nonlinear Response of RC Shear Deficient T-Beam Subjected to Cyclic Loading", *Computers and Concrete*, Vol.10, No.4, pp. 413–428, 2012.
- [69] Padmarajaiah, S.K., and Ramaswamy, A.A., "Finite Element Assessment of Flexural Strength of Prestressed Concrete Beams with Fiber Reinforcement", *Cement Concrete Composite*, Vol.41, pp.24-229, 2002.
- [70] European Committee for Standardization (CEN), Eurocode 3, "Design of Steel Structures", Part 1.1: General Rules and Rules for Building, DD ENV, EC3, 1993.
- [71] Al-Sahlawi, Y.M.Y., "Strengthening of Self Compacting Reinforced Concrete T-Deep Beams with Opening by CFRP Sheet", M.Sc. Thesis , College of Engineering, University of Kufa, Iraq, 2018.
- [72] Wolanski, A.J., "Flexural Behavior of Reinforced and Prestressed Concrete Beams Using Finite Element Analysis", M.Sc. Thesis, University of Marquette, 2004.



## *References*

---

- [73] Kachlakev, D., Miller, T., Yim. S., Chansawat, K., Potisuk, T., "Finite Element Modeling of Reinforced Concrete Structures Strengthened with FRP Laminates", Report SPR 316, California Polytechnic State University, San Luis Obispo, 2001.
- [74] Huang, H., Han, L.H., and Zhao, X. L., "Investigation on Concrete Filled Double Skin Steel Tubes (CFDSTs) under Pure Torsion", Journal of Constructional Steel Research, Vol.90, pp.221-234, 2013.
- [75] Al-Tai, S., "Nonlinear behavior of Reinforced Concrete T- beam strengthened with CFRP subjected to shear", M.Sc. Thesis, College of Engineering, University of Babylon, Iraq, 2007.
- [76] ANSYS Manual, Version (13), USA, 2011.

# **APPENDIX -A-**

## ***FINITE ELEMENT MODELING***

---

---

### **A.1 Finite Element Modeling**

In this section, modeling of one specimen is performed. This specimen is beam from series one. The model is RCHBs with positive haunch angle.

In building of any FE model it is necessary to define the element types, element real constants and material properties. A mesh is generated by defining nodes and connecting them to define the elements. After completing this step, the solution process used to define the analysis type and analysis options, applying loads and boundary conditions.

#### **A.1.1 Used Element**

For the solid RCHBs with CFRP sheet (G1-M32), used element in the modeling of the concrete, steel reinforcement, steel plate, and CFRP sheet is shown below in Table (A-1).

Table (A-1): Used element of a model in ANSYS.

<b>Material Type</b>	<b>ANSYS Element</b>
Concrete	SOLID65
Steel reinforcement	LINK180
Steel plate	SOLID185
CFRP sheet	SHELL41

#### **A.1.2 Real Constants**

Another entity for proper modeling is the real constants. It is worth to mention that many real constants may be input for an individual element. All used real constants are tabulated below in Table (A-2). Due to the symmetry, modeling the reinforcement rebar performed by creating two bars only from the

bottom longitudinal reinforcement. Top bars included modeling one and ½ Ø25 is created at the cut off plane of symmetry.

Table (A-2): Real constant of the used element in ANSYS.

Real constant set	Element type	Constant			
			Real constant for rebar 1	Real constant for rebar 2	Real constant for rebar 3
1 (Concrete)	SOLID65	Material number	0	0	0
		Volume ratio	0	0	0
		Orientation angle	0	0	0
		Orientation angle	0	0	0
2 (Ø25 rebar)	LINK180	Cross-section area (mm2)	507		
2 (½ Ø25 rebar)	LINK180	Cross-section area (mm2)	254		
3 (Ø10 rebar)	LINK180	Cross-section area (mm2)	78.54		
4 (CFRP)	SHELL41	Shell thickness at Node I TK(I)	0.167		
		Node J TK(J)	0.167		
		Node K TK(K)	0.167		
		Node L TK(L)	0.167		
		Element x-axis rotation	0		
		Elastic foundation stiffness	0		
		Added mass/unit area	0		

### A.1.3 Material Properties

All parameters for the material models were illustrated in Tables. (A-3) to A-7). ANSYS element needs some properties for proper entities which are termed "linear isotropic, linear orthotropic, multilinear isotropic, and bilinear material" for different materials. Many of terms need to define. EX means the

concrete modulus of elasticity ( $E_c$ ). PRXY is the Poisson ratio ( $\mu$ ) which was assumed to be 0.2 for concrete and 0.3 for steel. The stress-strain curve of the concrete that obtained from the equation is used in the modeling of the multilinear isotropic.

Table (A-3): Material properties for concrete.

<b>Linear Isotropic</b>	
EX	25153 MPa
PRXY	0.2

<b>Multilinear Isotropic</b>		
Point 1	0.00025	6.288
Point 2	0.0005	11.99797
Point 3	0.00075	17.01861
Point 4	0.001	21.08666
Point 5	0.00125	24.16132
Point 6	0.0015	26.31299
Point 7	0.00175	27.67462
Point 8	0.002	28.40027
Point 9	0.0025	28.51579
Point 10	0.0035	28.24

<b>Concrete</b>	
ShrCf-Op	0.4
ShrCf-Cl	0.9
UnTensSt	2.86
UnCompSt	28.64
BiCompSt	0
HydroPrs	0
BiCompSt	0
UnTensSt	0
TenCrFac	0.9

Table (A-4): Material properties for Ø25 rebar (longitudinal bar).

<b>Linear Isotropic</b>	
EX	200000 MPa
PRXY	0.3
<b>Bilinear Isotropic</b>	
Yield Stss	427 MPa
Tang Mod	448 MPa

Table (A-5): Material properties for Ø10 rebar (stirrups).

<b>Linear Isotropic</b>	
EX	200000 MPa
PRXY	0.3
<b>Bilinear Isotropic</b>	
Yield Stss	451 MPa
Tang Mod	452 MPa

Table (A-6): Material properties for CFRP sheet.

<b>Linear orthotropic</b>	
EX	240000 MPa
EY	1
EZ	1
PRXY	0.3
PRYZ	0
PRXZ	0
Gxy	1
Gyz	1
Gxz	1

Table (A-7): Material properties for steel plate.

<b>Linear Isotropic</b>	
EX	210000 MPa
PRXY	0.3

#### **A.1.4 Modeling and Meshing**

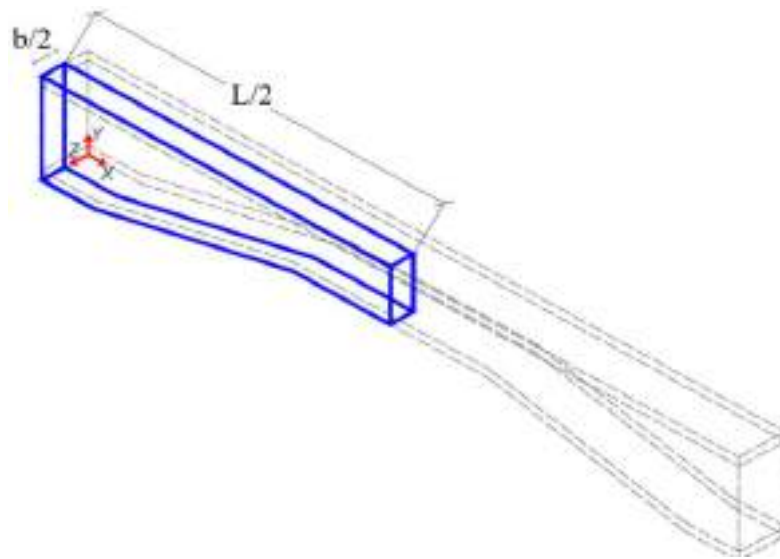
A three-dimension model of the concrete structure is built using ANSYS. Modelling haunched beam in Cartesian coordinate system is created with number of elements about 9400. All beams in this work have number of elements (8000-9700).

The process involved creating these type of beam in three regions. The first and third regions (prismatic zone) were created in X and Y axes while the second region (haunch zone) created in inclined axes  $\zeta$  and  $\eta$  axes. The region creating was done by generate the first node and take the advantage of the contract copying feature to complement the beam modelling. Then the concrete element was created by using command prompt line input in each region and take advantage of the contract copying feature too.

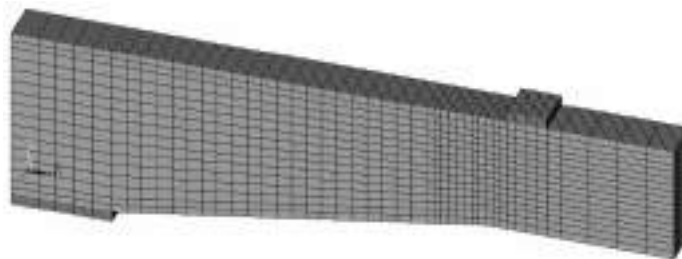
The concrete beam was modelled using a special concrete element SOLID 65. It enables to define up to the rebar materials within the concrete. In the current work, modelling the reinforcement by Link 180 is assumed to be discrete modelling throughout the element. The bond between the concrete and steel bars assumed as perfect bonding between them.

In order to reduce the computational effort, symmetry conditions for the studied RCHB were taken into account, only one quarter of the beam to be modeled. Therefore, the corresponding length for the haunched beam section modeled is  $L/2$  with a width of  $b/2$ , as depicted in Fig. (A-1 a).

It is worth noting that the meshing for each RCHB varies in each beam, additional stirrups were placed at different spacing from the vertex formed by the intersection of tapered sections with the prismatic section, to account for the vertical force introduced by the inclined longitudinal steel reinforcement in tension due to the change of direction. The concrete beam and the loading and support plates are identified in Fig. (A-1 b). Also, the meshing corresponding to the flexural and shear reinforcement.



**(a) Haunched beam section modeled (continuous line).**



**(b) Mesh for the concrete, and loading & support bearing plates**

**Figure (A-1): Haunched beam modeling.**

Flexural and shear steel reinforcement have some shared nodes as revealed in Fig. (A-2).

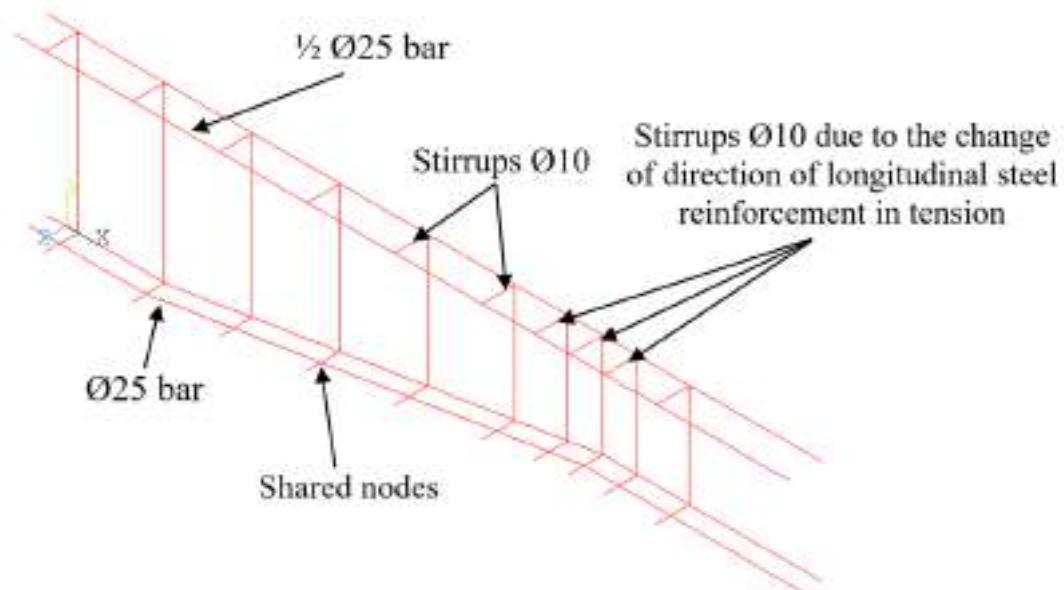


**Figure (A-2): Details of the flexural and shear reinforcement.**

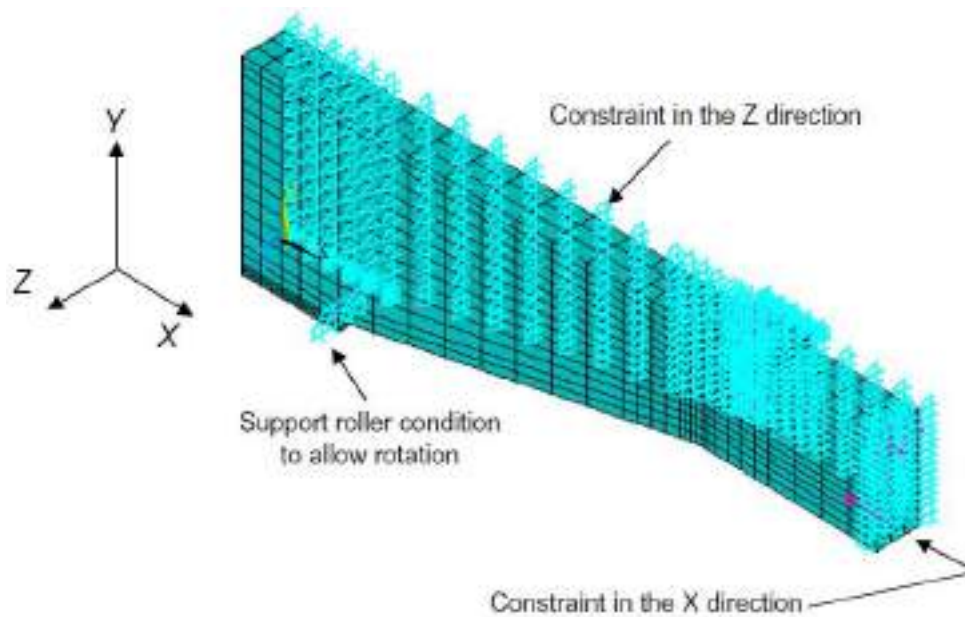
### **A.1.5 Boundary Conditions and Loading**

It has been found that the simulation of the applied load and the supports has significant effect on the results of the finite element analysis. Bearing plate has been used to distribute the applied load on an area to get a unique solution. To ensure that the model acts the same way as the experimental beam, the boundary conditions needed to be applied at points of symmetry and where the supports exist as depicted in Fig. (A-3 a). The boundary conditions are:

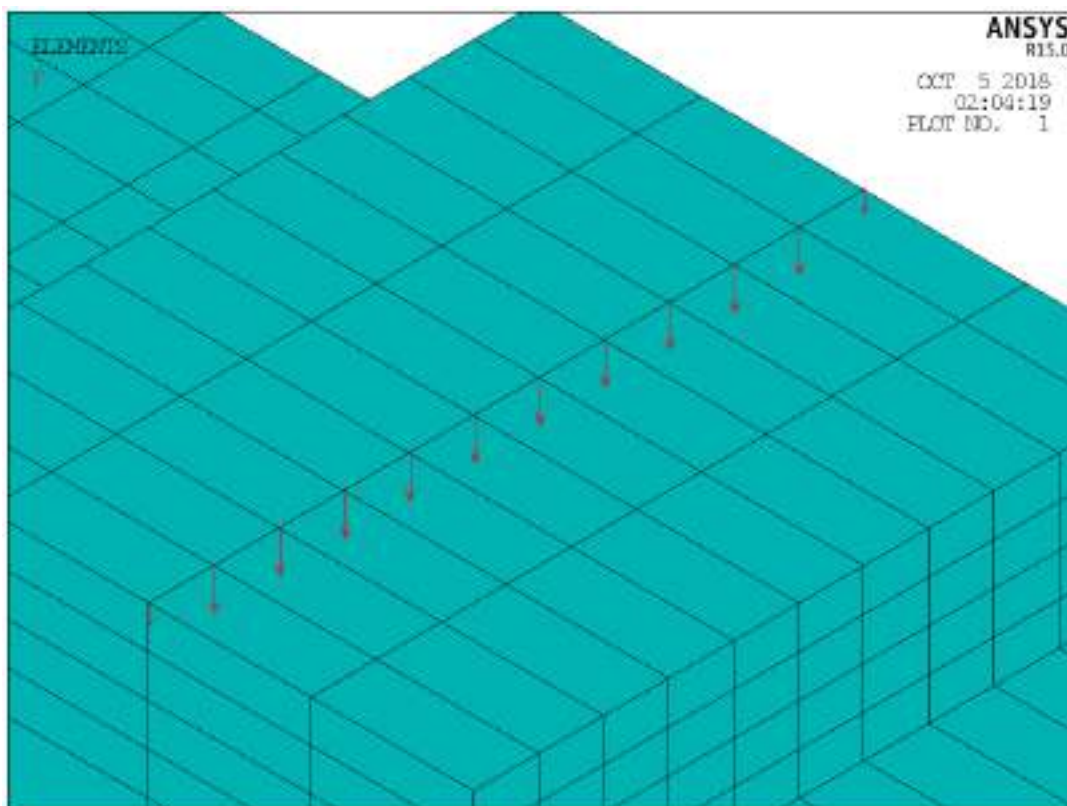
- 1) The concrete beam was supported by roller at the bottom with a distance 200 mm wide from the edge of the beam with no displacement of the nodes in the Y and Z direction.
- 2) The model being used is symmetry about two planes. The symmetric boundary conditions are applied at the two cut planes XY and XZ parallel to axis of the beam and all nodes on each plane of symmetry were supported in their direction only in the direction normal to that plane.
- 3) A concentrated load was applied on the single line of a steel plate which was placed in 100 mm wide from the vertex. The distribution of the applied load on the nodes is that the load divided on the number of nodes, the nodes at the



edge of plate will carry the half value of internal nodes as illustrated in Fig. (A-3 b).



(a) Boundary condition of RCHBs model.



(b) Loading method for RCHBs model.

Figure (A-3): Loading and boundary condition of RCHBs.

### **A.1.6 Analysis Type**

Actually, the static analysis was used for analyzed the models of all beams utilized in this study. The analysis was taken as small displacement and static which Performs a linear static analysis, i.e., a static analysis in which large deformation effects are ignored. The time at the end of the load step refers to the ending load per load step and the total time refers to total applied load. The time step refers to the time increment with maximum and minimum size. While the commands of the nonlinear algorithm and convergence criteria are used as tabulated in Table (A-8).

Table (A-8): The analysis commands in ANSYS.

<b>Designation</b>	<b>Command</b>
Analysis option	Small displacement
Calculate prestress effect	No
Time at end of Loadstep	Per applied load
Time step size	On
Maximum time step	1
Minimum time step	0.005
Write Items to Results File	All soluton items
Frequency	Write every substep

The aim in this study is to ensure that all selections are adequate to model the members. Tables (A-9) to (A-11) shows the commands of FE procedure used for the analysis of RCHBs.

Table (A-9): The analysis commands.

Equation Solvers	Sparse Direct
Number of restart file 1	1
Frequency	Write every substep

Table (A-10): The solution commands.

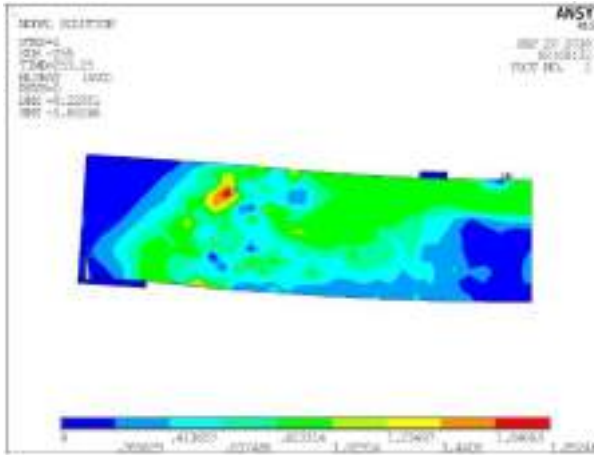
Line Search	on
DOF solution predictor	Prog. Chosen
Maximum number of iteration	200
Cutback control	Cutback according to predicted number of iter.
Equiv. Plastic Strain	0.15
Explicit Creep ratio	0.1
Implicit Creep ratio	0
Incremental displacement	10000000
Points per cycle	13
Set Convergence Criteria	
Label	F
Ref. Value	Calculated
Tolerance	0.05
Norm	Infinite norm
Min. Ref	Not applicable

Table (A-11): Commands for finishing analysis.

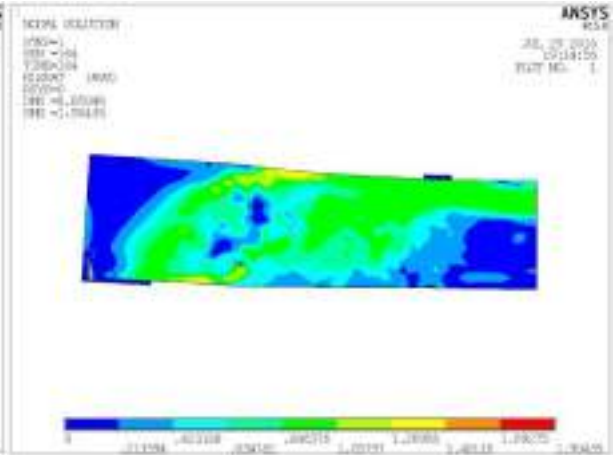
Program behavior upon non-convergence	Terminate but do not exit
Nodal DOF sol'n	0
Cumulative iter.	0
Elapsed time	0
CPU time	0

## APPENDIX -B-

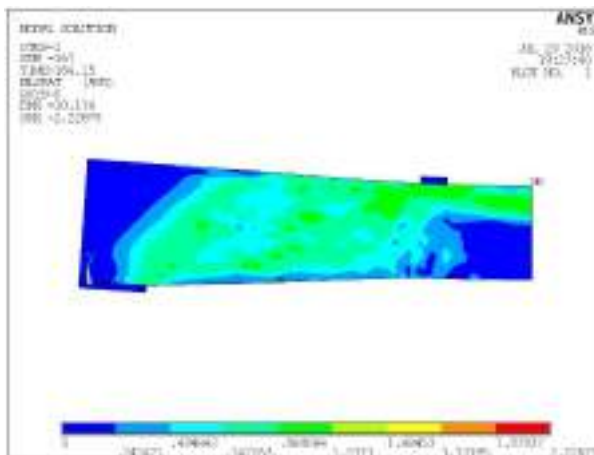
### *SHEAR STRESS DISTRIBUTION OF SERIES TWO*



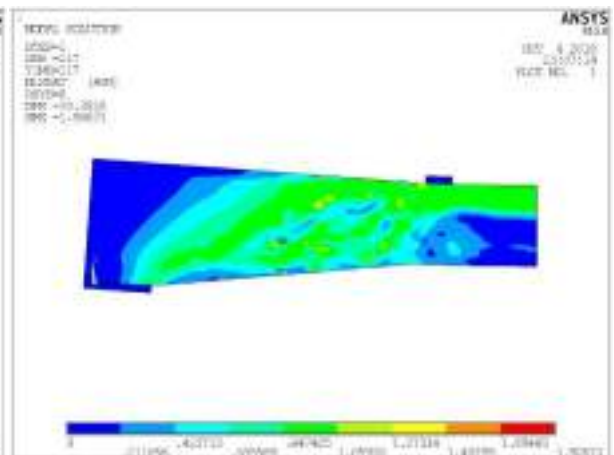
(a) Beam RB30-0.



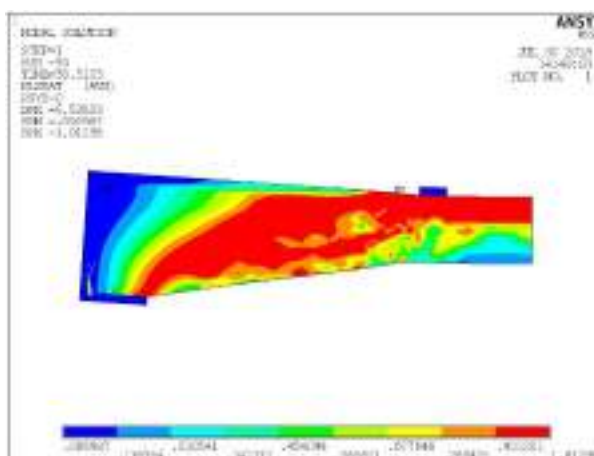
(b) Beam HB30-3.



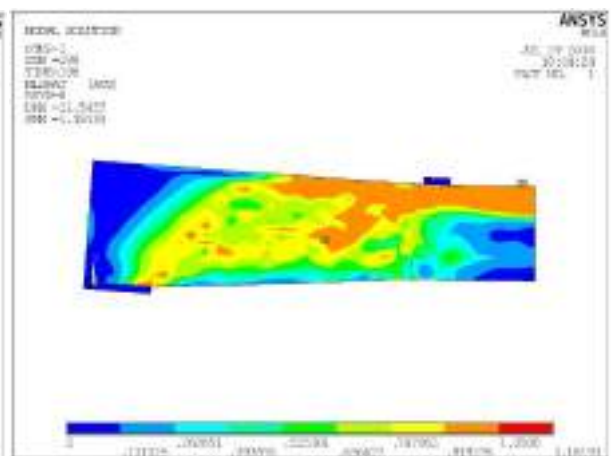
(c) Beam HB30-6.



(d) Beam HB30-9.

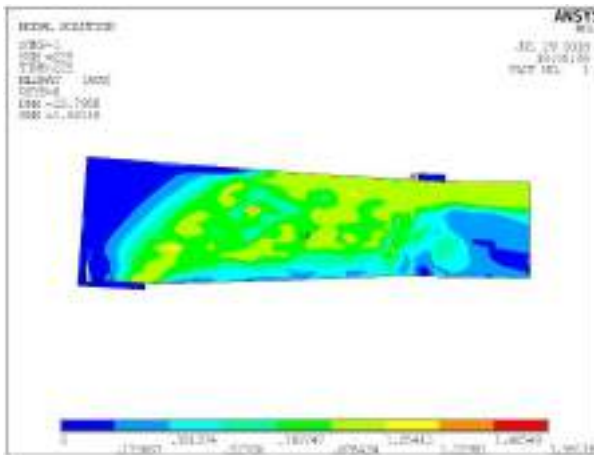


(e) Beam HB30-12.

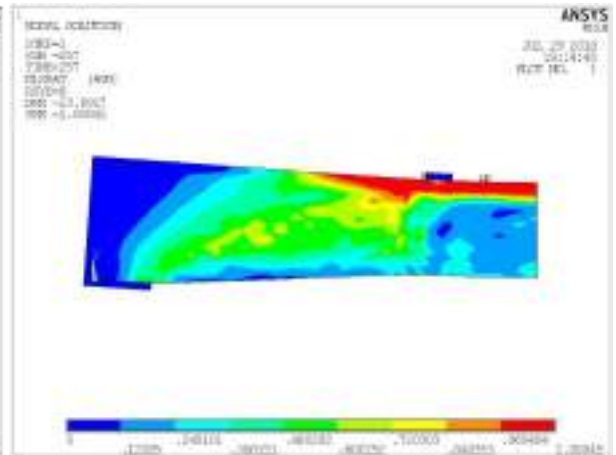


(f) Beam HB40-6.

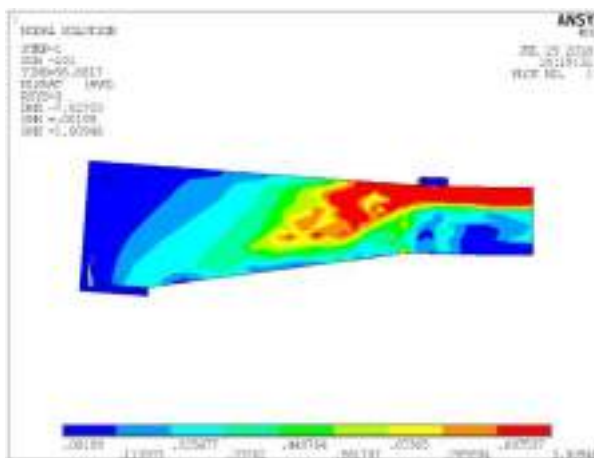
Fig. (B-1): Shear stress distribution for series two beams.



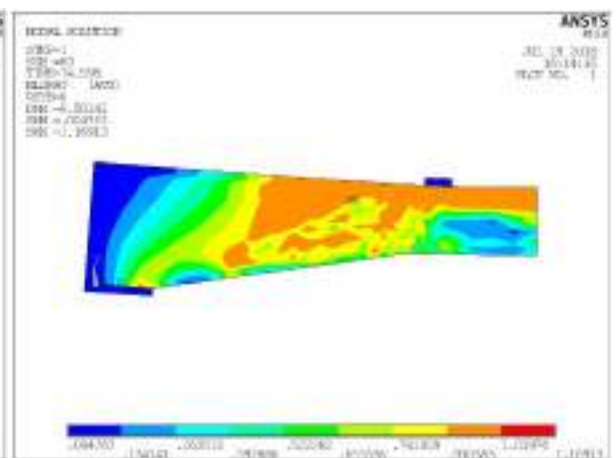
(g) Beam HB50-6.



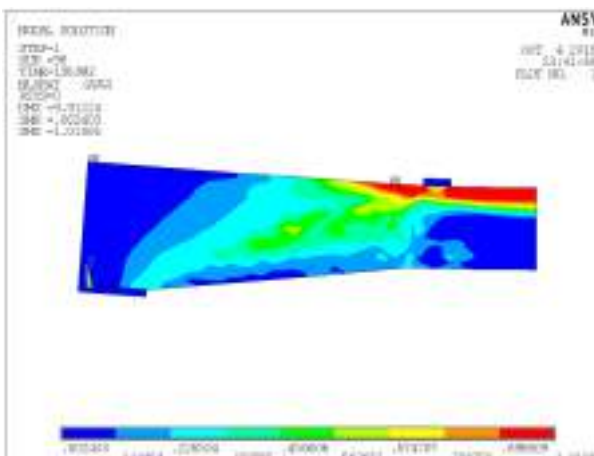
(h) Beam HB70-6.



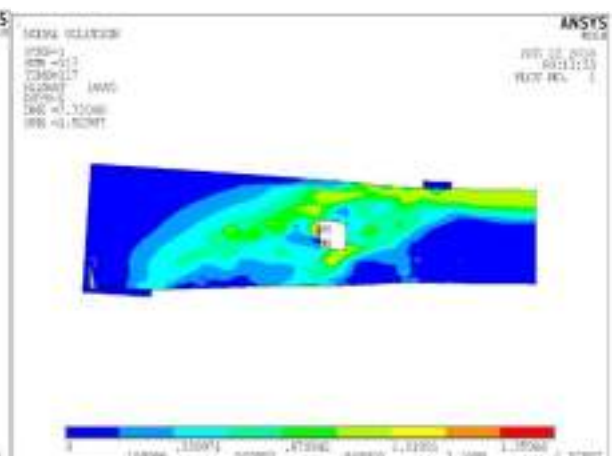
(i) Beam HB40-12.



(j) Beam HB50-12.



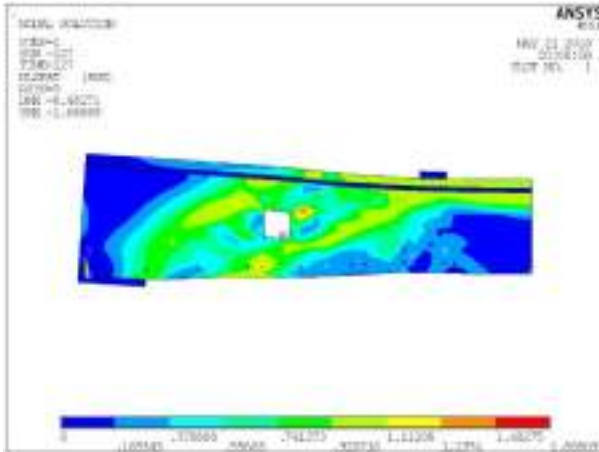
(k) Beam HB70-12.



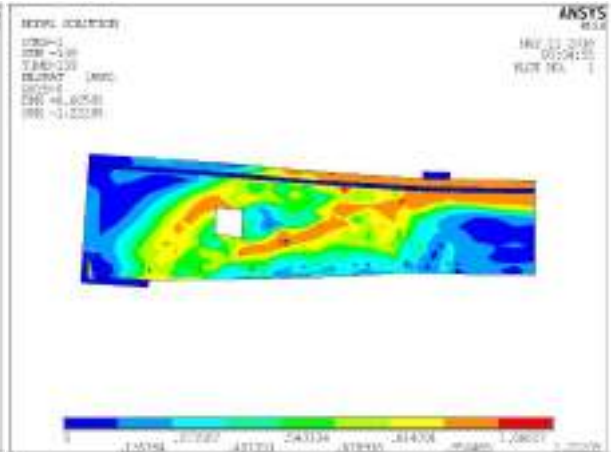
(l) Beam HB30-TO1.

Fig. (B-1): Cont.

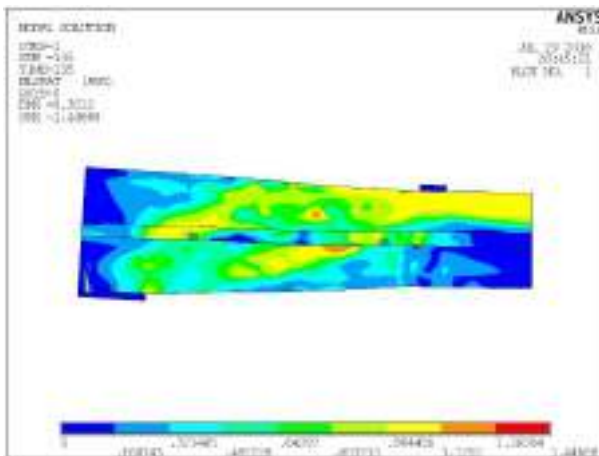




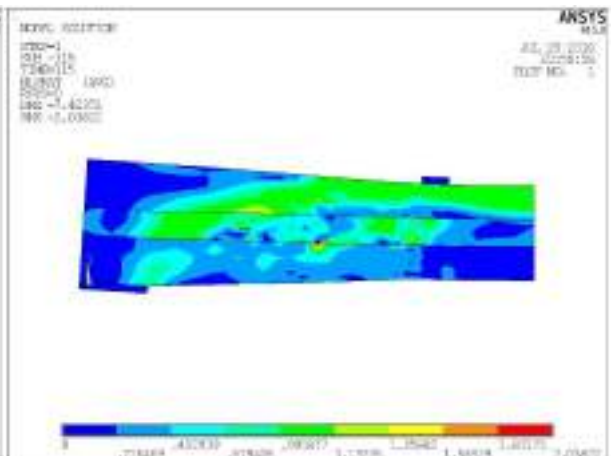
(m) Beam HB30-TO2.



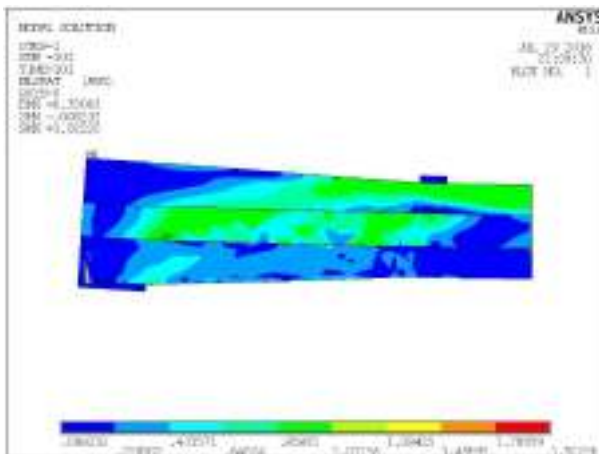
(n) Beam HB30-TO3.



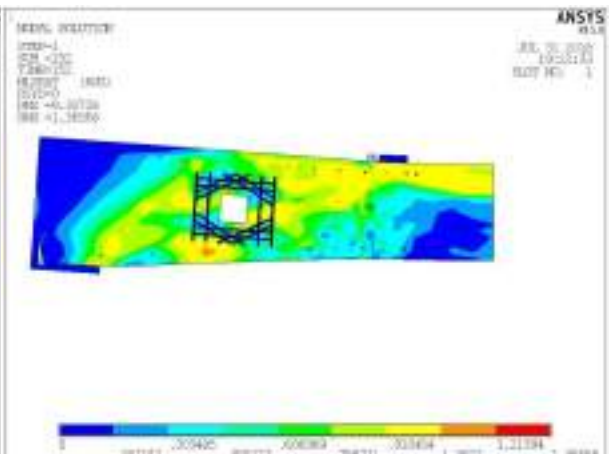
(o) Beam HB30-LO1.



(p) Beam HB30-LO2.

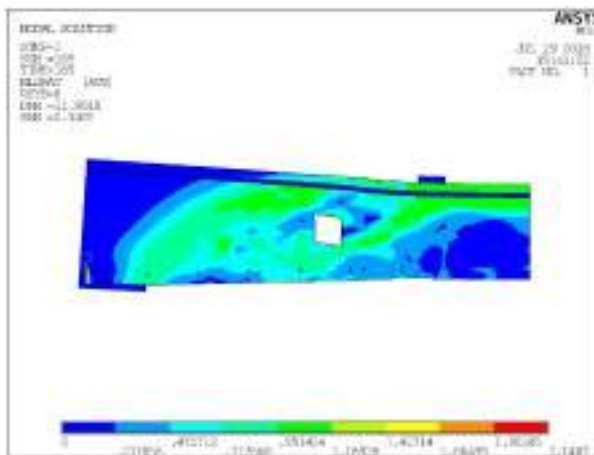


(q) Beam HB30-LO3.

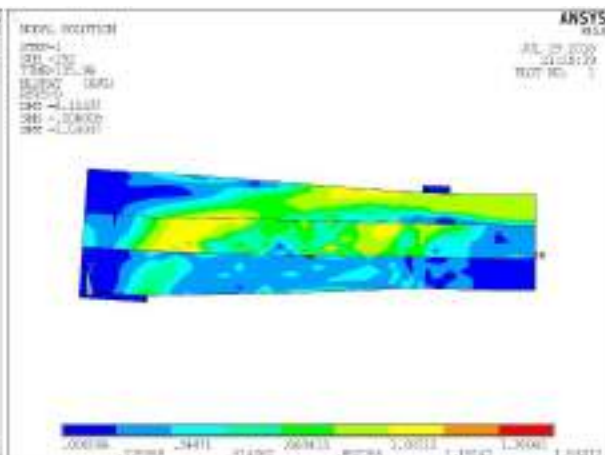


(r) Beam HB30-RO2.

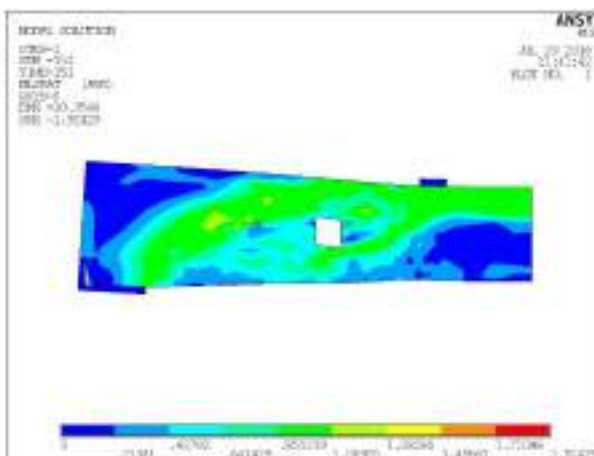
Fig. (B-1): Cont



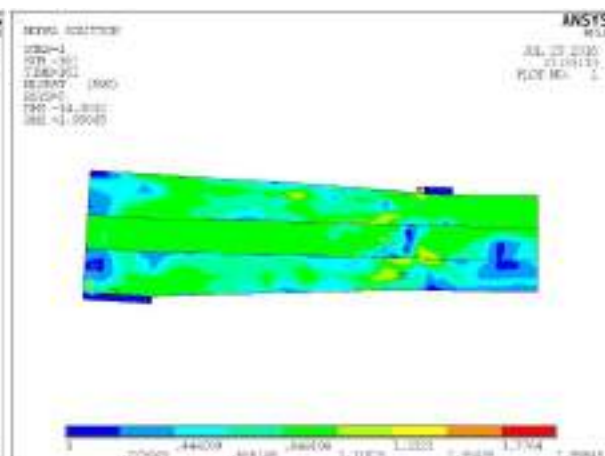
(s) Beam HB50-TO1.



(t) Beam HB40-LO3.



(u) Beam HB30-CT1.



(v) Beam HB40-CL3.

Fig. (B-1): Cont

## الخلاصة

هذه الدراسة تقدم التحريات النظرية لسلوك الانحناء والقص لـ43 عتبة من العتبات غير المشورية المسلحة مع او بدون الفتحات للخرسانة ذات المقاومة العادية وعالية المقاومة بسيطة الاسناد وتحت احمال ساكنة. بالاضافة الى ذلك تم استخدام التقوية بواسطة الياف الكربون البوليمرية (CFRP Sheet).

ينقسم العمل الحالي الى ثلاث مجاميع, تم تنفيذ. عملية التحقق نفذت على عتبات خرسانية من النوع الناتئ وتم تحليلها بواسطة التحليل اللاخطي باستخدام نظرية العناصر المحددة باستخدام برنامج (ANSYS V.15). للتأكد من صحة ودقة الخطوات المستخدمة في الحل والتي قدمت بواسطة عدة باحثين. نتيجة التحقق اظهرت تطابقا جيدا في المقارنة بين نتائج العملي والنظري حيث تضمنت منحنى القوة-الازاحة ونمط التشقق. كذلك تمت دراسة متغيرات عدة على هذا انواع مختلفة من العتبات الناتئة. المجموعة الأولى تضمنت تحليل القص للعتبات الناتئة المقلوبة بينما المجموعة الثانية والثالثة تضمنت عتبات ناتئة ذات ميل موجب وسالب تباعا. المتغيرات التي تمت دراستها هي زيادة مقاومة الانضغط, وجود فتحات عرضية , وجود فتحات طولية, واستخدام الياف الكربون البوليمرية لتقوية العتبات ومعالجة النقص الحاصل نتيجة وجود الفتحة. أظهرت النتائج ان ان هذا النوع من العتبات لديه قابلية عالية على التشوه وامتصاص الطاقة وان زيادة زاوية الميل تقلل من مقاومة القص للعتبات غير المشورية. ان الزيادة في مقاومة الانضغاط ادت الى زيادة في مقاومة القص للعتبات الخرسانية غير المشورية الفاشلة بالقص. وجود الفتحات قام بتقليل مقاومة القص والانتشاء والجساءة للعتبات. اقصى هبوط للمقاومة حدث بوجود الفتحة العرضية (100\*100) هو بقيمة 29% من مقاومة العتبة. اقصى هبوط بالمقاومة عند وجود فتحة طولية (125\*125) ملم كان بمقدار 39%. بالاضافة الى ان تسليح الفتحة بواسطة قضبان الحديد واستخدام خرسانة ذات مقاومة عالية قد استعادت النقص الحاصل نتيجة وجود الفتحات وعززت من المطيلية.

استخدام الياف الكربون البوليمرية لتقوية العتبات الخرسانية غير المشورية مع او بدون فتحات اظهر تحسينات جيدة علي مقاومة القص لهذه العتبات. استخدام الياف الكربون لتقوية العتبات



الحاوية على فتحات عرضية قد استعاد معظم الخسارة الحاصلة بالمقاومة مع مؤشر على زيادة الليونة.

العنبات الحاوية على فتحات اظهرت انتشار قليل للتشققات بينما كان استخدام الياف الكربون قد عزز انتشار التشققات. تغيير مقاومة الانضغاط للعنبات ذات الميل الموجب لم تؤثر على انتشار وكمية التشققات لكن الزيادة تكون مؤثرة فقط للعنبات غير الموشورية المقلوبة حيث اظهرت ان هناك تشققات قص وانثناء اضافية قد حدثت.



جمهورية العراق  
وزارة التعليم العالي والبحث العلمي  
جامعة ميسان  
كلية الهندسة  
قسم الهندسة المدنية



## التحليل اللاخطي للعتبات الخرسانية غير الموشورية بأستخدام نظرية العناصر المحددة

رسالة

مقدمة إلى كلية الهندسة في جامعة ميسان  
كجزء من متطلبات نيل درجة الماجستير في علوم الهندسة المدنية/ إنشاءات

من قبل

علي واثق عبد الغني

( بكالوريوس هندسة مدنية 2016 )

أشرف

الأستاذ المساعد الدكتور: عبد الخالق عبد اليمه جعفر

شعبان 1440

نيسان 2019

